



A Dynamic Neural Fields Model for Spinal Motor Control

A thesis submitted in fulfilment of the degree of
Doctor of Philosophy in Cybernetics

School of Psychology and Clinical Language Sciences

University of Reading

Gabriella Cefalù

November 2021

DECLARATION OF AUTHORSHIP

I, the undersigned GABRIELLA CEFALÙ, confirm that this is my own work and the use of all material from other sources has been properly and fully acknowledged.

Date: 30 November 2021

Signature:

(Gabriella Cefalù)

"When we leave this room is gone."

— Bon Iver

Grazie.

Abstract

One of the most debated processes of motor control is how biological systems solve the degrees of freedom problem, using the redundancy of the motor system advantageously. Optimisation strategies and control theory result in models that are task specific and limited at generalising. In this thesis, motor redundancy is addressed from a biologically inspired perspective, developing a model for spinal motor control in dynamic field theory (DFT). Empirical studies show that patterns of muscle activation contribute to coordination, emerging from the integration of cortical and spinal sensorimotor information. These patterns, called motor primitives, are at the core of the proposed model and are represented as attractors in two-dimensional neural fields. Weighted by cortical activations and combined with sensory feedback carrying the position of the end effector, primitives are combined in a resultant force field, associated to the motor plan. This process is formalised by a control law that, giving the forces at the joints of the manipulator, allows for the direct simulation of the forward dynamics. Other processes in the spinal cord are modelled, including a neural controller for the autonomous development of the task, an adaptive threshold enabling stable representations of motor features, and synaptic nodes converting neural representations into motor variables used to calculate the forces at the next time-step. Results show a generalised reaching repertoire, emerging from a few motor primitives and successful straight trajectories, with unimodal velocity profiles. Introducing two-dimensional traveling peak solutions as elemental behaviour shows how the developed methodology can be used to add physiologically inspired elements to cognitive robotics. The findings of this thesis connect existing models in DFT to biomechanical accounts based on motor primitives, resulting in a fully embodied account for motor control and opening the way for a unified framework to understand hand-eye coordination and develop bio-inspired robotics.

Contents

List of Abbreviations	v
1 Introduction	1
1.1 Aims of the Thesis	10
1.2 Overview of the Chapters	13
2 Movement and Motor Control	15
2.1 Introduction	15
2.2 Physiology of Motor Control	17
2.2.1 Cortical Organization	17
2.2.2 The Spinal Cord and Muscle Activation	23
2.2.3 Invariant Properties of Voluntary Movements	31
2.3 The Degrees of Freedom Problem	36
2.3.1 Muscles Synergies	40
2.3.2 The Motor Primitives Summation Hypothesis	43
2.4 Conclusions	47
3 Neural Fields for Embodied Motor Control	48
3.1 Introduction	48

Contents

3.2	Embodied Cognition	51
3.3	Dynamic Field Theory	57
3.3.1	Introduction to Neural Field Dynamics	61
3.3.2	From Peaks of Activation to Cognition	67
3.4	Sensory-Motor Coupling, Autonomy and Learning	70
3.4.1	Cognitive Robotics	76
3.5	Conclusions	86
4	Methods	87
4.1	Introduction	87
4.2	Stability of Neural Field Solutions	89
4.2.1	Evans Functions for the Study of Stability	94
4.2.2	Stability of Self-Sustaining Peak Solutions	99
4.2.3	Stability of Self-Stabilising Peak Solutions	104
4.3	Dynamic Neural Fields in 2D	109
4.3.1	The Amari equation in 2D	109
4.3.2	Stability of Self-Sustaining Solutions in 2D	114
4.3.3	Adaptation and Drifting Instability	117
4.4	Robotic Control Dynamics	122
4.4.1	Kinematics and Dynamics of a 2-R Manipulator	122
4.4.2	Design and Stability of Robotic Controls	128
4.5	Conclusions	136
5	A Physiologically Based Model for Spinal Motor Control	137
5.1	Introduction	137

Contents

5.2	Proposed Model for Trajectory Formation	139
5.2.1	S.A.M.: The Spinal Attractor Model	145
5.3	Neural Fields Control Design for S.A.M.	150
5.3.1	Model Overview	150
5.3.2	Mathematical Implementation	154
5.4	Simulations and Results	165
5.4.1	Numerical Methods	165
5.4.2	Simulating a Reaching Task	169
5.4.3	The Drifting Instability	175
5.5	Conclusions	180
6	Discussion	181
6.1	Introduction	181
6.2	A Coherent Framework for Embodied Motor Control	183
6.2.1	<i>Contribution 1.</i> The spinal attractor model for direct movement formation	188
6.2.2	<i>Contribution 2.</i> Task monitoring: a model for autonomous spinal response	194
6.2.3	<i>Contribution 3.</i> Synaptic nodes as a model for the neuromuscular junction	196
6.2.4	<i>Contribution 4.</i> A unified methodology to design and simulate controllers in the DFT account	198
6.3	Future Developments	202
6.4	Conclusions	206
	Bibliography	208

A Appendix: Matlab Code Scripts and Functions	219
A.1 Code for a Reaching Task	219
A.1.1 Function Files	224
A.2 Code for a Traveling Peak Solution	228

List of Abbreviations

a-DNF Activation DNF

ACh Acetylcholine

CNS Central Nervous System

CoS Condition of Satisfaction

DFT Dynamic Field Theory

DNF Dynamic Neural Field

DoF Degrees of Freedom

EB Elemental Behaviour

EMG Electromyography

EPP End Plate Potential

FFT Fast Fourier Transform

HCT Hand Centred Target Map

m-DNF Motor Primitive DNF

mAP Muscular Action Potential

NMJ Neuromuscular Junction

PD Proportional and Derivative

SAM Spinal Attractor Model

tm-DNF Task Monitoring DNF

Chapter 1

Introduction

The original title of this research project was ‘Frog in Silico: Understanding Hand-Eye Coordination’. The initial idea was to develop a model linking a sensory input (visual) to the development of a motor plan expressed in terms of a force field able to guide a robotic interface. This was inspired by the encoding of visual input in patterns in the frog’s retina and by electrophysiological experiments linking recorded spinal force fields to patterns of muscle activation in the frog’s spinal cord (Giszter et al., 1993; Lettvin et al., 1959).

This simple task requires the simulation of several processes that go from visual mapping of the target to some motor reference for reaching, and from some representation of the motor plan to the effective muscle pattern of activation. It is also necessary to include a recurrent pathway to adjust online the trajectory, based on sensory input, and some mechanism to detect task completion and avoid overshoot.

The sequence just described, with the addition of some learning process necessary to acquire and perfect existing motor skills, defines what is referred to as *motor control* (Rosenbaum, 2010). Modelling visuospatial coordination means appropriately representing and interconnecting these processes, mindful of the properties of the body and of the environment in which it senses and acts.

A number of models already exist in literature revolving around motor control

and its components represented in Fig. 1.1. They all share a common aim that is to study and understand how biological systems move autonomously, performing tasks situated in time (*autonomy & timing* block in Fig. 1.1), constantly adapting to the environment (*sensory-motor integration* block in Fig. 1.1), selecting effortlessly suitable muscle activations for the ongoing motor goals (*motor activation selection* block in Fig. 1.1) and continuously learning and improving their adaptive motor response (*learning* block in Fig. 1.1)(Rosenbaum, 2010).

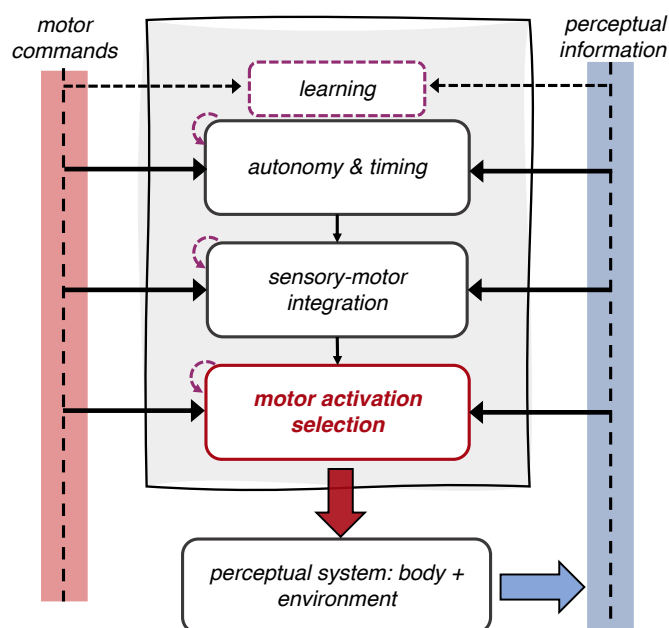


Figure 1.1: A schematic representation of the processes involved in motor control. Red and blue side bar represent the stream of information coming from the brain to the motor system and to the brain from the perceptual system. Existing models for motor control have already addressed to some extent autonomy, timing and sensory-motor integration in the embodied framework. The way in which motor activations are selected, that is *the degrees of freedom problem*, is still poorly understood. In the present thesis this problem is addressed linking dynamic fields as neural representation and motor primitives for movement formation.

The traditional approach to motor control considers a hierarchical development of it, assigning all the planning to the cortical regions in order to optimise some control variable (Todorov, 2004; Uno et al., 1989; Wolpert, 1997, among the others).

A distributed theory of motor control is supported, on the other hand, by the development of the concept of *embodied cognition*, that considers the emergence of its processes, from higher cognition to spinal circuits integration, from the continuous exchange of information between the body and the environment (Bizzi et al., 1991; Brooks, 1991; Schöner, 2007; Shapiro, 2012; M. Wilson, 2002).

The ability of biological systems to take advantage of their redundant motor system (i.e., the body) is still little understood, despite the presence of a great number of studies that span from electrophysiology to mathematical modelling of voluntary movement. This is mirrored by the fact that biological levels of behavioural adaptability seem until now unattainable with traditional robotics (Brooks, 1991; Clark, 1997; Hart & Giszter, 2010; Pfeifer et al., 2007).

The study of the strategies used by a system to compensate for this redundancy, or to take advantage of it, to produce an appropriate motor outcome goes under the name of *the degrees of freedom problem* (Bongaardt & Meljer, 2000; Rosenbaum, 2010). Considering the processes of motor control distributed at different levels of sensory-motor integration from the cortex to the spinal cord, the degrees of freedom problem describes the appropriate motor selection at different stages accordingly. Understanding how this problem is handled by the central nervous system and coordinated at the level of the spinal cord is still debated.

At a cortical level, the degrees of freedom problem can be represented in terms of the selection of motor activations that are then sent down to the spinal cord, based on the representation of the current motor task emerging from sensory-motor integration. In other words, the first DoF problem encountered consists in the mapping of perceptual features into motor features.

Dynamic Field Theory (DFT) has supported the development of architectures based on the Dynamic Neural Field (DNF) to give a sensory-motor representation of elements of cognition. Elemental behaviours, according to this account, are encoded in the dynamics of localised peaks of activation on a multidimensional feature space. The formation of these peaks and their instabilities can be triggered by the process of integration of sensory input and motor representations in coupled

fields (Sandamirskaya et al., 2013; Schöner, 2007; Spencer et al., 2009).

Neural fields have been used already to model visuospatial integration, motor sequencing and autonomous motor plan development in an embodied framework, moving the degrees of freedom problem down the line, at least to the point in which motor activations are selected to produce appropriate joint forces (Erlhagen & Bicho, 2006; Fard et al., 2015; Rudolph et al., 2015; Sandamirskaya & Schöner, 2010; Sandamirskaya & Storck, 2014).

Empirical studies show that motor commands are sent from the cortex to the spinal cord, where they form synapses with single motor neurons or with local spinal circuitry. At this level, the degrees of freedom problem is given by the recruitment of muscles to produce the correct forces at the joints. The redundancy of the musculoskeletal system gives multiple possible patterns of muscle activation that satisfy the motor task. Local spinal circuitry also provides local sensory motor integration and pre-shaped networks that contribute to the synergic activation of muscles (Luppino & Rizzolatti, 2000).

Existing models that attempt to solve the DoF problem at this level, including those that use DNFs, compute the torques at the joints directly solving the so-called *inverse dynamic problem*. The solution of the inverse dynamics consists in inferring the torques to apply at the joints of the desired actuator (i.e., the body or the robotic set-up) from the desired *kinematics* (i.e., the final displacement and orientation) satisfying the motor task. This solution can be estimated using analytical strategies that minimise cost functions representative of the motor goals, using traditional robotic control techniques (feedback control (Jazar, 2007), feedforward control or internal models (Miall & Wolpert, 1996) and adaptive observers (Wolpert, 1997) or abstract attractor/repeller control laws (Bicho & Schöner, 1997).

Using these strategies, it is possible to simulate reaching tasks based on sensory motor integration resulting in hand-eye coordination (Fard et al., 2015; Johnson et al., 2008). Nonetheless, these methods are not based on the physiology of the motor system and the solution of the DoF problem in this sense doesn't match the embodiment of the associated accounts. What is more, the computation of the torques using robotic controls and optimisation strategies does not provide the correct

framework to understand how the motor plan develops in biological systems, since algorithms and cost functions do not have a physiological counterpart (Latash, 2012).

It was decided then to develop an alternative approach to the DoF problem, introducing a model inspired by the physiological organisation of the spinal cord where, according to a growing number of empirical studies, this process of selection of muscle activation takes place, combining descending signals from the brain and local sensory feedback (Bizzi et al., 1991; Giszter, 2015; Giszter & Hart, 2013; Mussa-Ivaldi et al., 1994; Overduin et al., 2008).

The concept of spinal modularity emerged from the first studies on spinalised frogs. Giszter et al. (1993) noted that spinal stimulation of deafferented frogs elicited structured motor activation (muscle synergies). These can be represented in terms of an associated force field, recorded by keeping the limb position fixed in different points of the workspace. Each force field is characterised by an equilibrium point that is the point in the workspace where the forces acting on the limb are null and the limb keeps the equilibrium position. Superimposition of force fields yields to the formation of a resultant force field with its equilibrium point: superimposition of force fields can account for a greater motor repertoire. This concept was formalised by Mussa-Ivaldi et al. (1994) and goes under the name of *the motor summation hypothesis*. The modular elements encoding muscle synergies in the spinal cord are called *motor primitives*.

Supported by these findings, the focus of the project becomes modelling the spinal cord using dynamic fields to build an embodied layer where cortical activations, resulting from higher sensory-motor integration, can be combined with local sensory feedback, activating pre-shaped motor patterns (the motor primitives) to give the resultant forces at the joints, mirroring empirical results (Overduin et al., 2008).

In this sense, the degrees of freedom problem is addressed in this thesis from the *cybernetic* point of view. Cybernetics defines a broad field of research characterised by a common element: understanding the functioning of both artificial and biological systems in a unified account based on control mechanisms that regulate the exchange of information between the system and the environment in which it operates (Wiener,

1948). A bottom-up design process characterises the proposed model, that is not based on an algorithm satisfying some task related constraint, as traditional artificial intelligence would do. On the contrary, it builds from physiological and behavioural findings and from the understanding of stability of both DNFs and robotic controllers.

Describing the development of the forces at the level of the joints leaves open the problem of muscle recruitment down the line. This is addressed by a number of studies that extend the initial results on motor primitives, using clustering and extraction techniques to analyse muscle activation in intact animals (D'Avella et al., 2003; Flash & Hochner, 2005; Hart & Giszter, 2010, for instance) and, using electromyogram (EMG) recordings, in humans (Giszter, 2015; Giszter & Hart, 2013; Kurt A. & Reza, 2000). From these emerges that, complex movements can be represented in terms of a few motor primitives representing groups of muscles that are co-activated, appropriately scaled and shifted in time. The scaling and shifting coefficients can be represented by the cortical activations mentioned above, responsible for the selection of the primitives and resulting from sensorimotor integration at a cortical level.

Regardless of the kinematic or dynamic nature of motor primitives, biomechanical models for motor control have developed based on the following main assumptions: a limited number of motor primitives can account for a larger movement repertoire; such repertoire is implemented using a simple recruitment rule that sums weighted motor primitives; sensory-motor integration of proprioceptive and central commands at the level of the spine is mediated by interneuron circuits, giving the neural substrate for the synergic muscles activation (Alessandro et al., 2013; Flash & Hochner, 2005; Hart & Giszter, 2010).

Both the elements presented above, dynamic fields for cognition and motor primitives-based models, share the same embodied embedding:

- elements of cognition in DFT and force fields associated to motor primitives are described in terms of *attractor dynamics* on a two-dimensional feature space;
- both cognitive and motor representation in the embodied framework require continuous sensory-motor integration;

- complex cognitive or motor representation can be modelled using simple scaling and additive operation, despite the highly nonlinear underlying biological processes.

These shared features lead to the development of a novel model where motor primitives are represented as stable attractors, using the dynamic field equation in two dimensions. Cortical activations are assumed known and represented for convenience as stable attractors in one-dimensional neural fields. These could be computed in the same framework using sensory motor integration and motor learning by existing architectures in DFT, or extracted from biological datasets. The hypothesis of motor summation is translated into a control law based on the weighted sum of the motor output of motor primitives and activations neural fields, referred to as *the spinal attractor model* (SAM). The SAM provides robotic controls for the robotic model used for simulation, computing the force field at every position in the workspace based on the DNF representation of the motor plan and the current position of the end effector.

Controllers for autonomous motor development and for a stable representation of motor features in the spinal cord are developed to complement the spinal attractor model. Two other physiologically based elements are modelled and integrated in the DNFs architecture: an adaptive threshold that activates working memory representations of spinal motor features, namely motor primitives and cortical activation signals; a model for motor output mapping that resembles the function of the physical junction between motoneuron and muscle.

The system is tested in a reaching task: the position of the target, the value of the activations and the attractor-like motor primitives are passed to the model and represented in DFT. The information on the distance from the target is used to monitor task completion and to activate working memory instabilities to retain stable representations of the motor features. The motor variables are extracted from their field representation by means of motor junction synaptic models (*synaptic nodes*) and then used to compute the torques at the joints using the SAM control law. This gives the forces necessary for the planar link to move. The next position of the end effector is obtained computing the *forward dynamics*. This information is sent in feedback to

update that state of the motor task, in a way that is inspired by spinal reflexes.

The results show successful reaching tasks presenting some relevant motor invariants, such as trajectory straightness and a unimodal velocity profile. The representation of the motor plan in the spinal cord using dynamic fields as the weighted sum of planar motor primitives, together with the sensory feedback carrying the position of the end effector, provides at every step of the simulation a resultant force field on the workspace where the movement is taking place. This is the model correlate of empirically recorded spinal force fields.

Existing mathematical methods to study the stability of neural fields controllers are adapted to build this spinal motor control representation, creating a unified framework to design neural controllers that show the appropriate instabilities and elemental behaviours when triggered. Understanding stability (and the conditions that trigger instability) is fundamental to model strategies that are compatible with the empirical findings or, as it is done with synaptic nodes, to reunite existing elements in DFT with biological elements of motor control. The proposed methodology can be also used to introduce new attractor dynamics for a more physiological neural representation. An example is the proposed method to build travelling peaks on two dimensional neural fields to encode motor plans.

The proposed model for spinal motor control reconciles traditional control theory for the study of stability, biomechanical models based on spinal modularity and dynamic neural fields for cognition, contributing to the development of an architecture for motor control that can include more physiological elements and use the abundance of degrees of freedom of the motor system to produce flexible and adaptive behaviour.

The SAM proves that it is possible to simulate voluntary movements without the direct solution of the inverse problem. This is done here at the level of the computation of the forces at the joints using the concept of spinal force fields. These are representative of motor primitives and are associated to muscles recruitment which, in future developments, could be modelled using more sophisticated biomechanic datasets from behavioural experiments or simulations that include motor learning. Using existing models based on primitives for movement formation together with

architectures for cortical motor control in DFT, the problem of selection of the appropriate motor strategy can be finally studied in a unified embodied framework.

Future developments of the proposed approach could promote advances in understanding neural mechanisms underlying motor control and shed light onto the emergence of invariants typical of voluntary movements. An example could be represented by velocity profiles of voluntary movements that result unimodal in the proposed account, but not bell-shaped as found in behavioural studies (Plamondon et al., 1993). Results from simulation of the spinal level could confirm whether this invariant emerges from cortical processing (Fard et al., 2015) or as a consequence of the shape of the motor primitives (Miranda et al., 2018). The outlined account could also encourage the development of a new generation of robotics, benefitting from the flexibility typical of the motor primitive-based models for movement formation and embedded dynamic neural fields controllers.

1.1 Aims of the Thesis

The connection between dynamic models for neural systems and biomechanical models for motor control, based on a modular organisation of motor primitives, is the distinctive aspect of this thesis. In fact, it creates a bridge between neural attractors and biomechanical attractors, in a structure that supports both the flexibility and the stability needed for motor control in the context of embodied cognition.

This link fills the existing gap between the simulation of cortical structure involved in motor planning and the biomechanical modelling of movement formation at a lower level, both fields aiming at understanding the processes related to motor control.

The main goal of this project is to outline a system of controllers, both neural and biomechanical, for the study of voluntary movement coordination at the level of the spinal cord. This primary goal is addressed within the following four aims. These aims are addressed in detail in the following chapters. The associated contributions are discussed in detail in Chapter 6 and summarised below.

List of Aims:

- 1. Developing a model for motor control based on physiological findings that uses the motor primitive summation hypothesis, overcoming the need for optimisation tools to solve the inverse dynamics.**
- 2. Implementing appropriate neural controllers for spinal motor control in the Dynamic Field Theory (DFT).**
- 3. Introducing new types of elements of cognition in the DFT that can account for cognitive processes in terms of propagation of peaks of activation.**
- 4. Simulating a reaching task with the architecture satisfying Aims (1-3), using a simple robotic interface with two planar joints.**

To address the first aim, it was necessary to think about a control law for a robotic manipulator whose position could be updated without reverse-engineering its dynamics. From considerations on the organisation of motor primitives in the spinal cord and on the empirical finding of recorded spinal force fields, a new control law is formalised that gives stable reaching behaviours. This is possible calculating the resultant force field on the workspace from dynamic field representations of cortical activations, motor primitives and sensory feedback, modelling the motor summation hypothesis in DFT. This control law represents the fundamental step to bridge existing models for motor control that use neural fields to existing models for movement formation that represent muscle synergies in terms of spinal motor primitives (see *Contribution 1* in Section 6.2.1). In this framework, it will be possible to address in the future the degrees of freedom problem in terms of muscle recruitment and selection of cortical activations, connecting the proposed architecture with existing DNFs models and with biomechanical datasets (see Section 6.3 for future developments).

To address the second aim, the study of solution of the neural field equation is carried out and controllers are developed inspired by physiological findings on the spinal circuitry and the connection to the ascending (sensory) and descending (motor) pathway. In particular, a model for autonomous motor response is developed considering spinal reflexes and represented using detection/forgetting instabilities in a one-dimensional neural field (see *Contribution 2* in Section 6.2.2). Motor features for the ongoing motor plan are represented triggering a working memory instability in one and two-dimensional neural fields, for cortical activations and motor primitives respectively. These spinal motor features are stabilised using a threshold mechanism for the duration of the task. The conversion of neural representations into motor variables is modelled using instantaneous synapses, usually called neural nodes in DFT, here considered as a simplified representation of the neuromuscular junction (see *Contribution 3* in Section 6.2.3). Activations, in future developments, could be computed from sensorimotor integration, using existing models that include learning to solve the degrees of freedom problem at a cortical level. More refined motor primitives and patterns of muscle activations could give more detail to the proposed model, for instance, using more complex biomechanical models or behavioural datasets

(see further developments in Section 6.3).

The development of a unified framework for the study of stability, as well as the conditions to trigger instability, led to consider traveling peak solutions as interesting elements of cognition in DFT. In this thesis, methods for the analytical study of perturbation are reviewed and numerical methods to simulate the drifting behaviour are outlined (see *Contribution 4* in Section 6.2.4). The use of traveling peaks to model cognition is discussed in Section 6.3 and left as a future development of the proposed account. It is anticipated that more physiological elemental behaviours, including drifting solutions to the field equation, can be used to model more complex tasks, such as obstacle avoidance and periodic motor patterns, without the need for a new motor plan to emerge.

As regards the last aim, simulations of the controllers modelling spinal motor control are performed using a planar two revolute joint manipulator. Numerical methods used are outlined, with particular attention to Fourier methods for convolution. The results are successful reaching trajectories that, despite the simplified cortical activations and motor primitives, are straight and show unimodal velocity profiles. These features emerge directly from sensory motor integration and are not the result of optimisation processes or inverse models (see Section 5.4.2 for results and *Contribution 1* in Section 6.2.1 for a discussion on motor invariants and limitations of the proposed approach).

1.2 Overview of the Chapters

Chapter 1: Introduction

The field of study is introduced leading to the identification of an existing knowledge gap in the development of models that address the degrees of freedom problem. The concepts that have inspired the development of the proposed model are presented together with an anticipation of results and future applications. The list of aims of the thesis is detailed.

Chapter 2: Movement and Motor Control

The core problems of motor control are discussed, together with relevant neural and musculoskeletal structures involved in the development of voluntary movements. The degrees of freedom problem is described in terms of limitations and opportunities offered by motor redundancy. It follows the introduction of the concept of motor primitive and motor summation. These have a key role in the development of a model based on empirical findings that gives motor activations without direct solution of inverse dynamics (**Aim 1**).

Chapter 3: Neural Fields for Embodied Motor Control

The perspective offered by embodied cognition is the one used in the proposed framework for motor control and finds its formalism in the Dynamic Field Theory. Elements of DFT are introduced in order to build the substrate from which controllers for the proposed spinal model are designed (**Aim 2**) and highlight the limitations of the current approach to motor control. By doing so, the existing gap between sensory motor representation of motor plans and sensory motor representation of motor activations at the level of the spine is identified.

Chapter 4: Methods

A unified methodology is developed to design neural controllers using the neural field equation. The proposed method, adapted from the study of the field equation with transmission delays, gives a clear representation of the dynamics of neural fields in one and two dimensions, proving to be well suited to develop controllers that are physiologically based. Control theory elements necessary for the design of the spinal attractor model are presented together with the biomechanical description of the robotic interface used for simulations (**Aims 2-4**).

Chapter 5: A Physiologically Based Architecture for Motor Control

The proposed architecture for motor control in the spinal cord is presented. Mathematical and numerical implementation are detailed; results from a simulation of a reaching task are given, completing the development of **Aims 1, 2** and **4**. The description of numerical methods for travelling peak solutions and relative simulation partly address **Aim 3**.

Chapter 6: Discussion

The proposed model for spinal motor control is discussed in comparison with other existing frameworks. A list of contributions is detailed considering simulation results and the developed methodology, highlighting how these findings are related to the initial aims of the project. Future developments are presented, considering future task simulations, links to other existing DFT architectures and datasets of simulated or behavioural motor primitives. Long term implications of physiologically based models for motor control on neuroscience and robotics are considered.

Chapter 2

Movement and Motor Control

2.1 Introduction

The term Motor Control identifies the field that studies the processes underlying purposeful coordinated movement formation and stability. This term encloses different high level human behaviours such as motor planning, performance monitoring and attentional enhancement, that emerge from continuous integration of internal and external environmental information. Motor control is ultimately responsible for behavioural flexibility and adaptivity, achieved by means of feedback mechanisms for monitoring and learning.

The questions at the core of this field can be summarised as follows (Rosenbaum, 2010):

- *the perceptual-motor integration problem*, that responds for the flexible adaptation of motor plans to the ever-changing environment in which the system operates;
- *the sequencing and timing problem*, that encompasses the strategies to create ordered sequences of motor activations to accomplish a motor task;
- *the learning problem*, that is how motor skills are acquired and adjusted

in time;

- *the degrees of freedom problem* or *motor redundancy*, that addresses the selection of a particular set of motor activations among the many possibilities offered by the musculoskeletal system to achieve some motor goals.

In this chapter, elements to address such problems are presented in light of the available knowledge on the structures involved, from the central nervous system to the spinal cord and the muscles.

In Section 2.2, the role of the parts of the Central Nervous System (CNS) in the development of voluntary movement is presented: from the cortex involvement in motor planning and in the representation of salient motor features, to the structure of the spine and its role in local sensory-motor integration. The overview continues with a description of the neuromuscular junction and the contractile properties of muscular tissue, highlighting the number of variables at play during motor coordination. Invariant properties of voluntary movements are reviewed along with considerations regarding motor planning and existing models for motor control.

Section 2.3 focuses specifically on the degrees of freedom (DoF) problem, considering the traditional approach to motor redundancy and a new account that sees it as an evolutionary advantage. In this second account, the concept of motor primitive and of motor primitives summation is introduced, considering behavioural experiments and modelling strategies.

This theoretical background offers the context necessary for the development of the proposed model that, drawing inspiration from biological systems, addresses existing limitations in modelling motor control at the level of the spine (**Aim 1**).

2.2 Physiology of Motor Control

Voluntary movements are typically smooth, accurate and appropriately sequenced in time. This is possible thanks to the continuous integration of multi-sensorial and proprioceptive information and to the cooperation of cortical, subcortical and spinal structures that contribute to the development of the motor output (Kandel et al., 2012).

It is possible to distinguish two pathways, one carrying information to the Central Nervous System (CNS) and one streaming information from it:

- *the afferent pathway* conveys sensory information from visual input and proprioceptors through the spinal cord to the central nervous system;
- *the efferent pathway* carries information from motor areas of the cortex, through the spinal cord, to the ultimate effectors of the motor plan, the muscles.

In Fig. 2.1 the neural structures involved in motor control are illustrated. These include cerebral cortex, cerebellum, thalamus, basal ganglia, brainstem and spinal cord (Kandel et al., 2012).

2.2.1 Cortical Organization

Coming from the spinal cord, information access is gated by the thalamus that allows or prevents afferent signals enhancement according to the state of the system. This structure is formed by several defined nuclei: some receive sensory and somatic information to send to the neocortex; some project directly onto the frontal lobe; others play a role in motor control passing information to cerebellum and basal ganglia.

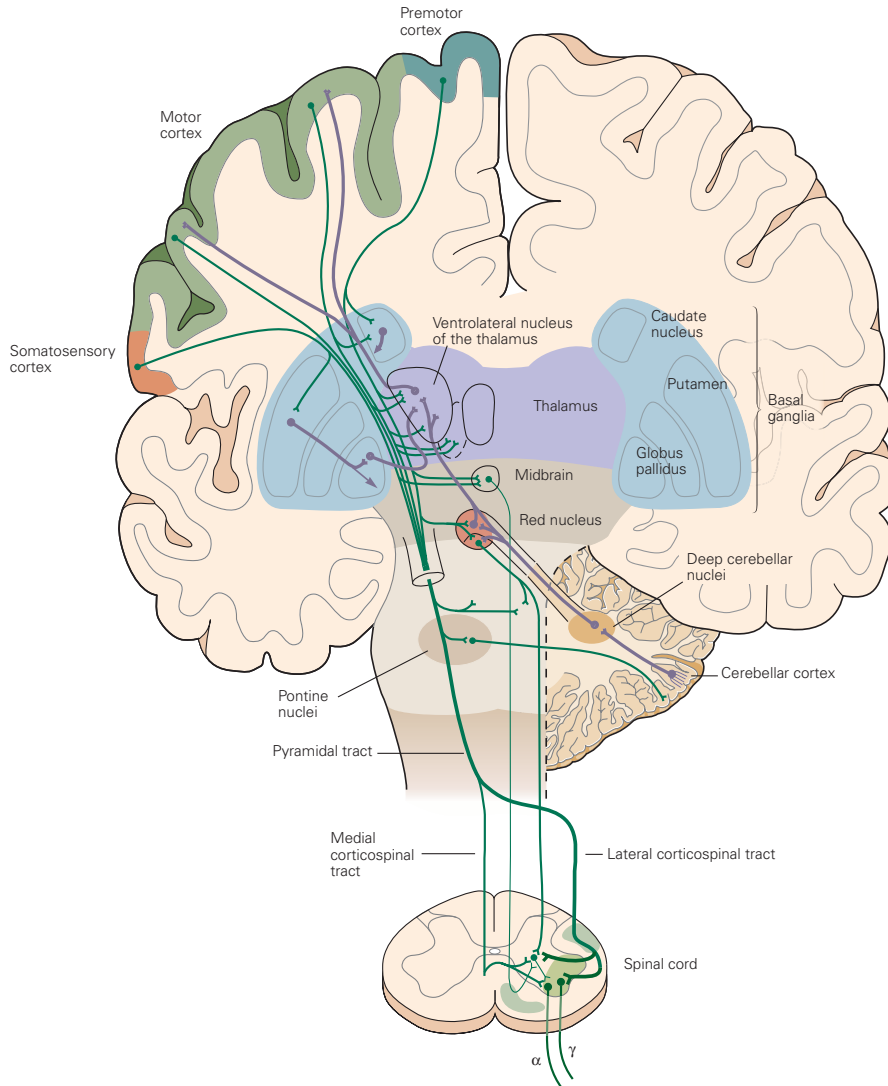


Figure 2.1: Descending pathways and the principal components of the of the CNS for voluntary movement control. In purple: local feedback projection; in green: principal descending projection. Adapted from *Principles of Neural Science, Fifth Edition* by Kandel et al. (2012).

Feedback loops among these regions are involved in producing smooth skilled movements based on a learning process and on the evaluation of the outcome of motor behaviour (Kandel et al., 2012). The cerebellum, in particular, is involved in motor learning triggered by unfavourable outcomes of motor actions (Ito, 2000) and in sequencing and timing (Johansson et al., 2016).

Receiving input directly or through the thalamus from the hypothalamus, mesencephalon and the limbic system, the prefrontal cortex has a crucial role elaborating information coming from the internal and external environment to update the internal state and motivation of the system (Fuster, 1981).

Prefrontal Areas and Internal Models

Prefrontal areas have been found to be essential for initiation, selection and monitoring of the development of the behaviour, although they are not directly responsible for the selection of single muscular contractions. The motor planning function, in fact, could be carried out in terms of representation of the motor task, and prefrontal cortex appears particularly activated when *internal models* are used to anticipate the motor outcome (Goldman-Rakic, 1987).

Such models are considered by the traditional cognitivist approach as a representation of the behaviour of the motor system and are thought to provide a solution to a number of problems concerning motor control. Internal models can be grouped in two categories (Miall & Wolpert, 1996):

- *forward models*, that predict the outcome of ongoing motor plans using a copy of efferent motor commands and the current state of the motor system, coming from the afferent pathway;
- *inverse models*, that generate appropriate output commands in order to achieve a desired state.

Forward models explain a number of empirical findings, such as the cancellation of sensory reafference, that is the afference generate by the system on the system

itself, and compensation for time delays arising from information elaboration (Miall & Wolpert, 1996).

Inverse models could represent the way in which the CNS ‘solves’ the degrees of freedom problem, providing appropriate motor commands from the available knowledge on the system and on the environment (Wolpert, 1997).

These concepts have been used extensively in the development of mathematical models for motor control and are further described in the next sections of this chapter. Nonetheless, the hierarchical organisation that is subsumed has been questioned and a more modular and distributed view of motor control, emerging from the features and the interactions of the motor system and the environment, has been considered as an alternative (or overlapping) control strategy (Giszter & Hart, 2013; Graziano et al., 2002). An integrated perspective that takes into account the recent embodied approach is presented in Chapter 3.

The Motor Cortex

Traditionally motor cortex is divided into three distinct areas (Meier et al., 2008):

- the primary motor cortex (Brodmann’s area 4), from which originates most of the output from the motor cortex, has most fibres that connect directly with motoneurons in *the corticospinal tract*;
- the premotor cortex (Brodmann’s area 6) is involved into movement preparation;
- the supplementary motor area (medial area 6) could have a role in coordination and postural stabilisation.

A peculiar feature of motor areas is the supposed somatotopic organisation. In particular, it was thought that the primary motor cortex included a topographic map of the body, where each point is associated with tension development in a single muscle (or a small group of muscles) and connections among different areas follow

a hierarchical organisation, so that premotor areas project onto motor areas that project onto the spinal cord (Fulton, 1939).

Recent studies on motor cortical areas have confirmed that a general somatotopic organisation exists, but with patterns of muscle activation mostly overlapping with each other and a gradual transition between primary and premotor cortex (Graziano et al., 2002). Patterns of connection among motor areas can be grouped in two major functional classes from this analysis:

- areas that receive sensory input and elaborate motor commands;
- areas that manage the sensory-motor transformation.

The interpretation of such findings together with the examination of spinal projection led to the hypothesis that some areas activate pre-shaped circuits at the spinal level that determine the global frame of the movement. At the same time, direct projections to the motor neurons allow fine regulation of movements breaking pre-shaped synergies (Luppino & Rizzolatti, 2000).

Another relevant hypothesis considers primary motor cortex as the locus in which relevant motor features are mapped. According to *in vivo* recording during pointing tasks, in fact, neurons of the motor cortex in primates are capable to produce a tuning response to some features of the movement. For example, it has been found that the firing rate of some pools of neural cells is higher for a preferred direction of the movement and decreases in the other directions (Georgopoulos et al., 1986).

These findings can be modelled using a function that links the firing rate and the direction of the movement of the type

$$d(\mathbf{M}) = b + k \cos \theta(\mathbf{M}), \quad (2.1)$$

where $\theta(\mathbf{M})$ is the angle between the preferred direction of the cell (i.e., the direction corresponding to the highest firing rate) and the direction of the movement \mathbf{M} ; $d(\mathbf{M})$ is the discharge rate.

It is possible to represent the neural population of cells, firing according to their

tuning curve, as the sum of each vector $\mathbf{N}_i(\mathbf{M})$ associated to the firing rate $d_i(\mathbf{M})$ of the i -th neuron, dependant on the direction of the movement. The resultant directional vector is called *the population vector* and gives the encoding of the direction of the movement represented by the neural population (Georgopoulos et al., 1986):

$$\mathbf{P}(\mathbf{M}) = \sum_i \mathbf{N}_i(\mathbf{M}). \quad (2.2)$$

This type of analysis has been used in several studies on the motor cortex and other brain areas to understand how salient motor features are represented (Georgopoulos, 1997).

A number of studies have investigated if there are neurons in the cortex responding to variations in direction, velocity, position of the joint angles and so on, performing voluntary movements, finding evidence for some kind of encoding for each one of them. Questioning whether motor control is based on one property or another could be the wrong strategy to understand it. It seems more likely, from recent cortical stimulation experiments in primates, that the organisation of movement control is structured in terms of a mixed representation of features that are behaviourally relevant for a specific task or posture (Graziano et al., 2002).

2.2.2 The Spinal Cord and Muscle Activation

The spinal cord is composed by a H-shape grey matter internal part enclosed into white matter, as shown in Fig. 2.2. The grey matter in the posterior part is called *dorsal horn*, whereas the grey matter in the anterior part is the *ventral horn*.

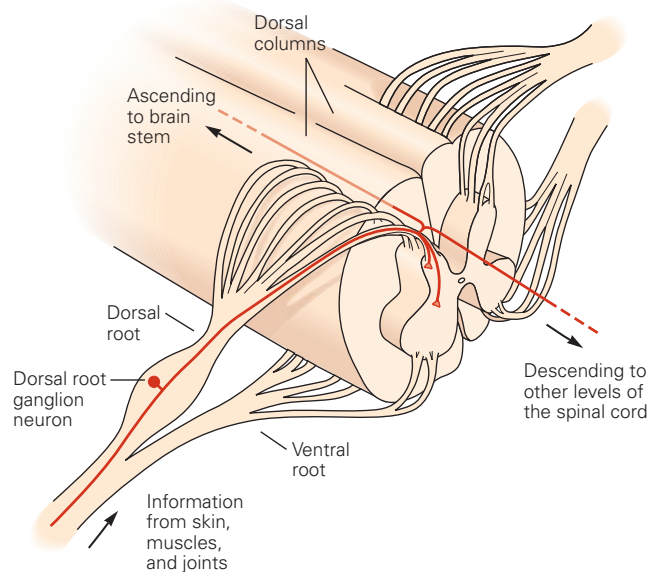


Figure 2.2: Schematic of dorsal and ventral root of the spinal cord with afferent and efferent pathways. From *Principles of Neural Science, Fifth Edition* by Kandel et al. (2012).

The afferent pathway brings somatosensory information coming from the body to higher centres for elaboration. This information enters in the dorsal horn of the spine where the sensory nuclei are found. In the efferent pathway, from cortical areas to the spinal cord, most motor fibres encounter pyramidal decussation at the junction between medulla and the spinal cord. Here, motor nuclei, composed by the body of motoneurons, are situated in the ventral horn: their axons project to skeletal muscles forming columns that pass next to the spinal cord (Kandel et al., 2012).

The grey matter contains interneurons whose contribution to the development of movement is at the centre of a growing number of studies. Traditionally, spinal

interneurons are described in terms of evoked reflex responses, triggered by sensory feedback and leading to stereotyped behaviours that can be modulated by motor commands descending from cortical areas, encoding voluntary movements (Kandel et al., 2012).

Another approach to the study of interneurons classifies local spinal circuitry in terms of Central Pattern Generators, contributing to the development of rhythmic behaviour. At the same time, groups of spinal interneurons are considered involved in a modular organisation of movements, based on the evoked muscular response following intraspinal stimulation. The neural substrate of these muscle synergies is called *motor primitive* (Fetz et al., 2000; Flash & Hochner, 2005; Kandel et al., 2012). The role of motor primitives in movement formation is described in detail below.

A small part of fibres from the medulla crosses at the level of the motor neurons they innervate, making monosynaptic connections that are fundamental for fine hand movements and, forming synapses with interneurons of the spinal cord, for larger groups of muscles coordination (Kandel et al., 2012).

This ensemble of spinal internal connections and the collateral presence of axons coming directly from the cortex give to the spinal circuitry a role of mediator. The modulation of supraspinal commands with afferent local sensory information in the spinal cord specifies the state of activation of the musculoskeletal system (Levine et al., 2014; Overduin et al., 2008; Stelmach & Diggles, 1982). Not only spinal circuitry is able to produce autonomous motor activation without the the supraspinal intervention (Fetz et al., 2000; Giszter et al., 1993; Hart & Giszter, 2010), but it also provides elemental integration of sensory-motor information, coordinating a local level of motor control (Stelmach & Diggles, 1982).

The Neuromuscular Junction

The neuromuscular junction (NMJ) is the point at which the neural signal is converted into the chemical input that triggers muscle contraction. This synaptic junction between the motoneuron and the muscle fibre is located in the ventral root of the spinal cord.

The process of neuromuscular transmission consists in the release, caused by patterns of electrical activity in the motor neuron, of neurotransmitter in the synaptic junction that is carried by vesicles. It is the motor neuron that triggers a first depolarisation, mediated by acetylcholine (ACh), transmitted into packets ligated by a huge number of receptors on the muscle fibre. This process brings the membrane potential under the threshold of about $-50mV$ causing *the end plate potential* (EPP)(Kandel et al., 2012).

In vertebrates this is followed by the opening of voltage-gated channels, situated in the depth of the junction, leading to a much bigger flux of positive ions. This triggers the proper *muscular action potential* (mAP) that, propagating along fibres, causes contraction (Slater, 2017).

The structure of the neuromuscular junction is represented in Fig. 2.3, accompanied by the representation of channels distribution and of the time course of the membrane potential of the postsynaptic muscle fibre.

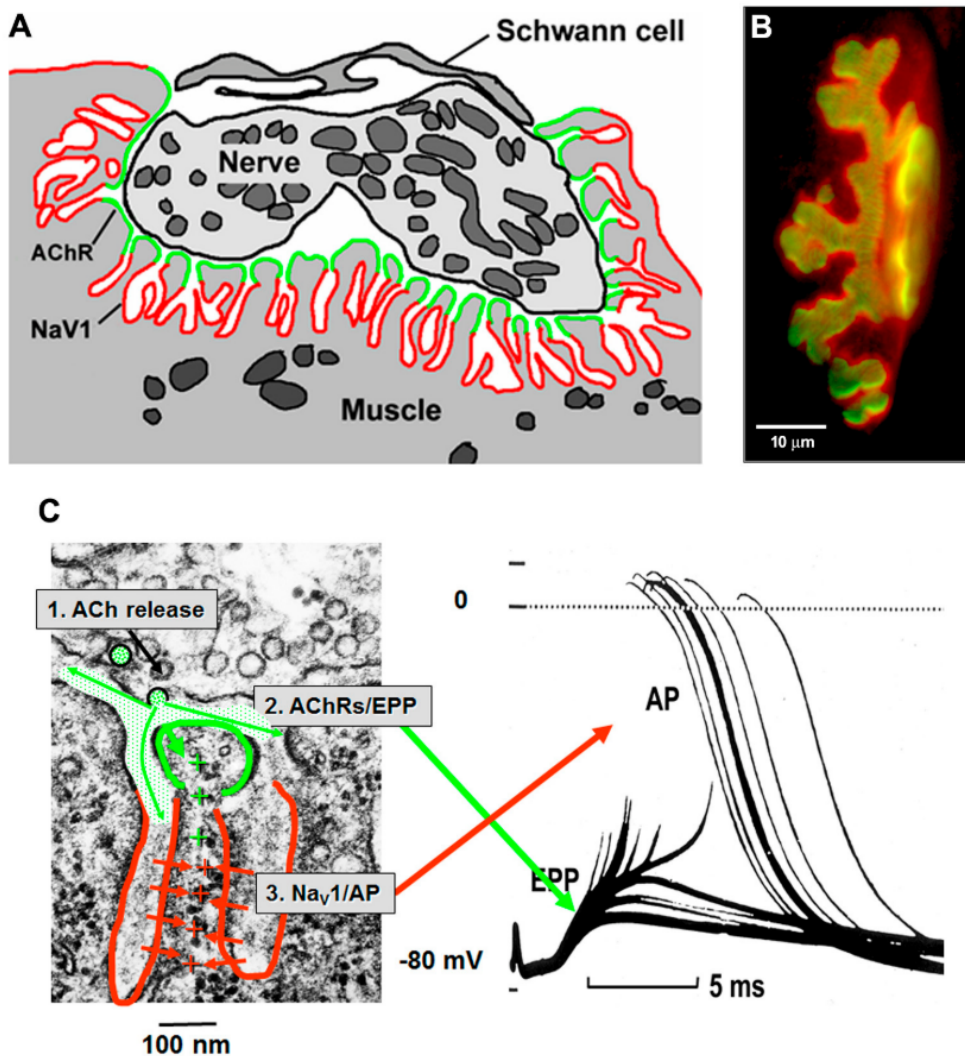


Figure 2.3: Anatomy of the NMJ and generation of the muscular action potential. (A) Diagram of the junction. Receptors for ACh in green are concentrated at the top of the folds of the postsynaptic membrane of the muscle. Voltage gated channels are found in the deeper part of the folds, represented in red. (B) Fluorescence of rat NMJ with the same colour code for the two types of receptors. (C) Generation of the mAP. The release of ACh (1) occurs in the region dense of ACh receptors giving rise to the first depolarisation (EPP) (2). This opens voltage-gated channels (3) allowing more positive ions to enter triggering the mAP. From ‘The structure of human neuromuscular junctions: Some unanswered molecular questions’ by Slater (2017).

The Structure of the Muscle

Each motoneuron innervates a motor unit that can include many fibres. Electromyography has elucidated the structure of the smaller contractile element in the muscle fibre called sarcomere.

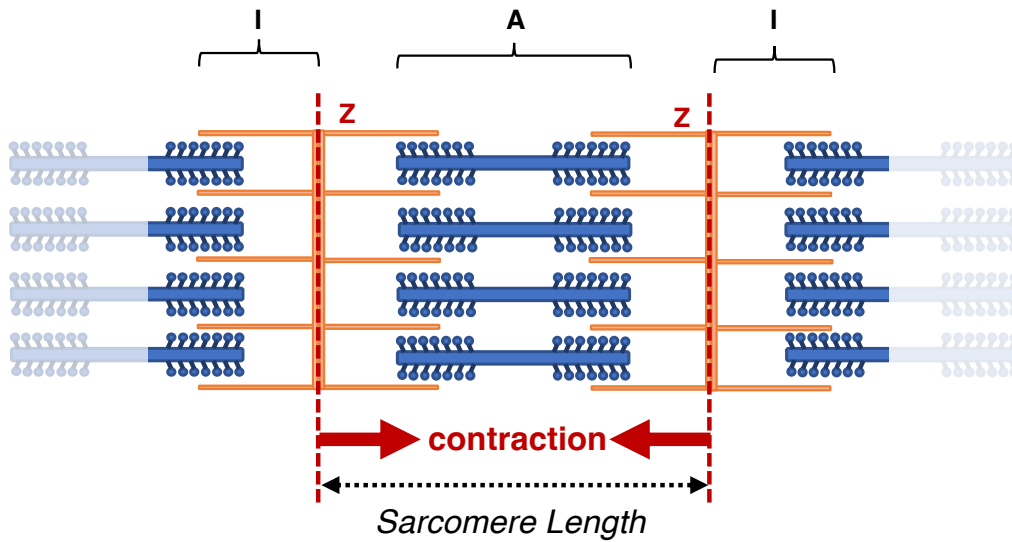


Figure 2.4: Structure of the sarcomere. The wider filament represents myosin with protruding myosin heads (**A**), the narrower actin (**I**). Maximum sarcomere length ($2\mathbf{I} + \mathbf{A}$) is limited by **Z** lines. The shortening of the sarcomere length generates contraction.

The sarcomere is composed by two bands of protein: the myosin, constituting the thicker filament, interposed between bands of actin, the thinner filament, arranged in a comb-like structure (Huxley, 1957, see Fig. 2.4).

The bonds between the two different types of filaments are called crossbridges. Sarcomere length is defined by the distance between two zeta lines and varies with contraction between $1.5\mu m$ and $2.5\mu m$. The contraction is due to the sliding motion of the two filaments caused by the tension released by myosin heads, that are the terminal part of the myosin filament that bonds with actin. This sliding is due to the conformational changing that myosin encounters caused by the variation of calcium concentration in the sarcomere following the arrival of the neural signal in

the neuromuscular junction. Sarcomeres are disposed in series, composing a myofibril. An ensemble of myofibrils disposed in parallel creates a muscle fibre. Muscle fibres form the muscle which is linked to the insertion point in the bone by means of the tendon, passive connective tissue (Huxley, 2004).

The shortening of the contractile element produces the contraction that can be modelled by a force-length curve (Gordon et al., 1966). Changing the sarcomere length and recording the maximum isometric tension, while keeping the length constant until the maximum force is reached, it is possible to obtain the curve in Fig. 2.5. It is found that the percentage of maximum isometric tension developed reaches a peak for an ideal overlap. From this point it decays either when filaments overlap to the point that crossbridges interfere with each other below l_0 , the resting length, or when the filaments are pulled apart to the point that crossbridges cannot form (Winter, 2009).

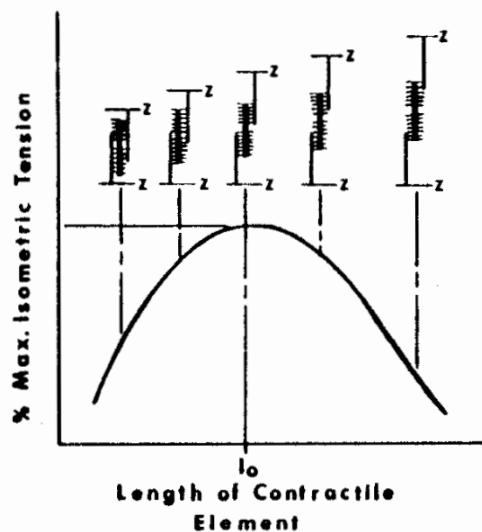


Figure 2.5: Length tension curve of the muscle expressed in percentage of maximum isometric tension with visual representation of the overlapping in the sarcomere. Z lines represent the extension of the sarcomere. From *Biomechanics and motor control of human movement* by Winter (2009).

Connective tissue surrounding the contractile element affects the length tension curve, acting like an elastic component. The behaviour of such component is found to be nonlinear. It exerts no tension when muscle length is $l < l_0$. After resting length

has been surpassed a slow initial tension is followed by a rapid increase as shown in Fig. 2.6, where contractile and elastic forces are represented, F_c and F_p respectively, together with the resultant characteristic F_t .

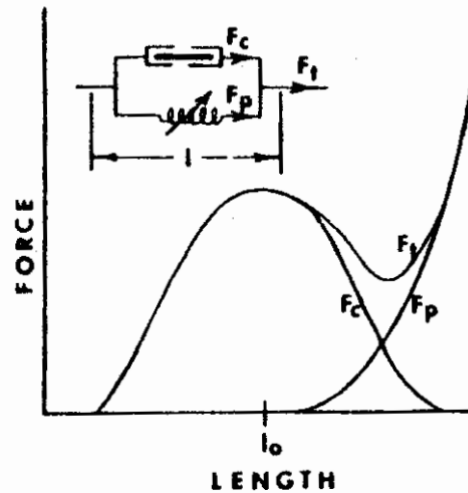


Figure 2.6: Length - force curve of the muscle considering the elastic parallel element. The resulting F_t is given by the sum of the force of the contractile element F_c plus the nonlinear elastic force F_p . Above the curve: electrical model for the muscle with a contractile element in parallel with the elastic component. From *Biomechanics and motor control of human movement* by Winter (2009).

The behaviour of the system can be modelled in terms of electrical components, with an active element representing the sliding filaments contraction, the connective tissue represented as a parallel elastic component and an optional elastic element in series element modelling connective tissue (i.e., tendon) (components in parallel are represented in Fig. 2.6).

The relationship between the shortening velocity and the tension developed is represented in Fig. 2.7. The latter is found to decrease as the former increases. This could be due to the loss in tension caused by crossbridges that need time to break and reform and to the damping effect of fluid viscosity (Winter, 2009).

From the perspective of modelling such behaviour, the relationship between the tension developed by the muscle and the speed at which the muscle length shortens

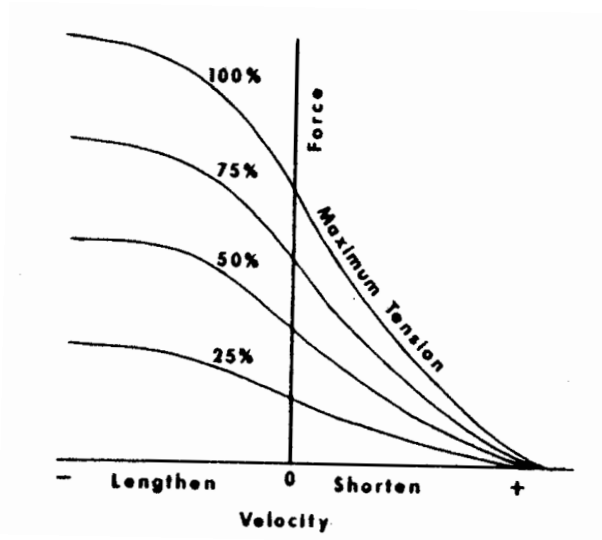


Figure 2.7: Velocity - force curves of the muscle as percentage of the maximum tension. From *Biomechanics and motor control of human movement* by Winter (2009).

can be expressed using the Hill model (Hill, 1938). This is typically formalised by the equation:

$$(P + a)v = b(P_0 - P), \quad (2.3)$$

where P is the muscle force, v is the velocity of muscle contraction, P_0 represents the maximum isometric force and a and b are called Hill constants. Scaling a and b it is possible to simulate the biomechanics of different muscles (see the work by Schmitt et al. (2013) for an example of application of the model to the simulation of artificial muscles).

Properties of the single muscle have been considered above, including how the neural signal is converted into contraction. A motor plan, though, is composed by a sequence of muscle activations and the degrees of freedom problem applies directly to the mapping of neural activity to muscle activity. The required sequence, in fact, can be implemented by many different patterns of neural activation and, at a lower level, with many different patterns of muscles activation. The problem exists whenever, in the motor control chain, a *many-to-one* mapping is necessary (Rosenbaum, 2010).

Even considering a simple Hill model for the muscle, it would be necessary to specify activations of agonist and antagonist muscles at each of the joints involved in the motor task and associate to them the pattern of neural activation to recruit muscle fibres.

Considering the number of variables at play highlighted in this review of the properties of the neuromuscular system involved in motor control, internal models and optimisation strategies have played an important role in modelling motor control, significantly reducing the number of degrees of freedom (Kawato, 1999; Wolpert, 1997). These are discussed in more detail in the next sections.

At the level of the spinal cord, empirical findings have pointed out that, instead of single muscle activations, motor encoding might be performed in terms of target configurations of the body that, regardless of the initial configuration, are responsible for purposeful movements (Flash & Hochner, 2005; Graziano et al., 2002). Before this hypothesis is further explored, some of the invariant properties of voluntary movements are reviewed.

2.2.3 Invariant Properties of Voluntary Movements

Several experimental studies considering, for instance, point-to-point reaching tasks or drawing curvilinear lines have shown that voluntary movements share a number of common features (Abend et al., 1982; Morasso, 1981; Plamondon et al., 1993; Soechting & Lacquaniti, 1981; Suzuki et al., 1997). These can be summarised as follows:

- trajectories linking two points are quasi-straight;
- tangential velocity at the hand has bell-shaped profile;
- joints angles may vary substantially among repetitions;
- curvilinear movements can be decomposed into sub-movements each of which showing the above properties.

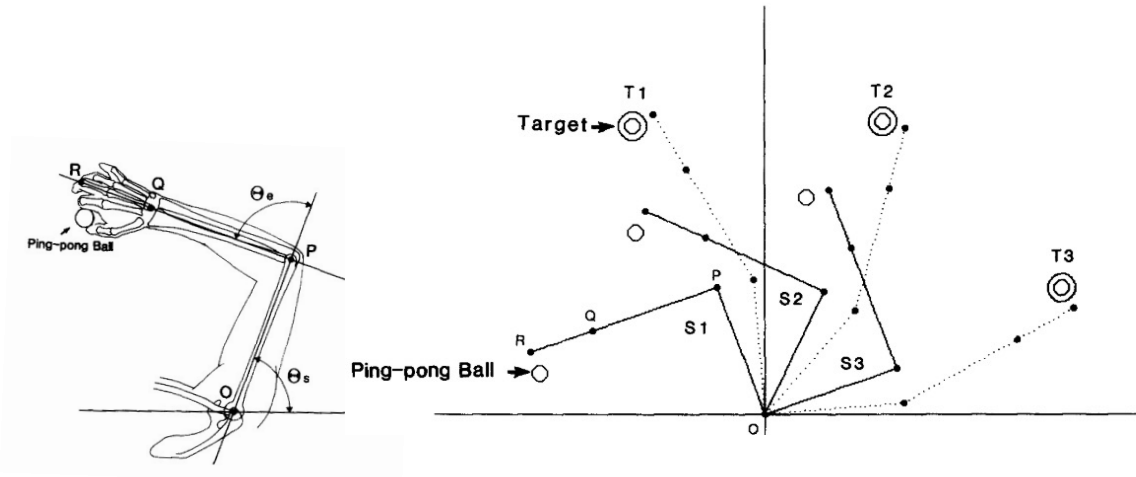


Figure 2.8: Example of experimental set-up to study kinematic and dynamic invariants of voluntary reaching movements. Adapted from ‘Trajectory formation of the center-of-mass of the arm during reaching movements’ by Suzuki et al. (1997).

In Fig. 2.9, an example of trajectories and velocity profiles relative to a reaching task are plotted. In the experiment, whose set-up is represented in Fig. 2.8, the subject was requested to move a ping-pong ball from the starting position S_1 to different target points (in Fig. 2.9, only target T_1 and T_3 are presented).

Experiments on restrained and unrestrained hand drawing movements have proved to follow some linear or power law, describing the invariant relationship between voluntary movements features. For instance, the relationship between the length of a reaching movement and its duration follows the so-called Fitts’ law (Fitts, 1954), that can be written as:

$$MT = a + b \log_2 \left(\frac{2D}{W} \right), \quad (2.4)$$

where MT is the average movement duration, D is the distance from the starting point, W is the width of the target along the axis of motion. In terms of regression, parameters a and b represent an initial delay and an acceleration term, respectively.

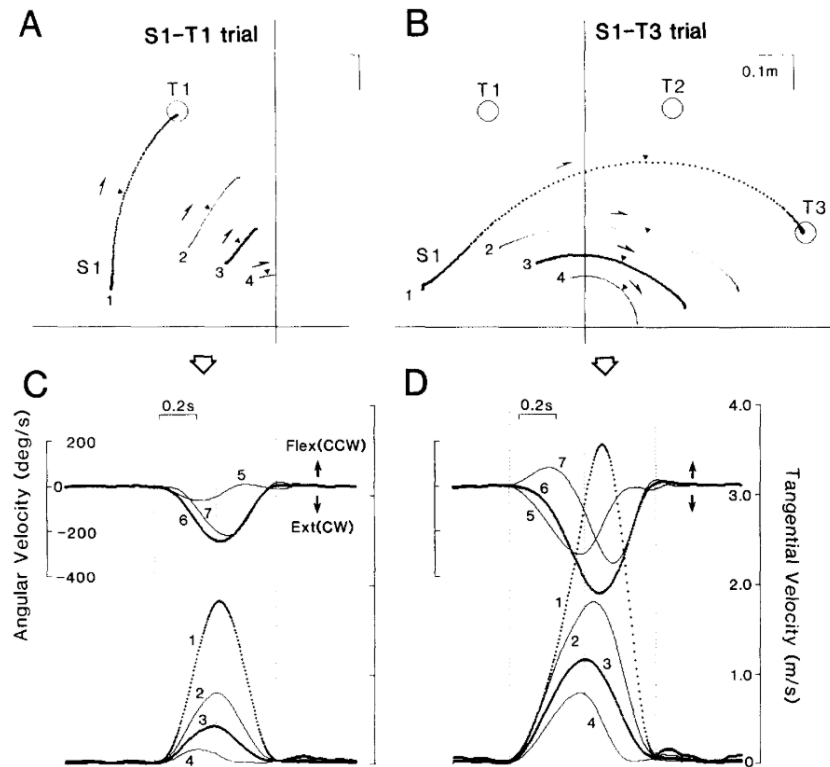


Figure 2.9: Trajectories and velocity profiles in two reaching tasks from S_1 to T_1 and to T_3 . (A-B): trajectory of the hand (1), of the centre of mass of the distal (2) and proximal (3) arm segment and of the entire arm (4); arrows indicate the direction of movement and triangles the peak velocity time. (C-D): time-course of the angular velocity at the shoulder (5), elbow (6) and distal arm (7), flexion and extension are directed counterclockwise (CCW) and clockwise (CW), respectively; below, tangential velocity associated to the trajectories (1-4) in the top panels (A-B) showing the bell-shaped profile. From ‘Trajectory formation of the center-of-mass of the arm during reaching movements’ by Suzuki et al. (1997).

As regards curvilinear trajectories, the two-thirds power law relates the instantaneous velocity of the movement and the radius of curvature associated with the hand trajectory. This law is also referred to as the Lacquaniti's law and can be written as follows (Lacquaniti et al., 1983):

$$v(t) \propto R(t)^{\frac{2}{3}}, \quad (2.5)$$

where v is the velocity tangential to the trajectory and R is its radius of curvature.

These findings seem to support the idea that control commands are planned in the space of the hand based on kinematic regularities and that there exists some control process that translates the kinematic requirements of the movement into dynamic activations compatible to the desired goal (Lacquaniti et al., 1983).

Conversely, other studies have pointed out that some part of the motion must be planned in the space of the joints. For example, other reaching experiments have shown that acceleration at the elbow and shoulder are linearly related to each other during the phase of deceleration of the movement (Soechting & Lacquaniti, 1981). This would suggest that some control is exerted in terms of joints excursion during the task, based on dynamic regularities.

Both accounts are at the core of the optimisation-based approach to solve the degrees of freedom problem and find appropriate motor activations for trajectory formation. These computational theories have been extensively tested, confirming a variety of predictions and motor invariants. Two of the main accounts are the *minimum jerk model*, as regards kinematic control, and the *minimum torque-change model*, as regards dynamic control. While the nature of the controlled variables is still debated, integration of these approaches has also been attempted (Kawato, 1999; Wolpert, 1997).

Instead of speculating from invariants which variables are more likely 'used' by the CNS for motor planning, the *uncontrolled manifold hypothesis* (UCM) offers a practical solution that could be easily applied to experimental data collected on voluntary movements. The idea behind this account is to investigate which control variables, arbitrarily defined, have less variance during a task (Scholz & Schöner,

1999).

It is useful then, according to the UCM, to hypothesise a set of relevant variables and to consider a configuration space for the task object of study. In a reaching task the space could be the one spanned by the joint angles involved. The control variables of choice could be functions of the same angles. The joint space can be divided, then, into two orthogonal subspaces for any set of control variables. The first subspace contains all the configurations of the joints that do not affect the control variables set, that is *the uncontrolled manifold*. The second, orthogonal to the first, is the space of joints configurations that affect the chosen control variables, that is *the controlled manifold*.

If, for the current choice of control variables and the given task, the variance of the uncontrolled subspace is greater than the variance of the controlled one then, according to this theory, the hypothesis on the control variables is acceptable. This means that that most of the variability in the selected feature space (i.e., the joints space) leaves the control variables unaffected (Latash, 2012; Scholz & Schöner, 1999). It must be remarked that the suitability of a set of variables to represent a defined motor task doesn't imply that said set is actually used by biological systems for motor planning.

2.3 The Degrees of Freedom Problem

If one considers the act of reaching with the arm to a target object, it is immediately evident that there are a number of configurations that the arm can assume to perform the same motor task. To each of these configurations, expressed in term of angles formed by the joints, one can associate torques at the joints. These, in turn, can be applied using several combinations of muscle activations.

As pointed out in the previous section, from a traditional perspective on cognition, the Central Nervous System (CNS) should be the one responsible for the process of selection among all the possible choices given by this underdetermined problem where there are more degrees of freedom than constraints (Latash et al., 2007).

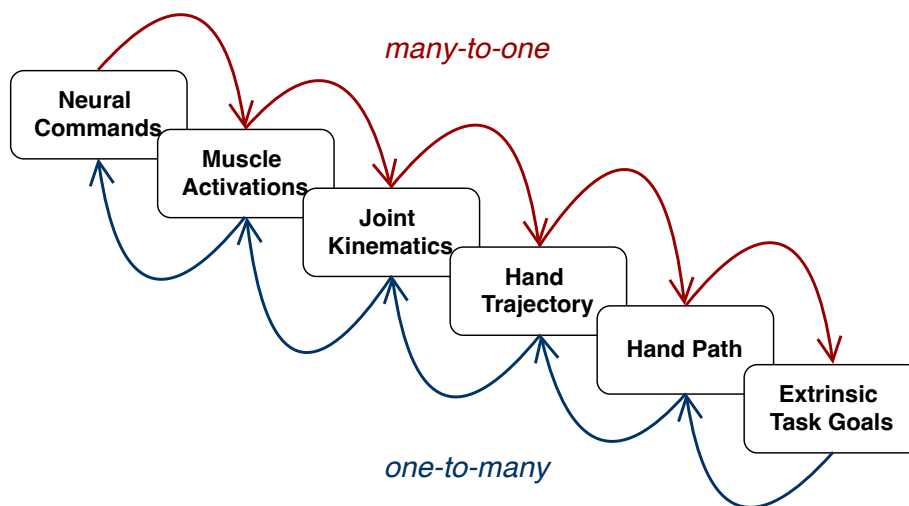


Figure 2.10: The degrees of freedom problem at different levels of motor planning. The *one-to-many* mapping represents the traditional formulation of the motor redundancy, where at each level one configuration corresponds to many possible options at the level above. The *many-to-one* mapping is the process of subsequent reduction of the degrees of freedom, implying a selection among motor activations equally satisfying task goals.

It was Bernstein who argued first that the degrees of freedom problem is handled by motor control strategies that required a circular flux of information (Rosenbaum, 2010). These strategies had to be hierarchically organised so that at the top level

there must be a representation of the motor outcome of the task, at the intermediate level the integration of sensory-motor information and at the bottom level the biomechanical properties of the movement. The two lower levels represent in his vision *the coordination of movement* that he defines as the process that overcomes the motor redundancy turning the motor apparatus in a system that can be controlled (Bongaardt & Meljer, 2000).

Intuitively, he also hypothesised that motor coordination could be understood in terms of a *motor field* that is the space in which the movement takes shape, encoded in a global nonlinear topology and not in a specific metric such as spatial details or torques. Control is achieved in relationship to a task or a goal, using this essential representation that is emerging from neural organisation rather than from processes related to single neurons. In a similar way, he thought that *motor synergies* are controlled at the level of the link between muscles and joints. There previous motor experience is also stored (Bongaardt & Meljer, 2000).

This theoretical approach is still valid and the main concept are taken into account in the proposed architecture, that encodes the same principles in terms of representation, sensory-motor integration and role of the spinal cord in motor control.

Motor Redundancy

In mathematical terms, the degrees of freedom of a system are the number of independent variables of the system itself. Solving the degrees of freedom problem means finding the criteria by which the number of independent variables of the system are reduced in a way that is appropriate for the selected task. The redundancy of the biomechanical system concerns the *kinematics* and the *kinetics* of it. The first represents the variety of positions that can be assumed in time by the system compatible with the task. The second concerns the forces exerted in order to reach this configuration, each of which implies a different pattern of muscle activation.

As mentioned above, some accounts propose that the CNS uses a cost function that has to be optimised to solve this problem. Namely, an efficiency criterion is used to solve the redundancy. It is intuitive that some motor strategies are preferred to

others because they minimise or maximise some variable. For example, efficiency is the reason why direct paths are preferred when doing movements and final configuration of the limbs are usually in the middle of the range of motion in order to allow for quicker response to secondary or unexpected tasks (Rosenbaum, 2010).

There is also the tendency for human movements to have minimum jerk, which is the mean squared rate of the variation of acceleration during the task, meaning that movements from one point to another tend to be as smooth as possible (Flash & Hogan, 1985). Other authors have considered, for example, the minimum torque change (Uno et al., 1989) or more complex cost functions (Todorov, 2004). There is no evidence though that any of these functions is actually used at some level to create motor strategies.

Another account addressing the reduction of degrees of freedom as the solution to the redundancy of the motor system assumes the existence of internal models of the motor system. These are divided into *inverse internal models* and *feedforward internal models* (Wolpert, 1997).

Inverse internal models allow for the computation of motor commands from the kinematic description of the trajectory of the limb that satisfies the task. They are based on an internal reverse representation of associated instances of movements and motor commands and have been traditionally used to produce coordinated movements by control theory and robotics. The level of generalisation of this inverse function can be hypothesised optimal, so that the whole space of motor representation is mapped. Alternatively, it can be assumed that generalisation is limited to the experienced trajectories, obtaining a local mapping. Models based on neural networks, for instance, show an intermediate level of generalisation (Bekey & Goldberg, 1993; Kawato, 1999).

Feedforward models anticipate the outcome of the action, so that the motor system can compensate for sensory reafference and feedback delays. In predictive control, forward models are used to generate an internal feedback on the outcome of the motor plan, receiving a copy of the motor commands. This is usually implemented introducing in the system an adaptive observer (see Section 3.4.1 for an example of application of this concept to cognitive robotics). Forward models can also provide

error estimates for motor learning (Miall & Wolpert, 1996; Wolpert, 1997).

Empirical evidence suggests the existence of neural circuitry that could support both forward and inverse internal models as the result of motor learning in the cerebellum (Kawato, 1999; Miall & Wolpert, 1996). A discussion on the connectionist account and examples of models for motor control that use mappings as internal models or adaptive observers to compensate for delays is presented in Chapter 3.

The main opposition to these approaches is that there is evidence of *variable means* in tasks performance. The phenomenon that Bernstein described as ‘repetition without repetition’ means that there is always some variability in the performance of a motor task even following extensive practice (Latash, 2012). This approach to motor coordination as a top-down mapping problem, structured hierarchically and abstractly addressed by the CNS as represented in Fig. 2.10, reflects the methodology typical of cognitivism (Haugeland, 1978).

Motor Abundance

There is an alternative view that considers the degrees of freedom problem not a problem, but more of a feature of the motor system to produce efficient, but not identical, movements in a way that is evolutionary advantageous. This concept is summarised as *the principle of motor abundance*. This perspective considers the *abundance* of degrees of freedom as an asset to produce stable but flexible motor behaviours. This positive redundancy creates the condition for an adaptive modulation of the motor output so that the motor system is able to better handle secondary tasks and unexpected perturbations (Latash et al., 2007).

In the model proposed in this thesis, the degrees of freedom problem is not addressed in terms of activation of muscle groups, but in terms of how patterns of muscles can be encoded at a neural level in the spinal cord to produce the forces necessary to perform purposeful movements at the joints of a robotic interface. The general perspective is the one assumed by *embodied cognition*, namely that motor control is distributed. The object of this thesis is adding another layer to the existing cortical models, representing the role of the spinal cord in motor control.

Internal representations of the motor systems and of patterns of activation might significantly contribute to motor planning. It can be speculated that the development of purposeful movements could emerge from a combination of these learned internal models with online sensory-motor integration at a cortical level. The possibility to reunite these two perspectives is further discussed in Chapter 3, where embodied cognition is discussed in more detail.

2.3.1 Muscles Synergies

A perspective based on the idea of motor abundance that explains purposeful movement formation lays its foundation on the concept of synergy. A muscle synergy is defined as a group of muscles whose co-activation allows for a reduction in the degrees of freedom of the system in function of the performed task, in a way that proves to be both stable and flexible (Giszter, 2015; Latash et al., 2007). The concept of muscle synergy stems from studies on the spinal circuitry in deafferented animals, showing that consistent patterns of muscle activation of the limbs arise when stimulating the spinal cord directly.

The first studies on patterns of muscle activation used spinal microstimulation in spinalised frog. If the brainstem and the spinal cord are surgically separated in the frog, it is found that residual motor skills are significantly present and coordinated synergic movements are still possible (Bizzi et al., 1991; Giszter et al., 1993).

The experimental set-up of this type of studies is shown in Fig. 2.11. Defined a workspace made of 9-16 points, reaction forces are recorded keeping fixed the ankle of the frog at each point, while stimulating through implanted electrodes in the grey matter of the spine. This measure of force spread on the workspace can be divided in two components:

$$F = F_r + F_a, \tag{2.6}$$

where F_r is the resting force, measured prior to the onset of the stimulation and due to the viscoelastic properties of the muscles of the frog; F_a , the active force, represents

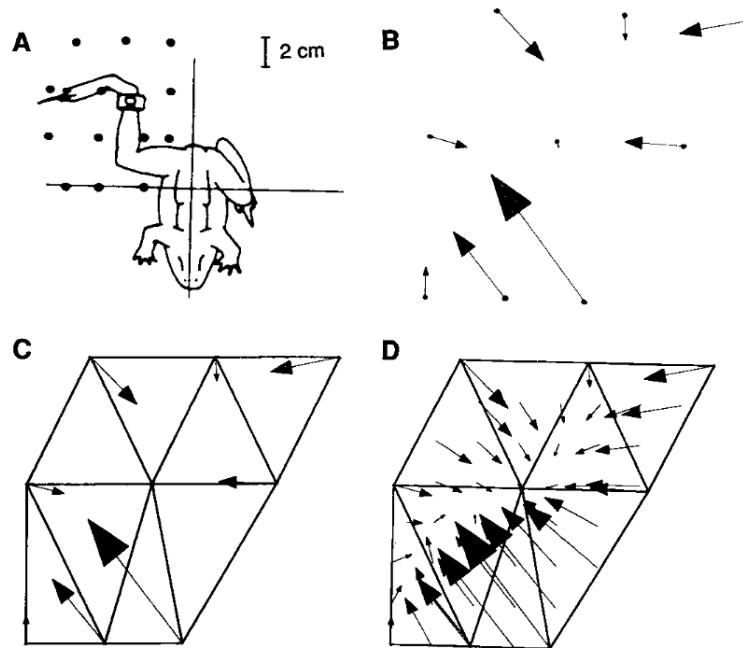


Figure 2.11: Experimental set up to evaluate the resting and active force field in the spinalised frog using micro-stimulation at the level of the spine. (A): representation of the workspace with the force recording points. (B): recorded force vectors at the workspace locations. (C): interpolation grid and recorded force vectors. (D) Interpolated field. From ‘Computations underlying the execution of movement: a biological perspective.’ by Bizzi et al. (1991)

the force elicited by muscular activation due to stimulation (Bizzi et al., 1991).

Keeping unchanged the site of stimulation, the total force field F changes across the workspace, presenting two main characteristics: convergence and a single *equilibrium point*. The equilibrium point (x_0, y_0) is the point in which both Cartesian components of the vector $F = (F_x, F_y)$ are equal to zero. In other words, it is the place towards which the limb would move if unconstrained and in which it would remain in steady state, since the total acting force null (Bizzi et al., 1991).

Subsequent studies have found that, modulating the stimulation, the force field changes over time and, as a consequence, the associate equilibrium point changes position too (Giszter et al., 1993). This sequence of positions describes a trajectory that goes from the initial resting position to a new position, corresponding to the

peak value of the stimulation, and back to the original position when stimulation ceases.

The interpretation given to these findings is that the trajectory spanned by the equilibrium point is the virtual position that the limb would reach in time if it wasn't constrained by the clamp. In Fig. 2.12 an example of the evolution of the force field during the stimulation is depicted together with the so-called *virtual trajectory*.

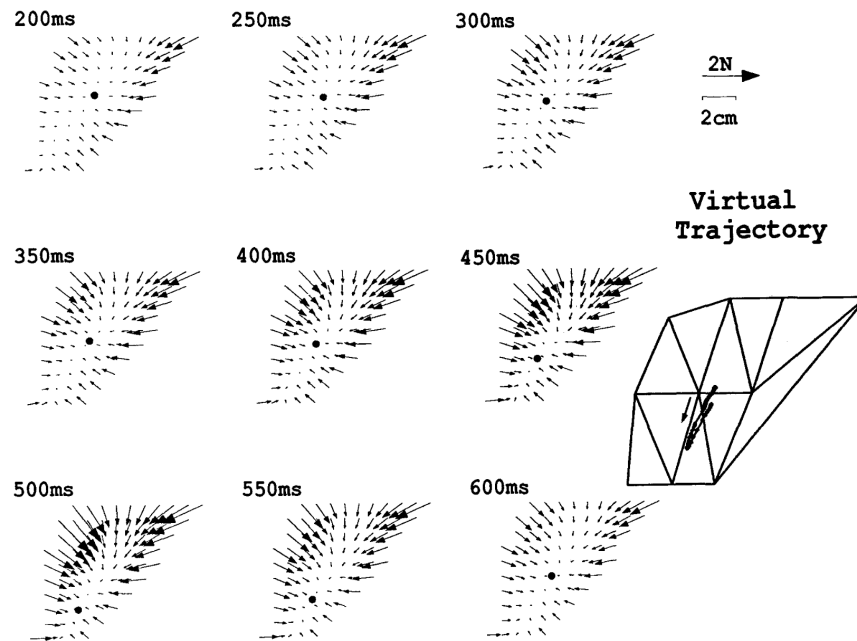


Figure 2.12: Evolution of the total force field F during increasing spinal stimulation. The equilibrium point (black dot) moves describing a trajectory in time represented in the interpolation grid on the right. From ‘Convergent force fields organized in the frog’s spinal cord.’ by Giszter et al. (1993).

Most importantly, separating the active force field from the total field, it was found that recorded force fields could be sorted in a few classes each of which originating from a portion of the spinal cord. Moreover, analysing the magnitude of the active force fields it was found that, although it changes over time, the direction of the force vectors is almost invariant and the equilibrium point is fixed (Giszter et al., 1993).

2.3.2 The Motor Primitives Summation Hypothesis

After these initial experiments on frogs, the idea that the CNS controls the redundancy of the system using a fixed combination of muscles, a *muscle synergy*, has been tested further. A growing amount of empirical evidence, including studies that use electromyographic (EMG) recordings in vertebrates together with techniques for components extraction, supports now the existence of the so-called synergies (see the review by Tresch and Jarc (2009) on the methods and by Flash and Hochner (2005) on primitives in vertebrates and invertebrates).

These findings have suggested a control strategy: suppose that efferent motor commands assign an equilibrium point, this is enough to produce a pattern of muscle activation that is selected among a group of sets stored in the spinal cord. At this point, the posture is maintained by the limb until descending signals specify another equilibrium associated with a set of muscle synergies (Giszter et al., 1993).

This approach overcomes the need to specify all the controls for the redundant system, in terms of single muscle activation. A spatial mapping of some motor patterns within the spinal cord, referred to as a *motor primitive*, is identified as the modular element from which more complex motor behaviour can be performed (Giszter, 2015).

A first model for motor control based on this idea was proposed by Mussa-Ivaldi et al. (1994), who introduced and tested *the motor summation hypothesis*. According to the authors, the resultant active force field F_{ac} , elicited by costimulation of two spinal sites 1 and 2 and measured using a set-up like the one presented in Fig. 2.11, can be modelled using the following linear relationship:

$$F_{ac}(x, y, t) \simeq s[F_{a_1}(x, y, t) + F_{a_2}(x, y, t)], \quad (2.7)$$

where $F_{a_{1,2}}$ are the measured active force fields recorded from the single stimulation points and s is a real scaling coefficient. Experiments on the frogs confirmed his hypothesis.

It was also confirmed that supraspinal modulation of spinal reflex can generate

a vast motor repertoire, selecting a combination of primitives that corresponds to the vectorial summation of associated force fields. The resultant equilibrium position of the limb during the costimulation, in fact, is found in an intermediate location between the equilibrium points of the component fields. This means that, considering for instance two linear fields $F_A(x) = s_a(x - x_A)$ and $F_B(x) = s_b(x - x_B)$, with equilibrium points x_A, x_B and s_a, s_b constants, the equilibrium point according to Eq. (2.7) is given by

$$x_E = (s_a + s_b)^{-1}(s_ax_A + s_bx_B), \quad (2.8)$$

that is the weighted sum of x_A and x_B (Mussa-Ivaldi et al., 1994).

From this simple movement formation paradigm, motor primitives have been at the core of the development of models for motor control that address the degrees of freedom problem in terms of modularity. To this purpose, they have been defined in a number of different ways. From the kinematic perspective, motor primitives are modelled in terms of bell-shaped velocity modules or segmentation units of the behaviour (*stroke* or *kinematic primitive*). From the kinetic point of view, they are described with the traditional formulation in terms of force fields or muscle time-varying patterns as presented above and used in the following. According to the underlying implementation, it is possible to define them in terms of robotic controllers (*multi-joint control units*) or neural substrate (*premotor drives*) (Flash & Hochner, 2005).

As regards the neural encoding of these elemental movements, the neural basis that could be associated to them is still an object of debate. Recent studies on spinal interneurons seem to indicate the existence of local neural circuitry that could account for spinal motor primitives (Hart & Giszter, 2010; Levine et al., 2014).

To present an example of motor summation using behavioural data, in Fig. 2.13 summation of two time-varying synergies extracted from EMG measurements in in-vivo frogs is presented (D'Avella et al., 2003). In this study, each synergy is given by the concurrent activation of three muscles (see Fig. 2.13 a). In order to generate a pattern of activation, each synergy can be scaled and translated in time (see Fig. 2.13

b). Obtained muscles profiles composing the synergy are then summed to obtain the activation pattern (see Fig. 2.13 c). A set of synergies can be used in this way to generate different patterns as resultant linear combination.

The model proposed by D’Avella et al. (2003) is able to explain most of the data on frog kicking collected from intact animals using only three time-varying synergies combined. The reduction in dimensionality of the space of all the possible synergies cannot arise simply from the constraints imposed by the task, given the intrinsic redundancy of the controlled system. As a consequence, the authors assume that the development of these patterns of muscle activation forms not just to satisfy elemental biomechanical functions, but also to be optimised with learning, leading to a greater level of generalisation. This means that the same set of synergies could be able to satisfy multiple motor tasks (D’Avella et al., 2003; Giszter & Hart, 2013).

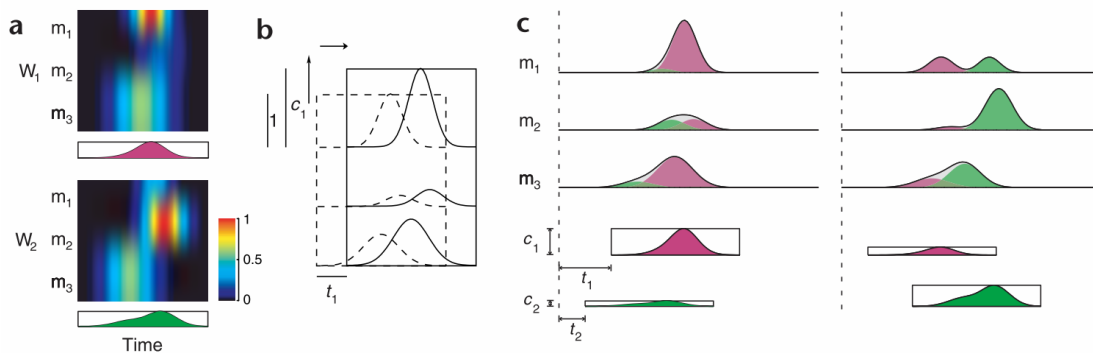


Figure 2.13: Motor summation with extracted EMG primitives. (a): representation of two synergies W_1 and W_2 . Rows: three different muscles involved in the synergy $m_{1,2,3}$ with activation encoded in colour and averaged time course across muscles represented in the box below. (b): muscles activation of W_1 scaled by constant c_1 and delayed by t_1 , dashed (full) lines represent W_1 after (before) scaling and shifting. (c): two examples of synergies summation, using modulated W_1 (magenta) and W_2 (green). $c_{1,2}$ are encoded in the width of the boxes below; $t_{1,2}$ in the position of their left corner. From ‘Combinations of muscle synergies in the construction of a natural motor behavior’ by D’Avella et al. (2003).

It has been argued that the motor summation hypothesis could be somewhat limiting the motor repertoire of the system. Nonetheless, reviewed models that

hypothesise the synergy-based modularity account for a separate motor path that can suppress, or modulate, spinal activation when necessary (i.e., whenever precision requires single muscle strategies). The physiological structure of the neuromuscular system supports this combined control strategy, with the modulation carried out by the corticospinal tract (Mussa-Ivaldi et al., 1994; Tresch & Jarc, 2009).

Another important observation is that this approach to the degrees of freedom problem could be considered in agreement with the uncontrolled manifold theory. Motor primitives could be seen as a smaller subspace of controlled variables in the space of the variables that are relevant for the task (Latash, 2012).

From an embodied perspective, some authors have suggested that synergies could actually not be responsible at all of a simplification in terms of variables to control. On the contrary, promoting the idea of motor abundance, the central nervous system could allow for a redundant representation of the system and of the environment that is capable of probabilistically anticipate the outcome of their interaction. The emergence of muscle synergies in this sense could arise as the result of reciprocal influence between the musculoskeletal system and the environment (Tresch & Jarc, 2009).

In conclusion, micro-stimulation of the premotor area of the spinal cord and more recent experiments on synergic muscle activation could account for the existence of some elemental motor representation, that is identified as a *motor primitive* (Hart & Giszter, 2010). A combination of a limited number of motor primitives can account for a greater number of movements, according to the motor primitives summation hypothesis. The activation of motor primitives is regulated and weighted by neural signals, including afferent inputs and descending motor commands (Mussa-Ivaldi et al., 1994). Both, in fact, have access to spinal premotor circuits where a certain level of integration can actually happen, as anticipated in Section 2.2.2, discussing the physiology of the spinal cord (Overduin et al., 2008). A review on the existing models for motor primitives can be found in the work by Giszter and Hart, 2013.

2.4 Conclusions

In this chapter the core themes of motor control are presented in an integrated perspective that includes physiological findings and existing hypothesis and models relative to voluntary movements and their properties.

The role of the different parts of the motor system is explored with particular attention to the motor cortex, the spinal cord, the neuromuscular junction and the development of contractile force in the muscle. Invariant properties of voluntary movements are reviewed.

This overview of the physiological system clarifies the number of controlled variables to be considered when modelling voluntary movement formation, often addressed in terms of optimisation criteria and hierarchical organisation of the motor system itself. The degrees of freedom problem, presented as the traditional motor redundancy problem, could be considered instead in terms of motor abundance, contributing to the distinctive adaptability of biological systems.

From this perspective, the concept of muscle synergy is introduced, presenting relevant bio-physiological experiments. The possibility to model a large motor repertoire using a small number of motor primitives is summarised by the hypothesis of motor primitives summation.

The proposed model for spinal motor control is largely inspired by this modularity (**Aim 1**), since the representation offered by motor primitives naturally matches the one offered by *dynamic fields*, presented as part of the embodied approach to understand motor control in Chapter 3.

Chapter 3

Neural Fields for Embodied Motor Control

3.1 Introduction

From a philosophical perspective, the cognitivist approach that characterise some of the explored theories of movement formation has its foundation in the Cartesian dualism: the dichotomy between mind and body. Cognition, being separated from the body, is given by the stream of subsequent abstractions that start with the representation of the sensory input coming *from* the environment *to* the body, ending in the brain where information elaboration takes place. This perspective lends itself to be modelled in terms of algorithms based on abstract representations (Haugeland, 1978; von Neumann, 1958).

In this perspective, the brain is portrayed similar to a computer and the study of motor control reduces to finding an algorithm that solves the redundancy problem. Motor commands are the output sent top-down, specifying activations and timing of actions. The physiology of the motor system, reviewed in the previous chapter, supports a more distributed and modular development of motor control.

In 1991, in his paper ‘Intelligence without representation’, Brooks brilliantly

points out with an allegory the limitations of *the computer brain* and the need for an integrated approach to understand complex phenomena such as cognition (Brooks, 1991):

Suppose it is the 1890s. Artificial flight is the glamor subject in science, engineering, and venture capital circles. A bunch of AF researchers are miraculously transported by a time machine to the 1980s for a few hours. They spend the whole time in the passenger cabin of a commercial passenger Boeing 747 on a medium duration flight. Returned to the 1890s they feel vigorated, knowing that AF is possible on a grand scale. They immediately set to work duplicating what they have seen. They make great progress in designing pitched seats, double pane windows, and know that if only they can figure out those weird "plastics" they will have their grail within their grasp. Meanwhile [...] They have come to agree that the project is too big to be worked on as a single entity and that they will need to become specialists in different areas.[...]On their observation flight none of the original group managed to get a glimpse of the driver's seat, but they have done some hard thinking and think they have established the major constraints on what should be there and how it should work. The pilot, as he will be called, sits in a seat above a glass floor so that he can see the ground below so he will know where to land. There are some side mirrors so he can watch behind for other approaching airplanes. His controls consist of a foot pedal to control speed (just as in these newfangled automobiles that are starting to appear), and a steering wheel to turn left and right. In addition, the wheel stem can be pushed forward and back to make the airplane go up and down. A clever arrangement of pipes measures airspeed of the airplane and displays it on a dial. What more could one want? Oh yes. There's a rather nice setup of louvers in the windows so that the driver can get fresh air without getting the full blast of the wind in his face.

A new perspective on motor control actually emerges in a number of studies in different disciplines that share a common vision: cognition is rooted in the interaction between the system that acts, the body or *agent*, and the environment, both participating actively in the experience of it.

In this chapter this perspective is introduced, leading to a description of the neural processes of motor control using models belonging to the Dynamic Field Theory (DFT), that are used to implement the neural controllers of the architecture proposed for spinal motor control (**Aim 2**).

In Section 3.2, a definition of embodiment is attempted, analysing claims that characterise this approach: modelling motor control in this perspective means finding an embodied representation for its core problems.

In Section 3.3 a number of relevant features of Dynamic Field Theory (DFT) are presented, encompassing the underlying neural processing and the qualitative construction of the Dynamic Neural Field equation. The representation of elements of cognition is introduced in terms of peaks of activation. This mathematical framework has proved ideal to model both the degree of flexibility and the robustness that go beyond the achievements of technical systems and are typical of living organisms.

In Section 3.4 the focus is on DFT principles applied to perceptual-motor integration, sequencing and timing, learning and, most importantly, solving the degrees of freedom problem in light of architectures that go towards the now trending bio-inspired robotics. This outlines the knowledge gap that the proposed model aims to fill.

3.2 Embodied Cognition

Defining embodied cognition is a challenging task, considering that the concept of *embodiment* is relatively new and that it has been developed in different fields, more as collection of perspectives that challenge traditional cognitivism than a structured discipline with own methods and goals (Shapiro, 2012).

According to cognitivism, cognition is the result of a computational process of progressive abstraction from the sensorial input. The subject receives this information passively and of this creates the first representation, then subsequent transformations (modelled by algorithms) produce some output representation. These representations can be processes, like perceiving or motor commands, or objects, like memories or perceptions. Symbolic structures, in both cases, independent from the features of the perceiver and of the environment, are the archetypes of cognition (Shapiro, 2012). A representation of this type of approach is illustrated in Fig. 3.1.

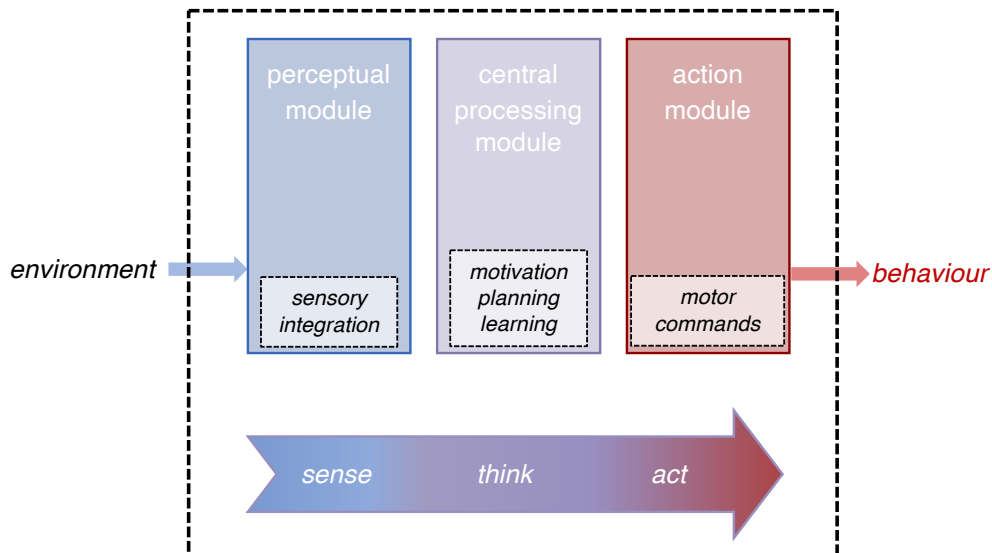


Figure 3.1: Cognition, according to a cognitivist perspective, can be represented as a sequence of abstraction from sensory input coming from the environment (*sense*), to a perceptual representation followed by information processing that gives motor plans (*think*) performed by the body to produce the behaviour (*act*).

In his review *Embodied Cognition*, Shapiro considers the first instance relative to embodied cognition ascribable to Gibson's work on visual perception and the school of *ecological psychology*. The experience of cognition, in this framework, is described in terms of the *affordances* that available information within the environment can specify to an *active agent*. Two main concepts emerge:

- the agent is *active*, meaning that it has a body able to interact with the environment;
- the environment provides affordances, meaning intuitive ways to interact with it, that are peculiar to the body of the agent and its perceptual and motor availability.

In other words, the focus moves from a passive sensing of the environment by the agent, to the emergence of perception as result of the interaction between agent and environment (Shapiro, 2012).

The Embodied Cognition Manifesto

The embodied perspective appears in a number of studies in different disciplines. Along the lines of 'Six views of embodied cognition' by M. Wilson (2002), a list of claims that emerges from these studies can help defining the core concepts of embodiment. These can be summed up as follows (M. Wilson, 2002):

- cognition is situated, perception and action are intrinsically linked to cognition that cannot take place if not immersed into an environment;
- cognition is for action, since the primary function of the mind is to produce appropriate motor behaviour, cognitive processes cannot be understood apart from their ultimate goal;
- offline cognition is body based, since cognition has developed for action, when decoupled from the environment mental activity uses the same mechanisms available for sensory-motor integration and motor control;

- cognition is time-pressured and so mental processes must take into account interaction with the environment in the appropriate time frame;
- cognitive work is off-loaded onto the environment, meaning that the environment is an instrument to compensate for limited processing abilities of the brain;
- the environment is part of the cognitive system, in the sense that it is impossible to draw a line between the mind and the environment given their continuous exchange of information.

By definition, situatedness is the theoretical approach regarding the mind as enmeshed with environmental, social and cultural factors from the functional and ontological perspective. According to this approach, there is no dualism between mind and world and the idea that mind is an interior separated entity that senses passively and produces outputs after representational evaluations is rejected (Costello, 2014). Since cognition arises from the interaction through the body with the environment, the properties of the body shape the products of cognition, defining a new methodological perspective on how cognition should be modelled (Shapiro, 2012; M. Wilson, 2002).

Intuitively, it's clear that cognitive processes have evolved, at least at the beginning, to guarantee the survival of the agent in the external environment. To cite Wolpert: 'The reason for brains is not think or feel but control movement' (Wolpert, 2011). It is sufficient to have a look at the evolution of intelligence in biological species to understand that most of the evolutionary time was spent developing the ability to move and survive within the environment. From this perspective it is easy to hypothesise that the basis for the development of cognition as it is known, inclusive of problem solving skills, language, expert knowledge and so on, has the same substrate (Brooks, 1991).

The claim that cognition has developed to address motor goals could be questioned considering that the same evolution has allowed for cognitive processes that are decoupled from an immediate interaction with the environment and happen *off-line*, for example planning and remembering (M. Wilson, 2002). Nonetheless, the fact

that cognition has developed in a motor-oriented fashion seems to be confirmed by experimental and cellular studies too.

Studies on visual perception, for example, have shown that some visual inputs can have a priming effect on motor areas without any ongoing motor task. When the agent is not directly interacting with the environment, cognition can be thought as ‘for action’ in a more sophisticated manner. It can be advantageous to memorise objects properties (visual input) in terms of affordances (motor pre-activation) so as to be able to recall them, if necessary, at some point in the future (M. Wilson, 2002).

The discovery of *mirror neurons* has contributed to strengthen the claim that cognition has a sensory-motor substrate (Shapiro, 2012). Mirror neurons are types of neurons discovered in the premotor cortex of the monkey that have bimodal discharge pattern: they result activated when actions are performed by the individual and when the individual observes the same actions performed by another individual (Rizzolatti, 2005).

The functional role of such neurons is still being debated but they have been linked with action and intention understanding, imitative behaviours, development of empathy and language among individuals. It has been pointed out that the function of mirror neurons might be common to all these processes. This function could be creating the neural substrate to connect motor and sensory system diffusely in the brain, collecting and distributing signals that generate internal simulations of motor behaviour, based on patterns of connectivity that can be learned (Damasio, 2008).

In the same way, cognition involved in more abstract tasks, such as mental imagery or episodic memory, although happening off-line, could use sensory-motor pathways to build such representations. These could emerge from internal simulations that use the same pathways as the one used to interact with the environment, this time with the purpose to perform abstract reasoning. Interestingly, models for mental concept formation, use the idea of a *perceptual symbol*, that is the re-activation of sensory-motor areas that were associated during the perceptual experience, suggesting that concepts could emerge from simulations involving cognitive primitives that have a sensory-motor foundation (Barsalou, 1999).

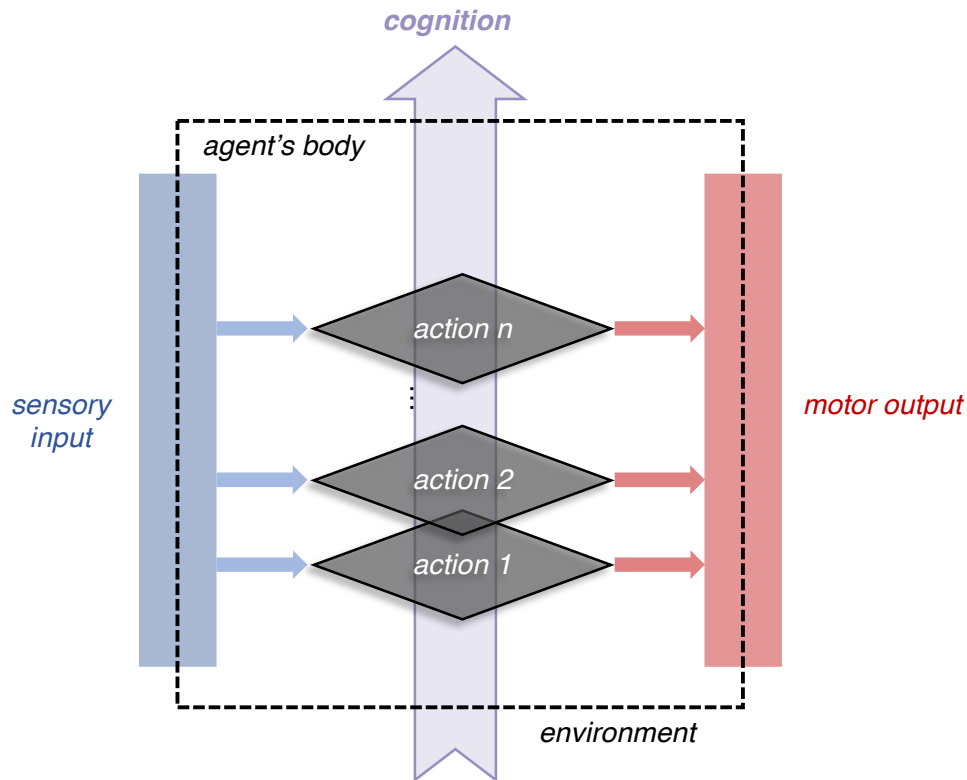


Figure 3.2: Representation of an embodied approach to robotics. Cognition emerges as the superimposition of simple embodied *actions*, modules that perform task-specific sensory-motor integration, accounting for the perceptual and motor features of the agent and their interaction with the environment. Illustration inspired by the work by Brooks (1991).

Situatedness in time of cognition has been one of the major challenges in traditional artificial intelligence and robotics. A hierarchical approach can limit the performance in real environment since the computation of internal models and the one-way path to subsequent abstractions lack the immediate sensory enmeshment that grants humans to react promptly to changes and unexpectedness. The focus on real-time responsiveness has led to the development of ‘behaviour-based robotics’ and models that use overlapping layers to build cognitive depth, each of which has sensory-motor instances as the one represented in Fig. 3.2 (Brooks, 1991; M. Wilson, 2002).

Brook’s *Creatures* are a radical example of architectures that do not require algorithms acting on abstract representation. These are based on the superimposition

of horizontal architectures that represent single activities (i.e., motor tasks) each of which has direct connections to sensing and action. Layers can be interconnected with each other, but their activity keeps running in parallel. For example: one activity of the creature is to avoid obstacles, a second layer is added to make the creature explore the environment reaching distant visible spots. Both layers have access to the sensory information and the second layer passes motor commands to the first that is going to divert its trajectory whenever a new obstacle is encountered without being aware of the goal of the second. In the same way, the second is not aware of the presence of obstacles. The system, in fact, works without some shared representation of goals or objects to avoid (Brooks, 1991).

Although simple behaviours could be explained in terms of small sensory-motor circuits superimposed (spinal reflexes, for instance), explaining human cognition as a whole might not be achievable by simply superimposing a layer for each *activity* (Brooks, 1991; Shapiro, 2012).

The active role exerted by the environment is the concept at the core of the *extended cognition*, according to which the environment is actually part of the cognitive system itself (Shapiro, 2012). The environment might contribute to higher cognitive processes storing information. It would be not necessary in this case to load the working memory of the system with representations of all the features of the environment because they are simply provided online by sensory-motor integration (Brooks, 1991, ‘the World is its own model’).

To conclude, although some of the claims could be oversimplifying the variety of processes that are grouped under the term *cognition*, the new perspective offered by embodied cognition could help improve our understanding of motor control and guide the development of better robotics that are more physiologically inspired. The future development of this multi-disciplinary account could hold space to integrate some aspects of the more traditional approach to cognition, in order to create a unified theory that is able to account for its higher and more abstract expressions (Shapiro, 2012).

3.3 Dynamic Field Theory

As Cognitive Sciences have regarded the mind as a processor that elaborates information abstractly, in the same way artificial intelligence has shared the same approach, developing in terms of models for symbolic processing. The claims of embodied cognition affected this field bringing the attention to sensory-motor processing rather than to centralised computation of inputs and outputs (M. Wilson, 2002).

Considering mind, body and environment as coupled dynamical systems, mathematical tools relative to such systems and based on coupled differential equations have found application in Cognitive Sciences. The Dynamic Field Theory (DFT) has provided a well-suited theoretical formalism for embodiment, representing sensory-motor integration and higher cognitive functions in a way that links directly to the principles underlying neural transmission (Schöner, 2007).

The DFT framework has been widely used to model perceptual systems according to the embodied cognition principles discussed above. Applications include models for cognitive development, motor planning, autonomous robotic control, models for visuospatial cognition and visual working memory (Spencer et al., 2009).

Neural dynamics are used to model units of cognition that are coupled in real-time to sensory-motor systems and are able to integrate processes over different timescales and to show behavioural flexibility. The computational element that makes possible the emergence of cognitive functions from models for neural dynamics is the Dynamic Neural Field (DNF) (Schöner, 2007). This is a mathematical structure spanning over two or more dimensions that is able to retain stable states of activation.

The stability of attractor dynamics is the key to address two crucial problems encountered when cognitive processes are modelled: the problem of *jumpy cognition* and the problem of *representation*. According to the embodied account, cognition emerges from continuous sensorimotor integration. While the position assumed by the hand in a reaching task develops continuously through space and time, motor plans in contrast can jump from one to another according to the requirements of the current task. An example of jumpy cognition could be when a sudden shift in the

target position forces the agent to change direction. Another one could be the shift from one thought to the other. When modelling cognition, it must be considered that continuous sensorimotor processes coexist with cognitive representations that can jump from one state to another, but still remaining embodied (Spencer et al., 2009).

This leads to the second problem, that is finding the appropriate representation to account for jumpy cognition and continuous sensory-motor processes. In other words, the abstract, symbolic representation of elements of cognition at the core of traditional artificial intelligence must be replaced with a different modality that is capable of interfacing cognitive systems with continuous sensorimotor processing. An example of this could be represented by the process of recalling the position of an object while the position of the observer is changing over time. Elements of cognition can be encoded by prototypes (e.g., left, right, top, bottom), whereas the position of the agent and the sensory afference develops continuously, resulting in jumpy cognitive representation. Movements of the agent cause the target to be first at a location labelled by ‘top left’, for instance, then ‘bottom right’ (Spencer et al., 2009).

The core concepts of DFT that satisfy both these aspects, giving an embodied representation of cognition anchored in sensorimotor processing, can be summed up as follows:

- a stable attractor, or peak of activation, is the representation of an *emergent behaviour*;
- bifurcations, or instabilities, of the system dynamics model behavioural flexibility;
- knowledge from previous experience can be learned and facilitate the formation of stable attractors.

Stable states in the dynamic system guarantee appropriate cognitive task representations that take into account the variation (and availability) of sensory input, providing successful motor output. At the same time, sensory or motivational input can move the system beyond a bifurcation point. Loss of stability allows for new

behaviours to emerge in the form of a new stable attractor. The possibility to retain information in time is fundamental for learning and adaptation.

Attractor dynamics can account for the elements of motor control outlined in Chapter 2, as regards both representation of sensory-motor features and appropriate control. An example of such dynamic is presented in Fig. 3.3, where a simple selection behaviour from a bimodal input is implemented with a two-dimensional neural field. The following section addresses how these features emerge from models for neural transmission and how this theoretical approach can model not just selection but several elements of cognition.

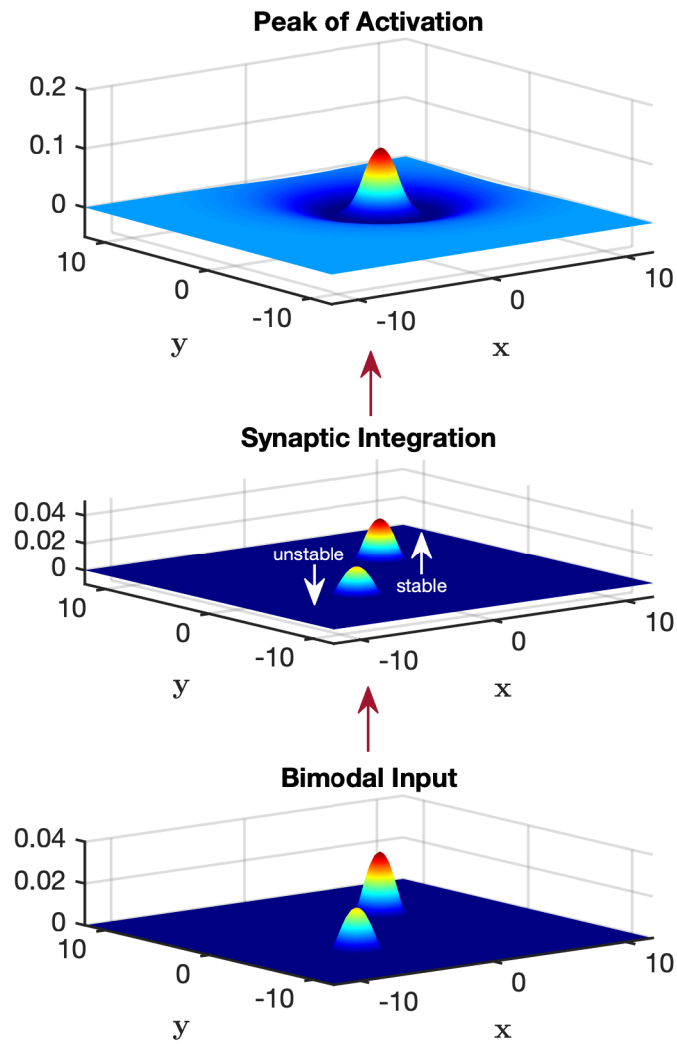


Figure 3.3: Dynamic neural field selecting between two inputs. From the bottom: bimodal input to the field; first step of simulation shows one of the inputs growing to a stable peak and one destabilising to the resting state; the selected input persists in a self-sustained activation that is able to retain information.

3.3.1 Introduction to Neural Field Dynamics

A multi-scale approach has been adopted through the years in the field of Computational Neuroscience due to the variety of neural activity features that can be studied using mathematical models: from the biochemical properties of the neuron and their role in axonal propagation, to complex behaviour emerging from networks of millions of interconnected neural cells. Models based on neural networks or more realistic descriptions of neurons and their connections have proved great to understand how neural transmission operates but limited capability to explain behaviours (Spencer et al., 2009).

Historically, the origin of dynamic neural fields can be found in the first models for mass of cells with neuron-like properties with random connection. Beurle in 1956, considering this ensemble of neurons, studied how simple forms of activity such as wave propagation, can emerge without interconnections between elements to be specified in advance (Beurle, 1956). Subsequently, Wilson and Cowan, studying the conductive properties of the axon, introduced inhibitory and excitatory populations of neurons and modelled neuron's refractory period (H. R. Wilson & Cowan, 1972).

Although it might present variations among layers, as shown in Fig. 3.4, the structure of cortical pyramidal neurons is made by the following parts:

- *the soma*, that is the cell body containing the nucleus,
- *the dendritic tree* (or basal dendrites), that is a tree-like structure conveying the input from other neurons into the soma;
- *the axon*, that is an elongated branch presenting ramifications (apical dendrites) emanating from the soma and conveying the electrical output of the neuron, *the action potential*.

Synapses are the place in which electrical activity from one neuron, *the presynaptic neuron*, is transmitted to the dendritic tree of the *postsynaptic neuron*. This electrical flow into the postsynaptic neuron is summed throughout the dendritic tree and, if this sum is enough to cross its intrinsic threshold, then a new action potential is

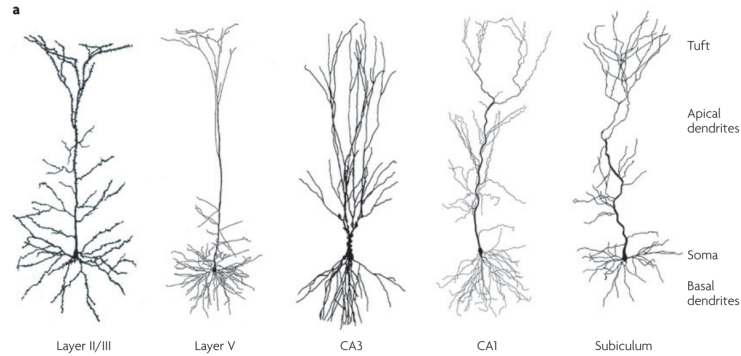


Figure 3.4: The structure of pyramidal neurons in different cortical layers. From ‘Pyramidal neurons: Dendritic structure and synaptic integration’ by Spruston (2008).

triggered. Integration of synaptic input is at the heart of the computational function of pyramidal neurons (Spruston, 2008).

As introduced in Chapter 2, studies on the firing patterns of neurons in the motor cortex during pointing tasks have highlighted that the direction of movement can be modelled using a population vector (Georgopoulos, 1997).

Each neuron can be associated to a tuning curve where the highest firing rate is reached for the preferred direction and the discharge rate decreases continuously moving away from it. Further experiments confirmed that resultant activation of a population of neurons can actually encode relevant sensory-motor features (Spencer et al., 2009).

Intuitively, this *field* of sensitivity for the single neuron and the concept of population encoding leads to the concept of *neural field* as a model to represent not the single cell firing but the tuning curve of the population it belongs to, spanning across the possible values of some salient feature with continuity (Sandamirskaya et al., 2013).

A neural field can be defined by a nonlinear differential equation that includes the following terms:

$$\tau \dot{u}(x, t) = -u(x, t) + \text{synaptic interaction} + \text{input} + \text{resting level}, \quad (3.1)$$

in which $u(x, t)$ represents the dynamic of a mean field variable varying with time constant τ . The other terms on the right-hand side are the synaptic input coming from the rest of the field with appropriate synaptic weights, an external input (e.g., sensory input) and the resting level that, like the resting potential of neural cells, is the value to which the field relaxes in absence of sustained activation (Schöner, 2007).

A formal simplified model of the type of Eq. (3.1) can be derived considering the synaptic current in conductance based model of the structure of the neuron (Bressloff, 2012). In a network composed by N coupled neurons with membrane potential $V_i(t)$ and synaptic input $u_i(t)$, the membrane potential varies according to the equation:

$$C \frac{dV_i}{dt} = -I_{con,i}(V_i, \dots) + u_i(t), \quad i = 1, \dots, N \quad (3.2)$$

with the generic ionic current $I_{con,i}$ defined as a function of the conductance and the reversal potential of the ionic species. Assigning the index j to the presynaptic neuron and i to the postsynaptic one, the firing times of the former can be expressed as $T_j^m, m \in \mathbb{Z}$, defined as the instants in which membrane potential $V_j(t)$ crosses a threshold potential V_h :

$$T_j^m = \inf\{t, t > T_j^{(m-1)} | V_j(t) = V_h, V_j'(t) > 0\}$$

where $V_j' = dV_j/dt$.

The net synaptic current entering the i -th neuron is given by the sum of the presynaptic action potentials, temporally filtered by the dendritic tree of the postsynaptic neuron. This processing can be expressed using a function $\Phi_{ij}(t)$ so that the current assumes the form $\sum_m \Phi_{ij}(t - T_j^m)$ (Bressloff, 2012). If linear summation is assumed for the system, $u_i(t)$ can be written as follows

$$u_i(t) = \sum_{j=1}^N \sum_m \Phi_{ij}(t - T_j^m) \quad (3.3)$$

Using the properties of the Dirac function, and writing the output spike train of the

j -th neuron as

$$a_j(t) = \sum_{m \in \mathbb{Z}} \delta(t - T_j^m),$$

the equation of the input current can be written as:

$$u_i(t) = \sum_{j=1}^N \int_{-\infty}^t \Phi_{ij}(t - t') a_j(t') dt'. \quad (3.4)$$

Considering this network of spiking neurons, it is possible to partition it in homogeneous populations. In each population neurons are considered as firing asynchronously. It follows that the synaptic input $u_i(t)$ represents the mean field current, that is the resultant short term temporal averaging. The output spike train can be replaced by an instantaneous firing rate function $f(u_j(t))$ (Bressloff, 2012). Equation (3.4) becomes:

$$u_i(t) = \int_{-\infty}^t \sum_{j=1}^N \Phi_{ij} f(u_j(t')) dt'. \quad (3.5)$$

Assuming that the population of neurons is distributed along one dimension with spacing d , that synapses between the n -th and m -th population only depend on the discrete location of the population, and taking the limit for $d \rightarrow 0$, it is possible to derive the following integral representation for a continuous state variable from Eq. (3.5) (Bressloff, 2012):

$$u(x, t) = \int_{-\infty}^{\infty} \int_{-\infty}^t \Phi(x, x', t - t') f(u(x', t')) dt' dx'. \quad (3.6)$$

In Eq. (3.6), the term on the right-hand side represents the synaptic filtering. The function Φ takes into account the distribution in space of the dendritic tree. The function f models the threshold characteristic of neurons, allowing only supra-threshold contribution to be considered. Since most neurons do not fire below some threshold h and fire up to a maximum rate limited by the refractory period, typically this function is assumed to be sigmoidal:

$$f(u(x, t)) = \frac{1}{1 + e^{-\beta(u(x, t) - h)}}, \quad (3.7)$$

where β models the steepness.

For analytical convenience, in DFT the output function is usually modelled with a piecewise linear approximation (Coombes & Schmidt, 2010) or, considering $\beta \rightarrow \infty$, with the Heaviside function (see Methods, Chapter 4). Sigmoidal and Heaviside synaptic filtering functions are plotted in Fig. 3.5.

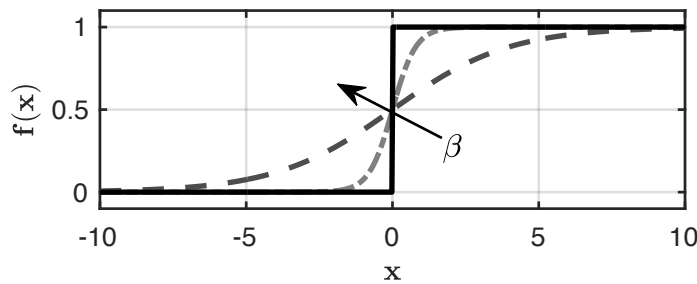


Figure 3.5: Example of nonlinear threshold functions.

The integral kernel can be conveniently decomposed in a temporal kernel, identical for pre- and postsynaptic neurons, and a weighting function w that is usually referred to as *the synaptic footprint* dependent on the position on the field:

$$\Phi(x, x', t) = w(x, x')\Phi(t) \quad \Phi(t) = e^{-t/\tau}H(t). \quad (3.8)$$

The mathematical formulation of neural fields, as it is used in Dynamic Field Theory, builds from the analysis carried out by Amari on pattern formation in continuous models for neural activity (Amari, 1977). Also known as the Amari equation, the differential form of Eq. (3.6) can be written as:

$$\tau \dot{u}(x, t) = -u(x, t) + \int_{-\infty}^{\infty} w(x, x')f(u(x', t))dx' + S(x, t) + h_{rest}, \quad (3.9)$$

where the second term on the right-hand side represents the synaptic interaction of Eq. (3.1). The external input is $S(x, t)$ and h_{rest} is the resting potential. Detailed derivation of this formulation and references for the assumptions made can be found in the work by Bressloff (2012).

Within this framework synaptic depression, dendritic filtering, axonal propagation delays and adaptive threshold dynamics can be modelled. The neural field in Eq. (3.9) supports a number of patterns and localised solution. Besides being the constitutive element of Dynamic Field Theory, whose application are explored in the following, neural fields have been used to model a variety of neurobiological phenomena involving cortical activity (Coombes et al., 2014; Liley et al., 1999, for instance), wave propagation in cortical slices (Bressloff et al., 2003) and EEG rhythms (Bojak et al., 2004).

In the analysis carried out by Amari, the synaptic footprint models the so-called *lateral inhibition*, that is based on a simplified model of the cortex that represents the connection within the field as excitatory in the short range and inhibitory on the long range (Pinto & Ermentrout, 2001). This representation of synaptic connections is usually modelled as dependant on the Euclidean distance between positions on the neural field so that $w(x, x') = w(|x - x'|)$.

The typical kernel used can be written as a function of two couples of parameters modelling strength ($A_{ex,in}$) and range ($\sigma_{ex,in}$) of excitatory and inhibitory connectivity:

$$w(x - x') = A_{ex}e^{-\frac{(x-x')^2}{2\sigma_{ex}^2}} - A_{in}e^{-\frac{(x-x')^2}{2\sigma_{in}^2}}. \quad (3.10)$$

A representation of this kernel, which is commonly referred to as Mexican hat function, is given in Fig. 3.6.

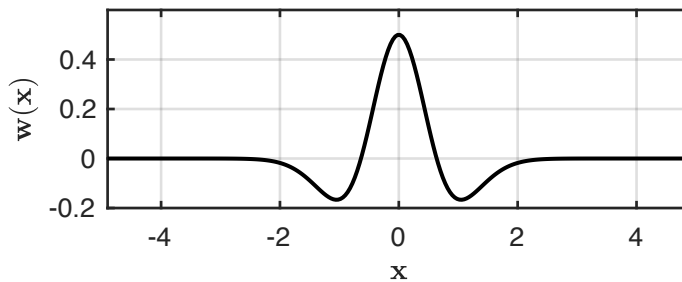


Figure 3.6: Example of Mexican Hat function.

This distribution is convenient for the representation of cognitive functions since a kernel shaped as such allows for the explicit construction of localised solutions

and the study of their stability (Amari, 1977). At the same time, a continuous field variable allows for the study of stability and bifurcations of relevant solutions using traditional methods for nonlinear systems (Coombes & Owen, 2004, see Chapter 4).

3.3.2 From Peaks of Activation to Cognition

The fundamental concept behind Dynamic Field Theory (DFT) is that the representation of basic elements of cognition, that are also called *elemental behaviours* (EB), corresponds to stable peaks of activation on a Dynamic Neural Field (DNF) (Sandamirskaya, 2013).

The mathematical formalism of DNF and the study of stability is presented in detail in Chapter 4. Consider here instead the DNF qualitatively, as a variable describing the activation of a neural population $u(x, t)$ over the dimension x following the dynamic described by Eq. (3.9) with a resting level h_{rest} representing the quiescent state of the field and some external input to drive it $S(x, t)$.

It is intuitive from the descriptive formulation in Eq. (3.1) that in absence of synaptic interaction the attractor solution, $u(x, t) = \text{resting level} + \text{input}$, would only track the input. As shown in the example in Fig. 3.3, it is the synaptic interaction that stabilises local patterns of activation. The synaptic kernel of the type defined in Eq. (3.10) allows for sustained peaks of activation to form (Amari, 1977; Spencer et al., 2009).

The distribution of synaptic weights modelling lateral inhibition, together with the presence of a nonlinear output function, gives the characteristic threshold behaviour making sure that only the parts of the field that are sufficiently active (i.e., where input $S(x, t)$ is sufficiently strong) can generate sustained activity (Schöner, 2007).

As anticipated, self-stabilised peaks guarantee stable representation of sensory motor information, filtering noise and unwanted perturbations. They can also track gradual changes in the input or enter a self-sustained state retaining a certain representation in time suitable to model working memory processes. On the other hand, instabilities determine the emergence flexibility. Trespassing critical input

values (*bifurcation points*) can alter the dynamic of the system that will relax into a new attractor state or to the inactive state (Spencer et al., 2009).

It is possible to identify four types of instability, supported by the Amari equation, that constitute the elemental instances of cognition in the dynamic field framework (Sandamirskaya, 2013; Schöner, 2007):

- *the detection instability*, whenever the DNF switches from a quiescent state to a retained and self-stabilised activation;
- *the selection instability*, when the input to the DNF drives the field above threshold at several locations and lateral inhibition allows self-stabilised activation at a single preferred one, selected among the others;
- *the working memory instability*, when sufficiently strong lateral inhibition allows the field to retain a stable self-sustaining peak of activation that persists even after the input has been removed and that requires an external inhibiting input to bring the field back to the resting state;
- *the reverse detection instability* or *forgetting instability*, when a peak of activation ceases to exist and the field goes back to a quiescent state due to an external inhibitory input or a decrease in an external excitatory input.

Figure 3.7 gives a visual representation of the dynamics listed above.

Triggering appropriate instabilities makes DNF architectures capable of flexibility and adaptability. The type of peak solutions that can emerge depends not only on the input that the field receives, but also on the balance of excitation and inhibition typical of the synaptic footprint, by the resting level of the neural field and by the value of the threshold of the nonlinear function (Amari, 1977; Spencer et al., 2009).

Characterisation of DNF models and instability selection methods that were used to design the architecture in the proposed model are presented in detail in Section 4.2 and 4.3. In the following section, the core problems of motor control presented in Chapter 2 are explored using the principles of DFT.

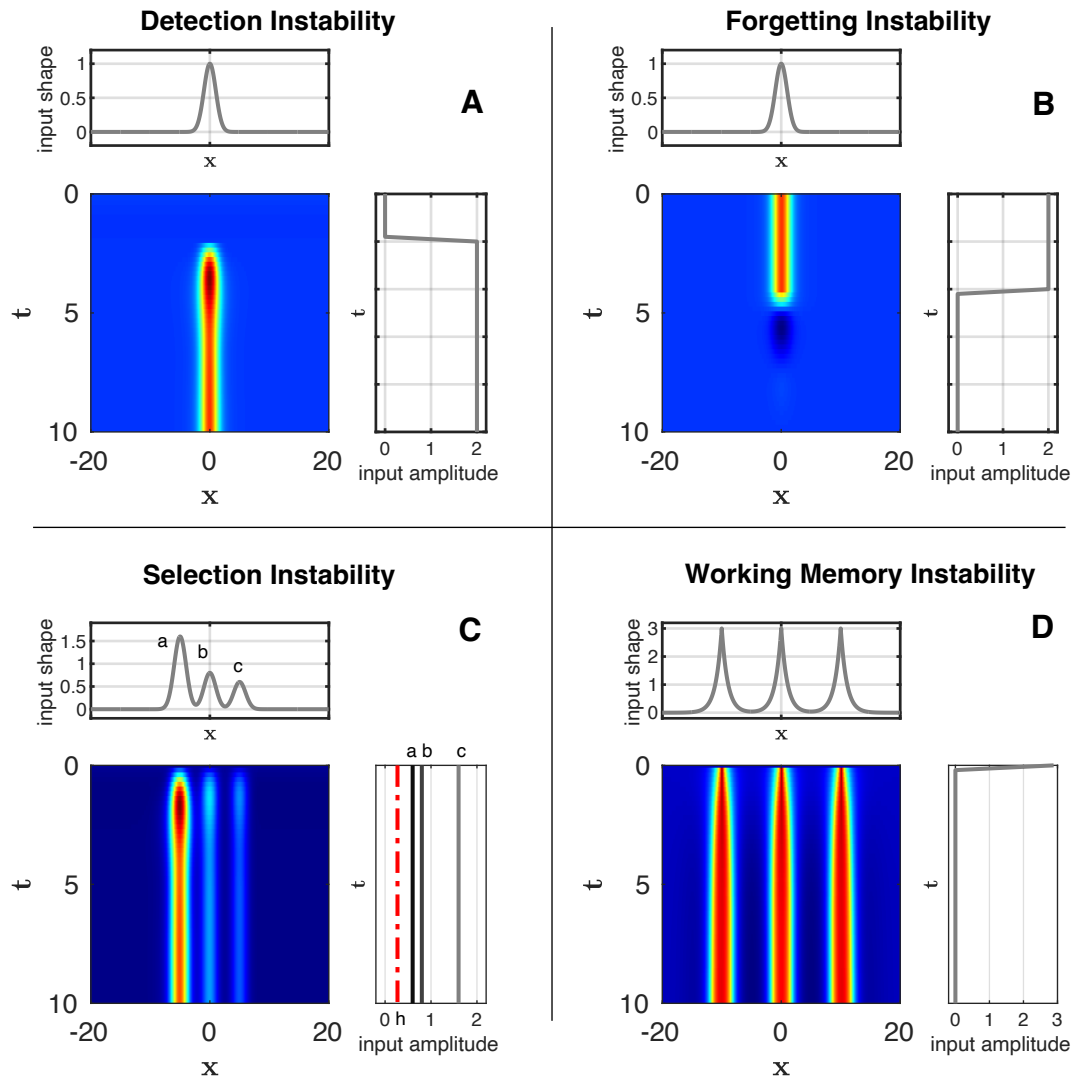


Figure 3.7: Elemental behaviours in DFT. 2D plots represent the evolution in time of a one-dimensional neural field $u(x)$, together with shape and amplitude of the input during simulation. Colormap shows activation above threshold in red and resting level in dark blue. **(A)**: the detection instability. **(B)**: the reverse detection instability. **(C)**: the selection instability (note that inputs a, b, c are all above the threshold h). **(D)**: the working memory instability.

3.4 Sensory-Motor Coupling, Autonomy and Learning

The dimensions spanned by the Dynamic Neural Fields (DNF) can be associated with features of perception or movement and encode goals and intentions. The corresponding level of activation specifies the presence of information relative to the features that the field represents.

The emergence of stable peaks not only represents the emergence of the elemental behaviour (EB), but it can also lead to other detection instabilities in coupled fields. Connecting dynamic fields with each other, in fact, allows for the development of architectures in which elemental behaviour can influence each other. It is possible to couple neural fields of different dimension, create mappings of sensory information onto motor features and develop autonomous motor plans and learning strategies (Sandamirskaya et al., 2013).

DNF architectures can be used to guide *embodied agents* that are system that interact physically or virtually with the environment. An embodied agent needs to solve the problem relative to the multimodal representation of a number of parameters affecting its behaviour in terms of both sensory and motor variables. In other words, integration of sensory input to motor commands and, ultimately, the degrees of freedom problem linked to a specific motor task must be solved.

Sensory-Motor Coupling

The representation of salient sensory-motor features can be achieved using multi-dimensional DNFs that are responsive to several behavioural parameters. Consider a two-dimensional neural field representing two features of a target objects, namely *hue* and *location*. Peaks of activation can represent the elaboration of visual stimuli leading to target detection that can subsequently trigger a motor response on coupled fields (Sandamirskaya, 2013).

In the representation of the field in Fig. 3.8, a neural field spanning the colour-

position space receives visual input from some visual sensor. Every object in the visual field causes a small peak of activation that is sub-threshold, in the sense that alone it does not allow a self-sustained peak to emerge.

Specification of the target colour can pre-shape the field, creating a ridge of activation corresponding to the desired target colour. The pre-shape facilitates the emergence of a sustained peak corresponding to the object of the desired colour. This supra-threshold activation is the emergence of the EB, namely a target detection. In fact, along the other dimension of the field is univocally specified the position of the target. This detection instability can then trigger a motor response appropriate for the task (Sandamirskaya et al., 2013).

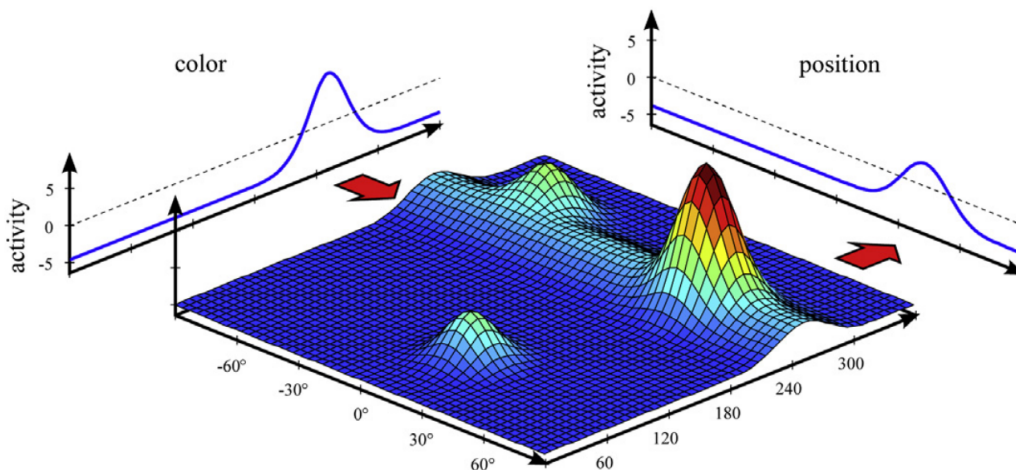


Figure 3.8: Example of target detection using a two-dimensional neural field mapping colour and position. From ‘Using Dynamic Field Theory to extend the embodiment stance toward higher cognition’ by Sandamirskaya et al. (2013).

A localised bump solution as the one shown in Fig. 3.8 represents elementary cognitive functions (in the example, the emergence of the attractor *answers* a question of the type ‘where is the blue object?’), creating symbolical and categorical representation from low level sensory-motor inputs.

Sensory-motor representations or instances can translate into appropriate motor activations. Coupling between fields allows not only for mapping of relevant features

but also for perceptual representations and working memory (Spencer et al., 2009).

DNFs with different dimension can interact with each other by means of a coupling matrix, also referred to as *mapping function*. The general equation of two coupled fields is simply:

$$\begin{aligned}\tau\dot{u}_1(x, t) &= -u_1(x, t) + \int f(u_1(x', t))w(x - x')dx' \\ &\quad + S_1(x, t) + h_{rest}, \\ \tau\dot{u}_2(y, t) &= -u_2(y, t) + \int f(u_2(y', t))w(y - y')dy' \\ &\quad + W_c(x, y)f(u_1(x, t)) \\ &\quad + S_2(y, t) + h_{rest},\end{aligned}\tag{3.11}$$

where u_1 and u_2 are two neural fields defined over two feature spaces x and y that can have different dimensionality. $W_c(x, y)$ is a function that maps the dimensions of x onto the dimension of y (Sandamirskaya, 2013). S_1 and S_2 are external inputs, w is the synaptic footprint and h_{rest} is the resting potential.

The position of the activity peak on the DNF carries the information relative to motor features that one wants to map onto a control variable for the motor dynamics of an agent (e.g., position, velocity or force of the end effector). This is usually computed in DFT using a structure called *neural node*, that is defined as follows:

$$\tau\dot{u}_\phi(t) = -u_\phi \int f(u(x, t))dx + \int \lambda(x)f(u(x, t))dx,\tag{3.12}$$

where $u(x, t)$ is a DNF representing possible values of the motor variable and u_ϕ is the input to the part of the system that performs motor tasks, i.e. *the behaving agent* (Sandamirskaya, 2013). A typical choice is $\lambda(x) = cx$, but this term can be subject to learning. An interpretation of neural nodes from a physiological perspective is proposed in Chapter 5 and discussed in Chapter 6, in light of the role that nodes play in the proposed architecture for spinal motor control.

Autonomy

Providing appropriate timing for actions is part of the tasks for which motor control is responsible (Rosenbaum, 2010). In this sense, development of systems that encode the time pressured feature of cognition means giving to the simulated sensory-motor process autonomy. This characteristic contributes to flexibility of behaviours since the duration of action is typically a consequence of the motor plan development and not assumed a priori. Duration of movements might also change in response to unannounced disturbances or more compelling inputs. Finally, plans that require sequences of movements require also that the system autonomously detects the end of one task to begin the next.

In the Dynamic Field Theory (DFT), some proposed models for autonomy consider a coupled representation in terms of attractor-dynamics representing *intentionality* and a *condition of satisfaction* (Sandamirskaya et al., 2013).

The first encodes one (or several) possible intentions of the agent, that could be motor or perceptual, and drives the motor system accordingly towards the goal within the environment. The second encodes the condition that must be satisfied to consider the task completed. When this condition is met the loop is closed by the suppression of the peak representing the intention. A model for this process can be written as follows (Rudolph et al., 2015; Sandamirskaya, 2013):

$$\begin{aligned}
 \tau \dot{u}_{int}(x, t) &= -u_{int}(x, t) + \int f(u_{int}(x', t))w(x - x')dx' \\
 &\quad - c_1 \int f(u_{CoS}(y, t))dy + S_1(x, t) + h_{rest}, \\
 \tau \dot{u}_{CoS}(y, t) &= -u_{CoS}(y, t) + \int f(u_{CoS}(y', t))w(y - y')dy' \\
 &\quad + c_2 W_c(x, y) f(u_{int}(x, t)) + S_2(y, t) + h_{rest},
 \end{aligned}
 \tag{3.13}$$

where u_{int} represent the intention DNF, u_{CoS} represents the Condition of Satisfaction (CoS) DNF. W_c establishes the coupling between them and it can be subject to

learning (see below). The coefficients c_1 and c_2 modulate the effect of the interaction between the fields. The first weights the negative term on the right-hand side, modelling the inhibition exerted by the CoS on the intention field; the second weights the pre-activation of the CoS field by the intention. S_1 and S_2 are external inputs, w is the synaptic footprint and h_{rest} is the resting potential, according to the usual notation.

The external input $S_1(x, t)$, that represent a sensory input indicating task initiation (e.g., target detection) or motivation, activates the intention u_{int} -DNF. Resultant activity is passed through neural mapping to the CoS-DNF that becomes selectively sensible or pre-activated.

The input S_2 at this point will trigger the emergence of a stable attractor in u_{Cos} only when the condition for termination of the task is met, adding up to the pre-activation brought by the intention. The selection instability of the CoS inhibits the intention DNF determining a reverse selection instability in the latter.

A new intention can become active at this point and the cycle can start again, creating an autonomous mechanism that determines the duration of the motor task and allows for the development of a sequence of tasks if multiple intentions are activated in sequence (Sandamirskaya & Schöner, 2010). For examples of architectures built using this coupling see the work by Sandamirskaya et al. (2013).

Learning

The learning problem relative to motor control regards how motor skills are learned, how motor performance can be improved and how this knowledge is stored, meaning what kind of memory representation underlies the process (Rosenbaum, 2010).

Dynamic Neural Fields allow for an embodied representation of motor learning in the sense that the trace of previous activation encoding sensory-motor processes can be stored modifying the topology of an overlapping field, that can be interpreted as a memory representation.

This preshape takes the name of *memory trace* and it is modelled as an additional layer that keeps a trace of previous above threshold activation on the perceptual neural field (Schöner, 2007). It usually has a slower time constant than the field from which it receives input and might include some homeostatic mechanisms that, with an even slower time constant, allow the preshape to decay in time. The memory trace follows an equation of the type (Sandamirskaya, 2013):

$$\begin{aligned} \tau_l \dot{P}(x, t) = & \lambda_{build} \left(-P(x, t) + f(u(x, t)) \right) f(u(x, t)) + \\ & - \lambda_{decay} P(x, t) (1 - f(u(x, t))), \end{aligned} \quad (3.14)$$

where $P(x, t)$ is the strength of the preshape and τ_l/λ_{build} and τ_l/λ_{decay} are the rates at which the memory trace builds up and decays.

The strength will increase where the field $u(x, t)$ forms peaks of activation above the threshold and decrease elsewhere. $P(x, t)$ is simply added to the dynamic of the Amari equation in Eq. (3.6). This accumulation and decay of the memory trace can be linked to models for category formation and long-term memory (Spencer et al., 2009).

Other examples of learning include (Sandamirskaya, 2013):

- *mappings* and *associations*, that are used to learn coupling rules between fields with higher dimensionality with a Hebbian-like learning rule of the type

$$\begin{aligned} \tau \dot{W}_c(x, y, t) = & \epsilon(t) \left(-W_c(x, y, t) + \right. \\ & \left. + f(u_1(x, t)) \times f(u_2(y, t)) \right), \end{aligned} \quad (3.15)$$

where the coupling function $W_c(x, y, t)$ after learning will have an attractor at the intersection between active parts of the fields u_1 and u_2 ;

- the *adaptation gain* learning rule, typically necessary to set the coupling gain λ between the space of features spanned by the dynamic neural field and the variable that controls some motor output, described by

$$\tau \dot{\lambda}(x, t) = \epsilon(t) f(u(x, t)). \quad (3.16)$$

$\epsilon(t)$ here denotes a learning window or some reward mechanism and the operator (\times) denotes the sum of the expansion of the output of u_1 along the dimensions of u_2 and vice versa. The first listed learning rule can be used to learn the mapping of coupled neural fields in Eq. (3.11); the second to adapt the gain function to the behaviour of the agent in Eq. (3.12).

3.4.1 Cognitive Robotics

Cognitive robotics complete the perspective on Dynamic Field Theory (DFT) and motor control, linking neural fields architectures with sensors and robotic actuators that interact with the real (or simulated) environment. It has been pointed out that traditional robotic systems, based on control engineering, often fail to perform adequately as soon as the conditions of the environment in which they operate slightly change. They lack the time-pressured and situated response that biological systems provide effortlessly (Brooks, 1991; Pfeifer et al., 2007; Shapiro, 2012).

So far, some constitutive elements of motor control and embodied cognition have been explored in the framework of the DFT. It was shown how dynamic neural fields can account for sensory-motor coupling, autonomy and learning, all aspects that an *autonomous agent* requires.

The last core problem to be addressed regards the solution of the degrees of freedom (DoF) problem that is ultimately linked to the physical properties of the agent and to the environment in which it operates. To contextualise the model proposed in this thesis, two relevant examples of architecture that attempt to address this problem are reviewed.

The DoF Problem: Using Mapping Learning

The architecture proposed by Rudolph et al. (2015) extends sensory-motor mapping models for saccades movements toward a target object (see, for example, the work by Sandamirskaya and Storck (2014)) with a body-centred target representation that controls the movement of the arm down the line.

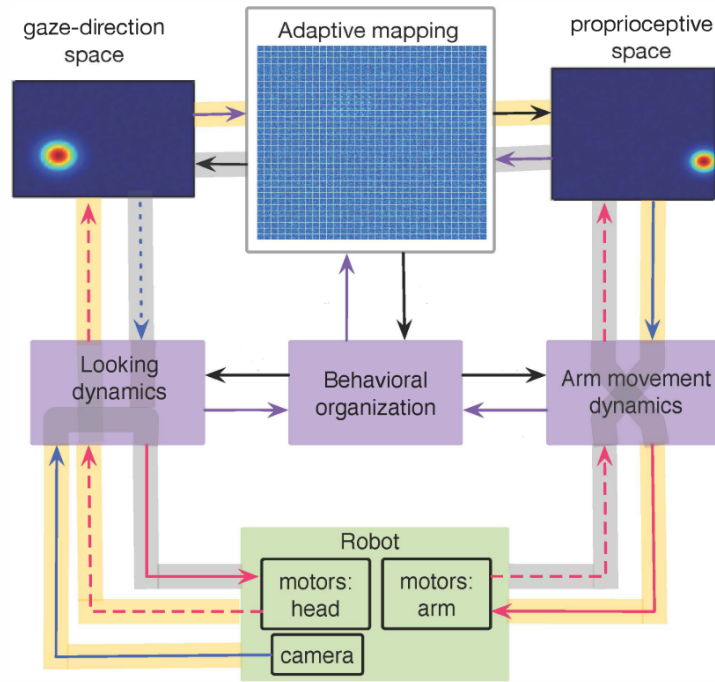


Figure 3.9: DNF architecture for looking and reaching. Adapted from ‘Learning to reach after learning to look: A study of autonomy in learning sensorimotor transformations’ by Rudolph et al. (2015), see text for a description of the model.

The hardware set-up includes a pan-tilt camera and a robotic arm. The DNF architecture is represented in Fig. 3.9. The first mapping associates the orientation of the camera (input from *motors: head*) to the visual field (input from *camera*) in the *gaze-direction space*, represented by the dynamic neural field $u_{gaze}(pan, tilt)$.

The additional mapping connects the *gaze-direction space* to the *proprioceptive space*, represented by $u_{hand}(x_{hand}, y_{hand})$ receiving inputs from the arm (*motors: arm*). The coupling between the two DNFs follows a learning rule similar to the one in Eq. (3.15). Simulation of the model starts with a learning phase during which the hand is randomly moved to map the workspace. At the end of the learning phase, the mapping is able to transform the position of the target in robot-centred coordinates.

The control of the biomechanics of the robotic arm is left to a model based on attractor dynamics: an attractor force component drives the end-effector towards the target and a repeller force component drives it away from eventual obstacles.

Joint torques are computed with traditional inverse kinematics methods (see Methods Section 4.4 for *the inverse kinematic problem*).

The autonomy and timing of the system is regulated by two architectures labelled under the name *Behavioral organization* in Fig. 3.9. This block includes interconnected intentions and conditions of satisfaction defined in Eq. (3.13). The first architecture encodes the timing for guided learning (grey pathway), following the sequence *first-move-then-look* and signalling the end of a learning session. The second (yellow pathway) guides the sequence *first-look-then-move* implementing the reaching task and signals task completion (detailed explanation of both architectures can be found in ‘Learning to reach after learning to look: A study of autonomy in learning sensorimotor transformations’ by Rudolph et al. (2015)).

Reaching experiments show that the learned mapping can account for human reaching and looking variability and every task, from target selection to movement performance and completion detection, can be carried out autonomously. Nonetheless, mapping is dependent both on the learning process and on the learning environment; a full mapping would require different scenes for learning where the target is moved around (Rudolph et al., 2015).

The degrees of freedom problem is solved at a cortical level, in a way that is comparable to neural networks models for trajectory formation (Bekey & Goldberg, 1993), showing some degree of generalisation. The concept of inverse internal model of the motor system can be then represented in a way that is grounded in sensorimotor integration, compatible with the embodied framework of DFT (see Section 2.3 for a discussion on internal models). Although this architecture presents an embodied solution to the representation of the target, mapping the visual space in the space of motor features, motor activations are still computed using traditional methods. The DoF problem at a lower level, in fact, is still addressed using the traditional robotic controls, lacking a physiological counterpart (i.e., the equivalent of the spinal level).

The proposed model for motor control, introduced in the following chapters, can be thought as an intermediate layer between architectures like the one presented above and models for movement generation by muscle synergies. Using the model by Rudolph

et al. (2015), for instance, to find the correct mapping necessary for a reaching task gives *the cortical motor activations*. These can be used in the proposed architecture to compute the forces at the joints in combination with motor primitives encoded in the spinal cord and sensory feedback. This creates a direct bridge between existing models, that solve the DoF problem in terms of motor planning, and biomechanical models, that associate motor primitives with patterns of muscles recruitment such as the one presented in Section 2.3.2

The DoF Problem: Implementing an Adaptive Observer

In the model presented by Fard et al. (2015), there is an explicit attempt to build a control system for arm reaching tasks that is biologically motivated. The authors propose a mixed approach in which a DNF architecture is placed side by side to a closed loop controller: an *adaptive observer*.

The concept of adaptive observer is borrowed from control theory in engineering and represents a dynamic system that estimates the current state of the plant system, to which it runs in parallel, based on the monitoring of sensory feedback and the *efferent copy* of motor commands. Using this information such systems provide robustness whenever sensory input is uncertain and they can compensate for transduction delays in sensory afference (Wolpert, 1997).

Using this adaptive internal model, the architecture represented in Fig. 3.10 is able to generalise accurate arm movements from a small learning set and accounts for realistic delays and absence of visual input (Fard et al., 2015).

The architecture includes a DNF encoding the position of the end effector, the *end-effector map*, and one for the location of the target in the visual field, the *target-map*. Convolution of the two maps gives the *hand centred target map* or HCT map, that specifies orientation and distance between the map and the target, in end effector coordinates.

Motor features are mapped in terms of velocity of the end-effector in the *velocity map*. This receives a broadened input from the HCT map together with a pre-shaped Gaussian activation at the centre of the map. This central activation represents the

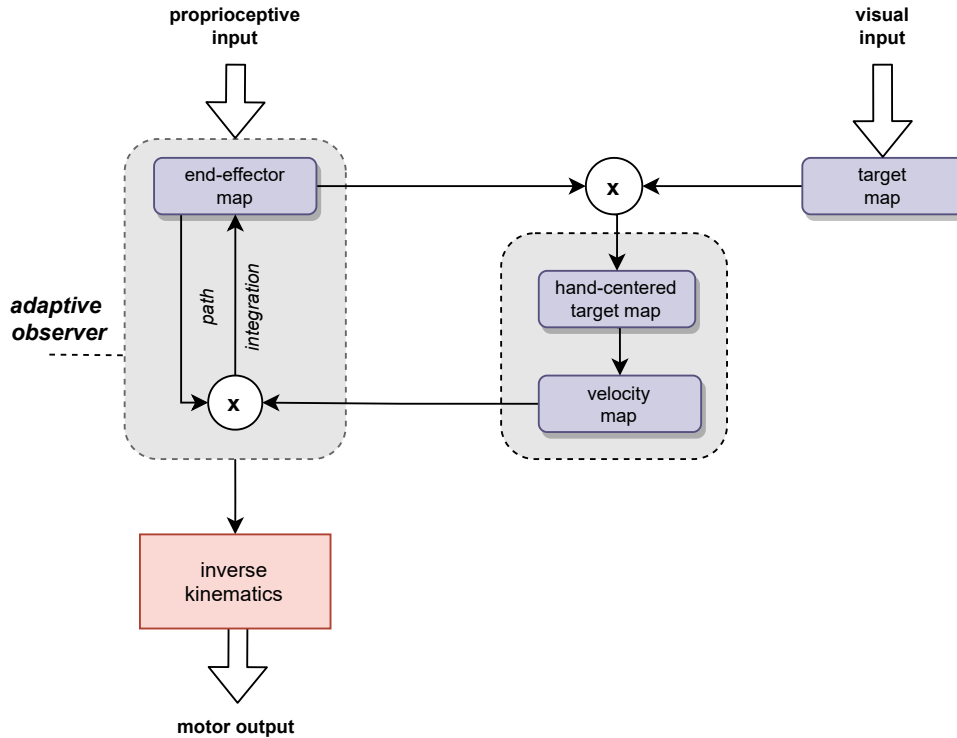


Figure 3.10: DNF architecture adapted from ‘Modeling human target reaching with an adaptive observer implemented with dynamic neural fields’ by Fard et al. (2015).

resting condition (i.e., zero velocity condition). The resultant peak in the velocity map gives a measure of the speed of the movement and is taken as the *centre of mass* of the field (Fard et al., 2015). A formal definition of this concept is given in Section 5.3 and a physiological interpretation of *the centre of mass* of a neural field is proposed in Chapter 5 and discussed in Chapter 6.

Autonomy of the system does not build on the typical intention-CoS architecture in Eq. (3.13). At the beginning of the movement the attractor in the velocity map is close to the centre (due to the Gaussian pre-activation); as the input from HCT arrives, it creates a second peak of activity: the resultant peak moves away from the centre of the velocity map causing an increase in velocity. As the distance between target and hand effector decreases during the task, the peak returns to the centre signalling the end of the reaching movement (Fard et al., 2015).

This organisation provides a different approach to autonomy that uses the dynamic of peak formation and interactions between peak solutions, showing that autonomy can be achieved in different ways using the principles of Dynamic Field Theory. Remarkably, this mechanism also gives to the velocity profile of the trajectories of the end effector the typical bell shape. This supports those account that consider the resultant velocity profile as a consequence of motor planning (Fard et al., 2015).

The computation of the next position of the end effector is based on the prediction given by the adaptive observer and then the usual inverse dynamics have to be computed. The prediction is based on learning from a training set and using *path integration*, that is implementing a Hebbian-like rule on the synaptic footprint of the end-effector map (Stringer et al., 2002). This process makes the synaptic kernel asymmetric. Convolution is then sufficient to trigger a movement of the peak towards the desired direction regardless of its starting position. This gives the predicted location. Once again, a type of internal model, feedforward in this case, is represented in an embodied framework in DFT.

Three strategies are proposed to generalise from the training set to all possible directions of movements:

- numerically rotate the asymmetric kernel in the desired direction;
- taking the asymmetric kernel of the closest learned position;
- using a population decoding scheme and interpolate between the two closest kernels among learned directions.

The most interesting result of this study is that testing these three options it is found that a rudimentary population decoding implemented on a few learned kernels is enough to give good movement predictions in directions that do not belong to the training set, as shown in Fig. 3.11 (Fard et al., 2015). This means that movements across the workspace can be generalised from a limited set, this is reminiscent of the concept of *motor primitives* explored in Chapter 2.

The reviewed architecture by Fard et al. (2015) shows that it is possible to model features of cortical motor control that give autonomy to the development of the

motor plan and compensate for delays and occluded sensory input, adding up to those introduced by Rudolph et al. (2015). This study also confirms that the use of dynamic neural fields to build models for cognition that are embodied is compatible with the concept of internal model, as long as the process of learning is grounded in sensorimotor integration.

Building from this review, the aim of the proposed architecture can be clarified once again. Considering that the computation of the forces at the joints is left to the computation of the inverse dynamics in both examples, it is impossible to reunite accounts for cortical motor control with models for motor control based on synergic muscles activations. The interface point between them is the concept of motor primitive, that represents the neural correlate at the level of the spinal cord of coordinate muscles recruitment. For this reason, the proposed model represents the spinal cord using the properties of dynamic fields, adding to the existing accounts another layer of sensorimotor integration that directly provides the forces at the joints using motor summation.

Anticipating the results obtained from simulations, the model for spinal motor control presented here is able to simulate reflex-like autonomy, and to produce straight trajectories computing directly the forward dynamics. This can be achieved using the forces at the joints resulting from sensorimotor integration in terms of a force field spanning the workspace. Interestingly, the unimodal velocity profiles found are not bell-shaped, confirming the hypothesis that this feature is the result of cortical processing, as in the model by Fard et al. (2015).

The concept of motor primitive, represented in DFT in the proposed architecture, can be linked in future developments with models that connect motor primitives to patterns of muscles activations, as mentioned above, proving that modelling motor control in the spinal cord was the missing piece to create a unified account to understand motor control, from cortical processes to muscles recruitment.

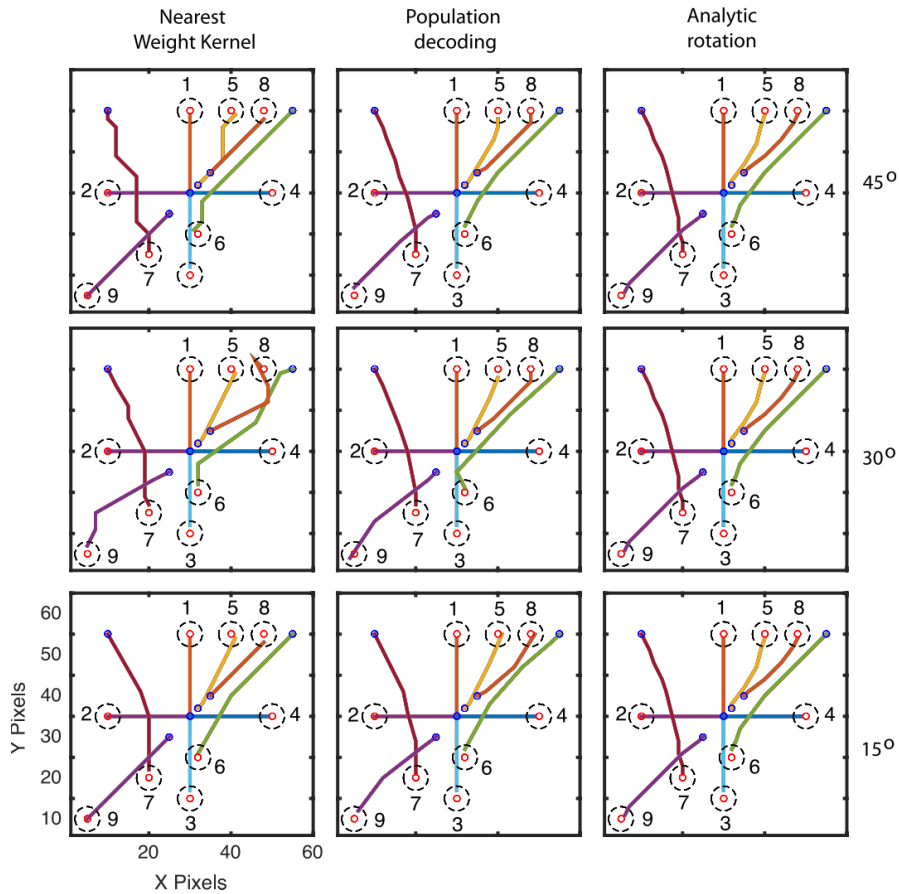


Figure 3.11: Comparison of three strategies of generalisation after path integration learning. Columns indicate the type of algorithm used to generalise, rows the direction spacing during training session. Blue dots indicate starting point of each of the nine trajectories; red dots the final position; black dashed circles represent the target zone of each destination. From ‘Modeling human target reaching with an adaptive observer implemented with dynamic neural fields’ by Fard et al. (2015).

Bio-inspired Robotics

In the first example, the DoF problem was dealt with using two mapping processes that lead to an explicit representation of the end effector and of the target in the same reference coordinates (Rudolph et al., 2015). Although this process is indeed autonomous, involves learning, and can explain to some extent how the central nervous system is involved in motor planning, motor activations are still calculated using Control Theory. The quest for task specific motor activations that give the correct forces at the joints, emerging from sensorimotor integration as it happens in the spinal cord, is not directly addressed.

The second shows how it is possible to approach problems related to motor planning using different strategies obtaining a similar result in terms of sensory-motor representation and autonomy. The role to convert motor planning into motor output is assigned this time to a predictive model that uses DFT methods and proves better at generalising (Fard et al., 2015; Rudolph et al., 2015). The concept of adaptive observer, borrowed from traditional Control Theory, is actually implemented in a more physiological manner, proving again that at a cortical level the concept of internal model can be reinvented using dynamic representations that are embodied. Nonetheless, it produces an estimate representation of the position that cannot be connected directly to motor activations or to models for the musculoskeletal system.

In summary, both architectures represent well cortical processes of motor control, but they reach to the point where some abstract representation, that does not share the same embodied features of the rest of the architecture, is assumed to compute the inverse dynamics and give the forces necessary for the movement to take place. The model developed in this thesis aims at filling this gap, modelling the motor in the spinal cord inspired by physiological findings and experimental results.

This is supported by the current research trend in robotics that draw increasingly inspiration from biology, aspiring at increasing levels of adaptivity and robustness that seems to be better addressed by the systems that are embodied. The trend seems to be going towards self-organisation and behavioural emergence, leaving the traditional top-down control on the side, at least to some extent (Pfeifer et al., 2007).

In this perspective, what seems to lack to these autonomous agents is an adequate representation of motor activations in an embodied sense. From this review on motor control, that includes the physiological perspective and the embodied approach to modelling offered by the DFT, emerges that the biological concept of motor primitive discussed in Section 2.3 is the natural match to the required representation. This creates the opportunity to link DFT representations to a biologically based biomechanical model in the proposed architecture for spinal motor control.

In the following chapter, the methods to develop a model that aims at reconciling physiologically inspired controllers to physiologically inspired representations of motor features are introduced. A further comparison between the model presented in Chapter 5 and existing architectures is discussed in Chapter 6.

3.5 Conclusions

In this chapter, the embodied approach to cognition is introduced first from a general perspective and subsequently in terms of its implications in the study of motor control and other higher cognitive functions.

The focus is then moved to a modelling approach that can account for this coupling between the agent's body and the environment, giving a suitable representation of basic behaviours and motor features in the embodied sense, based on the properties of neural tissue. Dynamic Field Theory complies with these requirements, with a growing body of architectures modelling several aspects of cognition: from sensory-motor integration, to motor learning and planning.

Of particular relevance is the possibility to represent salient features of the motor plan onto multi-dimensional structures that are able to retain topological states of activation in time, allowing at the same time for the development of autonomous processes where learning from previous experience can be integrated.

Two examples of architectures that try to address the degrees of freedom problem at a cortical level in this framework are discussed. This clarifies the need for a representation of motor activations compatible with the embodied account and more physiologically plausible (**Aim 2**).

From these premises, the idea to develop a model for spinal motor control using a dynamic field representation of motor primitives emerged. In the next chapter, relevant methods for the development of the proposed model are introduced to study stability and, equally importantly, instability in the DFT framework and in robotic modelling.

Chapter 4

Methods

4.1 Introduction

As introduced in Chapter 2, understanding motor control means understanding the processes underlying movement and stability. This perspective is mirrored by the Dynamic Field Theory that, in the embodied stance outlined in Chapter 3, defines the emergence of cognition as a shift in the stability of attractor dynamics. Stability and flexibility are also desirable features for robotic applications.

In this chapter, mathematical methods to study the stability of solutions of the Dynamic Neural Field (DNF) equation are explored together with a general introduction on stability of robotic controllers. Understanding the dynamics of neural fields and of the robotic interface is the starting point for the design and simulation of the proposed model for motor control (**Aims 2** and **4**).

In Section 4.2, methods to study the stability of solutions for the Amari equation are presented. First, an intuitive argument is outlined to prove the existence of different solution patterns and to better understand the role played by the synaptic footprint and other parameters in shaping the dynamics of the system. Subsequently, a general method for the analysis of stability, that reduces the problem to the computation of the zeros of a linear operator, is adapted to the case of negligible

space dependant delays. The obtained Evans functions for the self-sustaining and the self-stabilising peak solutions give the parameters necessary for simulations and for the development of a control strategy to trigger instability.

In Section 4.3, methods for the study of stability of solutions in two-dimensional neural fields are reviewed. In particular, the conditions to simulate stable self-sustaining peaks are presented analysing both radial and azimuthal perturbations. This type of solution is used in the proposed model to represent motor primitives. The conditions necessary for the construction of travelling peak solutions are presented, aiming at expanding the repertoire of elemental behaviour in DFT with the drifting instability (**Aim 3**).

In Section 4.4 kinematics and dynamics of the manipulator model used as robotic interface for the DNF model are described followed by an overview of robotic control theory. Traditional feedback and feedforward mechanisms are presented to discuss stability of control laws and to introduce the difference between joint and workspace control design. The latter approach is selected to build the proposed physiologically based control law for the robotic arm, based on considerations regarding the invariant properties of voluntary movement trajectories and empirical findings on motor primitives.

4.2 Stability of Neural Field Solutions

The study of dynamical systems allows to describe qualitatively the dynamics that a system can model in terms of equilibria (or *attractors*) using a topological representation, namely the phase plane. It is possible to describe how a system can shift from an attractor dynamic to another outlining a diagram in which such changes are represented in terms of trajectories linking critical points called *bifurcations* (Sejnowski & Poggio, 2007).

To understand how parameters tuning impacts the dynamics of the system, and how it is possible to control the emergence and disappearance of elemental behaviours in the DFT sense (see Chapter 3), the analysis of the field equation is presented starting from the description given by Amari.

The Amari Argument

The fundamental equation based on which neural fields models used in DFT have been developed is the Amari equation, already presented in Eq. (3.9) and re-written here as follows:

$$\frac{1}{\alpha} \frac{\partial u(x, t)}{\partial t} = -u(x, t) + \int_{-\infty}^{\infty} w(x - x') f(u(x', t)) dx' + h_{rest}. \quad (4.1)$$

This equation describes the evolution of the mean field $u(x, t)$ over time as the result of a spatial convolution between a weighting function $w(x)$ and the synaptic firing rate function $f(u(x, t))$, with time constant $\tau = 1/\alpha$ and h_{rest} resting potential of the field.

Amari studied the emergence of non-homogeneous patterns within a homogenous field, starting from this single layer, one-dimensional field equation where delays in time are considered negligible. The output function is modelled as the Heaviside function

$$f(u) = \begin{cases} 0 & u \leq 0 \\ 1 & u > 0 \end{cases},$$

and the synaptic footprint $w(x)$, introduced in Eq. (3.10) and illustrated in Fig. 3.6, models proximal excitatory and distal inhibitory connections and is assumed symmetrical, $w(x) = w(-x)$ (Amari, 1977).

The study of equilibrium solutions, with these premises and in absence of input, shows the existence of the resting solution or \emptyset -*solution*, that is the condition in which no region of the field is above threshold; the ∞ -*solution*, that is the equilibrium for which the whole field is excited; a localised excitation solution, called a -*solution*, that is when only part of the field of finite length a is above threshold (Amari, 1977).

In his work ‘Dynamics of pattern formation in lateral inhibition type neural fields’, Amari proves that the existence of different types of solution can be determined simply using the integral of the connection function $w(x)$, defined as follows

$$W(x) = \int_0^x w(x')dx', \quad (4.2)$$

and the quantities

$$W_m = \max_{x>0} W(x),$$

$$W_\infty = \lim_{x \rightarrow \infty} W(x),$$

compared with h_{rest} . Results can be summarised as follows:

- the \emptyset - *solution* exists if and only if $h_{rest} < 0$;
- the ∞ - *solution* exists if and only if $2W_\infty > -h_{rest}$;
- the a - *solution* exists if and only if $W(a) + h_{rest} = 0$ with $h_{rest} < 0$ and $a > 0$;
- spatially periodic patterns of excitation exist when $0 < h_{rest} < -2W_\infty$ with $W_\infty < 0$.

Proof of these results is given in the appendix of the mentioned study (Amari, 1977). Here, the focus is on the study of stability of the *a-solution*, also referred to as *peak of activation*, *bump* or *pulse*.

Considering a general solution $u(x, t)$, since $f(u)$ is non-zero only within the excited region, it is useful to defined this active region as a function of the two points at zero crossing $x_1(t)$ and $x_2(t)$ (Amari, 1977):

$$R[u(x, t)] = \{x_1(t), x_2(t)\}.$$

At the boundary it holds that $u(x_{1,2}, t) = 0$. From Eq. (4.1), defined the region of activation, it follows that:

$$\begin{aligned} \frac{1}{\alpha} \frac{\partial u(x_{1,2}, t)}{\partial t} &= \int_{x_1}^{x_2} w(x - x') dx' + h_{rest} = \\ &= W(x_2 - x_1) + h_{rest}. \end{aligned} \tag{4.3}$$

Defining

$$c_1 = \frac{\partial u(x_1, t)}{\partial x} \quad \text{and} \quad -c_2 = \frac{\partial u(x_2, t)}{\partial x},$$

and Taylor expanding the condition at the boundaries $u(x_{1,2} + dx_{1,2}, t + dt) = 0$, for $x_{1,2}(t + dt) = x_{1,2} + dx_{1,2}$, it is found:

$$\left. \frac{\partial u(x, t)}{\partial x} \right|_{x=x_{1,2}} dx_{1,2} + \frac{\partial u(x_{1,2}, t)}{\partial t} dt = 0.$$

It is possible, then, to calculate the gradient at the boundary as follows:

$$\begin{aligned} \frac{dx_1}{dt} &= \frac{-\partial u}{\partial t} \bigg/ \frac{\partial u}{\partial x} = -\frac{\alpha}{c_1} [W(x_2 - x_1) + h_{rest}] \\ \frac{dx_2}{dt} &= \frac{\alpha}{c_2} [W(x_2 - x_1) + h_{rest}] \end{aligned} \tag{4.4}$$

The dynamic of the system can be reduced to the sole change at the boundaries, defining $a(t) = x_1(t) - x_2(t)$ and writing the equation describing the variation of the amplitude of the peak solution as follows (Amari, 1977):

$$\frac{da}{dt} = \alpha \left(\frac{1}{c_1} + \frac{1}{c_2} \right) [W(a) + h_{rest}]. \quad (4.5)$$

The condition of existence of the peak solution of length a is then simply:

$$W(a) + h_{rest} = 0 \quad (4.6)$$

and the condition for stability can be written as:

$$\frac{dW(a)}{da} < 0. \quad (4.7)$$

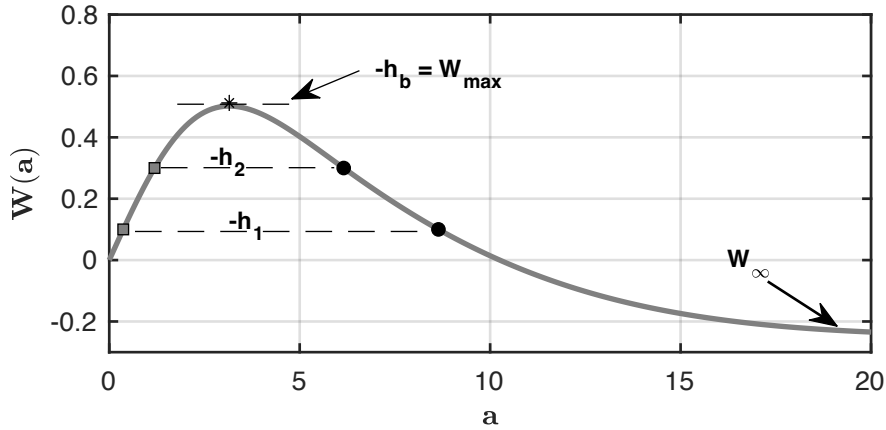


Figure 4.1: Plot of the integral of the synaptic footprint $W(a)$ and the values W_{max} and W_{∞} , together with the condition of existence of peak solutions $W(a) + h = 0$. For $h_1 = -0.1$ and $h_2 = -0.2$ two solutions are found, one stable (black dot) and one unstable (grey square). For $h = h_b$ the two branches of solution merge into one; above h_b there are no a -solutions. Parameters: $[A_{ex}, A_{in}, \sigma_{ex}, \sigma_{in}] = [1.5, 1, 2, \sqrt{2}]$.

From the representation in Fig. 4.1, it is easy to see that according to the shape of the synaptic function w the field equation will admit two, one or no localised peak solutions. It is also clear that if Eq. (4.6) has two solutions, a_1 and a_2 , using the condition in Eq. (4.7), for two generic solutions $a_1 < a_2$, the smallest bump solution is always unstable. Both branches of solution encounter a fold bifurcation at the critical value $h_b = -W_{max}$. This visually clarifies how it is possible to design a neural

field that admits stable localised peak solutions, namely selecting the appropriate synaptic footprint and resting level from Eq. (4.6).

This simple but effective approach developed by Amari, that considers the evolution of the boundary instead of the behaviour of the global field to study the existence and stability of solutions, has been developed further and is used in the following to determine shape and stability of travelling spots in two-dimensional fields (Bressloff & Coombes, 2013; Coombes et al., 2012).

For the development of the proposed model, consider the output function as the Heaviside function defined with a general threshold h :

$$f(u) = \begin{cases} 0 & u \leq h \\ 1 & u > h \end{cases}. \quad (4.8)$$

A secondary coupled field is also introduced, called *the adaptation field*, to add a more realistic inhibitory dynamic (Bressloff, 2012). Studies on travelling pulses in neural field models use simple linear forms of adaptation (Pinto & Ermentrout, 2001). The effective interaction kernel of the two coupled fields has the Mexican hat shape of the Amari argument, for an appropriate choice of exponential synaptic kernels (Coombes & Owen, 2004).

Adding the dynamic of the adaptation field it is found:

$$\begin{aligned} \frac{1}{\alpha} \frac{\partial u(x, t)}{\partial t} = & -u(x, t) + \int_{-\infty}^{\infty} w(x - x') f(u(x', t)) dx' \\ & - g \int_{-\infty}^{\infty} w_a(x - x') a(x, t) + h_{rest} \end{aligned} \quad (4.9)$$

$$\frac{1}{\beta} \frac{\partial a(x, t)}{\partial t} = -a(x, t) + f(u(x, t)),$$

where $g > 0$ modulates the effect of adaptation on the main field and $1/\beta$ is the time constant of the adaptation field and w_a is the associated synaptic footprint. Equation (4.9) defines the mathematical model for the neural controllers of the proposed architecture.

4.2.1 Evans Functions for the Study of Stability

In order to understand the behaviour of solution classes, a convenient approach is the one that reduces to the study of bifurcations of a linearised operator, that is the Evans function corresponding to the solution. This method proved to be well suited to select the desired behaviour for the neural field controllers of the proposed model and to assign parameters accordingly for numerical simulations. The rationale behind this approach can be presented using a general travelling pulse solution; results for a standing bump can be simply obtained considering $c = 0$.

Understanding the conditions that determine the dynamics of the system is crucial to design desired elemental behaviour for cognitive architectures in the DFT account. With the hypothesis of Heaviside firing rate the linear operator associated with the solutions of interest has the form of an analytic function with complex values, whose zeros represent the eigenvalues of the system (Bressloff, 2012). Using this representation of the stability of solutions, the desired type of attractor for the embodied system and the desired type of instability can be selected, setting parameters appropriately.

The four steps analysis that follows has been obtained following the procedure in the study by Coombes and Owen (2004). The methodological contribution that is given here consist in calculating the Evans functions for the solutions of interest considering space-dependent delays negligible. The fact that the method developed here is a particular application of a more general approach contributes to creating a unified methodology where more physiological detail can be added at any point. For a review on methods for neural fields with finite conduction velocity see the work by Coombes et al. (2003).

1. Write the Solution in Integral Form

The first step is to find an expression for a travelling pulse solution in the integral form. Consider the neural field with adaptation in Eq. (4.9) in a useful compact notation (Bressloff, 2012):

$$\begin{aligned} Qu(x, t) &= (w \otimes f * u)(x, t) - g(w_a \otimes a)(x, t) \\ Q_a a(x, t) &= f * u(x, t) \end{aligned} \tag{4.10}$$

where Q and Q_a are the two linear operators defined according to Eq. (4.9), associated with the respective Green's function $\eta(t)$ and $\eta_a(t)$, with $\eta(t), \eta_a(t) = 0$ for $t < 0$; w and w_a are the synaptic footprints. The notation (\otimes) describes convolution in space and $(f * u)(x, t) = f(u(x, t))$ represents the result of the output function in Eq. (4.8) applied to the field variable $u(x, t)$. In the following it is assumed $h_{rest}=0$ for simplicity.

The integral form of the model, as formulated in the study by Coombes et al. (2014) with the usual condition $w(x) = w(|x|)$ and $w_a(x) = w_a(|x|)$, is rewritten here considering negligible space-dependant delays:

$$\begin{aligned} u(x, t) = \left[\int_{-\infty}^{\infty} dx' w(x') \int_0^{\infty} ds \eta(s) + \right. \\ \left. -g \int_{-\infty}^{\infty} dx' w_a(x') \int_0^{\infty} ds \eta_b(s) \right] f \left(u(x - x', t - s) \right) \end{aligned} \tag{4.11}$$

where $\eta_b = \eta \oplus \eta_a$ and (\oplus) represents convolution in time between the synaptic filters. In compact notation Eq. (4.11) becomes:

$$u = [\eta \oplus w \otimes -g\eta_b \oplus w_a \otimes] f * u. \tag{4.12}$$

Considering a general travelling peak solution, the integral solution $U(\xi, t)$ is obtained simply substituting the variable $\xi = x - ct$ in Eq. (4.11), giving:

$$U(\xi, t) = \left[\int_{-\infty}^{\infty} dx' w(x') \int_0^{\infty} ds \eta(s) + \right. \\ \left. -g \int_{-\infty}^{\infty} dx' w_a(x') \int_0^{\infty} ds \eta_b(s) \right] f \left(U(\xi - x' + cs, t - s) \right). \quad (4.13)$$

2. Linearise Around the Solution

The second step consists in the linearisation of the general solution $U(\xi, t)$ around a stationary travelling pulse. Following the methodology proposed in the review by Coombes and Owen (2004), it can be written $U(\xi, t) = q(\xi) + u(\xi, t)$. For the case with negligible delays considered here, the stationary solution $q(\xi)$ is:

$$q(\xi) = \left[\int_{-\infty}^{\infty} dx' w(x') \int_0^{\infty} ds \eta(s) + \right. \\ \left. -g \int_{-\infty}^{\infty} dx' w_a(x') \int_0^{\infty} ds \eta_b(s) \right] f \left(q(\xi - x' + cs) \right). \quad (4.14)$$

Taylor expanding Eq. (4.13) around $q(\xi)$ in Eq. (4.14), the expression for the perturbation of the solution is found to be:

$$u(\xi, t) = \left[\int_{-\infty}^{\infty} dx' w(x') \int_0^{\infty} ds \eta(s) \right. \\ \left. -g \int_{-\infty}^{\infty} dx' w_a(x') \int_0^{\infty} ds \eta_b(s) \right] \cdot \\ \cdot f \left(q(\xi - x' + cs) \right) u(\xi - x' + cs, t - s) \quad (4.15)$$

where $\dot{f}(u(x, t)) = \partial f(u(x, t)) / \partial t$.

Considering those solutions that are bounded and smooth on \mathbb{R} for each t , the solution has the form $u(\xi, t) = u(\xi)e^{\lambda t}$; substituting and changing variables ($\xi - x' + cs \rightarrow \zeta, \zeta \rightarrow s$) leads to the eigenvalue equation in the form $u = \mathcal{L}u - g\mathcal{J}u$ (Coombes & Owen, 2004). Here the equation obtained with the hypothesis of infinite conduction velocity is found to be:

$$u(\xi) = \left[\int_{-\infty}^{\infty} dx' w(x') \int_{\xi-x'}^{\infty} \frac{ds}{c} \eta \left(-\frac{\xi}{c} + \frac{x'}{c} + \frac{s}{c} \right) - g \int_{-\infty}^{\infty} dx' w_a(x') \int_{\xi-x'}^{\infty} \frac{ds}{c} \eta_b \left(-\frac{\xi}{c} + \frac{x'}{c} + \frac{s}{c} \right) \right] \cdot \dot{f}(q(s)) e^{-\lambda \left(-\frac{\xi}{c} + \frac{x'}{c} + \frac{s}{c} \right)} u(s). \quad (4.16)$$

Having found the linear operator associated with the travelling peak solution, it is possible to further simplify the last equation defining $z = q(s)$ and changing variables accordingly (Coombes & Owen, 2004):

$$s = q^{-1}(z) \quad \text{and} \quad ds \rightarrow d(q^{-1}(z)) = \frac{dz}{|\dot{q}(q^{-1}(z))|}.$$

Substituting, it is found:

$$u(\xi) = \left[\int_{-\infty}^{\infty} dx' w(x') \int_{q(\xi-x')}^{q(\infty)} \frac{dz}{c} \eta \left(\frac{q^{-1}(z)}{c} - \frac{\xi}{c} + \frac{x'}{c} \right) - g \int_{-\infty}^{\infty} dx' w_a(x') \int_{q(\xi-x')}^{q(\infty)} \frac{dz}{c} \eta_b \left(\frac{q^{-1}(z)}{c} - \frac{\xi}{c} + \frac{x'}{c} \right) \right] \cdot \frac{\delta(z-h)}{|\dot{q}(q^{-1}(z))|} e^{-\lambda \left(\frac{q^{-1}(z)}{c} - \frac{\xi}{c} + \frac{x'}{c} \right)} u(q^{-1}(z)). \quad (4.17)$$

Remembering the properties of the Heaviside function, the eigenvalue equation with the hypothesis made on the delays is obtained:

$$u(\xi) = \frac{1}{c|\dot{q}^{-1}(h)|} \left[\int_{-\infty}^{\infty} dx' w(x') \eta \left(\frac{q^{-1}(h)}{c} - \frac{\xi}{c} + \frac{x'}{c} \right) - g \int_{-\infty}^{\infty} dx' w_a(x') \eta_b \left(\frac{q^{-1}(h)}{c} - \frac{\xi}{c} + \frac{x'}{c} \right) \right] \cdot e^{-\lambda \left(\frac{q^{-1}(h)}{c} - \frac{\xi}{c} + \frac{x'}{c} \right)} u(q^{-1}(h)). \quad (4.18)$$

3. Apply Boundary Conditions

For the travelling pulse solution $q^{-1}(h) = 0$ and $q^{-1}(h) = \Delta$ (Amari, 1977; Coombes & Owen, 2004). The third step consist in using these conditions, obtaining from Eq. (4.17) the following system:

$$\mathcal{L}u(\xi) = A(\xi, \lambda)u(0) + B(\xi, \lambda)u(\Delta), \quad (4.19)$$

$$\mathcal{J}u(\xi) = C(\xi, \lambda)u(0) + D(\xi, \lambda)u(\Delta), \quad (4.20)$$

where the operators \mathcal{L} and \mathcal{J} for the case of negligible space-dependant delays are:

$$\begin{aligned} A(\xi, \lambda) &= \frac{1}{c|\dot{q}(0)|} \int_{\xi}^{\infty} dx' w(x') \eta \left(-\frac{\xi}{c} + \frac{x'}{c} \right) e^{-\lambda \frac{(x'-\xi)}{c}} \\ B(\xi, \lambda) &= \frac{1}{c|\dot{q}(\Delta)|} \int_{\xi-\Delta}^{\infty} dx' w(x') \eta \left(-\frac{\xi-\Delta}{c} + \frac{x'}{c} \right) e^{-\lambda \frac{(x'-(\xi-\Delta))}{c}} \\ C(\xi, \lambda) &= \frac{1}{c|\dot{q}(0)|} \int_{\xi}^{\infty} dx' w_a(x') \eta_b \left(-\frac{\xi}{c} + \frac{x'}{c} \right) e^{\lambda \frac{(x'-\xi)}{c}} \\ D(\xi, \lambda) &= \frac{1}{c|\dot{q}(\Delta)|} \int_{\xi-\Delta}^{\infty} dx' w_a(x') \eta_b \left(-\frac{\xi-\Delta}{c} + \frac{x'}{c} \right) e^{-\lambda \frac{(x'-(\xi-\Delta))}{c}}. \end{aligned} \quad (4.21)$$

4. Impose Self-Consistency

In order for Eqs. (4.19) and (4.20) to be self-consistent, it must be verified that:

$$\begin{bmatrix} u(0) \\ u(\Delta) \end{bmatrix} = \mathcal{A}(\lambda) \begin{bmatrix} u(0) \\ u(\Delta) \end{bmatrix} \quad (4.22)$$

where

$$\mathcal{A}(\lambda) = \begin{bmatrix} A(0, \lambda) - gC(0, \lambda) & B(0, \lambda) - gD(0, \lambda) \\ A(\Delta, \lambda) - gC(\Delta, \lambda) & B(\Delta, \lambda) - gD(\Delta, \lambda) \end{bmatrix}. \quad (4.23)$$

Finally, it is found

$$\mathcal{E}(\lambda) = \det(\mathcal{A}(\lambda) - I) \quad (4.24)$$

where $\mathcal{E}(\lambda)$ is the Evans function associated with a travelling solution of the type in Eq. (4.13) (Coombes & Owen, 2004).

In order to study the stability, or the condition to trigger instability, for the desired elemental behaviour, the Evans function associated with the peak solution can be numerically computed from Eq. (4.24). The plot of the zero level of the real and imaginary part of $\mathcal{E}(\lambda)$ for $\lambda = \nu + j\omega$ gives the isolated eigenvalues as the point of intersection.

4.2.2 Stability of Self-Sustaining Peak Solutions

Self-sustained peaks are used in the DFT to model working memory processes or motor output that requires the persistence of information even when the input is removed. This type of solution is used in the proposed model to encode descending activation signals that select motor primitives. For this reason, a representation that is stable until the motor task is achieved is necessary.

Applying the methodology presented above to a stable peak solution, parameters for controllers can be set and a condition on the threshold to trigger reverse detection

instability (for instance, to reset the controller when the task is over) is outlined.

For a stationary standing peak solution, as the one presented in Fig. 4.2, it is $c = 0$ and

$$Qu = u, \quad Qa = a.$$

Considering a peak of width Δ , the solution to the field equation takes the form:

$$q(\xi) = \int_0^\Delta w_b(\xi - x') dx', \quad (4.25)$$

where $w_b = w(x) - gw_a(x)$ is the resultant synaptic kernel (Coombes & Owen, 2004).

In order to compute the Evans function, $\dot{q}(\xi)$ is obtained from Eq. (4.25):

$$\dot{q}(\xi) = w_b(\xi) - w_b(\xi - \Delta), \quad (4.26)$$

and $|\dot{q}(0)| = |\dot{q}(\Delta)|$.

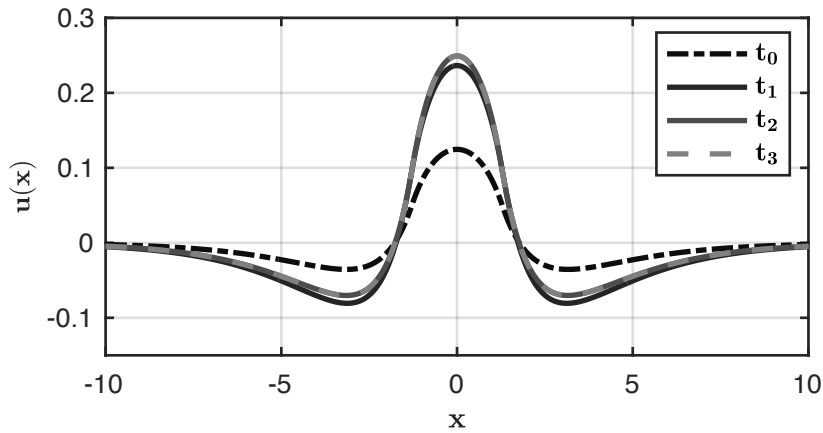


Figure 4.2: Example of self-sustaining peak solution at four simulation time steps.

Another simplification occurs in the evaluation of the Evans function since, for $c = 0$, both synaptic footprints can be considered flat compared to the terms including the filtering functions $\eta(y/c)e^{-\lambda y/c}$ and $\eta_b(y/c)e^{-\lambda y/c}$ (Coombes & Owen, 2004), so that Eqs. (4.21) become:

$$\begin{aligned}
 A(\xi, \lambda) &= \frac{1}{|\dot{q}(0)|} w(\xi) \hat{\eta}(-i\lambda) & B(\xi, \lambda) &= A(\Delta - \xi, \lambda) \\
 C(\xi, \lambda) &= \frac{1}{|\dot{q}(0)|} w_a(\xi) \hat{\eta}_b(-i\lambda), & D(\xi, \lambda) &= C(\Delta - \xi, \lambda),
 \end{aligned} \tag{4.27}$$

where the Fourier transforms of η and η_a are introduced, with the general definition of transform given by

$$\hat{\mathcal{F}}(k) = \int_{-\infty}^{\infty} \mathcal{F}(\zeta) e^{-ikx} d\zeta. \tag{4.28}$$

For the controllers implemented in Chapter 5, synaptic filters and footprint are chosen as follows:

$$\eta(t) = \alpha e^{-\alpha t}, \quad \eta_a(t) = e^{-t}, \quad w(x) = A_{ex} e^{-|x|}, \quad w_a = A_{in} e^{-|x|/\sigma_a} / 2\sigma_a,$$

where A_{ex} and A_{in} model the excitatory and inhibitory amplitude of lateral inhibition. The resultant footprint w_b consequently has the Mexican hat shape defined in Eq. (3.10), considering $\sigma_{ex} = 1$ and $\sigma_{in} = \sigma_a$ (Coombes & Owen, 2004). For simplicity, in the following it is considered $A_{ex} = A_{in} = 1/2$.

The solution $q(\xi)$ for the standing peak can be written as follows (Pinto & Ermentrout, 2001):

$$q(\xi) = \begin{cases} \frac{1}{2} (e^\xi - e^{(\xi-\Delta)}) - \frac{g}{2} (e^{\xi/\sigma_a} - e^{(\xi-\Delta)/\sigma_a}) & \xi \leq 0 \\ 1 - g - \frac{1}{2} (e^{-\xi} + e^{(\xi-\Delta)}) + \frac{g}{2} (e^{-\xi/\sigma_a} + e^{(\xi-\Delta)/\sigma_a}), & 0 < \xi < \Delta \\ \frac{1}{2} (e^{-(\xi-\Delta)} - e^{-\xi}) - \frac{g}{2} (e^{-(\xi-\Delta)/\sigma_a} - e^{-\xi/\sigma_a}) & \xi \geq \Delta. \end{cases} \tag{4.29}$$

Using the condition on the threshold h at the boundary, it is possible to find the condition of existence of the self-sustained peak solution $\Delta = \Delta(h)$:

$$\frac{1}{2} (1 - e^{-\Delta}) - \frac{g}{2} (1 - e^{-\Delta/\sigma_a}) = h. \tag{4.30}$$

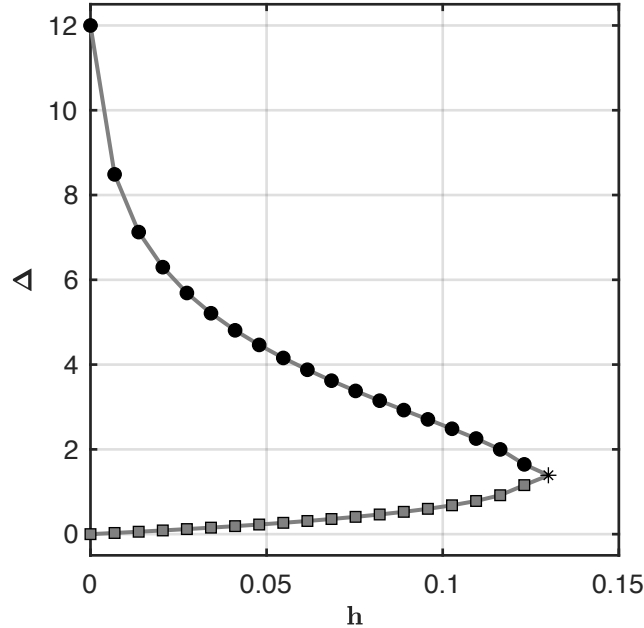


Figure 4.3: Plot of $\Delta = \Delta(h)$ for a self-sustaining peak solution. Parameters: $[A_{ex}, A_{in}, \sigma_a, g, \alpha] = [0.5, 0.5, 2, 1, 0.5]$.

Just like in the discussion presented by Amari (1977), the solution to this equation describes two branches, one wider and one narrower, showed in Fig. 4.3.

From this plot it is possible to set the parameters for neural controllers that show working memory instability. Moving the threshold above the bifurcation value, the field returns to the resting state. This method is used in Chapter 5 where an adaptive threshold mechanism triggers instability.

Evaluation of $\mathcal{E}(\lambda)$ from Eq. (4.24) using Eq. (4.27) gives the contour plots in Fig. 4.4 for one-dimensional neural controller used to represent motor primitives selection signals. It is found that solutions taken from the lower branch are unstable, confirming Amari's results, presented in Section 4.2. In order to simulate self-sustaining peaks it is necessary to stimulate the field with inputs that are sufficient to select the wider solution.

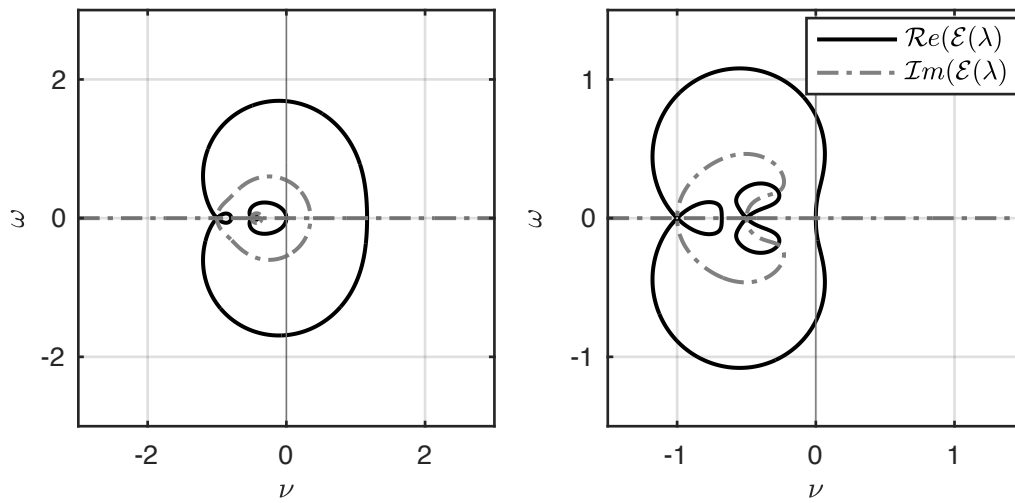


Figure 4.4: Plot of the zero-contour of the real and imaginary part of the Evans function associated with a self-sustaining peak solution for $\lambda = \nu + i\omega$. Left: solution taken from the lower branch. Right: solution taken from the upper branch. Parameters: $[A_{ex}, A_{in}, \sigma_a, g, \alpha, h] = [0.5, 0.5, 2, 1, 0.5, 0.1]$

4.2.3 Stability of Self-Stabilising Peak Solutions

Without the nonlinear adaptation self-sustaining peak solutions are always unstable. In fact, it is found that there is always a positive eigenvalue associate with them (Coombes & Owen, 2004). Nonetheless, if a nonhomogeneous input $I(x)$ with appropriate amplitude is introduced, the pinning of a stationary bump solution, a self-stabilising peak of activation, is observed. If the input is removed the field goes back to the resting potential.

This type of dynamics can be used to model detection and reverse instability: self-stabilising solutions can track sensory-motor features, providing the emergence of peaks only when an over-threshold input is detected and returning to the resting state when the input is not strong enough. In the proposed model, this type of neural controller allows for an autonomous development of the motor plan at the level of the spine (see in Chapter 5, *the task monitoring block*).

The model with linear adaptation is taken from the study by Bressloff et al. (2003) and has the simplified form:

$$\begin{aligned} \frac{1}{\alpha} \frac{\partial u(x, t)}{\partial t} &= -u(x, t) + \int_{-\infty}^{\infty} w(x - x') f(u(x, t)) dx' - ga(x, t) + I(x) \\ \frac{1}{\beta} \frac{\partial a(x, t)}{\partial t} &= -a(x, t) + u(x, t) \end{aligned} \quad (4.31)$$

In order to find the condition in which a self-stabilising peak solution emerges, consider a general travelling pulse solution satisfying Eq. (4.31):

$$q(\xi) = \int_0^{\infty} \eta(s) \psi(\xi + cs) ds - g \int_0^{\infty} \eta_b(s) q(\xi + cs) ds, \quad (4.32)$$

where $\psi(x, t) = Qu(x, t)$ when $g = 0$ (i.e., without adaptation) (Bressloff, 2012).

To obtain a closed expression for $q(\xi)$, the Fourier transform in Eq. (4.32) is computed:

$$\hat{q}(k) = \hat{\eta}_c(k) \hat{\psi}(k) \quad (4.33)$$

where

$$\hat{\eta}_c(k) = \frac{\hat{\eta}(k)}{1 + g\hat{\eta}_b(k)}. \quad (4.34)$$

Anti-transforming, it is found

$$q(\xi) = \int_0^\infty \eta_c(z)\psi(\xi + cz)dz \quad (4.35)$$

where

$$\eta_c(t) = \frac{1}{2\pi} \int_{-\infty}^\infty \hat{\eta}_c(k)e^{ikt}dk \quad (4.36)$$

with the condition $\eta_c(t) = 0$ for $t < 0$ (Bressloff et al., 2003).

Proceeding like in the previous sections, a linear operator associated with the system in Eq. (4.31) for the self-stabilised pulse with the form $\mathcal{J}_c u(\xi) = A_c(\xi, \lambda)u(0) + B_c(\xi, \lambda)u(\Delta)$ can be found (Coombes & Owen, 2004). Here the operator is derived for negligible spatial delays and it is found that:

$$\begin{aligned} A_c(\xi, \lambda) &= \frac{1}{c|\dot{q}(0)|} \int_\xi^\infty dx' w(x') \eta_c \left(-\frac{\xi}{c} + \frac{x'}{c} \right) e^{-\lambda \frac{(x'-\xi)}{c}} \\ B_c(\xi, \lambda) &= \frac{1}{c|\dot{q}(\Delta)|} \int_{\xi-\Delta}^\infty dx' w(x') \eta_c \left(-\frac{\xi-\Delta}{c} + \frac{x'}{c} \right) e^{-\lambda \frac{(x'-(\xi-\Delta))}{c}} \end{aligned} \quad (4.37)$$

Following the analysis in the study by Bressloff et al. (2003), the input function is defined as $I(x) = \mathcal{I}e^{-x^2/2\sigma^2}$, a Gaussian function with centre in zero, standard deviation σ and amplitude \mathcal{I} . The standing pulse solution, then, satisfies the condition at the boundary:

$$q(-\Delta/2) = q(\Delta/2) = h. \quad (4.38)$$

For the choice of synaptic filtering functions used to build a controller for autonomy in Chapter 5

$$\eta(t) = \alpha e^{-\alpha t}, \quad \eta_a(t) = e^{-\beta t}, \quad (4.39)$$

the explicit self-stabilising solution is:

$$q(\xi) = \hat{\eta}_c(0) \left[\int_{-\Delta/2}^{\Delta/2} w(\xi - x') dx' + I(\xi) \right] \quad (4.40)$$

where $\hat{\eta}_c(0) = 1/(1 + g)$ (Bressloff et al., 2003). It follows that:

$$|\dot{q}(-\Delta/2)| = |\dot{q}(\Delta/2)| = [w(\Delta) - w(0) + |\dot{I}(\pm\Delta/2)|]/(1 + g). \quad (4.41)$$

To find the relationship between the amplitude of the input \mathcal{I} and pulse width Δ , that gives the behavioural switching between detection/reverse instability for the desired controller, it is sufficient to apply the conditions at the boundary of the peak in Eq. (4.38) to Eq. (4.40) (Bressloff et al., 2003). The condition of existence of a self-sustaining pulse solution is then found to be:

$$(1 + g)h = \left[I \left(\frac{\Delta}{2} \right) + \frac{1 - e^{-\Delta}}{2} \right]. \quad (4.42)$$

In the threshold range $h(1 + g) > 0.5$, two solution branches are found again, one for a narrower self-stabilising solution and one for a wider one. For the choice $\beta > g$ the phase portrait shows a bifurcation. For a complete overview of solution branches see the original study by Bressloff et al. (2003).

In Fig. 4.5, the two branches are plotted. It is possible to see that for $\mathcal{I} < \mathcal{I}_{sn}$ such field equation does not support standing pulses, giving the condition to control the desired elemental behaviour.

The solution presents again two branches. To study their stability, the Evans functions are obtained using the four steps outlined above. It is possible to simplify, since $c = 0$, and consider again $w(x')$ relatively flat compared to the term $\eta_c(x'/c)e^{-\lambda x'/c}/c$ in Eq. (4.37). A result similar to the one in the study by Coombes and Owen (2004) is found again, here obtained without modelling space dependant delays:

$$A_c(\xi, \lambda) = \frac{1}{|\dot{q}(\Delta/2)|} \hat{\eta}_c(-i\lambda) w(\xi + \Delta/2), \quad B_c(\xi, \lambda) = A_c(\xi - \Delta, \lambda). \quad (4.43)$$

Applying self-consistency it is found:

$$\begin{bmatrix} u(-\Delta/2) \\ u(\Delta/2) \end{bmatrix} = \mathcal{A}_c(\lambda) \begin{bmatrix} u(-\Delta/2) \\ u(\Delta/2) \end{bmatrix} \quad (4.44)$$

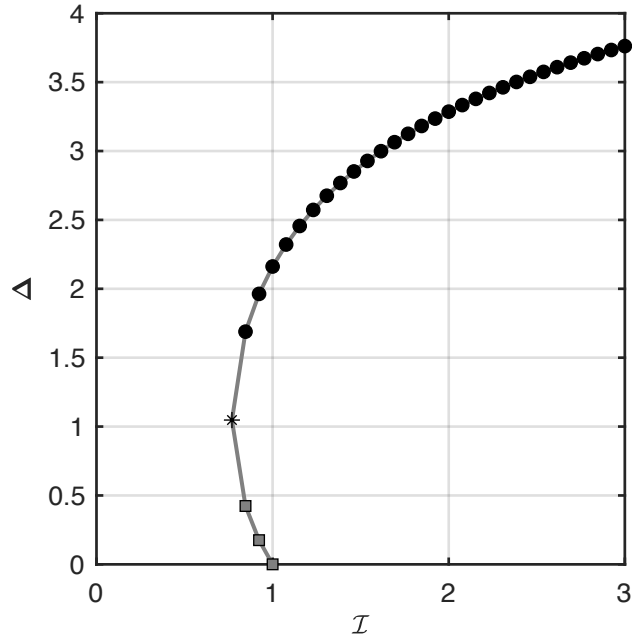


Figure 4.5: Bifurcation of the two branch solution for a neural field model with linear adaptation. Black dots represent stable solutions, grey squares unstable solutions, grey stars bifurcation points. Parameters: $[A_{ex}, A_{in}, \sigma_a, g, \alpha, h] = [0.5, 0, 1, 1, 1, 0.5]$.

where

$$\mathcal{A}_c(\lambda) = \begin{bmatrix} A_c(-\Delta/2, \lambda) & B_c(-\Delta/2, \lambda) \\ A_c(\Delta/2, \lambda) & B_c(\Delta/2, \lambda) \end{bmatrix}. \quad (4.45)$$

Computing Eq. (4.24) and plotting the real and imaginary part level zero as before, in Fig. 4.6 the Evans functions are shown for a self-stabilising peak solution. It is found again that the upper branch is stable. Using these results, it is possible to design a neural controller that retains a peak of activation as long as the amplitude of the input is big enough, selecting a solution from the upper branch.

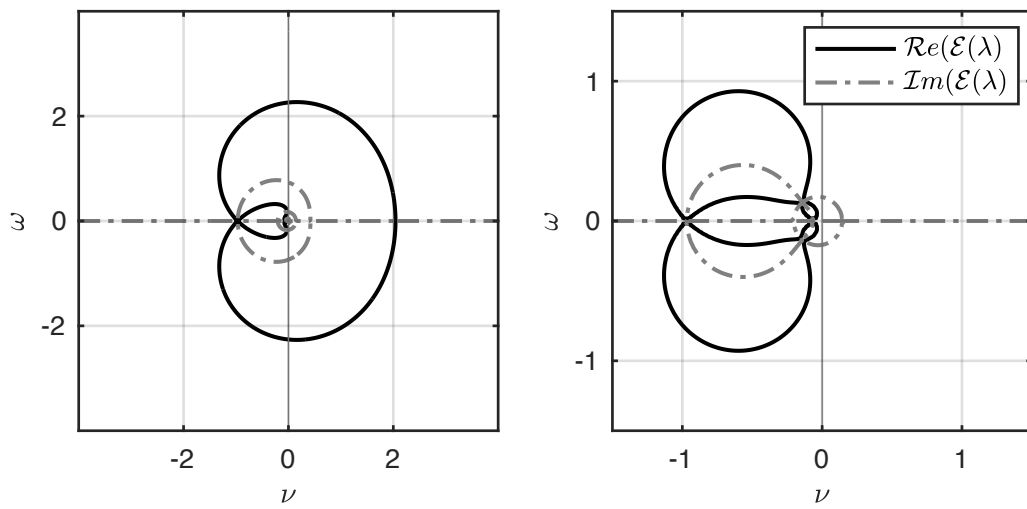


Figure 4.6: Plot of the zero-contour of the real and imaginary part of the Evans function associated with a self-sustaining peak solution for $\lambda = \nu + i\omega$. Left: solution taken from the lower branch for $\mathcal{I} = 0.8$; right: solution taken from the upper branch for $\mathcal{I} = 2$. Parameters: $[A_{ex}, A_{in}, \sigma_a, g, \alpha, h] = [0.5, 0, 1, 1, 1, 0.5]$

4.3 Dynamic Neural Fields in 2D

Two-dimensional fields are the building blocks used to model cortical cognitive processes in the Dynamic Field Theory (DFT) framework, as introduced in Chapter 3. In two dimensions, the study of solutions of the neural field equation has also found relevant applications in models of propagation of cortical activity (Bojak et al., 2004; Deco et al., 2008; Pinotsis et al., 2014).

In the proposed model for spinal motor control, the structure of two-dimensional Dynamic Neural Field (DNF) is considered ideal to map motor primitives (see Chapter 2 for the representation of motor primitives as planar force fields). These are represented in DFT using the working-memory instability that produces self-sustained peak solutions that are well suited to encode reliable input for motor agents (Sandamirskaya et al., 2013; Spencer et al., 2009).

The extension to two dimensions of the Amari equation and the investigation of stability has already been developed in the case of negligible space delays using Evans functions (Bressloff, 2012). The possibility to introduce another type of elemental behaviour, the *drifting instability*, leading to the emergence of travelling peaks solutions, requires the use of methods addressing not only radial but also azimuthal stability. These methods applied to both classes of solutions, self-sustained and drifting, are reviewed in the present section, completing the methodology used to develop the neural controllers for the proposed model presented in Chapter 5.

4.3.1 The Amari equation in 2D

The Amari equation for a two-dimensional neural field can be written using polar coordinates as follows:

$$\frac{1}{\alpha} \frac{\partial u(\mathbf{r}, t)}{\partial t} = -u(\mathbf{r}, t) + \int_{\mathbb{R}^2} w(|\mathbf{r} - \mathbf{r}'|) f(u(\mathbf{r}', t)) d\mathbf{r}' \quad (4.46)$$

where $\mathbf{r} = (r, \phi)$ and $\mathbf{r}' = (r', \phi')$. The variable $u(\mathbf{r}, t)$ represents the local activity of the field, $\tau = 1/\alpha$ is the time constant, $w(\mathbf{r}, t)$ is the synaptic footprint and $f(u(\mathbf{r}, t)) = H(u(\mathbf{r}, t) - h)$ is the Heaviside function with threshold h (Bressloff, 2012).

To model two-dimensional neural fields representing motor primitives and showing working memory instability, the condition of existence of the self-sustained solution is looked for. The type of solution to Eq. (4.46) of interest is a circular symmetric solution of radius Δ satisfying $u(\mathbf{r}, t) = q(r)$ and $q(\Delta) = h$, with $q(r) > h$ for $r < \Delta$ and $q(r) < h$ for $r > \Delta$, $\lim_{r \rightarrow \infty} q(r) = 0$. Such solution, shown in Fig. 4.7, can be written as

$$q(r) = \int_0^{2\pi} \int_0^\Delta w(|r - r'|) r' dr' d\phi. \quad (4.47)$$

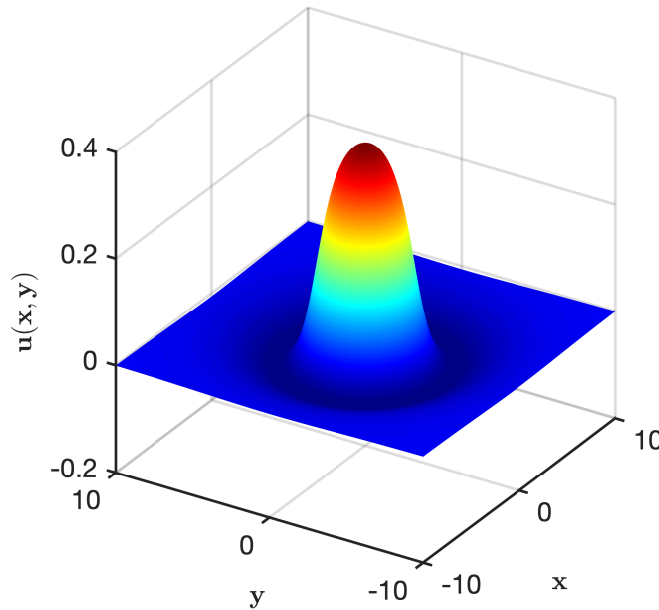


Figure 4.7: Radially symmetrical solution peak, or *bump* or *spot*, for the neural field equation in two dimensions with Mexican hat footprint. Parameters: $[A, \sigma, h, \alpha] = [0.25, 2, 0.12, 1]$.

In order to evaluate the integral in Eq. (4.47) and find a solution for the field

equation with the usual Mexican hat synaptic footprint, the procedure in the study by Bressloff (2012) is followed, leading to the construction of an explicit solution of the type:

$$q(r) = 2\pi\Delta \int_0^\infty \hat{w}(\rho) J_0(\rho r) J_1(\rho\Delta) d\rho, \quad (4.48)$$

where J_ν is the Bessel function of the first kind and order $\nu = 0, 1$ and \hat{w} is the Fourier transform of the synaptic footprint.

To make the computation of the solution easier (Bressloff, 2012; Bressloff & Coombes, 2013), it is possible to write the synaptic footprint using a function that is qualitatively similar to the Mexican hat of the type $w(r) = (2\pi)^{-1}(e^{-r} - Ae^{-r/\sigma})$:

$$w(r) = \frac{2}{3\pi}(K_0(r) - K_0(2r) - A(K_0(r/\sigma) - K_0(2r/\sigma))). \quad (4.49)$$

where K_0 is the modified Bessel function of the second kind and order zero and coefficients for lateral inhibition are $(A_{ex}, A_{in}, \sigma_{ex}, \sigma_{in}) = [1, A, 1, \sigma]$. It is possible to use the Hankel transform of $K_0(sr)$, that has the polynomial form $\mathcal{H}(\rho, s) = (\rho^2 + s^2)^{-1}$, to write the transform of w in Eq. (4.49):

$$\hat{w}(\rho) = \frac{2}{3\pi}(\mathcal{H}(\rho, 1) - \mathcal{H}(\rho, 2) - A(\mathcal{H}(\rho, 1/\sigma) - \mathcal{H}(\rho, 2/\sigma))). \quad (4.50)$$

Substituting Eq. (4.50) in Eq. (4.48) gives the expression for the radially symmetric peak solution:

$$q(r) = \frac{4\Delta}{3}(\mathcal{W}(\Delta, r, 1) - \mathcal{W}(\Delta, r, 2) - A(\mathcal{W}(\Delta, r, 1/\sigma) - \mathcal{W}(\Delta, r, 2/\sigma))), \quad (4.51)$$

where $\mathcal{W}(\Delta, r, s)$ is defined using the following identity

$$\begin{aligned} \mathcal{W}(\Delta, r, s) &= \int_0^\infty \frac{1}{\rho^2 + s^2} J_0(\rho r) J_1(\rho \Delta) d\rho = \\ &= \begin{cases} \frac{1}{s} I_1(s\Delta) K_0(sr), & r > \Delta \\ \frac{1}{s^2 \Delta} - \frac{1}{s} I_0(sr) K_1(s\Delta), & r < \Delta \end{cases} \end{aligned} \quad (4.52)$$

and I_ν is the Bessel function of the first kind and order $\nu = 0, 1$ (Bressloff & Coombes, 2013).

The condition for the existence of the radially symmetric peak is obtained applying the condition at the boundary $U(\Delta) = h$, giving:

$$\begin{aligned} h &= \frac{4\Delta}{3} \left(I_1(\Delta) K_0(\Delta) - \frac{1}{2} I_1(2\Delta) K_0(2\Delta) \right. \\ &\quad \left. - A\sigma \left(I_1(\Delta/\sigma) K_0(\Delta/\sigma) - \frac{1}{2} I_1(2\Delta/\sigma) K_0(2\Delta/\sigma) \right) \right). \end{aligned} \quad (4.53)$$

Equation (4.53) can be used to control the onset of the working memory instability, moving the threshold to the left of the bifurcation point, as shown in the $\Delta = \Delta(h)$ plot in Fig. 4.8. The controller can present a reverse detection instability increasing the threshold beyond the bifurcation point. This adaptive threshold mechanism is implemented in the proposed model to control the emergence of the motor plan at the level of the spine during the development of the task (see Chapter 5, *the spinal memory block*).

The condition on the threshold in Eq. (4.53) is necessary to the existence of the peak solution in Eq. (4.47), but not sufficient. In fact, it should be checked that threshold h is not crossed elsewhere. Proof that $q(r)$ is monotonically decreasing in r for a general monotonic synaptic weight function can be found in the study by Folias and Bressloff (2004), although with this kernel self-sustaining pulses in absence of input are always unstable, similarly to what was found in one dimension.

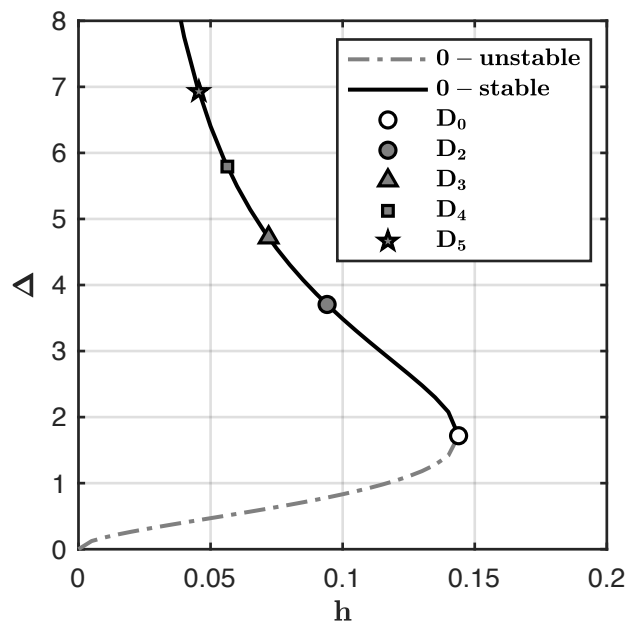


Figure 4.8: Plot of $\Delta = \Delta(h)$ for a two-dimensional neural field with Mexican hat synaptic footprint. Dashed grey line: lower branch, unstable to radially symmetric perturbations. Full black line: upper branch, stable to radially symmetric perturbations. The occurrence of azimuthal instabilities with D_m symmetry is depicted with different markers (see legend box). Parameters: $[A, \sigma, h, \alpha] = [0.25, 2, 0.12, 1]$.

4.3.2 Stability of Self-Sustaining Solutions in 2D

In the one-dimensional case the lower solution branch is always unstable, this result is confirmed for two-dimensional neural field following similar lines. On the contrary, the upper branch can encounter different types of bifurcations, leading to splitting and rotational instabilities (Owen et al., 2007). Those perturbations that can destabilise radially stable peak solution are called *azimuthal*. In this section, the focus is on finding the criteria to assign the correct parameters for self-sustaining peaks of activation used to model motor features so that they are radially and azimuthally stable.

Following the method in the study by Bressloff and Coombes (2013), a perturbation of the solution is written as $u(\mathbf{r}, t) = q(r) + u(\mathbf{r})e^{\lambda t}$. Substituting this into Eq. (4.46), and expanding to the first order gives the eigenvalue equation:

$$(\lambda + 1)u(\mathbf{r}) = \int_{\mathbb{R}^2} w(|\mathbf{r} - \mathbf{r}'|) \dot{f}(q(r')) u(\mathbf{r}) d\mathbf{r}', \quad (4.54)$$

where it is set $\alpha = 1$ to simplify notation.

The eigenvalue problem reduces to a simpler one in a similar fashion to the one-dimensional case. Rewriting Eq. (4.54) for the azimuthal perturbation $u(\Delta, \phi)$:

$$(\lambda + 1)u(\Delta, \phi) = \frac{\Delta}{|\dot{q}(\Delta)|} \int_0^{2\pi} w\left(2\Delta \sin\left(\frac{\phi - \phi'}{2}\right)\right) u(\Delta, \phi') d\phi', \quad (4.55)$$

and considering in terms of Fourier eigenmodes $u(\Delta, \phi) = u_m(\phi) = c_m e^{im\phi} + \bar{c}_m e^{-im\phi}$, leads to the expression (Bressloff & Coombes, 2013):

$$\mathcal{E}_m(\lambda) = (\lambda + 1) - \mu_m = 0 \quad (4.56)$$

where

$$\mu_m = \frac{\Delta}{|\dot{q}(\Delta)|} \int_0^{2\pi} w(2\Delta \sin(\phi/2)) e^{-im\phi} d\phi. \quad (4.57)$$

The functions $\mathcal{E}_m(\lambda)$ are a family of Evans functions for the two-dimensional peak solution (Owen et al., 2007). It is found again that λ_m is an eigenvalue for Eq. (4.46) if and only if $\mathcal{E}_m(\lambda_m) = 0$. It is possible to prove that the eigenvalue associated with the m -th mode λ_m is always real (Bressloff & Coombes, 2013).

Perturbations at the boundaries can be studied using the decomposition in terms of eigenmodes, simply taking $p(\Delta, \phi, t) = [c_m e^{in\phi} + c_m e^{-in\phi}] e^{\lambda t}$. A perturbation of order n has D_n symmetry. For instance, the $n = 0$ eigenmode represents uniform radially symmetric modifications of the boundary of the peak; the $n = 1$ represents perturbations of the spot along a symmetry axis; $n=2$ represents perturbations of the boundary that have two rotational and reflectional symmetry axes and so on (Bressloff & Coombes, 2013).

It is possible to find an expression for λ_m that can be computed numerically, using again the Bessel functions:

$$\lambda_m = -1 + \frac{\int_0^\infty \hat{w}(\rho) J_n(\rho r) J_n(\rho \Delta) \rho d\rho}{\int_0^\infty \hat{w}(\rho) J_1(\rho r) J_1(\rho \Delta) \rho d\rho}. \quad (4.58)$$

A 2D peak solution is linearly stable if $\lambda_m < 0$ for all m , $m \neq 1$ (i.e., $\lambda_1 = 0$). To find the point at which bifurcations occur, it is possible to impose $\lambda_m = 0$ in Eq. (4.58), giving:

$$1 = \mu_m = \frac{\sum_{i=1}^4 A_i K_m(\alpha_i \Delta) I_m(\alpha_i \Delta)}{\sum_{i=1}^N A_i K_1(\alpha_i \Delta) I_1(\alpha_i \Delta)} \quad (4.59)$$

where, for w defined in Eq. (4.49), $(A_1, A_2, A_3, A_4; \alpha_1, \alpha_2, \alpha_3, \alpha_4) = [1, -1, -A, A; 1, 2, 1/\sigma, 2/\sigma]$, $A, \sigma > 0$ (Bressloff & Coombes, 2013).

The calculation of the second of the points given by Eq. (4.59) (D_2 in Fig. 4.8) gives the criterion for the selection of the threshold value that guarantees stable peaks in two-dimensional neural fields, fixed the parameters relative to the synaptic footprint A and σ . This type of stability is required to represent the set of motor primitives (see Chapter 5 *the spinal memory block*).

Considering the upper branch solution in Fig. 4.8, decreasing the threshold leads

to bifurcations that break rotational symmetry reflecting the order m of the eigenvalue that is dominant. A numerical simulation of the shapes assumed by the destabilised peak solution is shown in Fig. 4.9 for illustrative purpose.

Splitting and rotational instabilities due to angular perturbations are further discussed in the study by Owen et al. (2007), where the emergence of multi-bump solutions and labyrinthine patterns is analysed. These patterns could be of interest for the future developments of elemental behaviour (EB) in the DFT, encoding more complex motor patterns.

In the present study, it was decided to include, as an additional EB, a stable peak solution that can travel on the space of features spanned by the neural field. In the next section the condition to trigger this type of instability are presented.

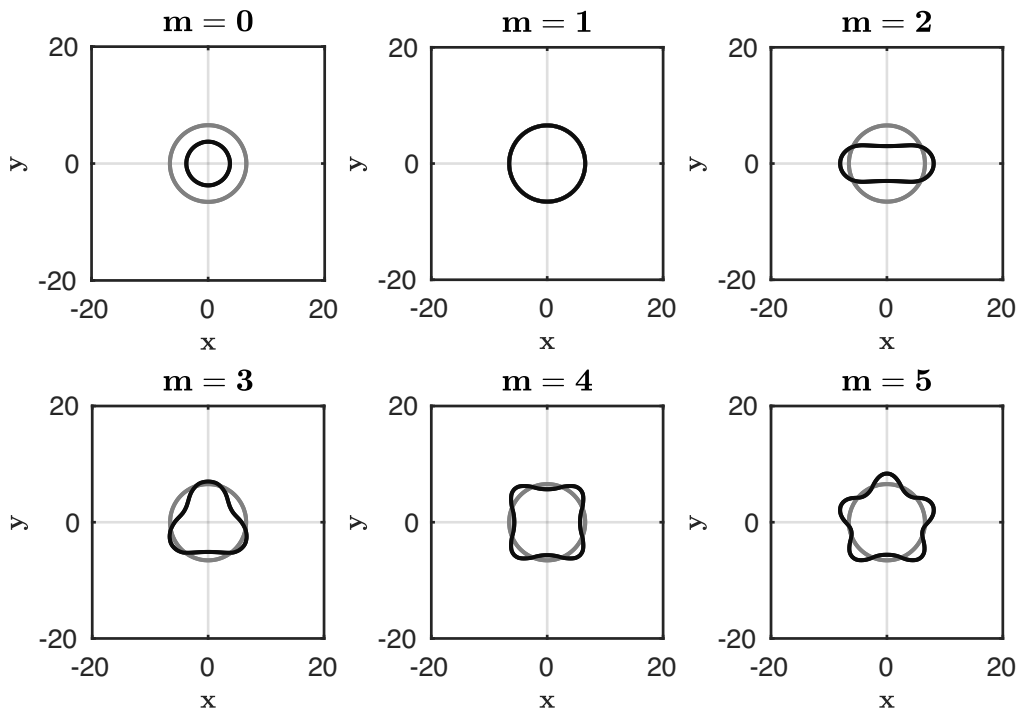


Figure 4.9: Examples of D_m -symmetry solutions for instabilities with dominant modes m from 0 to 5. In black: solutions after bifurcation point; in grey: radially symmetrical stable solution. Parameters: $[A, \sigma, h_{stable}, \alpha] = [0.25, 2, 0.12, 1]$; critical threshold for the m -th mode $h_m = [0.1439, n/a, 0.0941, 0.0720, 0.0564, 0.0456]$.

4.3.3 Adaptation and Drifting Instability

Modelling adaptation separately in two-dimensional neural fields leads to a secondary bifurcation that includes the formation of rotating waves and, for strong enough adaptation weight g , of the travelling peak solution of interest (Owen et al., 2007). Here, methods to investigate the emergence of *the drifting instability* are reviewed, following the study on boundary perturbations by Coombes et al. (2012). Numerical methods to build travelling peaks (or travelling spots) are developed in Chapter 5 and their role in DNFs architectures is discussed in Chapter 6.

The field with linear adaptation in two dimensions is defined by:

$$\begin{aligned} \frac{1}{\alpha} \frac{\partial u(\mathbf{r}, t)}{\partial t} &= -u(\mathbf{r}, t) + \int_{\mathbb{R}^2} w(|\mathbf{r} - \mathbf{r}'|) f(u(\mathbf{r}', t)) d\mathbf{r}' - ga(\mathbf{r}, t) \\ \frac{\partial a(\mathbf{r}, t)}{\partial t} &= -a(\mathbf{r}, t) + u(\mathbf{r}, t). \end{aligned} \quad (4.60)$$

It is possible to construct a radially symmetrical solution of radius Δ , following a similar procedure to the one presented in the previous section, and then find the condition for its propagation. For compactness, it is introduced the following function

$$\begin{aligned} \Psi(r) &= \int_0^{2\pi} \int_0^\Delta w(|r - r'|) r' dr' d\phi = \\ &= \frac{4\Delta}{3} (\mathcal{W}(\Delta, r, 1) - \mathcal{W}(\Delta, r, 2) - A(\mathcal{W}(\Delta, r, 1/\sigma) - \mathcal{W}(\Delta, r, 2/\sigma))), \end{aligned} \quad (4.61)$$

where $\mathcal{W}(\Delta, r, s)$ is defined in Eq. (4.52).

A radially symmetrical solution for the field with adaptation in Eq. (4.60) is simply a scaled version of Eq. (4.47) (Coombes et al., 2012):

$$q(r) = \frac{1}{(1+g)} \Psi(r). \quad (4.62)$$

The necessary condition for existence can be found substituting $h \rightarrow h(1+g)$ in Eq. (4.53), giving:

$$\begin{aligned}
 h(1+g) &= \frac{4\Delta}{3} \left(I_1(\Delta)K_0(\Delta) - \frac{1}{2}I_1(2\Delta)K_0(2\Delta) + \right. \\
 &\quad \left. - A\sigma \left(I_1(\Delta/\sigma)K_0(\Delta/\sigma) - \frac{1}{2}I_1(2\Delta/\sigma)K_0(2\Delta/\sigma) \right) \right) \\
 &\equiv F(\Delta),
 \end{aligned} \tag{4.63}$$

Solving $F'(\Delta_c) = 0$ gives the critical value of the radius of the bump $\Delta = \Delta_c$, corresponding to a fold bifurcation. In the phase plane (h, Δ) existence of solutions is limited by $h < F(\Delta_c)/(1+g)$. This gives the condition to simulate self-sustaining peak solutions in a two-dimensional neural field with adaptation. Plots of the curves $\Delta = \Delta(h)$ and $\Delta = \Delta(g)$ are shown in Fig. 4.10.

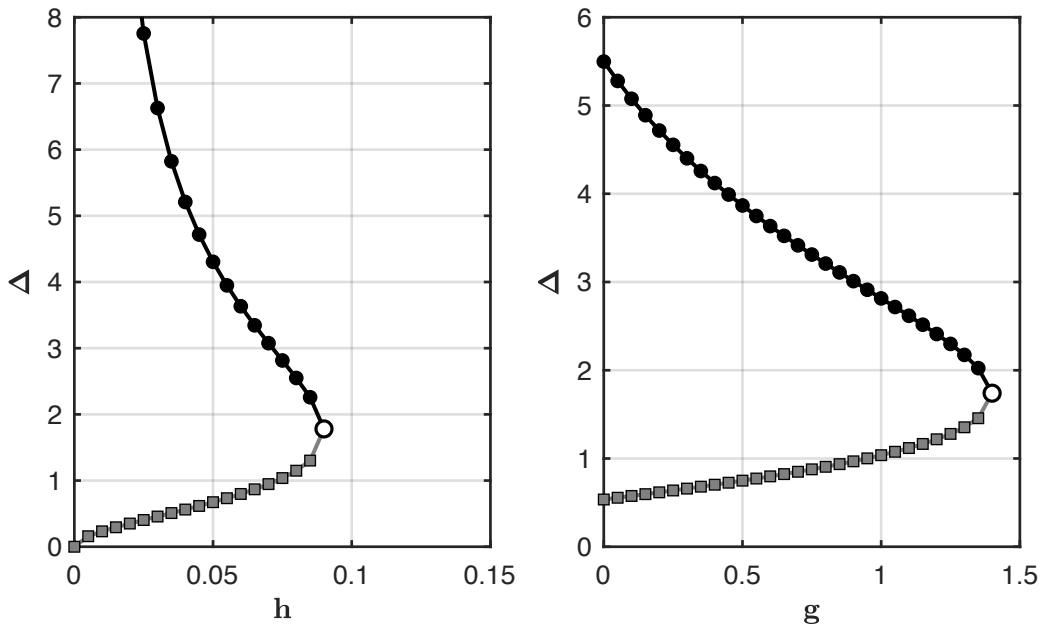


Figure 4.10: Bifurcation plots for a two-dimensional neural field with adaptation. Solution radius Δ is plotted as a function of threshold h (left) and adaptation gain g (right). Grey squares: lower branch, unstable. Black dots: upper branch, for details on stability of this branch see text. Parameters: $[A, \sigma, \alpha] = [0.25, 2, 1]$.

Following the analysis carried out in the study by Coombes et al. (2012), travelling peaks are describes as emerging from the dynamic of the field as drifting instabilities

occurring as a consequence of variations in α , with speed and direction defined by the vector \mathbf{c} , $c = |\mathbf{c}|$.

To represent a travelling spot solution, the field in Eq. (4.46) can be written in a co-moving framework $\xi = \mathbf{x} + \mathbf{c}t$. The equation of the field becomes:

$$\begin{aligned}\frac{1}{\alpha} \mathbf{c} \cdot \nabla_{\xi} u &= -u + \Psi - ga \\ \mathbf{c} \cdot \nabla_{\xi} a &= -a + u.\end{aligned}\tag{4.64}$$

From Eq. (4.64), the authors consider a weak distortion of the circular wave, defining a moving framework $\xi = (\xi_1, \xi_2)$ and rewriting the travelling solution as follows (Coombes et al., 2012):

$$u(\xi_1, \xi_2) = \frac{1}{c} \int_{-\infty}^{\xi_1} dy \eta((\xi_1 - y)/c) \Psi\left(\sqrt{y^2 + \xi_2^2}\right),\tag{4.65}$$

where the usual Green's functions notation is used.

It can be noted that the boundary condition $u(\xi)|_{\xi=\mathbf{r}} = h$ holds only for a radially symmetrical bump (i.e., $\xi_1^2 + \xi_2^2 = \Delta^2$), and can therefore be met only if $c = 0$. The travelling solution in Eq. (4.65), in fact, depends on the general shifting direction θ by the coordinate ξ_1 .

To construct the Evans function associated with the travelling solution, it is sufficient to find the eigenvalues λ_m associated with perturbations of the radius of the pulse of the type $\delta\Delta(\theta, t) = \epsilon e^{\lambda_m t} \cos(m\theta)$, δ and ϵ small.

For this particular case, it is found that (Coombes et al., 2012):

$$\mathcal{E}_m(\lambda) = \frac{1}{\hat{\eta}(\lambda)} - (1 + g)\mu_m,\tag{4.66}$$

Taking w as in Eq. (4.49), the expression of μ_m is the same given in Eq. (4.59), with the same parameters and the transform of the synaptic filtering function

$$\hat{\eta}(\lambda) = \frac{\alpha(1 + \lambda)}{(\lambda + \lambda_+)(\lambda + \lambda_-)},\tag{4.67}$$

with

$$\lambda_{\pm} = \frac{1 + \alpha \pm \sqrt{(1 + \alpha)^2 - 4\alpha(1 + g)}}{2}. \quad (4.68)$$

The mode of interest to simulate a traveling peak solution is $m = 1$, for which $\mu_m = 1$. The associated eigenvalues, given by the solutions of $\hat{\eta}(\lambda) = 1/(1 + g)$, are $\lambda = 0$ and $\lambda = \alpha g - 1$. The mode becomes unstable for the critical value $g \geq 1/\alpha$, as illustrated in Fig. 4.11, where the real and imaginary part zero contours are plotted, showing the crossing of the eigenvalue to the right-hand side of the plane (Coombes & Owen, 2004).

It can be noted that, for $m = 0$, Eq. (4.66) gives

$$\mu_0 = \frac{1 + \alpha}{\alpha(1 + g)} \quad (4.69)$$

so that for the same value $g \geq 1/\alpha$ a breathing instability can emerge with frequency $\omega = \sqrt{\alpha g - 1}$ (Coombes & Owen, 2004).

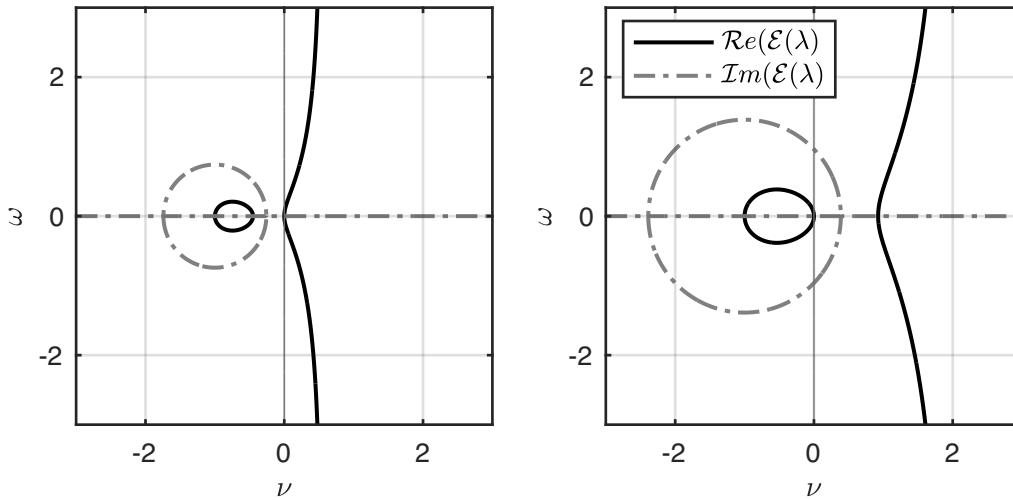


Figure 4.11: Plot of the zero contours of the real and imaginary part of the Evans function ($\lambda = \nu + i\omega$) associated with the bifurcation of a radially symmetric solution with respect to mode $m = 1$. Left: stable solution. Right: solution after bifurcation for $g > 1/\alpha$. Parameters: $[A, \sigma, g, h] = [0.25, 2, 0.55, 0.12/(1 + g)]$.

Simulating a drifting instability as a new element of cognition in DFT, the coexistence of a breather dynamic beyond the same bifurcation point must be taken

into account. Numerical construction of travelling spots, using the condition in Eq. (4.63) and choosing the adaptation gain above the critical value, is carried out in Section 5.4.3.

4.4 Robotic Control Dynamics

In the architecture for motor control proposed in this thesis, a control law for a robotic manipulator is designed drawing inspiration from the spatial organisation of circuitry of the spinal cord (Bizzi et al., 1992; Giszter et al., 1993; Mussa-Ivaldi et al., 1994) and from the concept of motor primitive introduced in Chapter 2.

To test the neural controllers developed for spinal motor control using Dynamic Neural Fields, a planar model of a two revolute joint actuator is used. In this last section of the Methods, the equations used to model the robotic interface are presented. Relevant concepts regarding robotic controls are reviewed: these are used in Chapter 5 to motivate the design and to assess the stability of the proposed control law, *the spinal attractor model*.

4.4.1 Kinematics and Dynamics of a 2-R Manipulator

A robotic manipulator is an ensemble of n rigid bodies called *links* connected by contact at a point called *joint* that can be *revolute* or *prismatic*. Revolute joints (R) allow for relative rotation between links; prismatic joints (P) allow for relative translation. For each joint axis, the coordinate called *joint coordinate* or *joint variable* describes the relative position of two links connected by a joint (Murray et al., 2017).

Each prismatic or revolute joint provides one degree of freedom to the robotic manipulator which typically possesses six degrees of freedom (DoF). A manipulator that has more than six degrees of freedom is called kinematically *redundant*. The term manipulator is used interchangeably with robot, although the manipulator is specifically the structural body made of links and joints, whereas the robot itself is composed by the manipulator and the control system that guides it (Murray et al., 2017).

The link that is grounded is called link 0. The distal part of the kinematic chain made by n links is referred to as *end effector*. This part is the one that performs the task for which the robot has been programmed. The space that the end effector can

reach is called *workspace*, which is subject to the geometry of the manipulator and the joint constraints.

Links and joints form the kinematic chain of the robot and the study of their displacement (change in position and/or orientation) in time of is called *kinematics*. Describing kinematically a manipulator is essential to write the system of equations that describe the *dynamics* of the system. These take into account the movement of the manipulator related to the torques applied at the joints. The equations of motion of the manipulator are used to design control strategies and to program the robot for the destination of use. This process goes under the name of *robot control* (Murray et al., 2017).

Kinematics

The two revolute joints (2-R) planar manipulator illustrated in Fig. 4.12 is used to perform simulations of voluntary movements using the proposed model for spinal motor control. The robot is composed by two rigid elements of length l_1 and l_2 linked to three joints:

- the joint (**0**) that allows the link l_1 to rotate on the plane;
- the joint (**1**) that connects segments l_1 and l_2 allowing relative rotation;
- the joint (**2**) that has zero DoF and represents the end effector of the manipulator.

The origin of a set of Cartesian axes is fixed in correspondence with joint (**0**). The joint variables of this system are the angles that describe the rotation of the links around the joint axes perpendicular to the plane: θ_1 and θ_2 .

Kinematic analysis of the robotic chain is formalised into two problems that are called the *forward kinematic problem* and the *inverse kinematic problem*. Solution to the forward kinematic problem consists in finding the position of the end effector, known the values of the joint variables. This can be written, for a set of coordinates

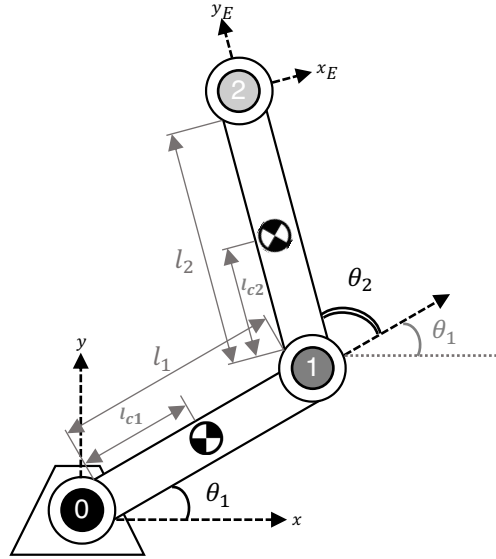


Figure 4.12: The planar manipulator with two revolute joints.

representing the position of the end effector (x_E, y_E) and a general n -link manipulator, as a function of the angles associated with each revolute joint (Murray et al., 2017):

$$(x_E, y_E) = f_{forward}(\theta_1, \theta_2, \dots, \theta_n). \quad (4.70)$$

Solution to the inverse kinematics consists in finding the configuration in terms of joint variables for which the end effector will reach the required target position in the workspace:

$$(\theta_1, \theta_2, \dots, \theta_n) = f_{inverse}(x_E, y_E). \quad (4.71)$$

For the two-link manipulator of choice, the position of the end effector (x_E, y_E) can be written as a function of the angles θ_1 and θ_2 as follows:

$$\begin{aligned} x_E &= x_1 + l_2 \cos(\theta_1 + \theta_2), \\ y_E &= y_1 + l_2 \sin(\theta_1 + \theta_2), \end{aligned} \quad (4.72)$$

where (x_1, y_1) are the coordinates defining the position of joint (1)

$$\begin{aligned} x_1 &= l_1 \cos \theta_1, \\ y_1 &= l_1 \sin \theta_1. \end{aligned} \tag{4.73}$$

Equations (4.72) represent the forward kinematic description of the robot of choice and they are used to compute the position of the end effector during simulations (Jazar, 2007). Variations in time of the end effector coordinates produce the trajectory

$$\mathcal{T}(t) = (x_E(t), y_E(t)). \tag{4.74}$$

Dynamics

The movement of the robotic chain in time can be studied writing the equations of motion of the system of interest. This step allows for simulations of motion and for the design and control of the robotic system; i.e., to program the manipulator to perform the desired trajectory. In a similar way, it is possible to identify the so-called *forward dynamic problem* and the *inverse dynamic problem* (Murray et al., 2017).

Direct dynamics evaluation consists in predicting the motion of the manipulator for a given initial state $\mathcal{T}(0)$ and under some known torques $\boldsymbol{\tau}$ active at the joints:

$$\mathcal{T}(t) = f_{forward}(\boldsymbol{\tau}, \mathcal{T}(0)). \tag{4.75}$$

This is equivalent to simulating the system behaviour for some torques applied at the joints.

Inverse dynamics aims at finding the activations, forces or torques, that give as a result a desired trajectory, specified by a kinematic set of positions, velocities and accelerations:

$$\boldsymbol{\tau} = f_{inverse}(\mathcal{T}(t)). \tag{4.76}$$

This immediately translates into finding appropriate control signals so that the end effector moves in the desired way. It is found again, in terms of robotic controls, the degrees of freedom problem (see Chapter 2 for the DoF problem).

The Lagrange formulation can be used to describe the motion of a robotic manipulator. The Lagrange equation of motion for a generic manipulator with n links is (Jazar, 2007):

$$\mathbf{M}(\boldsymbol{\theta})\ddot{\boldsymbol{\theta}} + \mathbf{C}(\boldsymbol{\theta}, \dot{\boldsymbol{\theta}})\dot{\boldsymbol{\theta}} + \mathbf{G}(\boldsymbol{\theta}) = \boldsymbol{\tau} \quad (4.77)$$

where $\boldsymbol{\theta}$ is the vector of the joint state variables and $\boldsymbol{\tau}$ is the vector of external torques at the joints. Eq. (4.77) has three terms:

- *the inertial term* takes into account the inertial forces and $\mathbf{M}(\boldsymbol{\theta})$ is the $n \times n$ *inertia matrix* for the manipulator;
- *the velocity coupling term* represents velocity coupling between links and $\mathbf{C}(\boldsymbol{\theta}, \dot{\boldsymbol{\theta}})\dot{\boldsymbol{\theta}}$, also represented by the notation $\mathbf{H}(\boldsymbol{\theta}, \dot{\boldsymbol{\theta}})$, is referred to as the *velocity coupling vector*;
- *the gravitational term* represents the gravitational force acting on the manipulator and $\mathbf{G}(\boldsymbol{\theta})$ is the *gravitational force vector*.

For a detailed derivation of the Lagrange equation from the Lagrangean applied to a multi-link robot see the book by Jazar (2007).

Consider again the manipulator used here in Fig. 4.12, with links of length l_1 and l_2 , mass m_1 and m_2 , centre of mass l_{c1} and l_{c2} and moment of inertia I_1 and I_2 respectively. Since it is of interest the performance of reaching tasks where the robot is restrained to the plane, resultant gravitational forces acting on it are considered zero and Eq. (4.77) simplifies as follows:

$$\mathbf{M}(\boldsymbol{\theta})\ddot{\boldsymbol{\theta}} + \mathbf{C}(\boldsymbol{\theta}, \dot{\boldsymbol{\theta}})\dot{\boldsymbol{\theta}} = \boldsymbol{\tau}. \quad (4.78)$$

In the case of study, the state variables and the required torques at the joints are represented by 2×2 vectors:

$$\boldsymbol{\theta} = \begin{bmatrix} \theta_1 \\ \theta_2 \end{bmatrix},$$

and

$$\boldsymbol{\tau} = \begin{bmatrix} \tau_1 \\ \tau_2 \end{bmatrix},$$

The inertia matrix and the velocity coupling matrix are given by

$$\mathbf{M}(\boldsymbol{\theta}) = \begin{bmatrix} d_{11} & d_{12} \\ d_{21} & d_{22} \end{bmatrix}, \quad \mathbf{C}(\boldsymbol{\theta}, \dot{\boldsymbol{\theta}}) = c_h \begin{bmatrix} \dot{\theta}_2 & \dot{\theta}_1 + \dot{\theta}_2 \\ -\dot{\theta}_1 & 0 \end{bmatrix}, \quad (4.79)$$

where $c_h = -m_2 l_1 l_{c2} \sin(\theta_2)$ and the inertia matrix coefficients are

$$\begin{aligned} d_{11} &= m_1 l_{c1}^2 + m_2 (l_1^2 + l_{c2}^2 + 2l_1 l_{c2} \cos \theta_2) + I_1 + I_2, \\ d_{12} &= m_2 (l_{c2}^2 + 2l_1 l_{c2} \cos \theta_2) + I_2, \\ d_{22} &= m_2 l_{c2}^2 + I_2, \\ d_{12} &= d_{21}. \end{aligned} \quad (4.80)$$

Equation (4.78) represents the description of the dynamics of the system. Solution to this equation and to the direct kinematics in Eq. (4.72) give the trajectory in time of the end effector. Determining the appropriate torques for the desired motor task is also a core problem of robotic control design. A schematic representation of the forward and inverse problems is presented in Fig. 4.13.

From the perspective of human motor control, strategies to address the DoF problem are discussed using the traditional and the embodied approach in Chapter 2 and in Chapter 3, respectively.

In contrast to the reviewed architecture in the DFT framework in Section 3.4.1, the model proposed in Chapter 5 does not require the solution of the inverse dynamics in Eq. (4.76). The desired behaviour is achieved building a control law physiologically inspired to guide the manipulator. It is necessary to consider principles of control dynamics, introduced in the following section, to understand the proposed design and to address the stability of the proposed control law.

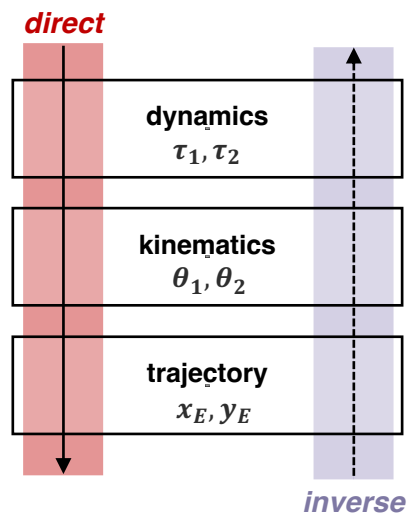


Figure 4.13: Representation of the forward and inverse problem, giving the equivalent of the degrees of freedom problem in robotic control theory.

4.4.2 Design and Stability of Robotic Controls

To determine the trajectory of the end effector in Cartesian space, it is necessary to transform it in joint space, solving the inverse kinematics in Eq. (4.71). Directly solving the inverse dynamic in Eq. (4.76) gives the appropriate motor commands to guide a robotic manipulator.

Supposing to have solved this problem and to have a trajectory $\mathcal{T}(t)$ and the associated kinematics expressed by $\theta_d(t)$, strategies from traditional control theory allow for the torque update during simulations and error compensation using the online position of the joints, in order to get the end effector to perform the desired trajectory with a certain robustness against perturbations (Jazar, 2007).

In this section, elements of robotic controls are reviewed. In the following, they are used to formalise the physiologically inspired control law for the model of the spinal cord. The information encoded using neural fields and the concept of motor summation, in fact, have to be translated into the torques (or the forces) at the joints directly, resulting in a robotic system that is stable. This is tested performing reaching tasks without recurring to the solution of its inverse dynamics satisfying the

fourth aim (see Chapter 1 for the list of aims).

Firstly, the introduction of feedback dynamics to stabilise the controller is motivated, considering the poor performances of open loop controls and briefly discussing the implications of Lyapounov and asymptotic stability. Subsequently, attractor dynamic controllers are presented. The final formulation of the spinal attractor model, in fact, includes two terms that can be rewritten as a function of the error signal (i.e., current position – set point) resembling a proportional and derivative controller. This gives the criteria by which parameters of the control law can be set to have the desired stability for the proposed model.

Lastly, the desired trajectory can be achieved considering robotic controls designed in joint space (*joint space control*) or, avoiding the direct solution of inverse kinematics, directly in workspace coordinates (*workspace control*) (Murray et al., 2017). The reason behind the development of the model using the latter is clarified, considering the difference of the simulated trajectories. It is shown that the space in which the control law is designed affects one of the most important invariants when considering reaching tasks: using a control law developed in workspace coordinates grants trajectories that are straight (see Section 2.2.3 for relevant invariants of voluntary movements). Furthermore, using the Lagrange equations in the same space for simulations avoids the computation of the inverse kinematics.

Open loop and feedback control

Given the manipulator dynamics as described in Eq. (4.78), consider the desired joint trajectory $\theta_d(t)$ to be tracked by the end effector. Consider the initial conditions $\theta(0) = \theta_d(0)$ and $\dot{\theta}(0) = \dot{\theta}_d(0)$, appropriate control torques are simply:

$$\tau = \mathbf{M}(\theta_d)\ddot{\theta}_d + \mathbf{C}(\theta_d, \dot{\theta}_d)\dot{\theta}_d. \quad (4.81)$$

It follows that $\theta(t) = \theta_d(t)$ for all $t \geq 0$. This type of control does not use the current state of the system to update input torques and, for this reason, it is an example of *open-loop* control. Open loop control does not allow for error correction

and thus it is not very robust (Murray et al., 2017). Selected a configuration near the desired one at the beginning, the trajectory of the robot will not necessarily follow it at all times, since the system cannot compensate for noise, delays or adjust the trajectory based on information on the current position online (Murray et al., 2017; Wolpert, 1997).

Open loop control cannot account for online sensory-motor integration, that is one of the prerequisites to model voluntary movements in the embodied account. In order to have the manipulator trajectory converging to the desired one using some level of sensory-motor integration, one can introduce an appropriate feedback mechanism in our control system (e.g., a visual input).

Allowing initial conditions to be corrected by the dynamic of the system requires adding a feedback mechanism to Eq. (4.81). The resultant control law, refined using the current position and velocity of the manipulator at time t , can be written as follows:

$$\boldsymbol{\tau} = \mathbf{M}(\boldsymbol{\theta})(\ddot{\boldsymbol{\theta}}_d - \mathbf{K}_v\dot{\mathbf{e}} - \mathbf{K}_p\mathbf{e}) + \mathbf{C}(\boldsymbol{\theta}, \dot{\boldsymbol{\theta}})\dot{\boldsymbol{\theta}}, \quad (4.82)$$

where $\mathbf{e} = \boldsymbol{\theta} - \boldsymbol{\theta}_d$, \mathbf{K}_v and \mathbf{K}_p are constant gain matrices and both the current position of the end effector and of the target goal are considered.

Equation (4.82) goes by the name of *computed torque control law* (Murray et al., 2017). Since the inertia matrix is always positive definite, the dynamic of the error signal \mathbf{e} simply follows:

$$\ddot{\mathbf{e}} + \mathbf{K}_v\dot{\mathbf{e}} + \mathbf{K}_p\mathbf{e} = 0 \quad (4.83)$$

which is a linear differential equation that gives to the system the desired stability. In fact, for an appropriate choice of \mathbf{K}_v and \mathbf{K}_p , it is easy to prove that error \mathbf{e} tends to 0 exponentially for $t \rightarrow \infty$. In this sense, this is an example of *feedback linearisation* (Murray et al., 2017). Once feedback is introduced in the model, it is possible to analyse its stability using linear control tools applied to the dynamics of the feedback signal. Ideally, if the trajectory to follow consist in a single target point, the system

in closed loop should have a stable attractor at this point, asymptotically.

An alternative approach consists in the design of a controller that uses a linearised system around an operating point, in an attractor dynamic fashion. It is possible to prove that, when linearisation of a nonlinear system exists, the study of stability of the linearised system determines the local stability of the nonlinear system according to Lyapunov's methods (Murray et al., 2017). Since stability of the linearised system implies local stability of the full system, it is often possible to give proof of global stability using Lyapunov's methods for this type of controllers (Murray et al., 2017). A relevant example is the Proportional and Derivative (PD) control law that has the form:

$$\boldsymbol{\tau} = -\mathbf{K}_v \dot{\mathbf{e}} - \mathbf{K}_p \mathbf{e}, \quad (4.84)$$

\mathbf{K}_v and \mathbf{K}_p are positive definite matrices and $\mathbf{e} = \boldsymbol{\theta} - \boldsymbol{\theta}_d$ is the error signal, as before. It can be proved that this type of controller gives setpoint stabilisation asymptotically (Murray et al., 2017).

The model proposed to simulate the development of a motor plan at the level of the spine uses sensory feedback that guarantees convergence to the equilibrium point set using a combination of motor primitives and efferent activation signals. The result is a stable attractor dynamic for the same feedback linearisation principle (see Chapter 5). Elements of bifurcation theory applied to nonlinear systems that use such methods go beyond the purpose of this section; for a comprehensive discussion see the book by Kuznetsov (1996).

Workspace control

Until now, the control problem has been addressed considering a configuration of the end effector as a function of time and solving the inverse kinematic so as to find the desired joint angles for the desired trajectory.

In the proposed architecture for motor control, control dynamics of the end effector are designed in workspace coordinates. This choice was made considering that most

of the empirical findings on pointing and reaching tasks describe typical features of voluntary movement in terms of features of the end effector trajectory, for example straightness and bell-shaped velocity profiles (see Chapter 2 for a review of properties of voluntary movements). In support of this choice, empirical studies have found that clustering of voluntary movements analysed in workspace coordinates (i.e., Cartesian) are successfully represented by a small number of motor primitives (Miranda et al., 2018, see Chapter 6).

The set used to parameterise the workspace is the one introduced in Eq. (4.72) that can be compactly written as follows:

$$\mathbf{x} = \begin{bmatrix} x_E \\ y_E \end{bmatrix}.$$

The Jacobian matrix associated with the configuration of the manipulator in Fig. 4.12 is a function of joint variables $\boldsymbol{\theta}$ and can be written from Eq. (4.72) as follows:

$$\mathbf{J}(\boldsymbol{\theta}) = \begin{bmatrix} -l_1 \sin(\theta_1) - l_2 \sin(\theta_1 + \theta_2) & -l_2 \sin(\theta_1 + \theta_2) \\ l_1 \cos(\theta_1) + l_2 \cos(\theta_1 + \theta_2) & l_2 \cos(\theta_1 + \theta_2) \end{bmatrix}. \quad (4.85)$$

Using the relationships

$$\dot{\boldsymbol{\theta}} = \mathbf{J}^{-1} \dot{\mathbf{x}} \quad \text{and} \quad \ddot{\boldsymbol{\theta}} = \mathbf{J}^{-1} \ddot{\mathbf{x}} + \frac{d}{dt} (\mathbf{J}^{-1}) \dot{\mathbf{x}}, \quad (4.86)$$

The dynamics of the manipulator in workspace coordinates are given by (Murray et al., 2017):

$$\widetilde{\mathbf{M}}(\boldsymbol{\theta}) \ddot{\mathbf{x}} + \widetilde{\mathbf{C}}(\boldsymbol{\theta}, \dot{\boldsymbol{\theta}}) \dot{\mathbf{x}} = \mathbf{F} \quad (4.87)$$

where $\widetilde{\mathbf{M}}$ and $\widetilde{\mathbf{C}}$ are called the *effective* parameters of the system and they are given by the following transformations:

$$\begin{aligned} \widetilde{\mathbf{M}} &= \mathbf{J}^{-T} \mathbf{M} \mathbf{J}^{-1}, \\ \widetilde{\mathbf{C}} &= \mathbf{J}^{-T} \left(\mathbf{C} \mathbf{J}^{-1} + \mathbf{M} \frac{d}{dt} (\mathbf{J}^{-1}) \right), \\ \mathbf{F} &= \mathbf{J}^{-T} \boldsymbol{\tau}. \end{aligned} \quad (4.88)$$

Using Eqs. (4.88) it is possible to eliminate θ from Eq. (4.87) so that an expression identical to the Lagrange formulation in Eq. (4.78) is found again, transformed in workspace coordinates. Results on the stability of the previous control laws in open loop, feedback and the proportional derivative control, can be immediately extended to workspace coordinates (Asada & Slotine, 1991). The computed torque law in Eq. (4.82) becomes for instance:

$$\mathbf{F} = \widetilde{\mathbf{M}}(\mathbf{x})(\ddot{\mathbf{x}}_d - \mathbf{K}_v\dot{\mathbf{e}} - \mathbf{K}_p\mathbf{e}) + \mathbf{C}(\mathbf{x}, \dot{\mathbf{x}})\dot{\mathbf{x}}, \quad (4.89)$$

where \mathbf{x}_d is the desired trajectory in workspace coordinates and error is defined as $\mathbf{e} = \mathbf{x} - \mathbf{x}_d$. Linear stability depends on the dynamics of the error signal that can be expressed as in Eq. (4.83). In a similar fashion, the PD control law can be written as follows:

$$\mathbf{F} = -\mathbf{K}_v\dot{\mathbf{e}} - \mathbf{K}_p\mathbf{e}. \quad (4.90)$$

The difference between joint and workspace control is easy to understand using the following example. Consider the computed torque control in Eq. (4.82), for instance, and apply it to the planar manipulator defined in Eq. (4.72) in both spaces, (θ_1, θ_2) and (x_E, y_E) . Joint control gives straight trajectories in joint space $\boldsymbol{\theta}$ and curved trajectories in workspace coordinates \mathbf{x} , as shown in Fig. 4.14 where trajectories in both spaces are presented.

Workspace control produces straight trajectories in the workspace coordinates \mathbf{x} and curved ones in the joint space $\boldsymbol{\theta}$, as shown in Fig. 4.15 (Murray et al., 2017). Using workspace control is then ideal for the present study, where the aim is to create and test physiologically inspired controllers that produce trajectories with human-like features.

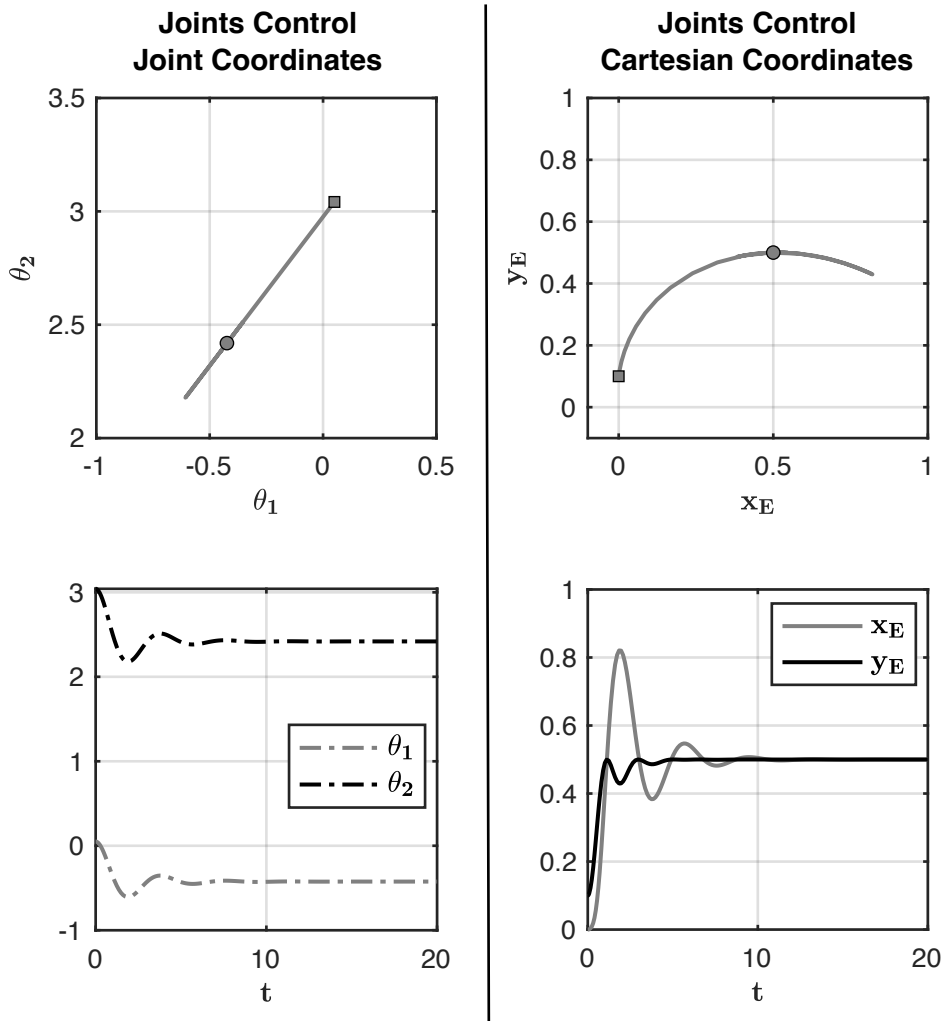


Figure 4.14: Joint space control using the computed torque control law for a 2-R planar manipulator. Top left: resultant trajectory in joint space (square = initial position, circle = target); bottom left: joints variables time course. Top right: same trajectory in Cartesian coordinates; bottom right: workspace coordinates time course.

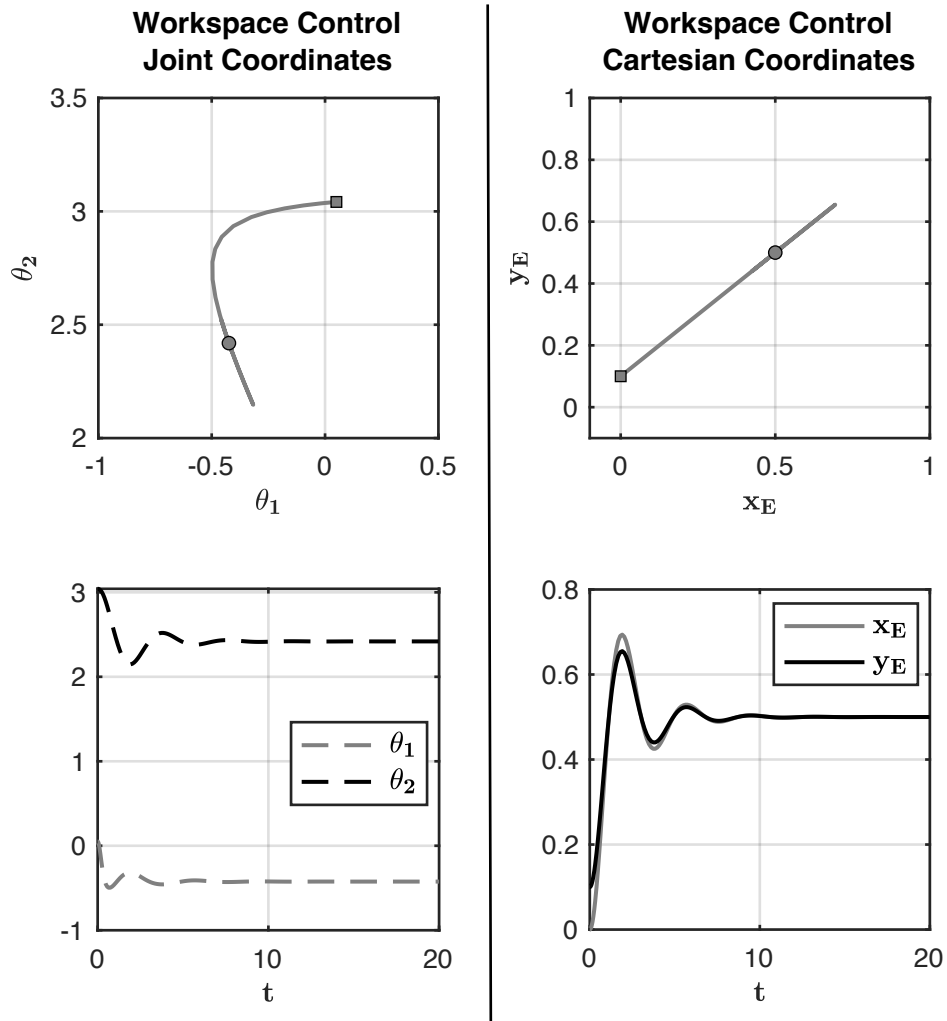


Figure 4.15: Workspace control using the computed torque control law for a 2-R planar manipulator. Top left: resultant trajectory of the end effector in joint space (square = initial position, circle = target); bottom left: joints variables time course. Top right: same trajectory in Cartesian coordinates; bottom right: workspace coordinates time course.

4.5 Conclusions

In this chapter a unified methodology to perform bifurcation analysis for the neural field equation is introduced together with the mathematical formulation of the robotic interface, used for simulations, and elements of robotic controls.

From the initial study on stability of solutions to the neural field equation carried out by Amari, methods that use an associated linear operator to find the bifurcation points have been developed. Here this approach is derived for a one-dimensional neural field in the case of negligible space dependant delays. The appropriate selection of parameters for neural controllers allows for self-sustaining and self-stabilising peaks used to model activations and autonomy in the proposed model (**Aim 2**).

Methods for the study of stability of self-sustaining peak solutions in two-dimensional neural fields are reviewed for the construction of a DNFs representation of motor primitives (**Aim 2**). This study of stability represents a powerful tool to develop neural controllers in DFT and it could also expand the repertoire of elemental behaviours. For this reason, the study of drifting instability is presented (**Aim 3**).

The planar manipulator used to test the behaviours of DNFs architecture is described (**Aim 4**) together with the robotic formulation of the degrees of freedom problem. Considerations on robotic stability are reviewed, using an example of feedforward and feedback control techniques. A description of the motor task in terms of invariant properties of voluntary movements and empirical findings on motor primitives justifies the selection of workspace control design (**Aim 1**).

In the following chapter, the neural controllers outlined here are linked together to give the proposed model for spinal motor control. The study of stability gives the criteria to model selection, working memory and reverse instability and to simulate a new elemental behaviour. A novel control law, developed in workspace coordinates and based on motor primitives summation in DFT, replaces the computation of inverse dynamics and kinematics.

Chapter 5

A Physiologically Based Model for Spinal Motor Control

5.1 Introduction

The main goal of the proposed approach is to create a new framework for modelling motor control where physiological mechanisms can be easily introduced, in the attempt to find better solutions for the ultimate problem of motor redundancy. Despite the existence of architectures that model autonomy, sensory-motor integration and learning with a good level of embodiment, this problem is often left to traditional control theory (see Chapter 3).

Furthermore, this kind of approach cannot be used to infer physiological processes involving the musculoskeletal system and its interaction with the environment, from which, ultimately, movement emerges. A better understanding of how the abundance of solutions that biological systems offer to motor problems could contribute to improved robotic solutions in return. In fact, traditional control strategies have shown limited adaptability in unconstrained environments (i.e., every environment except the one they were built for; Brooks, 1991; Pfeifer et al., 2007).

In the proposed framework, the redundancy problem is addressed at the level of

the spinal cord by designing a simple model for motor primitives summation in a DFT-based architecture, tested using a planar manipulator performing reaching tasks. The proposed model, inspired by the empirical finding of spinal force fields (see Chapter 2), gives a mathematical representation of the concept of motor primitive. Each primitive describes a field converging to a fixed point that can be easily represented with the *attractor dynamic* offered by neural fields. A combination of spinal attractors, selected by signals that can be modelled using existing neural fields for cortical motor planning and motor learning (as the one presented in Section 3.4.1), gives the DNF representation of the resultant motor plan at the spinal level, in a way that is compatible with models of muscle synergies (like the one presented in Section 2.3).

In Section 5.2 the concept of motor primitive is formalised mathematically, introducing the attractor dynamic applied to a point mass to exemplify the motor primitives summation concept. The model is then extended to the 2-R link manipulator described in Chapter 4, giving the final control law representative of the proposed model, called *the spinal attractor model* (SAM).

In Section 5.3 the neural field architecture that models motor control is presented in its parts: one encoding the principle of motor summation and one regulating the development of the motor plan in the spinal cord, using an adaptive threshold to guide elemental behaviours. Mathematical implementation of these processes is outlined considering the study of stability presented in Chapter 4.

In Section 5.4, numerical implementation of the model is presented together with simulations of a reaching behaviour. A method to build travelling peak solutions is tested in a simulation environment to extend the repertoire of elementary behaviour representable with dynamical fields.

5.2 Proposed Model for Trajectory Formation

In the present section, a novel approach to model movement generation at the level of the spine is introduced. The idea for the development of this models was inspired by the concept of motor primitive (Tresch & Jarc, 2009) and associated spinal force fields (Bizzi et al., 1991; Giszter et al., 1993; Mussa-Ivaldi et al., 1994), explored in Chapter 2. The physiological counterpart of the proposed model is the theory of movement formation by synergic activation of muscles (Alessandro et al., 2013; D'Avella et al., 2003).

The goal here is to give a mathematical representation of this process of summation of motor patterns to produce movement. The concept of attractor dynamics, matching the DFT rationale, gives the appropriate mathematical representation for *the spinal attractor model* (SAM).

Introducing SAM: one-dimensional attractor

Consider the simplified one-dimensional system represented in Fig. 5.1 A, consisting of a mass m moving along the x coordinate axis under a force F , with a damping factor β . The system can be described by the following differential equation:

$$\ddot{x} = -\frac{\beta}{m}\dot{x} + \frac{F(x)}{m} \quad (5.1)$$

with $\beta, m > 0$.

Define on the workspace (the x axis) P points $x^{M_1}, x^{M_2}, \dots, x^{M_P}$ that will be called *attractors* of the system in Eq. (5.1), described by the energy function of a linear spring obeying Hooke's law (Shukla & Anchal, 2006):

$$E_k(x) = \frac{1}{2}(x - x^{M_k})^2, \quad k = 1, 2, \dots, P. \quad (5.2)$$

The force F acting on the point mass can be written as a linear combination of the force exerted by each attractor modelled by Eq. (5.2):

$$F(x) = - \sum_{k=1}^P s_k (x - x^{M_k}) \quad (5.3)$$

where coefficients s_k , acting like the spring elastic constants, are referred to as *activations* associated to the attractor x_{M_k} .

For instance, consider $M = 2$ and set an attractor in $x^{M_1} = 0$ and a second attractor in $x^{M_2} = 1$, as shown in Fig. 5.1 B. If the vector of activation is $s = [1, 0]$, starting from the position x_0 , the point mass will move until it reaches the active attractor x^{M_1} in 0, regardless of the position of other attractors. For the choice of activations $s = [0, 1]$, the point mass will reach the second attractor in 1.

Using this two-attractor repertoire the point mass can be moved in between. Using a different combination of activations, for example $s = [0.5, 0.5]$, the dynamic of the system includes the intermediate point 0.5 to the list of equilibrium positions, as shown in Fig. 5.1 C. If multiple attractors are active at the same time, then, the point mass moves towards the resultant position of equilibrium that is given by the equation:

$$x_E = \frac{\sum_{k=1}^P s_k x^{M_k}}{\sum_{k=1}^P s_k} \quad (5.4)$$

A simulation of these attractor dynamics is shown in Fig. 5.1 D where position x and velocity v for the point mass are plotted. The eigenvalues associated with this model have the general form:

$$\lambda_{1,2} = \frac{1}{2} \left(-\frac{\beta}{m} \pm \sqrt{\frac{\beta^2}{m^2} - \frac{4}{m} \sum_{j=1}^P s_k} \right) \quad (5.5)$$

and the attractors created by summation defined in Eq. (5.4) are stable equilibria as long as $s_k \geq 0$; stable nodes if the condition $\sum s_k \leq \beta^2/4m$ holds (Kuznetsov, 1996).

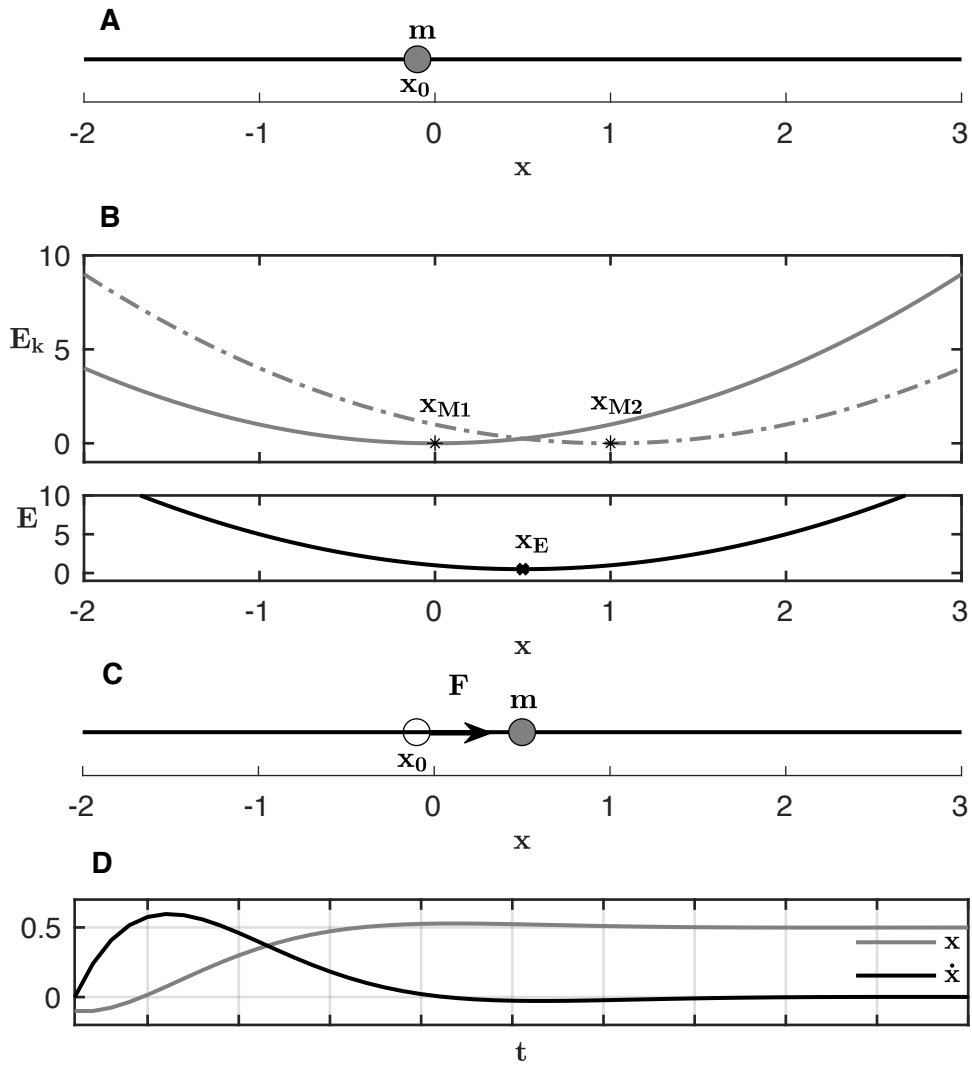


Figure 5.1: One-dimensional attractor dynamic. A point mass m with starting position $x_0 = -0.1$ (A) moves towards the equilibrium point $x = x_E$ (C) as the result of the force imposed by two attractors x^{M_1} and x^{M_2} , with energy E_k ($k = 1, 2$). The resultant energy function is $E = s_1 E_1 + s_2 E_2$ (B). Kinematics of the point mass are shown in D.

Introducing SAM: two-dimensional attractor

Consider now to extend the workspace to two dimensions, defining $\mathbf{x} = (x_1, x_2)$ and considering to apply a force $\mathbf{F}(\mathbf{x})$ to a point mass m with damping coefficient $\boldsymbol{\beta} = [\beta_1, \beta_2]$.

The energy field \mathbf{E}_k associated with an attractor $\mathbf{x}^{M_k} = [x_1^{M_k}, x_2^{M_k}]$ this time has the form given by the Hooke's law (Shukla & Anchal, 2006):

$$\mathbf{E}_k = \frac{1}{2}(\mathbf{x} - \mathbf{x}^{M_k})^T (\mathbf{x} - \mathbf{x}^{M_k}), \quad (5.6)$$

so that the resultant energy is:

$$\mathbf{E} = \sum_{k=1}^P s_k \mathbf{E}_k. \quad (5.7)$$

Force can be expressed as its two components on the workspace axes $\mathbf{F} = [F_1, F_2]$:

$$F_i = -\frac{\partial \mathbf{E}}{\partial x_i} = -s_k (x_i - x_i^{M_k}) \quad i = 1, 2. \quad (5.8)$$

The resulting system is described by the following equations:

$$\begin{aligned} \ddot{x}_1 &= -\frac{\beta_1}{m} \dot{x}_1 - \frac{1}{m} \sum_{k=1}^P s_k (x_1 - x_1^{M_k}), \\ \ddot{x}_2 &= -\frac{\beta_2}{m} \dot{x}_2 - \frac{1}{m} \sum_{k=1}^P s_k (x_2 - x_2^{M_k}), \end{aligned} \quad (5.9)$$

and the general equilibrium, given by a linear combination of attractors, can be written as follows:

$$x_i^E = \frac{\sum_{k=1}^P s_k x_i^{M_k}}{\sum_{k=1}^P s_k}, \quad i = 1, 2. \quad (5.10)$$

The stability of the equilibrium point is given by the associated eigenvalues:

$$\begin{aligned}\lambda_{1,2} &= \frac{1}{2} \left(-\frac{\beta_1}{m} \pm \sqrt{\frac{\beta_1^2}{m^2} - \frac{4}{m} \sum_{k=1}^P s_k} \right), \\ \lambda_{3,4} &= \frac{1}{2} \left(-\frac{\beta_2}{m} \pm \sqrt{\frac{\beta_2^2}{m^2} - \frac{4}{m} \sum_{k=1}^P s_k} \right).\end{aligned}\tag{5.11}$$

Equilibria are stable foci if and only if $\sum s_j \leq \max(\beta_1, \beta_2)^2/4m$, and $s_k \geq 0$ (Kuznetsov, 1996). An example of the dynamic of the system with two attractors is shown in Fig. 5.2.

Extending the attractor construction method presented here for a point mass, a new control law modelling movement formation is defined below for the dynamic of the planar 2-R manipulator, based on the hypothesis of motor primitives summation.

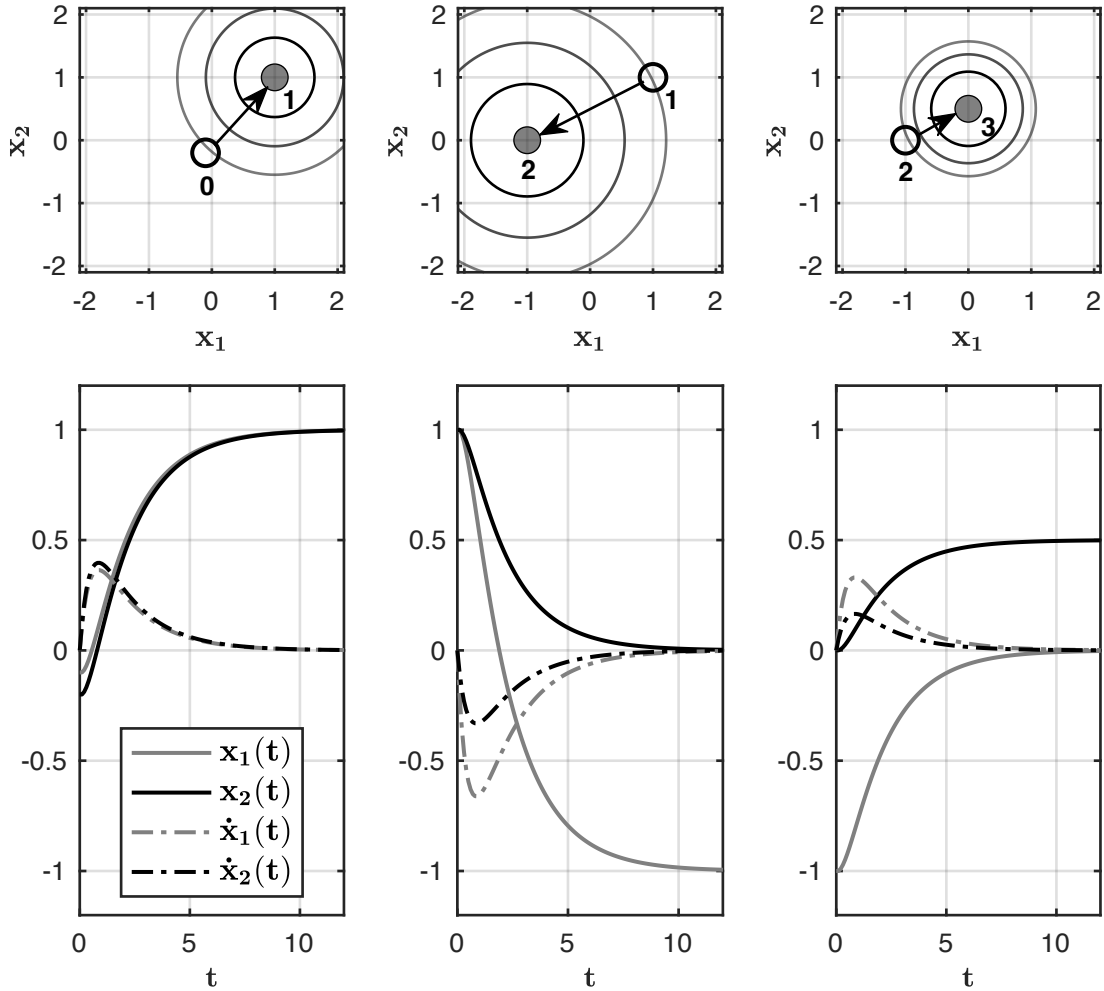


Figure 5.2: Attractor dynamic for a point of mass m (grey circle) in two dimensions. First row: contour plots of the energy function level-set (darker grey approaching minimum) and initial and final position of the mass. Second row: kinematics of the mass. The equilibrium point reaches the first attractor in $\mathbf{x}_E = \mathbf{x}^{M1} = [1, 1]$ ($0 \rightarrow 1$), then moves to the second in $\mathbf{x}_E = \mathbf{x}^{M2} = [0, 1]$ ($1 \rightarrow 2$) and to a point in between in $\mathbf{x} = [1, 0]$ ($2 \rightarrow 3$), changing activations from $s_{0 \rightarrow 1} = [1, 0]$, to $s_{1 \rightarrow 2} = [0, 1]$ and $s_{1 \rightarrow 2} = [0.5, 0.5]$.

5.2.1 S.A.M.: The Spinal Attractor Model

Consider the structure of the spinal cord, topologically organised as shown in Fig. 2.2. Direct stimulation of the premotor part, or descending motor commands resulting from cortical sensorimotor integration carried by the *efferent pathway*, can elicit the activation of a mapped group of muscles. Guided by Fig. 5.3, imagine representing this type of mapping onto layers of two-dimensional structures that can be selected using an input signal called *activation* (Fig. 5.3 A) and then summed to form a pattern of activation (Fig. 5.3 B).

The integration of this pattern with the sensory feedback, topologically carried in the dorsal horn of the spine, leads to the emergence of a representative force field (Fig. 5.3 C) that, in a similar fashion to what was found in empirical studies (Bizzi et al., 1991; Giszter et al., 1993), models the guiding force that the limb requires to move towards the desired position, the latter defined as the point in the field in which forces are null.

The position of the end effector of the link is carried by the *afferent pathway* and used locally in the spinal cord (i.e., as in spinal reflexes) or sent to the cortex for further elaboration of sensory input (e.g., proprioceptive, visual or multimodal) or for sensorimotor integration (e.g., updated target position in workspace coordinates) and then sent down to the spinal cord via *the efferent pathway*. The possibility to account for local spinal processes and to connect the proposed model to architectures that model cortical sensorimotor integration is represented in Fig. 5.3 by the dashed line. For simulation purpose, the connection of the afferent and efferent pathway creates a local feedback loop that is used to test the architecture in reaching tasks.

This process that describes a mechanism of selection of motor activations resulting in the computation of forces at the joint of the robotic model, inspired directly by the structure of the spine and by empirical findings on muscle activations, is defined here as *the spinal attractor model*.

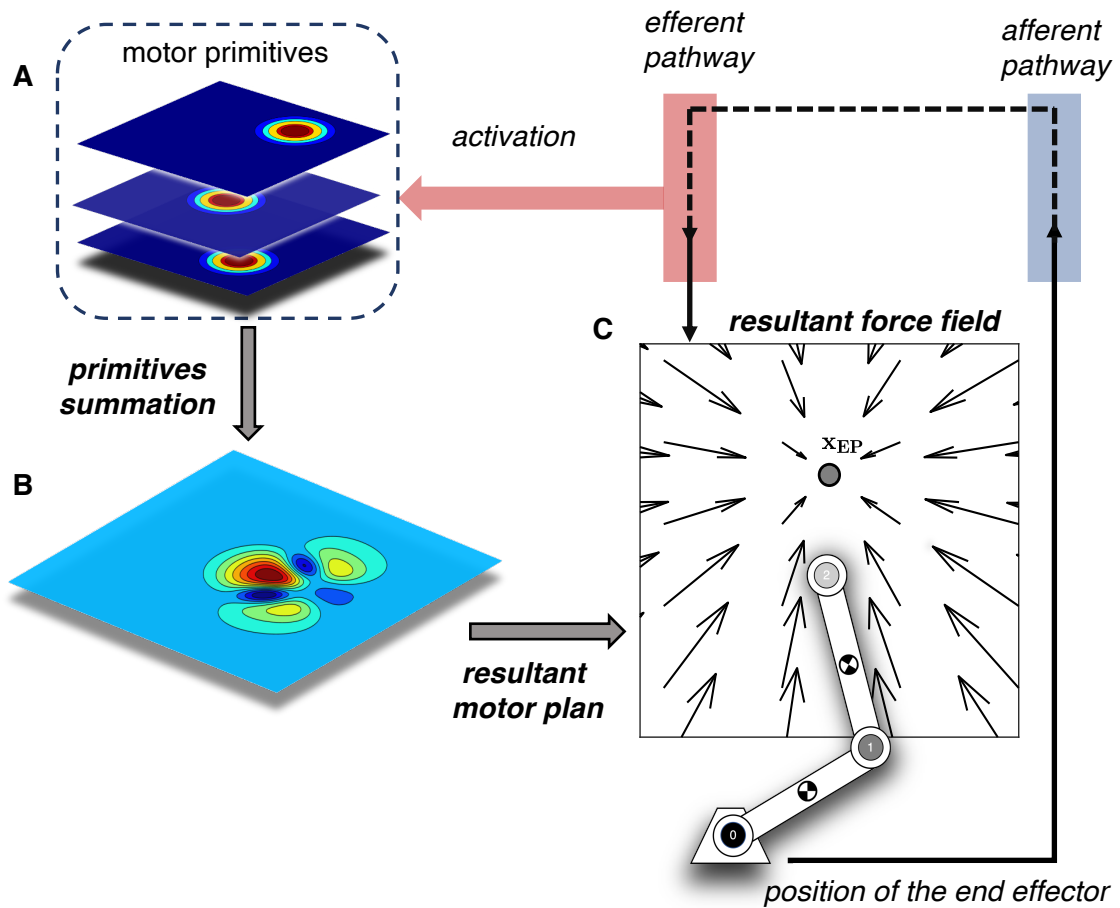


Figure 5.3: The *Spinal Attractor Model* (SAM). **(A)**: motor primitives are represented as planar structures that receive activation signals from the efferent pathway (i.e., motor commands). **(B)**: activated motor primitives are summed with appropriate weights to form a representation of the motor plan. **(C)**: sensory motor integration at the level of the spine gives the resultant force field that represents the forces necessary at the joint to complete the motor task. The dashed path indicates concurring local and cortical sensorimotor processes (see text for a detailed description).

Movement formation is based on the combination of a limited number of learned motor synergies, namely the motor primitives, and appropriate selection signals that allow to generalise to a greater motor repertoire. Here, the degrees of freedom is addressed in terms of neural activations in the spinal cord encoding forces at the joints. As experimental results suggest, motor primitives represent the neural correlates of muscles synergies (D’Avella et al., 2003; Mussa-Ivaldi et al., 1994, see Fig. 2.13 in Section 2.3.1), thus the control law formalised below opens the way to the development of a modelling account that can be used to simulate motor control from the cortical level to single muscles activations.

Considering Eq. (4.87), describing the dynamics of the manipulator in workspace coordinates of the end effector \mathbf{x} , the acting force \mathbf{F} is defined as the sum of two terms:

$$\mathbf{F} = \mathbf{F}_{\text{SAM},\mathbf{l}} + \mathbf{F}_{\text{SAM},\mathbf{d}} \quad (5.12)$$

where

$$\mathbf{F}_{\text{SAM},\mathbf{l}}(\mathbf{x}) = - \sum_{k=1}^P s_k (\mathbf{x} - \mathbf{x}^{\text{M}_k}) \quad (5.13)$$

represents the resultant force field exerted by P motor primitives. Equation (5.13) models *the principle of summation* presented in Eq. (2.7), considering $s \leq 0$ in the formulation proposed by Mussa-Ivaldi et al. (1994).

The second component is simply a weighted derivative term, obtained from Eq. (5.13), necessary to obtain a stable control law for the manipulator defined as follows:

$$\mathbf{F}_{\text{SAM},\mathbf{D}}(\dot{\mathbf{x}}) = - \sum_{k=1}^P \bar{s}_k (\dot{\mathbf{x}} - \dot{\mathbf{x}}^{\text{M}_k}). \quad (5.14)$$

with $\bar{s}_k = g_{\text{SAM},\mathbf{d}} s_k$.

The resultant control law that defines the *spinal attractor model* (SAM) is expressed by the following equation:

$$(\textit{spinal attractor model}) \quad \mathbf{F}_{\text{SAM}}(\mathbf{x}) = - \sum_{k=1}^P s_k (\mathbf{x} - \mathbf{x}^{\text{M}_k}) - \sum_{k=1}^P \bar{s}_k (\dot{\mathbf{x}} - \dot{\mathbf{x}}^{\text{M}_k}). \quad (5.15)$$

The introduced local (or *spinal*, in the physiological reference) feedback in the control law models sensory-motor integration, so that Eq. 5.15 gives the equivalent of the recorded force fields in the spinal cord, dependent on the position of the end effector and converging towards a single point. This resultant set point for the motor system given by the combination of motor primitives mirrors the force field equilibrium found in empirical studies (see Section 2.3.1) and modelled by Mussa-Ivaldi et al. (1994) in Eq. (2.8):

$$\mathbf{x}_{\text{EP}} = \frac{\sum_{k=1}^P s_k \mathbf{x}^{\text{M}_k}}{\sum_{k=1}^P s_k} \quad (5.16)$$

Equation (5.16) describes the point in the force field in which the end effector is at equilibrium (i.e., stops moving).

To investigate the stability of the new control law defined by Eq. (5.15), necessary to perform successful reaching task simulations, one can define the error signal between the position of the end effector and the resultant equilibrium point $\mathbf{e} = \mathbf{x} - \mathbf{x}_{\text{EP}}$. It is possible, then, to rewrite the SAM control law as

$$\mathbf{F}_{\text{SAM}}(\mathbf{x}) = - \sum_{k=1}^P s_k \mathbf{e} - \sum_{k=1}^P \bar{s}_k \dot{\mathbf{e}}.$$

Remembering the discussion on robotic control theory in Chapter 4, it is possible to notice that the SAM model can be thought as version of a PD controller defined in Eq. (4.90). Results on Lyapunov stability can then be extended directly to the proposed model, that will produce stable dynamics if $s_k \geq 0$ for all k and $g_{\text{SAM},d} \leq 2\sqrt{2}$, considering $\sum_k s_k = 1$.

The computation of joint forces using the spinal attractor model requires a local representation of descending activation commands, a locally stored mapping of primitives and updated information on the position of the end-effector as represented

in Fig. 5.3. In the following, a DNFs architecture is described that matches the representation of motor primitives and motor activations given by the spinal attractor model.

5.3 Neural Fields Control Design for S.A.M.

In this section the implementation of neural controllers is presented for the spinal attractor model (SAM). The proposed architecture aims at linking the DFT framework, broadly used to model features belonging to motor control (Johnson et al., 2008; Sandamirskaya et al., 2013; Schöner, 2007), to the physiologically based model for movement formation, using the versatility typical of neural fields to represent sensory-motor variables in a planar space.

Planar dynamic neural fields seemed to be the natural match for the spinal attractor model, since both the emerging force field and the representation of the motor primitives have an attractor-like dynamic, developing onto a two-dimensional mapping.

The proposed architecture for motor control accounts for the following motor control components: sensory-motor integration, autonomy and a strategy to produce motor activation that does not require the solution of the inverse dynamics. Motor learning (e.g., to cluster motor primitives) is not developed here and goes beyond the purpose of this study; nonetheless, links to existing accounts are suggested and further discussed in Chapter 6.

The representation of motor control introduced in Fig. 1.1 in Chapter 1 is mirrored by the architecture presented in Fig. 5.4. Although a block representation is convenient, the circular stream of information carrying afferent and efferent content represents the embodied nature of this architecture and the possibility to link other layers through the afferent and efferent pathway, to/from the CNS.

5.3.1 Model Overview

As introduced in Chapter 2, motor control must provide the following functions: autonomy, sensory-motor integrations, a solution to the redundancy of the system, that is selecting appropriate motor activations, and some learning mechanism. Here these features are represented by the following components:

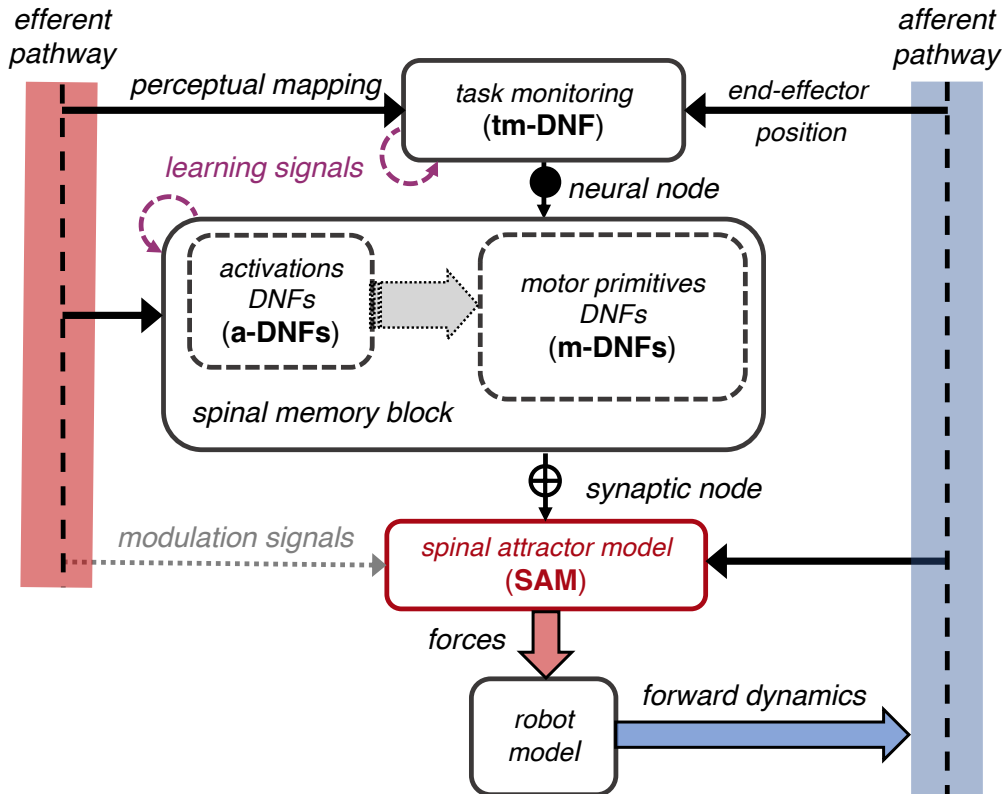


Figure 5.4: Overview of the proposed model for motor control. See text for a description of blocks and connections.

- *the task monitoring*, responsible for the autonomous development of the motor plan;
- *the spinal memory block*, composed of *the motor primitives block* and *the activations block*, representing the working memory of the system from which emerges the sensory-motor representation of the ongoing motor plan;
- *the spinal attractor model*, responsible for the encoding of appropriate motor activations for the robotic interface.

A reaching behaviour is used as reference to present the workflow of the proposed architecture.

Consider a task initiated by the detection of a visual input appearing within the environment or some motivational cue. External stimuli together with proprioceptive signals, adequately elaborated by some perceptual dynamic fields, can be represented in terms of a *perceptual mapping*, signalling the position of a target in hand-centred coordinates (see, for instance, the architecture in the study by Rudolph et al. (2015), presented in Chapter 3). This event of target detection triggers the onset of a motor plan.

The target detection signal arrives through the efferent branch to *the task monitoring* (tm-DNF), a one-dimensional neural field that receives an input proportional to the distance between the target and the current position of the end effector, the latter arriving from the afferent branch. If the distance is not zero, the field allows for self-stabilising peak solutions. The beginning of the task is represented by a detection instability, signalling the onset of the action to linked modules.

The activity of the tm-DNF is encoded by a *neural node* (black circle in Fig. 5.4) that is linked to the resting potential of the neural fields composing *the spinal memory block*. The state of this node is active when the task monitoring signals the presence of an ongoing motor plan. In this case, controlled dynamic fields can present a working memory instability and retain information for the duration of the task.

The spinal memory block is composed by two types of DNF architectures: the *activation* DNF (a-DNF) and the *motor primitive* DNF (m-DNF). The first represents the information relative to the motor selection process, for instance emerging from a sensorimotor coupled neural structure that includes learning from previous experience. Activation signals select and weight appropriately a number of motor primitives that, stored in the spinal memory block and learned at a developmental stage, are represented for the duration of the task by self-sustained peaks of activation in two-dimensional neural fields, the m-DNFs.

The spinal memory block retains the representations of salient motor features for the proposed motor control model. This guarantees robustness throughout the task since here are represented the motor commands that guide the behaviour. The encoding of the motor representation is carried out by *synaptic nodes* (black crossed

circle in Fig. 5.4). These convert the spatial DNF representation into motor variables giving the position of the peak on the field. Information coming from synaptic nodes, together with perceptual input, is brought to *the spinal attractor model* (SAM), where the resultant force field is evaluated integrating sensory information and active motor primitives.

The SAM block gives the online computation of the forces required by *the robot model block* to move purposefully. The robot used is the 2-R planar model in Fig. 4.12. The position of the end effector is computed solving the forward dynamics and is sent back as part of the afferent pathway, carrying proprioceptive and sensory information back into the modules of the architecture so that the motor task can be updated.

The end of the motor task is signalled by reverse detection instability in the tm-DNF, that sees the amplitude of its input progressively decrease together with the distance from the target, until the bifurcation point is encountered. Beyond that point, target has been reached and the self-sustaining peak representation collapses into the resting state solution. The task monitoring is now ready again to keep track of the development of another movement or another part of the motor sequence.

As a consequence of task completion, the representation of motor plans is no more necessary. The activity of the neural node linked to the tm-DNF moves to an inactive state and guides the spinal memory block towards the forgetting instability. At this point the system is ready to receive a new set of instructions.

In Fig. 5.4, purple looped connections represent learning; grey dotted arrows other kind of modulations such as performance monitoring, attentional enhancement or more refined motor strategies, involving the direct activation of single muscles for instance. Mechanisms relative to these connections are outlined in Chapter 2. Here they are represented for completeness, anticipating a discussion on the possibility to link this architecture to other DFT models (see Section 3.4 for relevant examples) and future developments (see Chapter 6).

5.3.2 Mathematical Implementation

In this section the mathematical implementation of each block is presented, considering the methods developed in Chapter 4. In Fig. 5.5, the proposed model is presented highlighting the neural and biomechanical variables that come into play, described by the following equations.

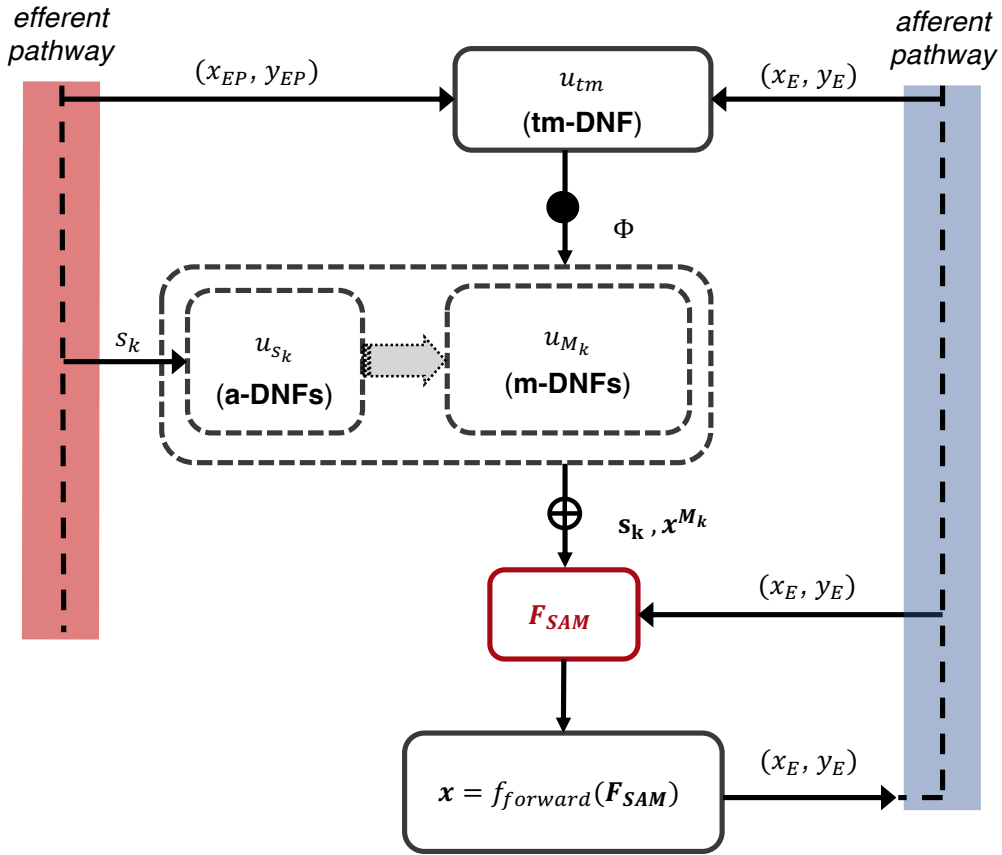


Figure 5.5: Developed components of the proposed architecture for motor control: detailed representation of the neural and motor variables.

Task Monitoring Block

The task monitoring block tracks the progress of the ongoing task. Considering a reaching task, this module signals the onset of movement pre-activating the modules

that represent motor features. When the target has been reached, it signals the end of the task and waits for new motor commands.

This behaviour is achieved using detection and forgetting instabilities, supported by models of self-stabilising peaks. The model used here is the one discussed in Section 4.2.3: it is a one-dimensional neural field with adaptation and exponential weighting function, encountering a saddle-node bifurcation as input amplitude \mathcal{I} is reduced (Bressloff et al., 2003).

The input amplitude is proportional to the distance between the end effector $\mathbf{x} = (x_E, y_E)$ and target position $\mathbf{x}_{\mathbf{EP}}$. Introducing a new notation for the one-dimensional neural field, this DNF is described by the variable u_{tm} with associated adaptation a_{tm} and dynamics derived from Eq. (4.31) that follow:

$$\begin{aligned} \frac{1}{\alpha_{tm}} \frac{\partial u_{tm}(x, t)}{\partial t} = & -u_{tm}(x, t) + \int_{-\infty}^{\infty} w_{tm}(x - x') f(u_{tm}(x', t)) dx' + \\ & - g_{tm} a_{tm}(x, t) + I_{tm}(x) \end{aligned} \quad (5.17)$$

$$\frac{1}{\beta_{tm}} \frac{\partial a_{tm}(x, t)}{\partial t} = -a_{tm}(x, t) + u_{tm}(x, t),$$

where the synaptic footprint is given by $w_{tm}(x) = A_{tm} e^{-|x|}$, with A_{tm} modelling the amplitude of synaptic excitation; g_{tm} is the adaptation gain and $f(u_{tm}) = H(u_{tm} - h_{tm})$; α_{tm} and β_{tm} model the decay to resting potential in absence of input.

The input function is defined as

$$I_{tm}(x, t) = \mathcal{I}(\mathbf{x}(t)) e^{-x^2/2\sigma_{tm}^2}. \quad (5.18)$$

The amplitude \mathcal{I} encodes the distance from target:

$$\mathcal{I}(\mathbf{x}(t)) = \mathcal{I}_{sn} + \frac{\|\mathbf{x}(t) - \mathbf{x}_{\mathbf{EP}}\|}{\|\mathbf{x}(0) - \mathbf{x}_{\mathbf{EP}}\|}, \quad (5.19)$$

where $\mathcal{I} \leq \mathcal{I}_{sn}$ gives the condition for the forgetting instability, that is when the target has been reached $\mathbf{x}(t) = \mathbf{x}_{\mathbf{EP}}$; it is assumed that in order for the motor plan to

exist $\mathbf{x}(0) \neq \mathbf{x}_{EP}$.

The analysis of bifurcations of the field in Eq. (5.17), presented in Fig. 4.5 with associated Evans functions in Fig. 4.6, allows for the construction of a neural controller that supports a self-stabilising peak solution, using the parameters listed in Table 5.1.

Task Monitoring: Self-Stabilising Peak		
inverse time constant	α_{tm}	8
adaptation inverse time constant	β_{tm}	0.03
synaptic footprint amplitude	A_{tm}	0.5
synaptic footprint dispersion	σ_{tm}	1
synaptic depression gain	g_{tm}	1
threshold	h_{tm}	0.5
bifurcation input amplitude	\mathcal{I}_{sn}	0.77
input dispersion	σ_{tm}	1

Table 5.1: List of parameters used to simulate a self-stabilising peak solution for the task monitoring module.

The Spinal Memory Block

The spinal memory block models the current representation of the ongoing motor plans. It receives the efferent commands for spinal primitives selection s_k as the input of the a-DNF block, and keeps an updated representation of the motor primitives, represented by \mathbf{x}^{M_k} in the spinal attractor model. These are encoded with attractor dynamics in the m-DNF.

The activation block is composed by P one-dimensional neural fields u_{s_k} , with adaptation a_{s_k} , supporting self-sustaining peak solutions as presented in Section 4.2.2. The equation for the neural field representing the k -th activation is written as follows:

$$\begin{aligned} \frac{1}{\alpha_s} \frac{\partial u_{s_k}(x, t)}{\partial t} = & -u_{s_k}(x, t) + \int_{-\infty}^{\infty} w_s(x - x', t) f(u_{s_k}(x', t)) dx' + \\ & - g_s \int_{-\infty}^{\infty} w_{s,a}(x - x', t) a_{s_k}(x', t) dx' + I_{s_k}(x, t) + h_{\Phi} \end{aligned} \quad (5.20)$$

$$\frac{1}{\beta_s} \frac{\partial a_{s_k}(x, t)}{\partial t} = -a_{s_k}(x, t) + f(u_{s_k}(x, t)),$$

where $w_s(x) = A_s e^{-|x|}$ and $w_{s,a}(x) = A_s e^{-|x|/\sigma_s} / \sigma_s$ so that the resultant synaptic footprint has the Mexican hat shape. A_s and σ_s model long range inhibition according to the lateral inhibition hypothesis; g_s is the adaptation gain and $f(u_{s_k}) = H(u_{s_k} - h_s)$; α_s and β_s model the decay to resting potential in absence of input.

The input function $I_{s_k}(x, t)$ carries the information on primitives selection encoded by stable attractors in terms of position on the x axis. The control variable h_{Φ} implements an adaptive threshold used to shift between the inactive ($h_{\Phi} = h_{rest} < 0$) and self-sustaining state ($h_{\Phi} = 0$), controlled by a neural node mapping the output of the task monitoring (see below).

Analysis of bifurcations of the activation field in Eq. (5.20), presented in Fig. 4.3 with associated Evans functions in Fig. 4.4, allows for the construction of neural controllers that can retain persistent self-sustained representations of activation, using the parameters listed in Table 5.2.

The motor primitive block is composed by P two-dimensional neural fields u_{M_k} with adaptation a_{M_k} , described by the model in Section 4.3.3. The equations that give the neural substrate for the representation of the k_{th} motor primitive is:

$$\begin{aligned} \frac{1}{\alpha_M} \frac{\partial u_{M_k}(\mathbf{r}, t)}{\partial t} = & -u_{M_k}(\mathbf{r}, t) + \int_{\mathbb{R}^2} w_M(\|\mathbf{r} - \mathbf{r}'\|) f(u_{M_k}(\mathbf{r}', t)) d\mathbf{r}' + \\ & - g_M a_{M_k}(\mathbf{r}, t) + I_{M_k}(\mathbf{r}, t) + h_{\Phi} \end{aligned} \quad (5.21)$$

$$\frac{1}{\beta_M} \frac{\partial a_{M_k}(\mathbf{r}, t)}{\partial t} = -a_{M_k}(\mathbf{r}, t) + u_{M_k}(\mathbf{r}, t)$$

a-DNFs: Self-Sustaining Solution		
inverse time constant	α_s	1
adaptation inverse time constant	β_s	1
synaptic footprint amplitude	A_s	0.5
synaptic footprint dispersion	σ_s	2
synaptic depression gain	g_s	0.5
threshold	h_s	0.27
inactivation threshold	h_{rest}	-0.1

Table 5.2: List of parameters used to simulate self-stabilising peak solutions in 1D a-DNFs.

where $w_M(r) = (2\pi)^{-1}(e^{-r} - A_M e^{-r/\sigma_M})$. A_M and σ_M model long range inhibition according to the lateral inhibition hypothesis; g_M is the adaptation gain and $f(u_{M_k}) = H(u_{M_k} - h_M)$; α_M and β_M model the decay to resting potential in absence of input.

The input function $I_{M_k}(\mathbf{r}, t)$ indicates a general efferent input encoding the equilibrium point of the k th motor primitive. For the mechanism of movement formation suggested here, the same result could be achieved using a pre-shape where the activation pattern is stored after learning (see Section 3.4 for the definition of the memory trace and learning). A visual representation of a *stack* of motor primitives represented by DNFs is illustrated in Fig. 5.3 A.

The control variable h_Φ is used to shift between the inactive ($h_\Phi = h_{rest} < 0$) and self-sustaining state ($h_\Phi = 0$) is the same way as in the a-DNFs (see below).

Analysis of bifurcations of the motor primitive field in Eq. (5.21), presented in Fig. 4.10, and the evaluation of the critical points using Eqs. (4.59) and (4.66) allow for the construction of neural controllers that can retain persistent self-sustained representations in two dimensions using the parameters listed in Table 5.3.

m-DNFs: Self-Sustaining Solution		
inverse time constant	α_M	1
adaptation inverse time constant	β_M	1
synaptic footprint amplitude	A_M	0.5
synaptic footprint dispersion	σ_M	2
synaptic depression gain	g_M	0.1
threshold	h_M	0.025
inactivation threshold	h_{rest}	-0.1

Table 5.3: List of parameters used to simulate self-stabilising peak solutions in 2D m-DNFs.

The Adaptive Threshold h_Φ

To encode some motor output associated with neural field dynamics, it is useful the concept of a *neural node*. A neural node is a zero-dimensional neural field described by an activation variable $\Phi(t)$ with dynamic here defined by:

$$\tau \frac{d\Phi}{dt} = -\Phi + \int_{\mathbb{R}^n} f(u(x, t)) dx, \quad x \in \mathbb{R}^n, \quad n = 1, 2 \quad (5.22)$$

where $u(x, t)$ could be the state variable of a one or two-dimensional neural field, $f(u(x, t))$ is the Heaviside function with threshold h and τ is the relaxation constant. Similar output rate variables are used in the DFT to represent CoS nodes, as introduced in Section 3.4.

In the proposed model, a neural node is used to control the activation of blocks down the line, based on the sensorimotor representation in the task monitoring. The dynamic described above, in fact, is responsible for the activation of neural fields belonging to the spinal memory block, guided by the task monitoring block. This is implemented using a neural node Φ_{tm} linked to u_{tm} driving the resting level h_Φ of the controlled DNFs in Eqs. (5.20) and (5.21) as follows:

$$\tau_\Phi \frac{d\Phi_{tm}}{dt} = -\Phi_{tm} + \int_{-\infty}^{\infty} f(u_{tm}(x, t)) dx, \quad (5.23)$$

$$h_{\Phi} = h_{rest}(1 - f(\Phi_{tm}(t))), \quad (5.24)$$

where $h_{rest} < 0$, τ_{Φ} is the time constant of the dynamic of the node, $f(u_{tm}) = H(u_{tm} - h_{tm})$ and $f(\Phi_{tm}) = H(\Phi_{tm} - \epsilon)$. The process is illustrated in Fig. 5.6.

At the beginning of the reaching task (see Fig. 5.6 A), the self-stabilising peak in the task monitoring u_{tm} causes an increase in the activity of the neural node Φ_{tm} . As soon as $\Phi_{tm} > \epsilon$, the adaptive threshold shifts to the value $h_{\Phi} = 0$. The choice of parameters for the spinal memory block allows for the emergence of self-sustaining peaks in the motor primitive and activation DNFs for this value of the resting level. The representation of the motor plan is active and the SAM model can compute the forward dynamics (see below).

When the target has been reached, the task monitoring peak solution destabilises (see Fig. 5.6 B). The activity in the neural node decreases until $\Phi_{tm} < \epsilon$. At this point, the threshold shifts to the inactivation value $h_{\Phi} = h_{rest} < 0$. This value, beyond the bifurcation point for both type of fields, causes a reverse detection instability in the a-DNFs and in the m-DNFs, bringing u_{s_k} and u_{M_k} to the resting state.

The monitoring block is then responsible for the activation of all the motor representations necessary to carry out the motor task, and for their reverse detection instability when the task is completed. This control process is implemented using a neural node linked to the resting level of the fields in the controlled blocks. Note that h_{rest} must be negative in order to force a \emptyset -solution (i.e., no localised solution exists; see Section 4.2) and that this procedure is equivalent to increasing the output function threshold h of the controlled fields; i.e., $h_{s,M} = -h_{\Phi}$.

The shifting of the resting potential of the field (and not of the neural threshold) is inspired by empirical findings. It is found that pre-activation of some neural pools involved in working memory processes occurs as a consequence of an increase in the baseline potential, here modelled by h_{Φ} (D'Esposito, 2007; Spencer et al., 2009).

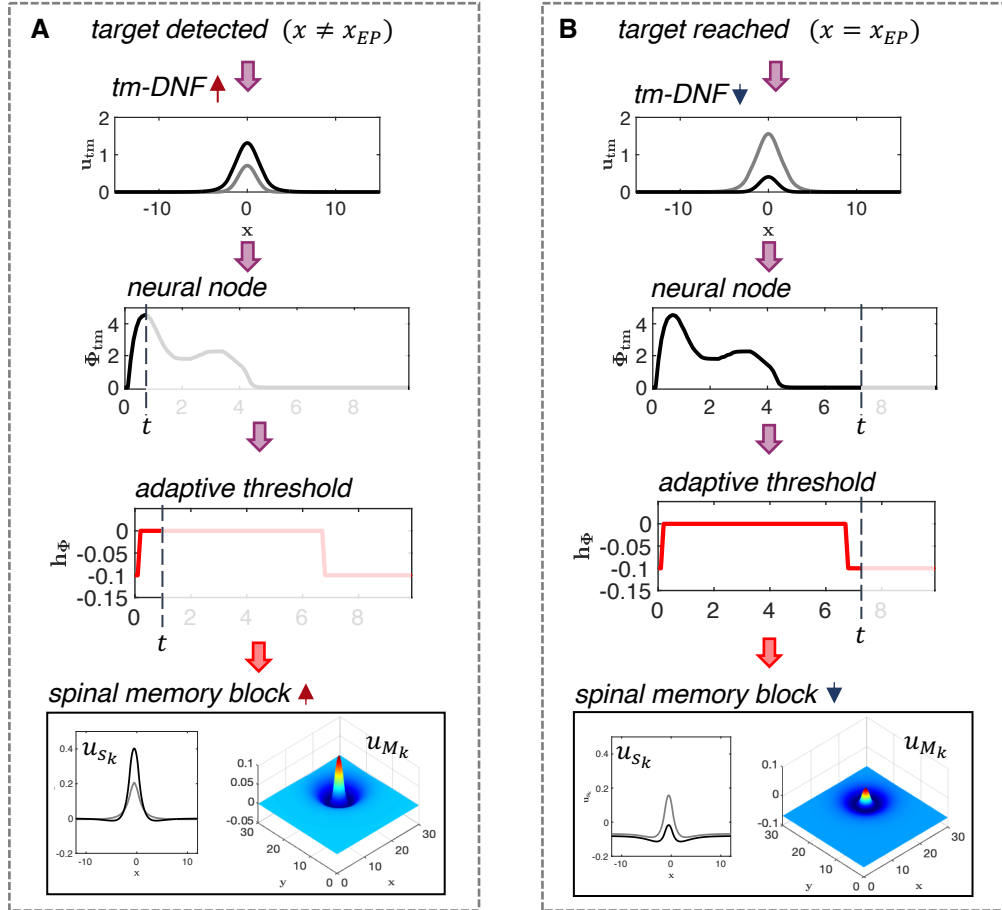


Figure 5.6: The adaptive threshold during a reaching task. **(A)**: target detection activates the task monitoring u_{tm} , the activity of the Φ_{tm} node increases so that $h_\Phi = 0$ allows for a stable motor representation in the spinal memory block (u_{S_k}, u_{M_k}). **(B)**: task completion triggers reverse detection instability in the tm-DNF; the activity of the Φ_{tm} node decays to zero. When $\Phi_{tm} < \epsilon$, $h_\Phi = h_{rest}$ and the DNFs in the spinal block destabilise. Red (blue) arrows represent detection (reverse) instability; t represents the timeframe considered for plots.

Computing Dynamics with SAM

The combination of persistent bump solutions weighted by activations, according to the spinal attractor model, represents the principle of motor summation, explored in Section 2.3.1. This principle can be modelled using the DNF representation follows:

$$u_{\mathbf{E}}(\mathbf{r}, t) = \sum_{k=1}^P s_k u_{M_k}(\mathbf{r}, t). \quad (5.25)$$

Equation (5.25) is the equivalent in the model for the spinal circuitry from which force fields can be recorded and is the representation in the Dynamic Field Theory account of the spinal attractor model (note that the derivative term in Eq. (5.25) is necessary to stabilise the dynamic of the manipulator model of choice). An example of motor primitives summation with the DNFs representation is given in Fig. 5.3 B.

The SAM block implements the spinal attractor model control law and gives the forces to guide the robotic model used to test the architecture, in this case, the 2-R planar model described in Section 4.4, with control law introduced in Section 5.2.1.

Attractor dynamics in the DNFs of the spinal memory block encode the SAM model in terms of motor features representation. The transduction of the peaks of activation into motor variables guides the robotic interface. This can be done using neural nodes as defined in Eq. (3.12) in Chapter 3 (Sandamirskaya, 2013).

Alternatively, some authors have borrowed from physics the concept of centre of mass, defining the position on the field corresponding to the highest activation as follows (Fard et al., 2015):

$$x_{MAX}(t) = \frac{\int_{R[u(x,t)]} u(x,t) x dx}{\int_{R[u(x,t)]} u(x,t) dx}. \quad (5.26)$$

where the part of the field considered is the one active above threshold $R[u(x,t)]$, defined Section 4.2. This is somehow reminiscent of the first method, encoding mapped features into rate variables using nodes (Sandamirskaya, 2013), but considering the process instantaneous.

Developing the model, it was noted that if one defines

$$w^u(x, t) = x / \left(\int_{R[u(x,t)]} u(x, t) dx \right), \quad (5.27)$$

Eq. (5.26) can be rearranged as follows:

$$x_{MAX}(t) = \int_{R[u(x,t)]} w^u(x, t) u(x, t) dx. \quad (5.28)$$

Considering that the integral of the field variable for localised solution is limited and can be reasonably assumed constant, it follows that $w_u(x, t) = w_u(x) = kx$. One can argue that this formulation can be interpreted as the integration of the field activation weighted by an activity-normalised synaptic footprint, that is the representation of a broad and instantaneous synapse transforming a neural input into a motor activation variable.

From this perspective, this model resembles the mechanism of the neuromuscular junction, where neural electric signal is converted into a biochemical signal that drives sarcomere recruitment (see Chapter 2). For this reason, Eq. (5.26) defines what is called in the following a *synaptic node*. This interpretation is further discussed in Chapter 6.

The synaptic node is used to extract from the field representation the values of activation needed to compute the spinal attractor model. In a similar fashion one can extend this concept associating some motor activation variables to two-dimensional neural fields:

$$\begin{aligned} x_{MAX}(t) &= \int_{R[u(\mathbf{r},t)]} w_x^u(x, t) u(\mathbf{r}, t) d\mathbf{r} \\ y_{MAX}(t) &= \int_{R[u(\mathbf{r},t)]} w_y^u(y, t) u(\mathbf{r}, t) d\mathbf{r}, \end{aligned} \quad (5.29)$$

where the weighting functions are defined as:

$$w_x^u(x, t) = \frac{x}{\int_{R[u(\mathbf{r},t)]} u(\mathbf{r}, t) d\mathbf{r}}, \quad w_y^u(y, t) = \frac{y}{\int_{R[u(\mathbf{r},t)]} u(\mathbf{r}, t) d\mathbf{r}},$$

with $(x, y) = (r \cos \theta, r \sin \theta)$.

Using synaptic nodes, defined by Eqs. (5.28) and (5.29), linked to both blocks composing the spinal memory block, it is possible to extract the values of the motor features. In particular, each activation s_k and each spinal attractor position $\mathbf{x}^{\mathbf{M}_k}$ is given by a synaptic node associated with the fields u_{s_k} and u_{M_k} respectively:

$$s_k(t) = \int_{R[u_{s_k}]} w^{u_s}(x, t) u_{s_k}(x, t) dx \quad (5.30)$$

$$\mathbf{x}^{\mathbf{M}_k}(t) = \int_{R[u_{M_k}]} \begin{bmatrix} w_x^{u_M}(\mathbf{r}, t) \\ w_y^{u_M}(\mathbf{r}, t) \end{bmatrix} u_{M_k}(\mathbf{r}, t) d\mathbf{r}.$$

The *SAM block* receives activations and spinal attractors, described in Eq. (5.30), and gives the forces necessary to move the joints, computed using Eq. (5.15). This results in a force field with an equilibrium point in which the force vector is zero, like the one plotted in Fig. 5.3 C.

For simplicity, this point is taken as the target point of the task; nonetheless, considering a series of signals $s_k(t)$ varying in time, such an equilibrium point could shift on the workspace modelling a more complex behaviour. Further considerations on the representation of motor primitives in the dynamic field framework and on how this could account for a greater motor repertoire are discussed in Chapter 6.

The *robotic model block* computes the new position of the end effector solving the Lagrange equation associated with the robot using the spinal attractor model forces:

$$\widetilde{\mathbf{M}}(\mathbf{x})\ddot{\mathbf{x}} + \widetilde{\mathbf{C}}(\mathbf{x}, \dot{\mathbf{x}})\dot{\mathbf{x}} = - \sum_{k=1}^P s_k \left(\mathbf{x} - \mathbf{x}^{\mathbf{M}_k} \right) - \sum_{k=1}^P \bar{s}_k(\dot{\mathbf{x}}), \quad (5.31)$$

where it is considered $\dot{\mathbf{x}}^{\mathbf{M}_k} = 0$ as a consequence of the jumpy representation of motor attractors offered by the adaptive threshold guided by the task monitoring. The result of the forward dynamic $\mathbf{x} = (x_E, y_E)$ is brought back to the task monitoring that determines if the current target has been reached.

5.4 Simulations and Results

The proposed architecture is implemented using Matlab (MATLAB, 2021). In the first part of this section, numerical methods for the model presented in Section 5.3 are discussed. In the second part, results of the simulation of a reaching task are presented and a method to construct travelling peaks is outlined, adding up to the repertoire of elemental behaviours in DFT. Relevant scripts and functions are attached in Appendix A.

5.4.1 Numerical Methods

Firstly, the space of features spanned by neural fields is discretised in a finite number of grid points. For a one-dimensional neural fields of finite length L , the number of points selected is $N = 2^n$, with $n \in \mathbb{Z}$, so that the spacing unit is $\Delta x = L/N$. It follows that $x_i = i\Delta x$, $i = -\frac{N}{2}, \dots, \frac{N}{2} - 1$. The discretised in space version of Eq. (4.1) becomes:

$$\frac{1}{\alpha} \frac{\partial u_i(t)}{\partial t} = -u_i(t) + \frac{L}{2N} \sum_{p=-N/2}^{N/2-2} [w_{i,p} f(u_p(t)) + w_{i,p+1} f(u_{p+1}(t))] + I_i(t) + h_{rest}, \quad (5.32)$$

where $u_i = u(x_i, t)$ represents the value of the discrete state variable at the i -th grid-point at time t ; $w_{i,j} = w(x_i - x_p)$ is the connection weight between presynaptic grid point location p and postsynaptic grid point location i in the grid space; I_i is a generic discrete input function. Integration in space is approximated using the trapezoidal rule (Glasgow, 2014).

Secondly, a discretisation in time is performed so that $t = k\Delta t$, for Δt small and $k \in \mathbb{Z}$. Application of the Euler method leads to Algorithm 1, describing numerical integration of the field equation, where $u[k]$ and $I[k]$ represent $N \times 1$ vectors and T is the duration of the simulation.

Lastly, to improve the performance of Algorithm 1, convolution can be performed using the *Fast Fourier Transform* (FFT) (Frigo & Johnson, 2014) as described by

Algorithm 1 Euler Method for 1D Neural Field Equation

```

for  $k = 1 : T$  do
  for  $i = 1 : N$  do
     $u_i[k + 1] = (1 - \alpha\Delta t)u_i[k] +$ 
       $+ \alpha\Delta t \left\{ \frac{\Delta x}{2} \sum_{p=-N/2}^{N/2-2} \left[ w_{i,p} f(u_p[k]) + w_{i,p+1} f(u_{p+1}[k]) \right] + \right.$ 
       $\left. + I_i[k] + h_{rest} \right\}$ 
  end for
end for

```

Algorithm 2 1D Neural Field Equation: Fast Fourier Transform for Convolution

```

 $\widehat{W} = \mathbf{fft}(W)$ 
for  $k = 1 : T$  do
   $u[k + 1] = (1 - \alpha\Delta t)u[k] +$ 
     $+ \alpha\Delta t \left\{ \Delta x \left[ \mathbf{ifft} \left( \widehat{W} \cdot \star \mathbf{fft}(f(u[k])) \right) \right] + I_i[k] + h_{rest} \right\}$ 
end for

```

Algorithm 2, where W is the $N \times 1$ synaptic weight vector and \widehat{W} is its 1D Fast Fourier Transform, computed once at the beginning of the simulation; $(\cdot \star)$ is the product element by element.

Some Matlab built-in functions are used: **fft** for direct Fourier transform and **ifft** for inverse transform. Frequencies are re-centred using the built-in function **fftshift**, necessary in Matlab environment (MATLAB, 2021). Toroidal conditions are implicitly applied, since FFT implements circular convolution. Integration in time of one-dimensional neural field in Eqs. (5.17) and (5.20) are computed using Algorithms 1 and 2 adapted for the field and the adaptation variable (see Appendix A.1 for the complete algorithm).

In a similar fashion, two-dimensional neural fields are defined over a $N \times N$ discretised space, with spacing units $\Delta x = \Delta y = L/N$, so that $x_i = i\Delta x$ and $y_j = j\Delta y$, for $i, j = -\frac{N}{2}, \dots, \frac{N}{2} - 1$. The discretised in space version of Eq. (4.46) is then:

$$\begin{aligned}
 \frac{1}{\alpha} \frac{\partial u_{i,j}(t)}{\partial t} = & -u_{i,j}(t) + \\
 & + \frac{L^2}{4N^2} \sum_{p,l=-N/2}^{N/2-2} [w_{ij,pl}f(u_{p,l}(t)) + w_{ij,(p+1)(l+1)}f(u_{(p+1),(l+1)}(t))] + \\
 & + I_{i,j}(t) + h_{rest},
 \end{aligned} \tag{5.33}$$

where $u_{i,j} = u(x_i, y_j, t)$ represents the value of the discrete state variable at the grid-point (i, j) , at time t ; $w_{ij,pl} = w(x_i - x_p, y_j - y_l)$ is the connection weight between presynaptic grid point location (i, j) and postsynaptic grid point location (p, l) ; $I_{i,j}$ is a generic discrete input function; integration in space is approximated using the trapezoidal rule (Glasgow, 2014).

Using time discretisation and the Euler method to integrate the neural field equation gives Algorithm 3. The convolution in two dimensions using the FFT algorithm (Frigo & Johnson, 2014) leads to Algorithm 4, where $u[k]$ and $I[k]$ represent $N \times N$ matrices, W is the $N \times N$ synaptic weight matrix and \widehat{W} is its 2D FFT.

Algorithm 3 Euler Method for 2D Neural Field Equation

```

for  $k = 1 \rightarrow T$  do
  for  $i = 1 \rightarrow N$  do
    for  $j = 1 \rightarrow N$  do
       $u_{i,j}[k + 1] = (1 - \alpha\Delta t)u_{i,j}[k] + \alpha\Delta t \left\{ \frac{\Delta x \Delta y}{4} \right.$ 
         $\sum_{p,l=-N/2}^{N/2-2} [w_{ij,pl}f(u_{p,l}[k]) + w_{ij,(p+1)(l+1)}f(u_{(p+1),(l+1)}[k])] +$ 
         $\left. + I_{i,j}[k] + h_{rest} \right\}$ 
    end for
  end for
end for
    
```

Matlab's two-dimensional FFT functions used are **fft2** for direct transform and **ifft2** for the inverse transform. Re-centering of zero frequencies requires the use of **fftshift** in Matlab environment (MATLAB, 2021). Toroidal conditions are implicitly applied, since FFT implements circular convolution. Numerical integration in time of

Algorithm 4 2D Neural Field Equation: Fast Fourier Transform for Convolution

```

 $\widehat{W} = \mathbf{fft}(W)$ 
for  $k = 1 \rightarrow T$  do
     $u[k + 1] = (1 - \alpha\Delta t)u[k] +$ 
         $+ \alpha\Delta t \left\{ \Delta x \Delta y \left[ \mathbf{ifft2} \left( \widehat{W} \cdot \star \mathbf{fft2}(f(u[k])) \right) \right] + I_{i,j}[k] + h_{rest} \right\}$ 
end for

```

two-dimensional neural fields in Eq. (5.21) uses Algorithms 3 and 4 adapted for the field and the adaptation variable (see Appendix A.1 for the complete algorithm).

The neural node in Eq. (5.24) is integrated using the Euler method. Synaptic nodes of Eqs. (5.28) and (5.29) are approximated with the Riemann sum (McLeod, 1979, see Appendix A.1.1).

Forward dynamics are calculated integrating Eq. (5.31) using Matlab Runge-Kutta solver function `ode45` (Shampine & Reichelt, 1997), presented in Algorithm 5. Each time step of the solver computation is considered one time-step in simulation time.

Algorithm 5 ODE Solver for Forward Dynamics

```

 $[\mathbf{x}[k], \dot{\mathbf{x}}[k]] = \mathbf{ode45} \left\{ \text{function handle (Eq. (5.31))}, [t[k], t[k + 1]], \mathbf{x}[k - 1] \right\}$ 

```

For the trajectory $\mathcal{T}[k] = \mathbf{x}[\mathbf{k}] = (x_E[k], y_E[k])$ the measure of straightness is computed using the straightness index (Batschelet, 1981):

$$S = \frac{\sum_{i=1}^T d[k]}{d_S}, \quad (5.34)$$

where $d[k]$ is the distance between two consecutive points of the trajectory and d_S is the length of the straight line connecting the first point of the trajectory to the last:

$$d[k] = \|\mathcal{T}[k + 1] - \mathcal{T}[k]\|,$$

$$d_S = \|\mathcal{T}[T] - \mathcal{T}[1]\|.$$

Straightness S is maximum (i.e. $S = 1$) when the trajectory is the straight line.

5.4.2 Simulating a Reaching Task

Algorithm 6 outlines the workflow used to simulate a reaching task. Parameters for the type of solutions of choice are loaded using the function **setparams** (*step 1*). The function **synapticfoot** specifies the exponential or Mexican hat shape of the synaptic footprint for each field (*step 2*).

Algorithm 6 Simulation: Reaching Task

- 1: loading parameters for neural fields models: **setparams**(*solution type*)
 - 2: computing synaptic footprints: **synapticfoot**(x, A, σ)
 - 3: initialising state variables
 - 4: Fourier Transform synaptic footprint for convolution: $W \rightarrow \widehat{W}$
 - 5: **for** $k=1:tspan-1$ **do**
 - 6: compute the transform of the output of DNFs variables: $f(u, h) \rightarrow \widehat{F}_U$
 - 7: perform convolution using transforms: $\widehat{W} \star \widehat{F}_U$
 - 8: update neural node and field variables (Euler Method)
 - 9: **if** $\Phi[k] > \epsilon$ **then** ▷ the motor task is taking place
 - 10: extract motor output for SAM: **synapticnode**(x, u, h)
 - 11: simulate forward dynamics: $ode45(@twolink, s_k, \mathbf{x}^{M_k}, \dots) \rightarrow \mathbf{x}$
 - 12: **end if**
 - 13: update task monitoring input
 - 14: **end for**
-

At the beginning of the simulation all fields are inactive and the task monitoring receives the position of the end effector and the position of the target in workspace coordinates (*step 3*). The synaptic footprints, by virtue of the properties of circular convolution, can be transformed once thanks to the FFT method for convolution (*step 4*).

Integration of the equations of the model (*steps 5-6*), using transforms for convolution (*step 7*), allows activations and motor primitives to be represented by stable peaks of activation, gated by the task monitoring node Φ (*step 8*) associated to u_{tm} . If the latter has signalled the onset of the task by means of a self-sustained peak, then the condition to evaluate motor output is met (*step 9*).

Synaptic nodes evaluate the information carried by a-DNFs and m-DNFs, using the function **synapticnode**, and drive the robotic set-up, setting the attractor dynamic for the control law used to solve the forward dynamics (*step 10*). Note that alternatively the resultant field of activation could be computed using Eq. (5.25). Possible uses of this representation of the resultant motor plan are discussed as further developments in Chapter 6.

Simulation of the dynamics, described in the function file **twolink**, gives \mathbf{x} that contains the kinematics relative to the position and velocity of the end effector of the robot (*step 11*). The former is used to update the input amplitude of the task monitoring, awaiting task completion (*steps 12-14*). When the target has been reached, the neural node becomes inactive ($\Phi[k] < \epsilon$) (*step 9*), the spinal memory block is brought back to inactivation, lowering the resting state level. No motor commands are available and the robot keeps the last position (*steps 13-14*).

The behaviour of the task monitoring, responsible for the autonomous development of the task, and of the associated node is represented in Fig. 5.7, where it is possible to observe the detection instability when the target is presented and the forgetting instability after target has been reached. Some modulation of the input value at zero distance, for instance a smaller value $\mathcal{I}(x_{EP}) \leq \mathcal{I}_{sn}$ or a different threshold ϵ , could be used to model different level of precision required for the reaching movement.

In Fig. 5.8 trajectories on the plane (x_E, y_E) are illustrated, together with related neural fields activity for three reaching tasks, using the same two motor primitives M_1 and M_2 and changing activation signals. In the first (reaching task A), activation selection is $s_{1,2} = [1, 0]$ so that the resultant motor plan is the first motor primitive with equilibrium point in $(x_E, y_E) = [20, 20]$ on the workspace. The second reaching task (reaching task B) uses $s_{1,2} = [0, 1]$, so that this time the active primitive is the second with equilibrium point in $(x_E, y_E) = [20, 30]$. The third task (reaching task C) shows the simultaneous activation of M_1 and M_2 , with selection signal $s_{1,2} = 0.5[1, 1]$. The resultant activation, given by motor summation, has equilibrium point in $(x_E, y_E) = [20, 25]$.

In Fig. 5.9, simulation C of Fig. 5.8 is presented in more detail, including the

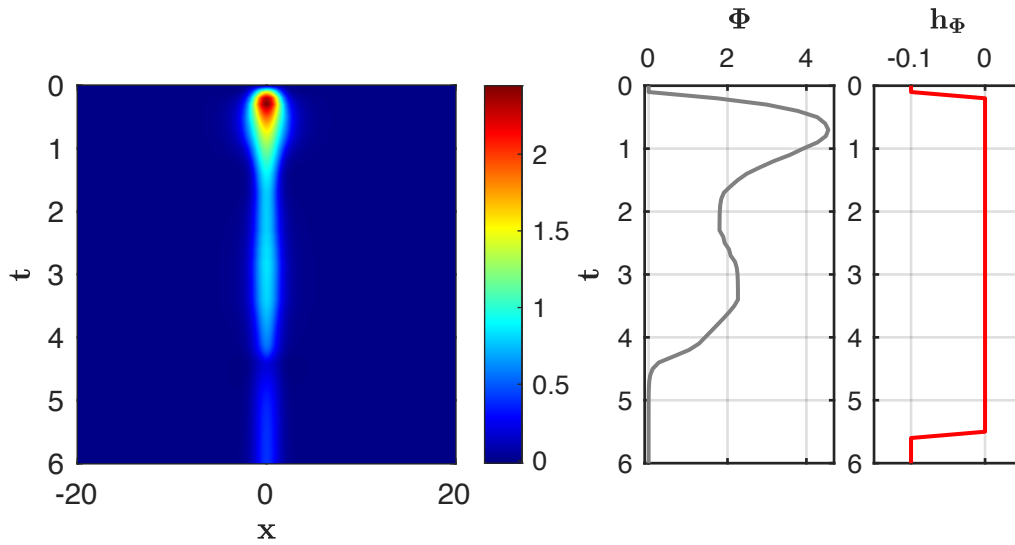


Figure 5.7: Task Monitoring Block. Left: time course of the task monitoring activation showing a self stabilising solution at the beginning of the motor task. As the distance between the target and end effector decreases the stable bump destabilises and disappears signalling task completion. Right: the activation of the associated neural node Φ and the adaptive threshold h_Φ .

time course of the coordinates of the robot links, associated velocity profiles and an example of resultant force field. It is possible to observe that the target point is successfully reached and that trajectories are quasi-straight with $S = 1.005$, calculated by Eq. (5.34). Velocity profiles present a peak but do not have the bell-shaped time course: considerations on how to model this finding on voluntary movements are further addressed in Chapter 6.

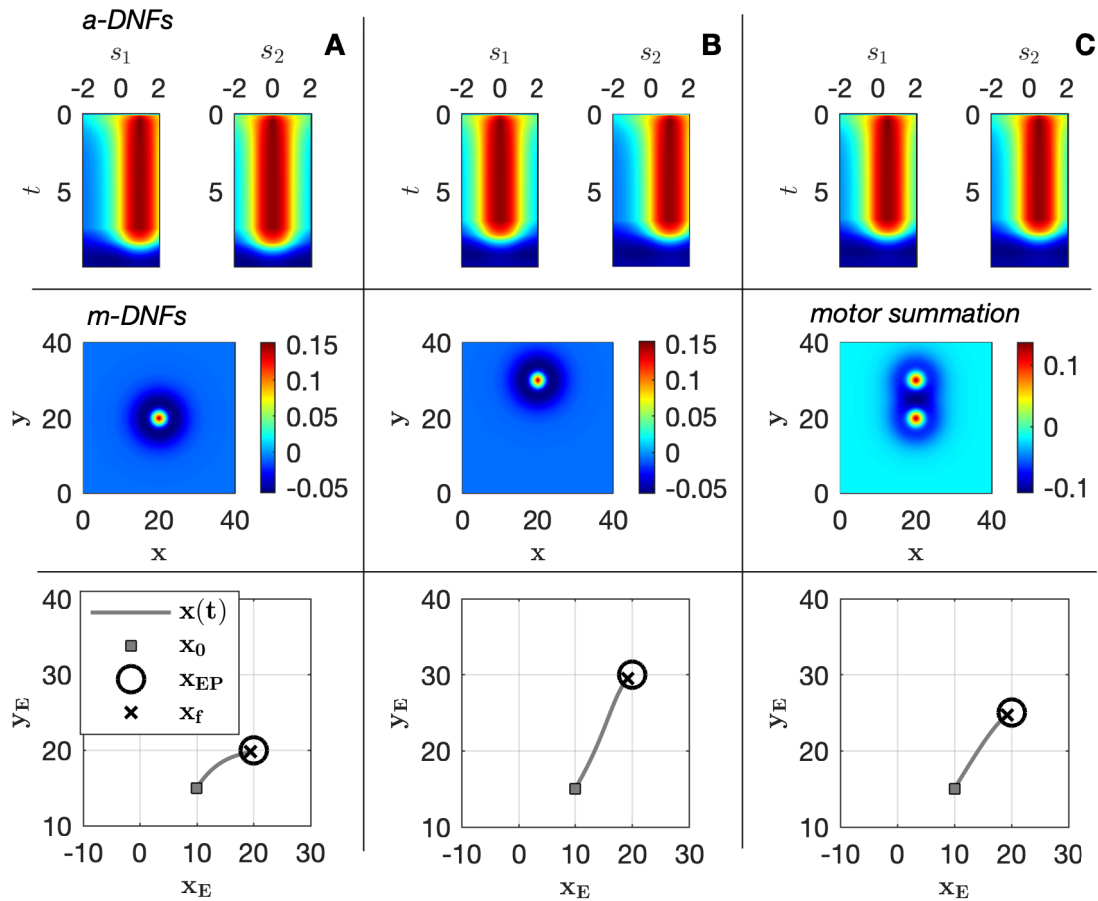


Figure 5.8: Results of three reaching tasks (A-C). First row: activation DNFs plot representing the selection signal. Second row: result of motor primitive selection. Third row: trajectories resultant from simulation of the forward dynamics. See text for further details.

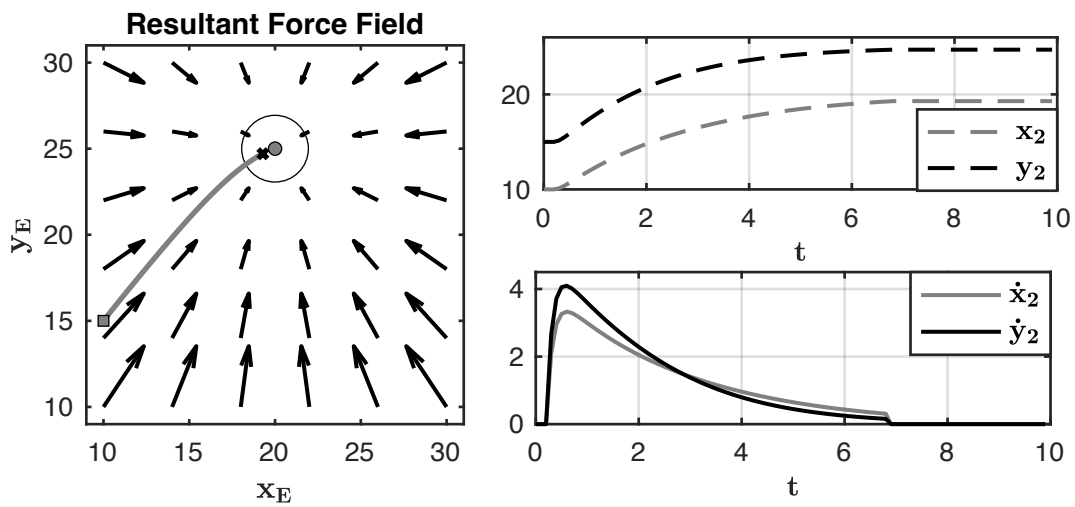


Figure 5.9: Example of resultant force field (left plot) for the reaching simulation C in Fig. 5.8 and kinematics of the end effector (right plots). In the resultant force field plot (black field vectors), the simulated trajectory (grey line), starting from the initial position (grey square) reaches the end position (black cross) in the target zone (black wide circle around the target, inner grey dot).

Code for the reaching simulation and functions in Algorithm 6 are provided in Appendix A.1. The parameter used for simulation are listed in Table 5.1 for the task monitoring, in Table 5.2 for the activation DNFs and in Table 5.3 for the motor primitives. Other parameters include the specifications for the robotic manipulator, reported in Table 5.4 and parameters relative to the numerical simulation, listed in Table 5.5.

Robotic Manipulator Parameters		
mass of segment (0)-(1)	m_1	1.74
mass of segment (1)-(2)	m_2	0.942
length of segment (0)-(1)	l_1	30
length of segment (1)-(2)	l_2	23.2
derivative SAM gain	$g_{SAM,d}$	2.4

Table 5.4: List of parameters for the 2-R planar robot. Mass and length of segments are taken from anthropomorphic tables (Winter, 2009), for height= 160 cm and weight= 60 kg.

Simulation Parameters		
number of grid points	$N \times N$	1024×1024
neural fields grid spacing	$\Delta x, \Delta y$	0.0781
Euler time step	dt	0.1
simulation time	T	100
threshold for neural node	ϵ	$1e - 10$
time constant for neural node	τ_Φ	0.25

Table 5.5: List of parameters for the reaching task simulations.

5.4.3 The Drifting Instability

The development of the architecture outlined above, together with the extensive application of the Evans function method to study the stability of solutions in the Dynamic Field Theory, leads to the consideration that control design can be further extended to other types of instabilities, which might be suitable to model processes of the brain. For example, one could argue that the on-off representation of sensory-motor coupling during the development of a motor plan is not very plausible. A representation including propagation over the feature space could actually be more biologically representative.

Travelling waves moving onto a one-dimensional space of features have already been used to model aspects of cognition. The movement of peaks of activation, in fact, can be used to represent extrapolatory perception and to predict the position of visual targets that are moving, even when occluding objects partly suspend sensory feedback. This is the result of combined sensorimotor integration and priming mechanisms that, increasing the baseline potential, allow for the emergence of a drifting solution. The shifting representation in this case behaves like an embodied internal model of the moving object (Erlhagen, 2003).

In two dimensions, the architecture by Fard et al. (2015) presented in Section 3.4.1 represents a possible application of traveling pulses on a planar features space that have a direct impact on movement invariants, determining the shape of the velocity profile as a consequence of a skewed synaptic footprint. In this section a strategy to design traveling peak solutions in two dimensions that leaves unaltered the connections of the field is presented.

In order to obtain a travelling spot, the first thing to determine is the type of perturbation necessary to destabilise a radially symmetric stable solution towards one preferred direction. Numerical simulations show that breathing and shifting instabilities can coexist, confirming the theoretical analysis reported in Section 4.3.3 (Coombes & Owen, 2004).

It was expected that pure breathing-like dynamics would arise simply as a con-

sequence of a choice of parameters beyond the bifurcation point and for radially symmetric perturbations, centred with respect to the initial standing peak solution. This was confirmed numerically and an example of such breathing behaviour is presented in Fig. 5.10.

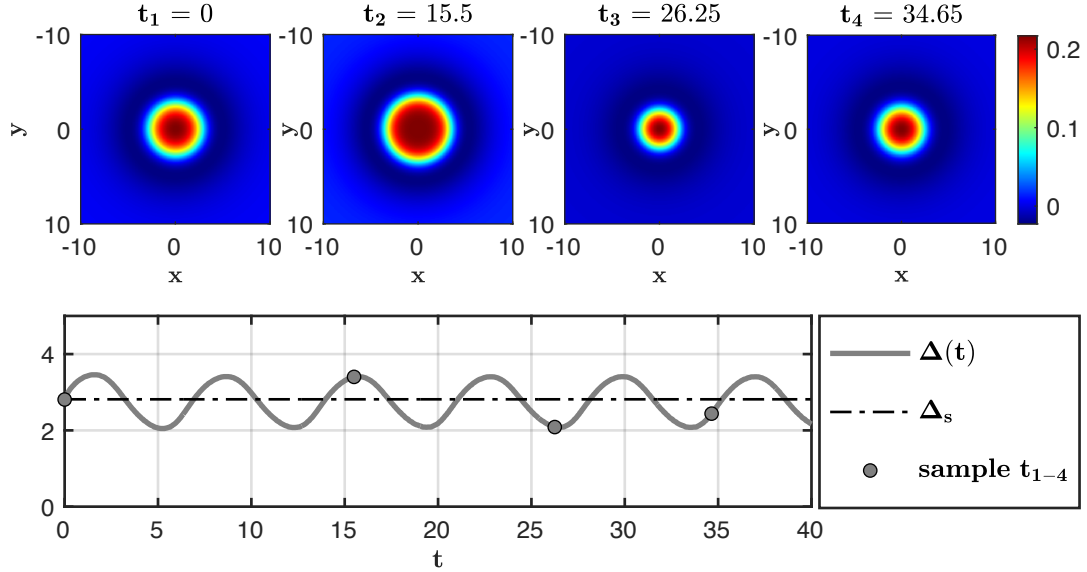


Figure 5.10: Breather-like behaviour from a $m = 0$ perturbation of a standing pulse solution. Top: 2D planar plot of the breather at four sample times shown as grey dots in the bottom panel. Bottom: evolution of the radius of the pulse in time (grey solid line). Parameters: $[A, \sigma, h, g, \alpha] = [0.25, 2, 0.12/(1+g), 0.7, 3]$ and $[\lambda_0, \lambda_1] = [10.15, 1.1]$. Numerical simulation parameters are listed in Table 5.7.

Perturbations centred at the boundary of the radial peak solution produce a shifting of the bump solution. Remembering that Δ_s is the radius of the unperturbed standing peak solution, a perturbation of this type is defined as follows:

$$I_p(\mathbf{r}, t) = \begin{cases} a_p e^{-(\mathbf{r}-\mathbf{r}_p)^2/2\sigma_p} & t \leq t_p \\ 0 & t > t_p \end{cases}, \quad (5.35)$$

where $\mathbf{r}_p = (\Delta_s, \phi_p)$ and a_p , ϕ_p , σ_p and t_p are the amplitude, the angular position, the dispersion and the duration in time of the Gaussian-shaped perturbation, respectively.

Simulation of the field equation in two dimensions in Eq. (4.60), with the input

perturbation defined in Eq. (5.35), is plotted in Fig. 5.11. The value ϕ_p , as expected, defines the direction of motion of the spot. A perturbation with angular position ϕ_p and amplitude $a_p < 0$ is equivalent to a perturbation at the boundary in $\phi_p - \pi$ with $a_p > 0$ in terms of direction of motion of the peak solution. Parameters for the drifting instability and for numerical simulation are listed in Tables 5.6 and 5.7.

Although some damped breathing oscillations are observed at the beginning of the simulation, travelling behaviour prevails for perturbation that are narrow and with sufficient amplitude. The duration of the perturbation must be kept small enough to avoid formation of multi-bump solutions. A higher value of g is used in comparison to the simulation of the breather in Fig. 5.10, clearly beyond the bifurcation point.

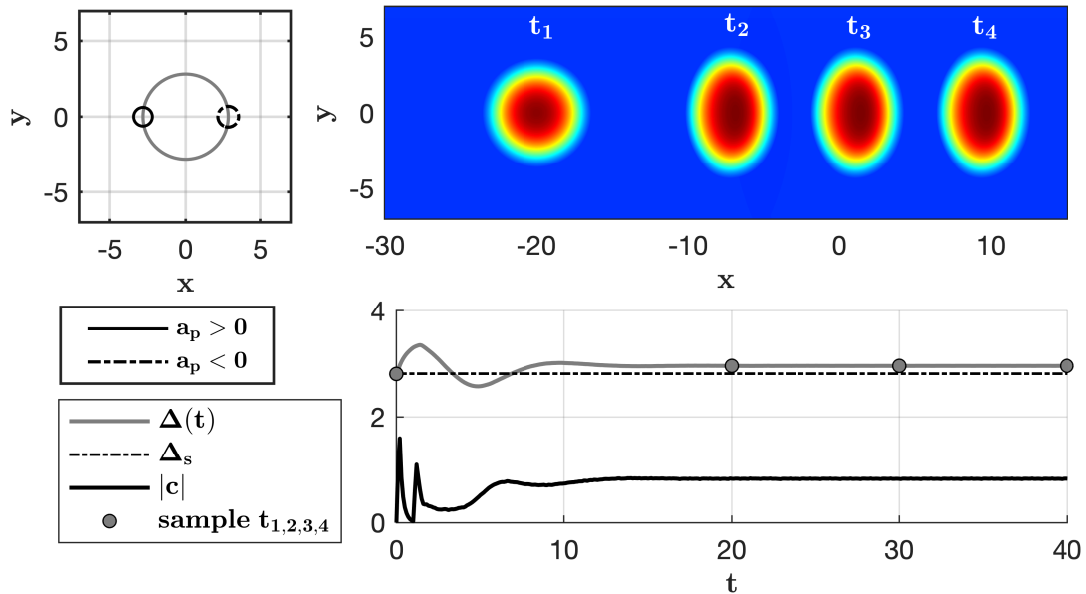


Figure 5.11: Travelling spot emerging from a $m = 1$ perturbation of a standing pulse solution. Top left: representation of the level set h of a standing solution and two equivalent perturbations for a desired direction of motion defined by $\phi_p = 0^\circ$. Top right: 2D planar plot of the travelling pulse at four sample times (grey dots in the bottom panel). Bottom: evolution of the radius of the pulse (grey line) and speed (black line) in time.

A discussion on the shape of travelling spots can be done for small c drifting instabilities arising at the bifurcation ($g_c = 1/\alpha$), proving that contraction of their shape occurs in the direction of propagation, whereas a widening is observable

orthogonally, both phenomena increasing with c (Coombes & Owen, 2004). These findings are illustrated in Fig. 5.12 where different velocities for the traveling peak are simulated increasing g .

It can be also observed that moving further from the critical value $g_c = 1/\alpha$, the breathing behaviour increases in frequency, as anticipated in the study by Coombes et al. (2012) and for greater values of adaptation gain, $g \gg g_c$, the solution collapses and the field returns to the \emptyset - solution, confirming the results of the analysis reported in Fig. (4.10).

The use of traveling solutions in the presented architecture is left to further developments. Considerations on the use of drifting instabilities in the DFT framework are discussed in Chapter 6. Code for simulation of traveling peaks is provided in Appendix A.2.

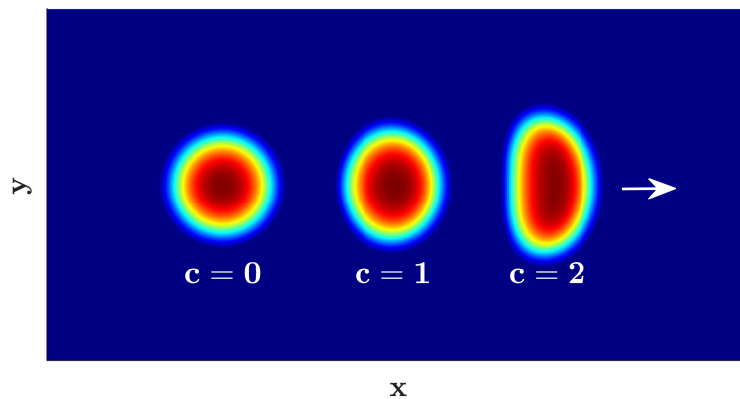


Figure 5.12: Contour plot of the travelling spot for $c = 0, 1, 2$. Colormap shows active zones above threshold in red and resting state in dark blue; the direction of motion is represented by the white arrow. Parameters are the same listed in Table 5.6, except for $\alpha = [3, 3.5]$ for $c = [1, 2]$ respectively.

Traveling Peak Solution		
inverse time constant	α	3
adaptation inverse time constant	β	0.5
synaptic footprint amplitude	A	0.25
synaptic footprint dispersion	σ	2
synaptic depression gain	g	0.5
threshold	h	0.0774
perturbation amplitude	a_p	2
perturbation dispersion	σ_p	0.25
perturbation duration	t_p	0.1

Table 5.6: List of parameters used to simulate a traveling peak solution in a 2D neural field with adaptation and perturbation at the boundary.

Simulation Parameters		
number of grid points	$N \times N$	1024 × 1024
neural fields grid spacing	dx, dy	0.0586
Euler time step	dt	0.1
simulation time	$tspan$	400

Table 5.7: List of parameters used for numerical simulation of a traveling peak solution.

5.5 Conclusions

In this chapter the two components of the proposed architecture for motor control are presented: a physiologically inspired model for movement formation in the spinal cord and an associated DNFs architecture for spinal motor control.

The first, formalised by the spinal attractor model, is defined in terms of a control law based on a two-dimensional representation of elemental motor activations: the motor primitives.

The second consists in a DNFs architecture for the spinal attractor model, that includes models for autonomy, sensory-motor integration and working memory. The equations describing each motor control task are presented and two types of nodes connecting them are introduced: the neural node, guiding an adaptive threshold, and the synaptic node transforming neural activity into motor activation for the SAM.

Numerical methods to simulate the proposed architecture are given, with particular attention to methods for convolution that use Fast Fourier Transforms. Simulations of reaching tasks with resultant trajectories and DNF activations are presented. A method, developed in parallel, for the construction of drifting instabilities is described together with an example of simulation of a traveling peak solution.

Chapter 6

Discussion

6.1 Introduction

In this last chapter, the results of the simulation of the proposed model for spinal motor control are discussed, considering the biomechanical and neural background knowledge presented in Chapters 2 and 3.

In Section 6.2, a critical perspective is offered on the contributions of this thesis listed below, in accordance with the aims outlined in Chapter 1. Physiological components of motor control modelled by the architecture presented in Chapter 5 are discussed, together with behavioural findings accounted for by the spinal attractor model. Limitations of the proposed model are explored.

In Section 6.3, further developments of the model are considered, including possible simulation scenarios as well as the impact on related fields.

List of Contributions:

- 1. The development of a coherent account for movement formation, based on a mathematical representation of spinal motor primitives and motor summation in the DFT framework, overcoming the need**

for inverse dynamics computation.

2. The development of a model for sensory-motor integration and autonomy in the spinal cord using DNFs;
3. The integration of existing methods for motor variables mapping into a unique account that is connected to the physiology of the motor system;
4. The development of a general methodology for the design of DNFs controllers, providing mathematical tools for stability analysis, numerical methods for simulation and introducing the drifting instability as a new elemental behaviour.

6.2 A Coherent Framework for Embodied Motor Control

Understanding motor control is at the core of the research of a several disciplines, including branches of physiology, neuroscience, biomechanics and robotics. The aim is always common: understanding coordination. This means understanding and simulating processes that go from microscopic, as could be the dynamics of calcium in muscles contractions, to macroscopic, as could be the development of anthropomorphic robotics, as discussed in Chapters 2 and 3.

Behind this coordination problem, there are concurring neural processes, deeply rooted in the particular interaction that the musculoskeletal system can afford within the environment. A number of models have been proposed to explain empirical findings. These include muscle force development patterns, kinematic and dynamic properties of voluntary movements, the topological organisation of the spine and of cortical regions involved in motor planning (see Section 2.2 for a review of these findings).

Reverse engineering strategies have been broadly used whenever confronting the challenges posed by the degrees of freedom problem. Traditional approaches to motor control are based on optimisation strategies and internal models, sharing the same perspective of a hierarchical organisation of motor control. According to these accounts, muscle activation selection is based on the minimisation of some cost function or on learned representations of the motor system that are able to anticipate the motor outcome, producing the correct muscles activation (see Section 2.3).

Analytical functions and robotic controls, despite accounting for some motor invariants and producing appropriate motor responses for the tasks they are built for, do not have a biological counterpart so that they are not well suited to infer or study the underlying processes. Robotic applications also show poor adaptivity whenever tested in new environments (see Section 3.4.1).

Despite the common neural substrate, models that use neural networks present a similar problem. Since motor redundancy is solved using learning algorithms, it

is represented as an output mapping that cannot be easily interpreted in terms of interactions between the neural and muscular substrate, both concurring to purposeful movement formation. In the same way, the need for tuning to adjust parameters affects the behaviour of the network with high sensitivity. This prevents from having a univocal physiological meaning assigned to them and from the possibility to use single parameters to model different cognitive behaviour.

The methodology described in this thesis, on the contrary, allows for a clear visualisation of the effects of parameters on the type of behaviour displayed by the fields. This gives the flexibility to obtain the desired type of attractors associating its emergence with parameters that have physiological relevance in the process. A clear example is the priming effect, modelled using an adaptive threshold, that allows for the emergence of working memory instabilities, leaving unaltered those parameters not concurring to the physiological process of interest.

Neural networks models tend to be successful in determining activation weights and clustering, addressing the trajectory generation problem (Bekey & Goldberg, 1993). Nonetheless the type of learning they implement is ultimately linked to an optimisation algorithm, too abstract for a biological interpretation and not able to generalise in a way that is comparable with biological systems.

The stance taken in this thesis supports the main criticism to these analytical approaches to motor redundancy, supported by a growing number of studies (Giszter & Hart, 2013; Graziano et al., 2002; Latash, 2012; Miranda et al., 2018). Cost functions, optimisation algorithms and internal models based on robotic controls and neural networks lack a physiological counterpart, representing input/output mapping functions that are often not only task specific, but highly dependent on parameters tuning and on the training set.

As discussed in this thesis, the DoF problem can be represented in terms of a sequence of reduction in the number of unconstrained variables of the musculoskeletal system for a given task. Alternatively, the abundance of configuration that satisfy a motor task can be considered as an asset. Rethinking the DoF problem in terms of a distributed mechanism responsible for the high adaptivity of biological system means

considering the problem from a new perspective. Motor control is then represented by those strategies that can be advantageously used for successful interactions with the environment, in terms of continuous sensorimotor integration. In this perspective, motor invariants emerge as a consequence of these processes and they are not considered anymore as criteria to reduce the number of independent variables of the system.

This view is supported by the embodied cognition ansatz that, representing a general opposition to the one directional top-down organisation of motor control, supports models that redistributes motor control (as in the architectures composed by embodied layers by Brooks (1991)). The solution to the DoF, in this account, emerges from multiple levels of sensory-motor integration: from cortical motor planning, to motor activation selection in the spinal cord (see Chapter 3). The general goal of understanding coordination translates into investigating how motor control is coordinated at every level, from the cortex to the spinal cord.

It can be hypothesised that some internal models might be reconciled to the embodied perspective, if one considers learning motor strategies in terms of sensory-motor mapping and not sequences of abstractions and functions. It has been pointed out already that refined motor control, as the one performed during voluntary movements in human, and other form of higher cognition cannot be simply reduced to reflex-like models (Shapiro, 2012).

Available models proposed in the DFT account already consider adequately sensorimotor integration and strategies for learning and timing. Furthermore, recent developments considered in Section 3.4, give an embodied substrate to elements of robotics control such as mapping, as seen in the architecture by Rudolph et al. (2015), and the adaptive observers developed by Fard et al. (2015). Both examples show how internal models can be included in the embodied framework using dynamic neural fields and how these can address the problem of motor activations selection at a higher level (i.e., the s_k signals in the proposed model).

The introduction of drifting peak solutions, already used to model perceptual extrapolation and predictive representations of visual inputs (Erlhagen, 2003), further

supports the possibility to develop model for cognition in DFT that include internal models emerging from sensorimotor integration and motor learning (see Section 6.3 below).

Although such models are very well suited to explain higher cognitive functions (e.g., motor planning, motor learning and visual and proprioceptive mapping), existing cognitive robotics models fail to address in the same embodied and biologically motivated manner the final stage of motor control. This consists in the computation of the forces at the joint, solving the degrees of freedom problem at the level of the spinal cord, where muscles are recruited. The use of strategies to compute the inverse dynamic problem (see Section 4.4) associated with the robotic interface, or models based on attractor dynamics, conceptually does not match the embodiment typical of the rest of the reviewed DNFs architectures. Furthermore, it limits the possibility to use such models to investigate the last stage of movement formation, involving the way in which muscles are recruited and organically activated to interact with the environment.

The neural fields architecture proposed here and the spinal attractor model aim at filling this gap, proposing a model for spinal movement formation that does not require the solution of the inverse dynamics of the motor system to compute the forces at the joints. The major challenge encountered modelling motor control, in this sense, was avoiding the development of another task-specific control architecture with limited capability to generalise and to increase our knowledge regarding physiological structures involved in motor control.

The proposed model contributes to the understanding of motor control adding the local processes carried out in the spinal cord. Considering empirical evidence regarding sensorimotor integration at this level, the architecture was developed in a way that is compatible with cognitive models in DFT. Controllers offer a representation of cortical motor plans, that could be encoded by cortical DNFs in further developments, as activations neural fields, and local memorised patterns of muscle activation, namely the motor primitives, encoded as two-dimensional attractors in dynamic fields spanning over the workspace. These motor features integrated with sensory signals are used for the computation of the forward dynamics and sent in

feedback to a monitoring field that can represent spinal reflexes, allowing for the architecture to run autonomously. An adaptive threshold stabilises the representation of motor features and the subsequent synaptic encoding, inspired by the neuromuscular junction, makes them available for the computation of the resultant force field, using the spinal attractor model control law.

This approach successfully leads to the emergence of some motor invariants, such as straight trajectories generalised to the whole workspace, and unimodal velocity profiles. The last result supports the idea that a more bell-shaped profile cannot be motivated by musculoskeletal properties but emerges from either cortical strategies or motor learning, the latter leading to more refined motor primitives.

This novel account is inspired by empirical findings and for this reason can easily be connected to models that use the summation hypothesis, associating motor primitives to direct muscles recruitment, that is the lower level of the DoF problem. Simulations of the sole spinal motor control model already confirm that a small number of muscles synergies, encoded by motor primitives as attractors of the field equation and selected by cortical activations, can account for a greater motor repertoire. Namely, two motor primitives are enough to generalise reaching tasks to the whole planar workspace.

In summary, the model described in Chapter 5 gives the forces in terms of a force field emerging from sensorimotor integration, representing the empirical correlate of force fields recorded in the spinal cord. It also represents the linking element between cognitive robotics that model cortical processes and motor learning. The spinal attractor model and the spinal controllers developed in this work can significantly contribute creating a unified, fully embodied framework to study motor control. Within this account, the construction of internal representations grounded on sensorimotor processes can be directly linked to existing biomechanical models that explain muscles synergic recruitment, addressing the degrees of freedom problem in full.

Future developments include a mapping of activations s_k carried out by cortical neural fields and the association of the motor primitives M_k used in the control law with models that map muscle activations onto them. The simulation of architectures

of this type, that include a model for the spinal cord like the one proposed in this thesis, can contribute shading light onto debated topics regarding motor control, testing inferences and developing experimental studies to confirm them whenever possible.

The clear definition of a methodology for the design of neural controllers and the proposed simulation framework for the field equation complete the account to explore motor control using DFT and robotic models. In the following, contributions in terms of simulation results and methodological advances are discussed in detail.

6.2.1 *Contribution 1. The spinal attractor model for direct movement formation*

The creative approach to modelling the coordination of motor control at the level of the spine stems from a review of the bio-physiological findings on motor control. Translation of such findings in terms of the available tools in the Dynamic Field Theory is the peculiarity of the proposed model.

From the first studies on deafferented and intact animals, suggesting a modular and topological organisation of synergic muscle patterns in the spinal tract, to recent study on vertebrates including EMG recording and clustering of muscle synergies, the concept of motor primitive emerged as an elemental motor behaviour, a *movemes* (i.e., the motor version of the element of speech, *phonemes*; Del Vecchio et al., 2003; Flash and Hochner, 2005). The fundamental hypothesis is that a combination of such primitives can be used to model a broader movement repertoire (Kargo et al., 2010, see Section 2.3.2).

In the DFT, the neural processing associated to motor control is represented by the concept of elemental behaviour (EB), that is the emergence of a peak of activation over two-dimensional neural fields (or their reverse transition to a homogeneous resting state). An embodied account requires the cognitive and motor instances of the agent to be coupled (Spencer et al., 2009), sharing the same representational substrate. From this consideration, the idea to represent motor primitives as attractors of neural

fields was developed.

The proposed model for motor control described in Chapter 5 is based on the hypothesis of motor primitives summation, giving a dynamic field representation of motor activation selection that is intrinsically embodied. The resulting framework for movement formation is compatible with existing DNFs architectures for higher cognition that, using *the spinal attractor model*, would not require the solution to the inverse problem to compute joint activations. This gives the main contribution of this thesis and fulfils the first of the aims of this project (see Chapter 1 for the list of aims).

Given the representation of motor primitives in the sense of DFT, introduced in Section 5.3, it is possible to obtain a resultant motor plan, provided appropriate activation signals. The location of the *centre of mass* of the resultant motor plan sets the equilibrium point for the attractor dynamic. Equation (5.31) defines the direct method to compute the dynamics of the system, by means of sensory-motor integration in the spinal cord giving a resultant force field dependant on the position of the end effector. The derivative term is added to stabilise the control law for the planar robot used for testing.

The spinal memory block encodes activations and motor primitives as self-sustained peaks for the duration of the task. These motor representations are encoded by synaptic nodes and passed to the SAM block that gives the forces necessary for successful reaching tasks, generalising the behaviour to any point in the workspace from a minimum number of two attractor-like motor primitives, as presented in Fig. 5.8.

The emerging motor plan, defined by Eq. (5.25), gives the model correlate of the recorded force fields, plotted along with the trajectory and the kinematics of a reaching task in Fig. 5.9. Results show that the model can account for the typical straightness of human reaching (Morasso, 1981), fulfilling the fourth aim of this project (see Chapter 1).

The proposed architecture, including the task monitoring model for timing that is discussed in detail below, offers a unified perspective on motor control. The possibility

to connected it to other existing architectures gives a unified embodied framework to understand the development of voluntary movements. From visual elaboration to muscle activations, this coherent approach to select appropriate motor activations completes the behavioural loop.

This account supports a growing number of studies on voluntary movements in vertebrates, indicating that the redundancy of the motor system is resourcefully used to compose the motor task by means of an ensemble of motor primitives, scaled and appropriately delayed. The architecture developed in Chapter 5 supports and models the following empirical findings on spinal circuitry and motor primitives:

- Motor primitives are *movemes* (Del Vecchio et al., 2003), invariant elemental units of motor activation (Overduin et al., 2008).
- The neural correlate of motor primitives is represented by interneuron circuitry in the spinal premotor area (Flash & Hochner, 2005; Hart & Giszter, 2010). It makes sense then to represent them with dynamic fields with a defined topological organisation as in the spinal memory block (note that this does not necessarily mean physical contiguity).
- Supraspinal modulation regulates the recruitment of motor primitives, as represented in the model by self-sustaining peaks encoding activation signals (Giszter & Hart, 2013; Hart & Giszter, 2010; Mussa-Ivaldi et al., 1994). A set of scaling signals (i.e., motor activations) is associated with the invariant nature of motor primitives in the spinal cord (Overduin et al., 2008).
- Despite the highly nonlinear nature of the structures at play, neural and muscular, motor primitives summation hypothesis can account for a broader movement repertoire. As shown by the simulations with two active attractors, empirical findings on synchronous stimulation of multiple spinal sites are confirmed by the SAM model (Flash & Hochner, 2005; Giszter & Hart, 2013; Mussa-Ivaldi et al., 1994, among the others).

- Measured spinal force fields are the result of sensory-motor coupling, depending on the position of the end effector and on efferent motor commands encoding the target position (Mussa-Ivaldi et al., 1994). As such, they are emerging in the proposed model from the combination of the motor primitives and the afferent signal from the manipulator, reconciling control theory and bio-inspired models by the definition of the control law in Eq. (5.15).
- In recent studies, complex upper limb movement are accounted for using a model of motor primitives with bell-shaped velocity profile, crucially represented in workspace Cartesian coordinates (Miranda et al., 2018). This result supports the design of the proposed control law, initially motivated by the invariant features of planar reaching (i.e., quasi-straight trajectories).
- Studies on mice have identified a population of interneurons called Motor Synergy Encoder (MSE) that seem to provide the neural substrate for the development of motor plans (Levine et al., 2014). From spinal integration of local proprioceptive input and central corticospinal signals, multiple motor pools are activated, mirroring the architecture in Fig. 5.4 and supporting the representation of motor pools in the spinal cord using neural fields.

Limitations

It could be argued that the representation of the resultant motor plan using neural fields is ‘just’ a representation, supported by physiological findings but not so important in terms of the simulation of motor behaviour, carried out using output motor variables guiding the SAM model.

It must be considered, though, that to the purpose of this thesis, this step represents the opportunity to reunite a vast repertoire of models that use motor primitives to a solid body of neural controllers represented by dynamic fields, broadly used to simulate processes of cognition.

This representation of motor primitives summation, described by Eq. (5.25), allows for the simulation of voluntary movements using a repertoire of motor primitives. This group of motor primitives could be extracted from empirical data, for instance, sharing the same planar representation, or it could be obtained from a DNFs fitting of behavioural data. The motor plan in terms of dynamic field could also offer the substrate for further local sensory-motor integration. Future developments, including the ones foreshadowed here, are discussed in Section 6.3.

Invariants of voluntary movements are only partly accounted for by this model. In particular, velocity profiles are not bell shaped and simulations of curvilinear movements should be implemented to test the two-thirds power law. Nonetheless, the main goal of the proposed architecture is bridging existing DNFs models for cognition and theoretical models for motor control based on motor primitives, giving an embodied representation of cognition and motor features. For this reason, the topological representation of motor primitives might seem oversimplified. Yet, results presented in Section 5.4.2 show that such a simple representation is already able to model generalised purposeful reaching with straight trajectories.

Testing the model using a cluster of motor primitives from empirical data (D'Avella et al., 2003; Miranda et al., 2018), or alternatively implementing learning and clustering using a robotic interface (Fard et al., 2015, reviewed in Section 3.4.1) could lead to more plausible kinematics. For example, velocity-based motor primitives used to model three-dimensional reaching tasks in the study by Miranda et al. (2018) give as a result movements that follow the two-thirds power law (Lacquaniti et al., 1983)), and show, by construction, bell-shaped velocity profiles.

Although several models have been proposed through the years to account for this feature of voluntary movements (Plamondon et al., 1993), there is not agreement whether this emerges from intrinsic properties of the motor system (Abend et al., 1982; Suzuki et al., 1997), from motor primitive features (Kurt A. & Reza, 2000; Miranda et al., 2018), or from planning in cortical areas of the brain (Fard et al., 2015; Flash & Hogan, 1985). For instance, recent studies have failed to associate features of the kinematics to cortical rhythms linked to motor control (Tatti et al., 2019). Indeed, hypotheses could be tested within this framework.

Discussing intrinsic limitations of an approach to motor control mediated by motor primitives goes beyond the purpose of this study, that does not aim at determining if or to what extent motor primitives are actually used to perform human voluntary movements. General limitations to this approach are discussed in the reviews by Giszter (2015) and Tresch and Jarc (2009) and, for completeness, summarised as follows:

- assuming movement formation based on motor synergies could limit the behavioural adaptivity, what is more, evidence of single muscle based control leads to the conclusion that other strategies must be accounted for in order to properly explain human motor capabilities;
- it is possible that a set of motor primitives does exist in human at an early stage of development, but it is unclear the impact of developmental modifications and the possibility to re-use parts of such patterns to develop new types of affordances, such as the ones offered by technology;
- interspecies extension of the behavioural results that concern interneurons circuitry underlying motor primitive activations should be considered carefully and further investigation on the matter is required.

As regards the first critique to this hypothesis, it must be noted that most of the recent studies on motor primitives include more refined control strategies that can override the simple primitive summation whenever needed (Alessandro et al., 2013; Giszter & Hart, 2013; Overduin et al., 2008). In the presented model they are not implemented but a representation is given in Fig. 5.4 in terms of general modulation signals, to be considered in further developments.

As regards the second, a simulated environment to study motor control, like the one proposed here, could be ideal to study evolution of motor primitives mediated by learning.

6.2.2 *Contribution 2. Task monitoring: a model for autonomous spinal response*

The architecture presented in Chapter 5 is intended to model the local organisation of motor patterns to produce appropriate motor selection at the level of the spine (i.e., joint forces or muscle synergic activation). Considering empirical findings on the role exerted by interneurons in mediating motor formation and reflex pathways, a model for a local monitoring in the spinal cord seemed necessary.

Using the coupling of two-dimensional fields, as found in the models presented by Rudolph et al. (2015), Sandamirskaya (2013) and Sandamirskaya and Schöner (2010) for instance, seemed to be overcomplicated. A simplified method is implemented in the proposed model for the spinal tract to provide appropriate timing to the motor output using a detection/reverse instability dynamic in a one-dimensional neural field.

Despite the fact that in DFT dynamic fields are usually shaped two-dimensional, it must be remembered that the neural derivation of the field equation, and the parallelism between 2D neural fields and the planar arrangement of cortical slices is not the relevant from the modelling perspective considered (i.e., modelling the spinal cord). The planar layout used is usually motivated by mapping reasons to represent visuospatial features (see Section 3.3) or, like in the present model, to encode some invariant attractor-like structure that requires a representation in workspace coordinates: the motor primitives.

A one-dimensional field and an associated neural node seemed sufficient, in this case, to regulate the motor task timing and results from simulation confirm that this model accounts for movement autonomous development, as presented in Fig. 5.7.

The distance between the end-effector and the target produces a stable peak representation during the task, that destabilises after the motor goal has been achieved. This information could arrive from cortical sensory-motor representation of salient task features, for instance. There exists behavioural evidence that the scaling of motor primitives could be based on movement amplitude (Overduin et al., 2008).

It is possible then to speculate that such information is available from sensory-motor integration. A DNFs architecture implementing mapping between fields that gives a measure of distance from target could be the one by Fard et al. (2015), introduced in Chapter 3.

At the same time, an equivalent physiological mechanism that this model could account for is the spinal reflex. Local spinal circuitry is able to provide rapid autonomous movement development, without waiting for visual and proprioceptive integration sent from higher centres (Fetz et al., 2000; Kandel et al., 2012). In this case, activations signals s_k might actually originate directly from local sensory-motor integration, and the measure of distance could be replaced by proprioceptive input.

In this framework, the task-monitoring represents a mechanism for autonomous local sensory-motor integration, that can be modulated by cortical signals as in the proposed simulation of a reaching task, resembling the function of some interneuron circuits in the spinal cord (Levine et al., 2014).

Limitations and Alternatives

Limitations of the model proposed for the task monitoring are associated with the function it was built for, that is providing local monitoring to a motor task. This model can track one single behaviour. If, for example, an avoidance behaviour needs to be modelled in parallel, another monitoring block would be necessary to track it. The former task monitoring for reaching would be able in parallel to track the reaching, but not to model both processes at the same time.

More complex sequencing and timing would require neural fields coupling to be modelled, mirroring the engagement of cortical centres in motor planning, involving the cerebellum for instance (Johansson et al., 2016).

6.2.3 *Contribution 3. Synaptic nodes as a model for the neuro- muscular junction*

Connecting DNFs blocks with each other and with the robotic interface is a critical process: the emergent behaviour of the architecture arises from such interconnections and stably linking neural fields representation to output motor variables is an indispensable requirement. The latter translates into finding the position of the peak of activation on the field, providing other DNFs or the robotic interface with the correct input from the features space spanned by the neural field (Sandamirskaya, 2013).

This problem could seem trivial mathematically speaking, considering that it is easy to numerically find the position of the peak of a unimodal distribution. Nonetheless, using an algorithm-based approach does not match the embodied account, nor the physiologically inspired approach to model cognition. The methodology to find the location of the peak of the localised solution had to present some level of synaptic integration. For this reason, the idea to use the position as a mapping function seemed more appropriate (see Eq. (5.27)).

Interestingly, a similar strategy is used by Fard et al. (2015) and, considering the process at steady state and the appropriate choice of λ , the same formulation is found from Eq. (3.12), used to model neural nodes introduced in Section 3.4.

The study of the physiological properties of the connection between the neural and muscular junction, presented in Section 2.2.2, leads to the speculation that synaptic nodes could be representative of the neuromuscular junction, in the sense of the DFT. The process described in Eq. (5.26) could represent the resultant summation in time of the release of neurotransmitter in the synaptic junction, based on the active neural distribution. The release of quanta of neurotransmitter matches the normalised description of weights with respect to the measure of neural activation on the whole field in Eq. (5.27).

In the proposed framework, the position of the attractors for the SAM control law can be thought as the resultant muscle activation from selected motor primitives that produces a certain amount of force at the joints. In the biological parallelism, quanta

determine if and to what extent contractile elements are recruited. This process reflects particularly well the association of synaptic nodes to encoded activations s_k that determine the weight of each motor primitive.

In conclusion, recent studies on interneuron populations in the spinal cord (Levine et al., 2014) support the synaptic node representation as a suitable mathematical model for local polysynaptic interactions. Together with the task monitoring function, the proposed spinal controllers can account for local signal integration and local motor pools recruitment.

Limitations

It is obvious that synaptic nodes are not suitable to model complex biochemical chain reactions responsible for the transduction of neural activation patterns into muscular ones.

The purpose of the above speculation is to reunite the representation of neural processes and cognition in the dynamic field theory with a unified method for the encoding of motor output features. This could prove useful, for instance, for the study of motor control using more sophisticated muscle models.

At the same time, the development of genetic studies on the functions exerted by interneurons could shed light on the presence of multiple concurring processes that might require more sophisticated modelling solutions than the one presented here (e.g., including a dynamic process or time delays).

6.2.4 *Contribution 4. A unified methodology to design and simulate controllers in the DFT account*

The choice of DNFs to implement neural controllers is supported by a growing number of studies in which they have a prominent role in modelling motor control, as introduced in Chapter 3.

This is due to the intrinsic embodied approach offered by the input-output coupling, the representational stability offered by the working memory behaviour providing robust motor outputs, and the underlying reference to neural processes from which such models can be derived. Finally, the possibility to implement DNFs models on integrated chip using their equivalence with winner-takes-all (WTA) architectures, makes DFTs the ideal substrate for hardware embodied controllers for cognitive robotics (Sandamirskaya, 2013).

Developing the proposed architecture, it was noted that the use of DNFs for cognition seems to be growing apart from the study of stability of the field equation. The design of these models is moving towards a block-based design of controllers that represent a limited number of instabilities, usually on a two-dimensional features space.

This is indeed advantageous in terms of favouring modularity, so that architectures can be easily interfaced or compared. On the other hand, from the perspective of extending our knowledge about the physiological substrate, having a clear understanding of how different dynamics emerge from the field equation is crucial. In fact, understanding the role played by parameters determining stability can be used not only to model physiological findings, but also to extend the repertoire of elemental behaviours.

Considering that one of the aims of this project was to design appropriate controllers for a biomechanical model for motor control (see Chapter 1), the research on analytical and numerical methods for the dynamic field equation led to a methodology that could be well suited to design more physiologically based controllers.

The construction of the Evans functions associated with the desired solution is not

new, per se. The main application of this method is mathematically advantageous for the study of the field equation including delays. In this thesis, the method is adapted and applied to the construction of self-stabilising, self-sustaining and drifting peak solutions (see Chapter 4). Having identified a type of solution of interest, it is easy within this framework to study the evolution of the system and highlight critical parameters that can alter the topology of the space of features spanned by the neural field.

The choice of different control strategies that trigger instabilities as elemental behaviours can then be motivated by the biological findings that one wants to model. New elements developed using this process included in the architecture presented in Chapter 5 are:

- the adaptive threshold controlling the spinal memory block, derived from the study of stability of the field equation and, at the same time, linked to the process of neural population pre-activation (D’Esposito, 2007);
- the task monitoring block, designed so that stability/instability is caused by input amplitude and linked to sensory-motor integration of local and cortical signals in the spinal cord (Levine et al., 2014; Overduin et al., 2008);
- spinal memory blocks, designed to show persistent neural activity using a working memory instability and creating the equivalent neural representation of motor primitives (Giszter, 2015).

Of course, the proposed design solutions for these processes are not unique. A number of different options can be used to model cognition. In the reviewed studies it has been shown, for instance, that sensory-motor coupling and mapping output functions can be performed using different strategies (see Section 3.4).

In the same way, spinal autonomy could have been designed using some distance mapping over the feature space. A sigmoidal memory trace with a negative left bound could destabilise a traveling peak solution at the zero-crossing point (this option was actually tested, but the pinning self-sustaining peak was preferred).

It is clear that, using the field equation, different dynamics can be tested for a given cognitive process and, at the same time, the same cognitive process can be modelled with alternative approaches. Maintaining this embodied block modularity is a desirable feature, contributing to the creation of an extended framework for the study of motor control. At the same time, a clear methodology to design controllers allows for more flexibility in testing the solutions that better match physiological processes and biomechanical or robotic constraints.

To the best of our knowledge, explicit description of numerical methods in Matlab environment is not available in literature and these are presented here, in Section 5.4.1, completing the design tools necessary to develop flexible controllers in the DFT. Relevant numerical methods for dynamic field equations can be found in the work by Hutt and Rougier (2014) and Lima and Buckwar (2015), confirming the fact that only a limited number of studies on numerical solutions of field equations is available. Explicit mention of the FFT methods applied to the field equation can be found in the studies by Coombes et al. (2012) and Fard et al. (2015).

It is suggested that a clear methodology to design and simulate controllers, as the one presented in this thesis, can provide the tools for a more flexible development of DNFs architecture and facilitate links to physiological findings. Ideally, the existence of a standard framework for design and simulation could be significantly helpful in linking architectures that model different aspects of motor control.

The possibility to use new classes of solutions, representative of new elements of cognition in the sense of DFT, can be achieved using such methods and is one of the aims of the project. In order to address it, drifting instabilities are presented and methods for their construction are outlined in Sections 4.3.3 and 5.4.3.

The initial goal was to integrate pulse propagation as a cognitive function within the model for spinal motor control, as stated by the third of the aims in Chapter 1. The use of traveling pulses to represent neural processes is more physiologically plausible. Considering recent studies on impulse propagation, this type of dynamic could also play a role at the level of the neuromuscular junction, converting and amplifying pulse propagation directly into the muscle fibre (Barz et al., 2013).

At this stage of development of the architecture, the degree of physiological detail of neural propagation is limited and so is the biomechanical detail of the robotic interface. Most of the effort was aimed at determining a strategy to address the degrees of freedom problem emerging from a coherent representation of cognitive and motor features.

For this reason, it seemed sufficient to represent cognition using a detection/-forgetting instability type of dynamic and working memory instabilities to model persistent neural activity (Major & Tank, 2004). A more physiological representation that takes into account propagation phenomena in the proposed architecture is left to further developments.

6.3 Future Developments

In light of the discussion on the contributions given by thesis, it is possible to outline possible future developments involving the proposed architecture. These are presented here in order of complexity: from extended simulations that use the architecture described in Chapter 5 as it is, to experiments including links to other DNF architectures, more detailed biomechanical models and datasets of motor primitives. Lastly, the impact of this approach to the study of motor control on related fields is discussed, from neuroscience to robotics.

Short-Term Developments

The proposed model for motor control at the spinal cord level could be further tested in a number of simulated tasks. Simulations of curvilinear movements, detailed as a sequence of activations specifying motor primitive recruitment $s_k(t)$, could be used to fit behavioural invariants modelled by power laws (see Section 2.2.3). Preliminary simulations seem to support a shorter movement latency for closer targets.

The spinal attractor model, formalised in Section 5.2, uses the concept of attractor dynamic in a physiological embedding given by the concept of motor primitives summation and spinal signal processing. In this framework, it is possible to extend the tasks supported by the architecture adding obstacle avoidance, simply by creating a repeller dynamic in the same fashion as the attractor one.

This could be done considering a force term in the control law that represents repellers, finding a model similar in formulation to the one by Bicho and Schoner (1997), but based on an encoding in terms of motor primitives. This would offer an alternative approach to the architectures proposed by Rudolph et al. (2015) and Sandamirskaya and Schöner (2010).

An alternative approach to obstacle avoidance, mentioned already in Section 6.2.2, could be inspired by the activity-layer structure proposed by Brooks (1991). An overlapping layer for avoidance could be identical to the one presented in Fig. 5.4, including a task monitoring for obstacle avoidance and a spinal memory block to

activate a stable representation of the obstacles.

At this point, a coupled convolution of the ongoing motor plan and of the obstacle DNFs representation could deviate trajectory appropriately. Equation (3.15) gives an example of mapping learning for coupled neural fields that could be used. As soon as the task monitoring for obstacle avoidance signals the end of the avoidant behaviour, the system goes back to target reaching, supervised by the task monitoring for reaching.

Introducing the traveling peak solution as a representation of an elemental behaviour could allow for a more flexible and physiologically based representation of cognitive processes in the DFT. Drifting instabilities could be used in the proposed architecture to model task switching, without the need for a new motor plan representation.

Consider again the sudden appearance of an obstacle. An alternative to the convolution approach outlined above could be destabilising the resultant motor plan into a traveling peak using the adaptation gain g (or equivalently α), so as to shift temporarily the motor representation. Once the obstacle has been avoided, the motor plan could drift back to the initial position. Tuning the adaptation gain would give again the stable initial representation so that the reaching task can continue.

Traveling peaks could also be used to model cortical motor sequencing, representing with the motion a sequence of spinal activations or more complex motor patterns where two or more elemental motor plans are used in sequence.

Long-Term Developments

The development of the proposed model for spinal motor control has been accompanied throughout by the intention to create an embodied block structure that can be easily interfaced with existing dynamic field models for cognition and more refined biomechanical models.

In Chapter 1, the broader goal of the project is presented in terms of understanding coordination, from perceptual input to motor output. In order to achieve this goal in

full, connecting the proposed architecture to higher levels of sensory-motor integration is essential. Neural and synaptic nodes, in this sense, provide two simple connecting structures that can be used to create links among architectures.

Connecting the present model to architectures implementing visuospatial mapping would provide a set-up to simulate hand-eye coordination (see, for instance, the work by Johnson et al. (2008) and Sandamirskaya and Storck (2014) for models of visual cognition in the DFT). At the same time, adding detail to the robotic interface could provide useful insight on the role exerted by cortical efferent and local afferent signals, combined at the level of the spine. A simple way to do so could be, for example, implementing a learning and clustering algorithm like the one presented by Fard et al. (2015), including a flexor/extensor muscle model at the elbow. This would provide an *in silico* batch of motor primitives to test coordination with.

It is expected that the connection to models of the cortex will improve velocity profiles for reaching movements and provide the correct framework to investigate the origin of voluntary movement invariants (see Section 2.2.3 for a review of invariants and muscle properties and Section 6.2.1 for relevant limitations of the proposed model).

A further step towards a unified approach could be represented by linking dynamic systems and behavioural datasets. This means being able to generate voluntary movements using different types of motor primitives (i.e., kinematic or dynamic) and the possibility to test results across species, at least in a simulated environment (see Section 2.3.1 for a review on empirical findings on motor primitives).

Future Implications for Related Disciplines

Understanding motor control is a complex problem at the core of a number of fields that use specific methods and modelling techniques matching the level of complexity of the processes object of study. Motor control can be described in terms of processes that go from microscopic to macroscopic, from biochemical reactions to complex patterns of muscle activation, developmentally shaped by the interactions between body and environment. These complementary processes shape voluntary movements

as they are (Rosenbaum, 2010).

The contributions of this thesis support the development of coherent models for the investigation of those processes that are hardly observable *in vivo*, due to physiological or ethical constraints, or due to their intrinsic distributed and embodied nature. The modularity of the DFT, together with the possibility to convert field representations, either from biomechanical models or empirical data, into motor activations potentially allows for the investigation of all the aspects of the motor system. Results from simulations could in turn be used to develop new experiments *in vivo* to test hypothesis and assumptions.

In the embodied approach to cognition, it would be interesting to see if the principle of summation of sensory motor representations, here presented and tested to model spinal circuitry involved in motor control, could be extended to more abstract cognitive functions. An example could be the perceptual theory of knowledge proposed by Barsalou (1999): *perceptual symbols* could be modelled as cognitive motor primitives, grounded on a sensory motor representation.

Gaining a better understanding of motor control processes from the perspective offered by neuroscience and biomechanics opens the way to exploring new strategies for better (or, at least, alternative) robotics, even when the model is developed in principle to investigate underlying physiological processes (Fard et al., 2015).

Behind this consideration lies the assumption that a greater understanding of the cognitive and behavioural processes that guarantee adaptability, reactivity and learning for motor control in humans, can be used to build a new generation of robotics that show levels of engagement with the environment typical of living beings (Clark, 1997). This trend is explored in the review by Pfeifer et al. (2007).

Robotic setups using motor primitive extraction from EMG signals like the one by Artemiadis and Kyriakopoulos (2010) could indeed benefit from the proposed direct approach that does not require the computation of the inverse dynamics. Finally, a better understanding of movement formation could be relevant for the development of better prosthetics guided by electromyographic signals and neuro-rehabilitation protocols (Zecca et al., 2017).

6.4 Conclusions

In this last chapter, the four main contributions given by this thesis are discussed considering relevant models for the degrees of freedom problem and physiological findings on the neuromusculoskeletal system.

The first consists in the development of the last missing piece for a fully embodied framework to model and simulate motor control using dynamic field controllers, avoiding the solution of the inverse dynamic problem. The proposed model fills this gap using physiologically inspired controllers that support relevant empirical studies.

The second and the third contributions regard the development of a model for two processes mediated by interneurons in the spinal cord. The first represents local autonomous or centrally mediated timing for movement development in *the task monitoring block*; the second modelling signal processing in the neuromuscular junction, transforming the neural fields features mapping into motor activations using *synaptic nodes*.

The last contribution is represented by the methodology used to study the stability of neural fields, necessary to build controllers biologically inspired and associated numerical methods for simulation. The outlined procedure can be used to include additional elemental behaviour to the DFT, such as the drifting instability, selected to simulate travelling peaks of activity.

Suggested future developments span from simulations that extend the behavioural repertoire of the architecture as it is, to a complete framework for hand-eye coordination that links the proposed model for spinal motor control to other existing architecture for visuospatial and motor primitives mapping.

Considering the variety of behavioural findings accounted for and the simulation possibilities given by the modularity of DNFs architectures, the proposed model successfully represents the intention to outline a framework for a multidisciplinary approach for the study of motor control.

The hope is to encourage a coherent progress, guided by a shared language among

relevant fields, aiming at understanding cognition and voluntary movement formation. A multifaceted problem like this one can be better addressed with coordinated multidisciplinary efforts.

Bibliography

- Abend, W., Bizzi, E. & Morasso, P. (1982). Human arm movement trajectory formation. *Brain*, 1(September), 331–348.
- Alessandro, C., Delis, I., Nori, F., Panzeri, S. & Berret, B. (2013). Muscle synergies in neuroscience and robotics: from input-space to task-space perspectives. *Front. Comput. Neurosci.*, 7(April), 1–16. <https://doi.org/10.3389/fncom.2013.00043>
- Amari, S.-i. (1977). Dynamics of pattern formation in lateral inhibition type neural fields. *Biol. Cybern.*, 27(2), 77–87. <https://doi.org/10.1007/BF00337259>
- Artemiadis, P. K. & Kyriakopoulos, K. J. (2010). EMG-based control of a robot arm using low-dimensional embeddings. *IEEE Trans. Robot.*, 26(2), 393–398. <https://doi.org/10.1109/TRO.2009.2039378>
- Asada, H. & Slotine, J.-J. (1991). Robot analysis and control. *Introd. to robot.* (p. 12). John Wiley & Sons.
- Barsalou, L. W. (1999). Perceptual symbol systems. *Behav. Brain Sci.*, 22(4), 560–577. <https://doi.org/10.1017/S0140525X99252144>
- Barz, H., Schreiber, A. & Barz, U. (2013). Impulses and pressure waves cause excitement and conduction in the nervous system. *Med. Hypotheses*, 81(5), 768–772. <https://doi.org/10.1016/j.mehy.2013.07.049>
- Batschelet, E. (1981). *Circular statistics in biology*. Academic Press London.
- Bekey, G. A. & Goldberg, K. Y. (1993). *Trajectory Generation* (1st ed.). Springer. <https://doi.org/https://doi.org/10.1007/978-1-4615-3180-7>
- Beurle, R. L. (1956). Properties of a Mass of Cells Capable of Regenerating Pulses. *Philos. Trans. R. Soc. London B Biol. Sci.*, 240(669), 55–94.

- Bicho, E. & Schoner, G. (1997). Target position estimation, target acquisition, and obstacle avoidance. *IEEE Int. Symp. Ind. Electron.*, *1*, 13–20. <https://doi.org/10.1109/isie.1997.651728>
- Bizzi, E., Hogan, N., Mussa-Ivaldi, F. A. & Giszter, S. (1992). Does the nervous system use equilibrium-point control to guide single and multiple joint movements? *Behav. Brain Sci.*, *15*, 603–13. <https://doi.org/10.1017/S0140525X00072538>
- Bizzi, E., Mussa-Ivaldi, F. A. & Giszter, S. F. (1991). Computations underlying the execution of movement: a biological perspective. *Science*, *253*(5017), 287–91. <https://doi.org/10.1126/science.1857964>
- Bojak, I., Liley, D. T., Cadusch, P. J. & Cheng, K. (2004). Electrorhythmogenesis and anaesthesia in a physiological mean field theory. *Neurocomputing*, *58-60*, 1197–1202. <https://doi.org/10.1016/j.neucom.2004.01.185>
- Bongaardt, R. & Meljer, O. G. (2000). Bernstein’s theory of movement behavior: Historical development and contemporary relevance. *J. Mot. Behav.*, *32*(1), 57–71. <https://doi.org/10.1080/00222890009601360>
- Bressloff, P. C. (2012). Spatiotemporal dynamics of continuum neural fields. *J. Phys. A Math. Theor.*, *45*(3), 033001. <https://doi.org/10.1088/1751-8113/45/3/033001>
- Bressloff, P. C. & Coombes, S. (2013). Neural ‘Bubble’ Dynamics Revisited. *Cognit. Comput.*, *5*(3), 281–294. <https://doi.org/10.1007/s12559-013-9214-3>
- Bressloff, P. C., Folias, S. E., Prat, A. & Li, Y.-X. (2003). Oscillatory waves in inhomogeneous neural media. *Phys. Rev. Lett.*, *91*(17), 178101. <https://doi.org/10.1103/PhysRevLett.91.178101>
- Brooks, R. A. (1991). Intelligence without representation. *Artif. Intell.*, *47*(1-3), 139–159. [https://doi.org/10.1016/0004-3702\(91\)90053-M](https://doi.org/10.1016/0004-3702(91)90053-M)
- Clark, A. (1997). *Being There: Putting Mind, Body, and World Together Again*. The MIT Press.
- Coombes, S., Lord, G. J. & Owen, M. R. (2003). Waves and bumps in neuronal networks with axo-dendritic synaptic interactions. *Phys. D Nonlinear Phenom.*, *178*(3-4), 219–241. [https://doi.org/10.1016/S0167-2789\(03\)00002-2](https://doi.org/10.1016/S0167-2789(03)00002-2)
- Coombes, S. & Owen, M. R. (2004). Evans functions for integral neural field equations with heaviside firing rate function. *SIAM J. Appl. Dyn. Syst.*, *3*(4), 574–600. <https://doi.org/10.1137/040605953>

- Coombes, S., Beim Graben, P., Potthast, R. & Wright, J. J. (2014). Neural fields: Theory and applications. *Neural Fields Theory Appl.* <https://doi.org/10.1007/978-3-642-54593-1>
- Coombes, S. & Schmidt, H. (2010). Neural fields with sigmoidal firing rates: Approximate solutions. *Discret. Contin. Dyn. Syst.*, *28*(4), 1369–1379. <https://doi.org/10.3934/dcds.2010.28.1369>
- Coombes, S., Schmidt, H. & Bojak, I. (2012). Interface dynamics in planar neural field models. *J. Math. Neurosci.*, *2*(1), 9. <https://doi.org/10.1186/2190-8567-2-9>
- Costello, M. (2014). Situatedness. In T. Teo (Ed.), *Encycl. crit. psychol.* (pp. 1757–1762). Springer New York. https://doi.org/10.1007/978-1-4614-5583-7_470
- Damasio, A. (2008). ESSAY Behind the looking-glass. *Nature*, *454* (July).
- D’Avella, A., Saltiel, P. & Bizzi, E. (2003). Combinations of muscle synergies in the construction of a natural motor behavior. *Nat. Neurosci.*, *6*(3), 300–308. <https://doi.org/10.1038/nn1010>
- Deco, G., Jirsa, V. K., Robinson, P. A., Breakspear, M. & Friston, K. (2008). The dynamic brain: From spiking neurons to neural masses and cortical fields. *PLoS Comput. Biol.*, *4*(8). <https://doi.org/10.1371/journal.pcbi.1000092>
- Del Vecchio, D., Murray, R. M. & Perona, P. (2003). Classification of human actions into dynamics based primitives with application to drawing tasks. *Eur. Control Conf. ECC 2003*, (July), 445–450. <https://doi.org/10.23919/ecc.2003.7084995>
- D’Esposito, M. (2007). From cognitive to neural models of working memory. *Philos. Trans. R. Soc. B Biol. Sci.*, *362*(1481), 761–772. <https://doi.org/10.1098/rstb.2007.2086>
- Erlhagen, W. (2003). Internal models for visual perception. *Biol. Cybern.*, *88*(5), 409–417. <https://doi.org/10.1007/s00422-002-0387-1>
- Erlhagen, W. & Bicho, E. (2006). The dynamic neural field approach to cognitive robotics. *J. Neural Eng.*, *3*, R36–R54. <https://doi.org/10.1088/1741-2560/3/3/R02>
- Fard, F. S., Hollensen, P., Heinke, D. & Trappenberg, T. P. (2015). Modeling human target reaching with an adaptive observer implemented with dynamic neural fields. *Neural Networks*, *72*, 13–30. <https://doi.org/10.1016/j.neunet.2015.10.003>

- Fetz, E. E., Perlmutter, S. I. & Prut, Y. (2000). Functions of mammalian spinal interneurons during movement. *Curr. Opin. Neurobiol.*, *10*(6), 699–707. [https://doi.org/10.1016/S0959-4388\(00\)00160-4](https://doi.org/10.1016/S0959-4388(00)00160-4)
- Fitts, P. M. (1954). The information capacity of the human motor system in controlling the amplitude of movement. *J. Exp. Psychol.*, *47*(6), 381–391.
- Flash, T. & Hogan, N. (1985). The coordination of arm movements: an experimentally confirmed mathematical model. *J. Neurosci.*, *5*(7), 1688–1703. <https://doi.org/4020415>
- Flash, T. & Hochner, B. (2005). Motor primitives in vertebrates and invertebrates. *Curr. Opin. Neurobiol.*, *15*(6), 660–666. <https://doi.org/10.1016/j.conb.2005.10.011>
- Folias, S. E. & Bressloff, P. C. (2004). Breathing Pulses in an Excitatory Neural Network. *SIAM J. Appl. Dyn. Syst.*, *3*(3), 378–407. <https://doi.org/10.1137/030602629>
- Frigo, M. & Johnson, S. G. (2014). *Fast Fourier Transform*. fftw@fftw.org
- Fulton, J. F. (1939). Physiology of the Nervous System. *Nature*, *144*(3638), 133–134. <https://doi.org/10.1038/144133a0>
- Fuster, J. M. (1981). Prefrontal Cortex in Motor Control. *Compr. Physiol.*, (May), 1149–1178. <https://doi.org/10.1002/cphy.cp010225>
- Georgopoulos, A. P. (1997). Neural Networks and motor control. *Neurosci.*, *3*(1), 52–60. <https://doi.org/10.1177/107385849700300115>
- Georgopoulos, A. P., Schwartz, A. B. & Kettner, R. E. (1986). Neuronal Population Coding of Movement Direction. *Science*, *233*, 1416–1419.
- Giszter, S. F. (2015). Motor primitives - new data and future questions. *Curr. Opin. Neurobiol.*, *33*, 156–165. <https://doi.org/10.1016/j.conb.2015.04.004>
- Giszter, S. F. & Hart, C. B. (2013). Motor primitives and synergies in the spinal cord and after injury - the current state of play. *Ann. N. Y. Acad. Sci.*, *1279*(1), 114–126. <https://doi.org/10.1111/nyas.12065>
- Giszter, S. F., Mussa-Ivaldi, F. A. & Bizzi, E. (1993). Convergent force fields organized in the frog's spinal cord. *J. Neurosci.*, *13*(2), 467–491.
- Glasgow, L. A. (2014). *Applied Mathematics for Science and Engineering*. John Wiley & Sons, Incorporated.

- Goldman-Rakic, P. S. (1987). Motor control function of the prefrontal cortex. *Ciba Found. Symp.*, 132, 187–200. <https://doi.org/10.1002/9780470513545.ch12>
- Gordon, A. M., Huxley, A. F. & Julian, F. J. (1966). The variation in isometric tension with sarcomere length in vertebrate muscle fibres. *J. Physiol.*, 184(1), 170–92. <https://doi.org/10.1113/jphysiol.1966.sp007909>
- Graziano, M. S. A., Taylor, C. S. R., Moore, T. & Cooke, D. F. (2002). The Cortical Control of Movement Revisited. *Neuron*, 36(3), 349–362.
- Hart, C. B. & Giszter, S. F. (2010). A neural basis for motor primitives in the spinal cord. *J. Neurosci.*, 30(4), 1322–1336. <https://doi.org/10.1523/JNEUROSCI.5894-08.2010>
- Haugeland, J. (1978). The nature and plausibility of Cognitivism. *Behav. Brain Sci.*, 1(2), 215–226. <https://doi.org/10.1017/S0140525X00074148>
- Hill, A. V. (1938). The Heat of Shortening and the Dynamic Constants of Muscle. *Proc. R. Soc. B Biol. Sci.*, 126(843), 136–195. <https://doi.org/10.1098/rspb.1938.0050>
- Hutt, A. & Rougier, N. (2014). Numerical simulation scheme of one- and two dimensional neural fields involving space-dependent delays. *Neural fields theory appl.* (pp. 175–185). https://doi.org/10.1007/978-3-642-54593-1_6
- Huxley, H. E. (1957). The double array of filaments in cross-striated muscle. *J. Biophys. Biochem. Cytol.*, 3(5), 631–648. <https://doi.org/10.1083/jcb.3.5.631>
- Huxley, H. E. (2004). Fifty years of muscle and the sliding filament hypothesis. *Eur. J. Biochem.*, 271(8), 1403–15. <https://doi.org/10.1111/j.1432-1033.2004.04044.x>
- Ito, M. (2000). Mechanisms of motor learning in the cerebellum. *Brain Res.*, 886, 237–245.
- Jazar, R. M. (2007). *Theory of Applied Robotics. Kinematics, Dynamics, and Control* (2nd ed.). Springer US.
- Johansson, F., Hesslow, G. & Medina, J. F. (2016). Mechanisms for motor timing in the cerebellar cortex. *Curr. Opin. Behav. Sci.*, 8(12), 53–59. <https://doi.org/10.1016/j.cobeha.2016.01.013>
- Johnson, J. S., Spencer, J. P. & Schöner, G. (2008). Moving to higher ground: The dynamic field theory and the dynamics of visual cognition. *New Ideas Psychol.*, 26(2), 227–251. <https://doi.org/10.1016/j.newideapsych.2007.07.007>

- Kandel, E., Schwartz, J., Jessell, D. o. B., Thomas, M. B., Siegelbaum, S. & Hudspeth, A. J. (2012). *Principles of Neural Science, Fifth Edition*. McGraw-Hill Publishing.
- Kargo, W. J., Ramakrishnan, A., Hart, C. B., Rome, L. C. & Giszter, S. F. (2010). A simple experimentally based model using proprioceptive regulation of motor primitives captures adjusted trajectory formation in spinal frogs. *J. Neurophysiol.*, *103*(1), 573–590. <https://doi.org/10.1152/jn.01054.2007>
- Kawato, M. (1999). Internal models for motor control and trajectory planning. *Curr. Opin. Neurobiol.*, *9*(6), 718–727. [https://doi.org/10.1016/S0959-4388\(99\)00028-8](https://doi.org/10.1016/S0959-4388(99)00028-8)
- Kurt A., T. & Reza, S. (2000). Learning of action through adaptive combination of motor primitives. *Nature*, *407*(6805), 742–747.
- Kuznetsov, Y. A. (1996). *Elements of applied bifurcation theory* (Vol. 33). Springer Science & Business Media. <https://doi.org/10.5860/choice.33-3370>
- Lacquaniti, F., Terzuolo, C. & Viviani, P. (1983). The law relating the kinematic and figural aspects of drawing movements. *Acta Psychol. (Amst.)*, *54*(1-3), 115–130. [https://doi.org/10.1016/0001-6918\(83\)90027-6](https://doi.org/10.1016/0001-6918(83)90027-6)
- Latash, M. L. (2012). The bliss (not the problem) of motor abundance (not redundancy). *Exp. Brain Res.*, *217*(1), 1–5. <https://doi.org/10.1007/s00221-012-3000-4>
- Latash, M. L., Scholz, J. P. & Schönner, G. (2007). Toward a new theory of motor synergies. *Motor Control*, *11*(3), 276–308. <https://doi.org/10.1123/mcj.11.3.276>
- Lettvin, J. Y., Maturana, H. R., McCulloch, W. S. & Pitts, W. H. (1959). What the Frog's Eye Tells the Frog's Brain. *Proc. IRE*, *47*(11), 1940–1951. <https://doi.org/10.1109/JRPROC.1959.287207>
- Levine, A. J., Hinckley, C. A., Hilde, K. L., Driscoll, S. P., Poon, T. H., Montgomery, J. M. & Pfaff, S. L. (2014). Identification of a cellular node for motor control pathways. *Nat. Neurosci.*, *17*(4), 586–593. <https://doi.org/10.1038/nn.3675>
- Liley, D. T. J., Cadusch, P. J. & Wright, J. J. (1999). A continuum theory of electro-cortical activity. *Neurocomputing*, *26-27*(May 2000), 795–800. [https://doi.org/https://doi.org/10.1016/S0925-2312\(98\)00149-0](https://doi.org/https://doi.org/10.1016/S0925-2312(98)00149-0)

- Lima, P. M. & Buckwar, E. (2015). Numerical solution of the neural field equation in the two-dimensional case. *SIAM J. Sci. Comput.*, *37*(6), B962–B979. <https://doi.org/10.1137/15M1022562>
- Luppino, G. & Rizzolatti, G. (2000). The Organization of the Frontal Motor Cortex. *News Physiol. Sci.*, *15*(October), 219–224. <http://www.ncbi.nlm.nih.gov/pubmed/11390914>
- Major, G. & Tank, D. (2004). Persistent neural activity: Prevalence and mechanisms. *Curr. Opin. Neurobiol.*, *14*(6), 675–684. <https://doi.org/10.1016/j.conb.2004.10.017>
- MATLAB. (2021). *version 9.10 (R2021a)*. The MathWorks Inc.
- McLeod, R. M. (1979). *Generalized Riemann integral*. American Mathematical Society.
- Meier, J. D., Aflalo, T. N., Kastner, S. & Graziano, M. S. A. (2008). Complex organization of human primary motor cortex: a high-resolution fMRI study (2008/08/06). *J. Neurophysiol.*, *100*(4), 1800–1812. <https://doi.org/10.1152/jn.90531.2008>
- Miall, R. & Wolpert, D. (1996). Forward Models for Physiological Motor Control. *Neural Networks*, *9*(8), 1265–1279. <https://doi.org/10.1016/S0893-608000035-4>
- Miranda, J. G. V., Daneault, J. F., Vergara-Diaz, G., Torres, Â. F. S. d. O. e. T., Quixadá, A. P., Fonseca, M. d. L., Vieira, J. P. B. C., dos Santos, V. S., da Figueiredo, T. C., Pinto, E. B., Peña, N. & Bonato, P. (2018). Complex Upper-Limb Movements Are Generated by Combining Motor Primitives that Scale with the Movement Size. *Sci. Rep.*, *8*(1), 1–11. <https://doi.org/10.1038/s41598-018-29470-y>
- Morasso, P. (1981). Spatial control of arm movements. *Exp. Brain Res.*, *42*(2), 223–227. <https://doi.org/10.1007/BF00236911>
- Murray, R. M., Li, Z. & Shankar Sastry, S. (2017). *A mathematical introduction to robotic manipulation*. CRC press. <https://doi.org/10.1201/9781315136370>
- Mussa-Ivaldi, F. A., Giszter, S. F. & Bizzi, E. (1994). Linear combinations of primitives in vertebrate motor control. *Proc. Natl. Acad. Sci. U. S. A.*, *91*(16), 7534–7538. <https://doi.org/10.1073/pnas.91.16.7534>

- Overduin, S. A., D'Avella, A., Roh, J. & Bizzi, E. (2008). Modulation of muscle synergy recruitment in primate grasping. *J. Neurosci.*, *28*(4), 880–892. <https://doi.org/10.1523/JNEUROSCI.2869-07.2008>
- Owen, M. R., Laing, C. R. & Coombes, S. (2007). Bumps and rings in a two-dimensional neural field: Splitting and rotational instabilities. *New J. Phys.*, *9*(10), 378–378. <https://doi.org/10.1088/1367-2630/9/10/378>
- Pfeifer, R., Lungarella, M. & Iida, F. (2007). Self-organization, embodiment, and biologically inspired robotics. *Science*, *318*(5853), 1088–1093. <https://doi.org/10.1126/science.1145803>
- Pinotsis, D., Robinson, P., Graben, P. B. & Friston, K. (2014). Neural masses and fields: Modeling the dynamics of brain activity. *Front. Comput. Neurosci.*, *8*(11). <https://doi.org/10.3389/fncom.2014.00149>
- Pinto, D. J. & Ermentrout, G. B. (2001). Spatially structured activity in synaptically coupled neuronal networks: II. Lateral inhibition and standing pulses. *SIAM J. Appl. Math.*, *62*(1), 226–243. <https://doi.org/10.1137/S0036139900346465>
- Plamondon, R., Alimi, A. M., Yergeau, P. & Leclerc, F. (1993). Modelling velocity profiles of rapid movements: a comparative study. *Biol. Cybern.*, *69*(2), 119–128. <https://doi.org/10.1007/BF00226195>
- Rizzolatti, G. (2005). The mirror neuron system and its function in humans. *Anat. Embryol. (Berl.)*, *210*(5-6), 419–421. <https://doi.org/10.1007/s00429-005-0039-z>
- Rosenbaum, D. A. (2010). *Human Motor Control* (Second Ed., pp. 11–41). Academic Press. <https://www.sciencedirect.com/science/article/pii/B9780123742261000024>
- Rudolph, C., Storck, T. & Sandamirskaya, Y. (2015). Learning to reach after learning to look: A study of autonomy in learning sensorimotor transformations. *Proc. Int. Jt. Conf. Neural Networks, 2015-Sept.* <https://doi.org/10.1109/IJCNN.2015.7280733>
- Sandamirskaya, Y. (2013). Dynamic neural fields as a step toward cognitive neuromorphic architectures. *Front. Neurosci.*, *7*(January), 276. <https://doi.org/10.3389/fnins.2013.00276>

- Sandamirskaya, Y. & Schöner, G. (2010). An embodied account of serial order: How instabilities drive sequence generation. *Neural Networks*, *23*(10), 1164–1179. <https://doi.org/10.1016/j.neunet.2010.07.012>
- Sandamirskaya, Y. & Storck, T. (2014). Neural-dynamic architecture for looking: Shift from visual to motor target representation for memory saccades. *IEEE ICDDL-EPIROB 2014 - 4th Jt. IEEE Int. Conf. Dev. Learn. Epigenetic Robot.*, (June 2015), 34–40. <https://doi.org/10.1109/DEVLRN.2014.6982951>
- Sandamirskaya, Y., Zibner, S. K., Schneegans, S. & Schöner, G. (2013). Using Dynamic Field Theory to extend the embodiment stance toward higher cognition. *New Ideas Psychol.*, *31*(3), 322–339. <https://doi.org/10.1016/j.newideapsych.2013.01.002>
- Schmitt, S., Günther, M., Rupp, T., Bayer, A. & Häufle, D. (2013). Theoretical hill-type muscle and stability: Numerical model and application. *Comput. Math. Methods Med.*, *2013*(7). <https://doi.org/10.1155/2013/570878>
- Scholz, J. P. & Schöner, G. (1999). The uncontrolled manifold concept: Identifying control variables for a functional task. *Exp. Brain Res.*, *126*(3), 289–306. <https://doi.org/10.1007/s002210050738>
- Schöner, G. (2007). Dynamical systems approaches to cognition. *Cambridge Handb. Comput. Psychol.* <https://doi.org/10.1017/CBO9780511816772.007>
- Sejnowski, T. J. & Poggio, T. A. (2007). Dynamical Systems in Neuroscience. *Dyn. Syst.*, *25*, 227–256.
- Shampine, L. & Reichelt, M. (1997). Ode Matlab Solvers. *J. Sci. Comput.*, *18*, 1–22.
- Shapiro, L. A. (2012). *Embodied Cognition*. <https://doi.org/10.1093/oxfordhb/9780195309799.013.0006>
- Shukla, R. K. & Anchal, S. (2006). Harmonic Motion. *Mechanics* (pp. 523–544). New Age International Ltd.
- Slater, C. R. (2017). The structure of human neuromuscular junctions: Some unanswered molecular questions. *Int. J. Mol. Sci.*, *18*(10). <https://doi.org/10.3390/ijms18102183>
- Soechting, J. F. & Lacquaniti, F. (1981). Invariant characteristics of a pointing movement in man. *J. Neurosci.*, *1*(7), 710–720. <https://doi.org/10.1523/JNEUROSCI.01-07-00710.1981>

- Spencer, J., Perone, S. & Johnson, J. (2009). Dynamic field theory and embodied cognitive dynamics. *Toward a unified theory of development: Connectionism and dynamic systems theory re-considered*. Oxford University Press. <https://doi.org/10.1093/acprof:oso/9780195300598.003.0005>
- Spruston, N. (2008). Pyramidal neurons: Dendritic structure and synaptic integration. <https://doi.org/10.1038/nrn2286>
- Stelmach, E. & Diggles, A. (1982). Control Theories in Motor Behavior. *Acta Psychol. (Amst)*., 50, 83–105.
- Stringer, S. M., Trappenberg, T. P., Rolls, E. T. & de Araujo, I. E. T. (2002). Self-organizing continuous attractor networks and path integration: one-dimensional models of head direction cells. *Network*, 13(2), 217–242. <https://doi.org/10.1088/0954-898X/13/2/304>
- Suzuki, M., Yamazaki, Y., Mizuno, N. & Matsunami, K. (1997). Trajectory formation of the center-of-mass of the arm during reaching movements. *Neuroscience*, 76(2), 597–610. [https://doi.org/10.1016/S0306-4522\(96\)00364-8](https://doi.org/10.1016/S0306-4522(96)00364-8)
- Tatti, E., Ricci, S., Mehraram, R., Lin, N., George, S., Nelson, A. B. & Ghilardi, M. F. (2019). Beta modulation depth is not linked to movement features. *Front. Behav. Neurosci.*, 13(March), 1–6. <https://doi.org/10.3389/fnbeh.2019.00049>
- Todorov, E. (2004). Optimality principles in sensorimotor control. *Nat. Neurosci.*, (7(9)), 907–915.
- Tresch, M. C. & Jarc, A. (2009). The case for and against muscle synergies. *Curr. Opin. Neurobiol.*, 19(6), 601–607. <https://doi.org/10.1016/j.conb.2009.09.002>
- Uno, Y., Kawato, M. & Suzuki, R. (1989). Formation and control of optimal trajectory in human multijoint arm movement. *Biol. Cybern.*, 61(2), 89–101. <https://doi.org/10.1007/BF00204593>
- von Neumann, J. (1958). *The Computer and the Brain*. Yale University Press.
- Wiener, N. (1948). Cybernetics. *Sci. Am.*, 179(5), 14–19.
- Wilson, H. R. & Cowan, J. D. (1972). Excitatory and inhibitory interactions in localized populations of model neurons. *Biophys. J.*, 12(1), 1–24. [https://doi.org/10.1016/S0006-3495\(72\)86068-5](https://doi.org/10.1016/S0006-3495(72)86068-5)
- Wilson, M. (2002). Six views of embodied cognition. *Psychom. Bull. Rev.*, 9(4), 625–636.

- Winter, D. (2009). *Biomechanics and motor control of human movement* (Wiley, Ed.).
- Wolpert, D. M. (1997). Computational approaches to motor control. *Nature*, 1 (September).
- Wolpert, D. M. The real reason for brains [Video]. In: *Ted conf.* 2011. https://www.ted.com/talks/daniel_wolpert_the_real_reason_for_brains
- Zecca, M., Micera, S., Carrozza, M. C. & Dario, P. (2017). Control of Multifunctional Prosthetic Hands by Processing the Electromyographic Signal. *Crit. Rev. Biomed. Eng.*, 45(1-6), 383–410. <https://doi.org/10.1615/CritRevBiomedEng.v45.i1-6.150>

Appendix A

Appendix: Matlab Code Scripts and Functions

A.1 Code for a Reaching Task

The code below for the reaching simulation displays the same numbering as in Algorithm 6.

```
%%%%%%%%% REACHING TASK SIMULATION WITH 2 SPINAL ATTRACTORS. %%%%%%%%%%
% 1) Setting Parameters
tspan=100;      % simulation time
dt=0.1;         % time step
N=2^10;         % N x N gridpoints
L=80;          % size of the space of features
t=0:dt:(tspan-1)*dt; % t
x=(-N/2:N/2-1)/N*L; %x
y=(-N/2:N/2-1)/N*L; %y
dx=x(2)-x(1); dy=y(2)-y(1); % grid spacing
[X,Y]=meshgrid(x,y);
R=sqrt(X.^2+Y.^2);
```

```

hrest=-0.1;      % resting potential for inactive fields
epsilon=1e-10;  % tollerance for the neural node
alpha_phi=6;    % neural node inverse of time constant

% tm-DNF
[a_tm,s_tm,g_tm,h_tm,alpha_tm,beta_tm]=setparam('pinning');
% ACTIVATION BLOCK - 1D NF params
[a_s1,s_s1,g_s1,h_s1,alpha_s1,beta_s1]=setparam('stable_1D');
[a_s2,s_s2,g_s2,h_s2,alpha_s2,beta_s2]=setparam('stable_1D');
% MOTOR PRIMITIVES BLOCK - 2D NF params
[a_m1,s_m1,g_m1,h_m1,alpha_m1,beta_m1]=setparam('stable_2D');
[a_m2,s_m2,g_m2,h_m2,alpha_m2,beta_m2]=setparam('stable_2D');
% 2R PLANAR LINK
H=160;  W=60;
m1=0.029*W;      m2=0.0157*W;
l1=(0.818-0.630)*H;  l2=(0.630-0.485)*H;
% SPINAL ATTRACTOR MODEL S
S=[1 1];          % activations s_k (both attractors active example)
S=S/sum(abs(S));  % normalising activations
xM=[20 20; 20 30]; % spinal attractors in workspace coordinates
xEP=S*xM/(sum(S)); % target point
gsam=2.4*eye(2);  % gain for the derivative term

%2) Computing Synaptic footprints
W0_tm=synapticfoot(x,a_tm,s_tm);    % tm-DNF
W_s1=synapticfoot(x,a_s1,1);        % w for a-DNFs
W_s2=synapticfoot(x,a_s2,1);
W_a_s1=synapticfoot(x,a_s1,s_s1);   % w_a for a-DNFs
W_a_s2=synapticfoot(x,a_s2,s_s2);
W_m1=synapticfoot(R,a_m1,s_m1);     % w for a-DNFs
W_m2=synapticfoot(R,a_m2,s_m2);

```

%3) Initialising State Variables and Inputs

```

% u fields                                %Inputs
U_tm=zeros(N,tspan);                      I_tm=zeros(N,tspan);
U_s1=zeros(N,tspan);                      I_s1=zeros(N,tspan);
U_s2=zeros(N,tspan);                      I_s2=zeros(N,tspan);
U_m1=zeros(N,N,tspan);                   I_m1=zeros(N,N,tspan);
U_m2=zeros(N,N,tspan);                   I_m2=zeros(N,N,tspan);

% a fields
A_tm=zeros(N,tspan);
A_s1=zeros(N,tspan);
A_s2=zeros(N,tspan);
A_m1=zeros(N,N,tspan);
A_m2=zeros(N,N,tspan);
phi=zeros(1,tspan);                      % neural node
hphi=zeros(1,tspan);                     % adaptive threshold

% Initial Conditions
I=4; s_in=2;                              % params for gaussian input
I_s1(:,1)=I*exp(-abs(x-S(1))/(s_in));
I_s2(:,1)=I*exp(-abs(x-S(2))/(s_in));
I_m1(:,:,1)=I*(exp(-sqrt((X-xM(1,1)).^2+(Y-xM(1,2)).^2)/s_in));
I_m2(:,:,1)=I*(exp(-sqrt((X-xM(2,1)).^2+(Y-xM(2,2)).^2)/s_in));
phi(1)=0;                                  % inactive phi node before task onset

% Initialising Robot Model
yout=[10 15 0 0];                          % initial position in workspace coordinates
d=zeros(1,tspan);                          % distance from target vector
d(1)=sqrt((xEP(1)-yout(1))^2+(xEP(2)-yout(1))^2); % initial distance
v=1;                                        % time indexing for ode solver
time(v)=0;                                  % stores time from ode solver
out=zeros(tspan,4);                         % stores forward dynamics
out(v,:)=yout';
v=v+1;

% tm-DNF input

```

```

sigma=1; % dispersion of the input function
Ifun=exp(-((x).^2)/(2*(sigma^2))); % input's shape
Isn=0.7692; % bifurcation value for tm-DNF
I_tm(:,1)=(Isn+(d(1)/d(1)))*Ifun; % tm-DNF input in Eq.(5.19)
%4) Fourier Transforming Synaptic Footprints
Wf_tm=fft(W0_tm);
Wf_s1=fft(W_s1); Wfa_s1=fft(Wa_s1);
Wf_s2=Wf_s1; Wfa_s2=Wfa_s1;
Wf_m1=fft2(W_m1);
Wf_m2=Wf_m1;
%5) SIMULATION LOOP
for k=1:(tspan)-1
    %6) Transform Output Functions f=(U<=h).
    fU_tm=f(U_tm(:,k),h_tm);
    fU_s1=f(U_s1(:,k),h_s1); fA_s1=f(A_s1(:,k),h_s1);
    fU_s2=f(U_s2(:,k),h_s2); fA_s2=f(A_s2(:,k),h_s2);
    fU_a1=f(U_m1(:,:,k),h_m1);
    fU_a2=f(U_m2(:,:,k),h_m2);
    %7) Perform Convolution
    B_tm=fftshift(iffshift(fftshift(Wf_tm'.*(fft(fU_tm)))))*dx;
    B_s1=fftshift(iffshift(fftshift(Wf_s1'.*(fft(fU_s1)))))*dx;
    B_s2=fftshift(iffshift(fftshift(Wf_s2'.*(fft(fU_s2)))))*dx;
    H_s1=fftshift(iffshift(fftshift(Wfa_s1'.*(fft(fA_s1)))))*dx;
    H_s2=fftshift(iffshift(fftshift(Wfa_s2'.*(fft(fA_s2)))))*dx;
    B_m1=fftshift(iffshift2(fftshift(Wf_m1'.*(fft2(fU_a1)))))*dx*dy;
    B_m2=fftshift(iffshift2(fftshift(Wf_m2'.*(fft2(fU_a2)))))*dx*dy;
    %8a) Update Neural Node
    phi(k+1)=phi(k)*(1-dt*alpha_phi)+sum(fU_tm)*dx*dt*alpha_phi;
    hphi(k+1)=hrest*(1-f(phi(k),epsilon));
    %8b) Update Field Variables
    % task monitoring
    U_tm(:,k+1)=(1-dt*alpha_tm)*U_tm(:,k)+(B_tm-g_tm*A_tm(:,k) ...

```

```

        +I_tm(:,k))*dt*alpha_tm;
A_tm(:,k+1)=(1-dt*beta_tm)*A_tm(:,k)+U_tm(:,k)*dt*beta_tm;
% a-DNFs
U_s1(:,k+1)=(1-dt*alpha_s1)*U_s1(:,k)+(B_s1 - g_s1*H_s1+...
        I_s1(:,k)+hphi(k))*dt*alpha_s1;
U_s2(:,k+1)=(1-dt*alpha_s2)*U_s2(:,k)+(B_s2 - g_s2*H_s2+...
        I_s2(:,k)+hphi(k))*dt*alpha_s2;
A_s1(:,k+1)=(1-dt*beta_s1)*A_s1(:,k)+fU_s1*dt*beta_s1;
A_s2(:,k+1)=(1-dt*beta_s2)*A_s2(:,k)+fU_s2*dt*beta_s2;
% m-DNFs
U_m1(:, :, k+1)=(1-dt*alpha_m1)*U_m1(:, :, k)+(B_m1-g_m1*A_m1(:, :, k)+
        ...
        hphi(k)+I_m1(:, :, k))*dt*alpha_m1;
U_m2(:, :, k+1)=(1-dt*alpha_m2)*U_m2(:, :, k)+(B_m2-g_m2*A_m2(:, :, k)+
        ...
        hphi(k)+I_m2(:, :, k))*dt*alpha_m2;
A_m1(:, :, k+1)=(1-dt*beta_m1)*A_m1(:, :, k)+U_m1(:, :, k)*dt*beta_m1;
A_m2(:, :, k+1)=(1-dt*beta_m2)*A_m2(:, :, k)+U_m2(:, :, k)*dt*beta_m2;
%9) Condition on the Neural Node
if phi(k)>epsilon % if true the motor task is taking place
%10) Extracting Motor Output for SAM
Mk(1,1:2)=synapticnode(X,U_m1(:, :, k),h_m1);
Mk(2,3:4)=synapticnode(X,U_m2(:, :, k),h_m1);
sk(1)=synapticnode(x',U_s1(:,k),h_s1);
sk(2)=synapticnode(x',U_s2(:,k),h_s1);
sk=sk*eye(2);
% target point for SAM
xEPs=sk*Mk/(sum(sk));
%11) Simulating Forward Dynamics
[tout,yout]=ode45(@(t,x)twolink(t,x,H,W,gsam,sk,Mk),
        ...
        [t(k) t(k+1)],yout(end,:)');

```

```

% updating distance from target
d(k+1)=sqrt((yout(end,1)-xEPs(1)).^2+...
            (yout(end,2)-xEPs(2)).^2);
% % % % % storing data % % % % %
time(v)=tout(end);
out(v,:)=yout(end,:);
v=v+1;
else %12) no motor plan available
d(k+1)=d(k);    %the robot does not move
time(v)=time(v-1);
out(v,1:2)=out(v-1,1:2);
v=v+1;
end
%13) Updating input to tm-DNF
I_tm(:,k+1)=(Isn+(d(k+1)/d(1)))*Ifun;
end

```

A.1.1 Function Files

setparam.m

```

function [A, s, g, h, alpha,beta ] = setparam( string )
% SETS PARAMETERS FOR THE TYPE OF SOLUTION
% string = desired field dynamics
if isequal(string,'stable_1D')
    A=0.5; s=2; h=0.27; g=0.5; alpha=1; beta=1;
end
if isequal(string,'stable_2D')
    A=0.5; s=2; h=0.025; g=0.1; alpha=1; beta=1;
end
if isequal(string,'pinning')
    A=0.5; s=1; h=0.5; g=1; alpha=8; beta=0.03;
end

```

end

end

synapticfoot.m

```
function [ w ] = synapticfoot( x,A,s )
% synaptic footprint function for 1D and 2D NF
    if (size(x,1))==1
        % 1D DNF – exponential footprint
        w=A*exp(-abs(x/s))/s;
    else
        % 2D DNF – Mexican hat function
        w=(2*pi)^(-1)*(exp(-x)-A*exp(-x/s));
    end
end
```

synapticnode.m

```
function [ C ] = synapticnode(x, U,h)
% finds the position of the peak of activation in 1D and 2D DNFs
% U=DNF; h=output function's threshold
    U=U.*(U>h); % selecting the active part of the field
    if (size(x,2))==1 % 1D
        C=(sum(x.*U))./(sum(U));
    else % 2D
        y=x';
        C(1,:)=sum(sum(x.*U))./(sum(sum(U)));
        C(2,:)=sum(sum(y.*U))./(sum(sum(U)));
    end
end
```

twolink.m

```

function xdd=twolink(t,xdot,H,W,gsam,s,xA)
% Models the 2-R planar robot dynamics using SAM model
% x = (x_E,y_E) coordinates q = (theta1, theta2)
x=xdot(1:2);
xdot=xdot(3:4);
% Robot Parameters
m1=0.029*W;          m2=0.0157*W;
l1=(0.818-0.630)*H;  l2=(0.630-0.485)*H;
I1=m1*l1^2/12;      I2=m2*l2^2/12;
lc1=l1/2;           lc2=l2/2;
% Joint Angles
r2=(x(1)^2+x(2)^2);
alpha=acos((l1^2+l2^2-r2)/(2*l1*l2));
beta=acos((r2+l1^2-l2^2)/(2*l1*sqrt(r2)));
q(1)=atan(x(2)/x(1))-beta;
q(2)=pi-alpha;
Jinv=jacobianmat_inv(q,l1,l2); % inverse of the Jacobian in Eq.(4.87)
% angular vel
qdot(1:2)=Jinv*xdot;
dJinv=jacobianmat_invdot(q,qdot,l1,l2);% t-derivative of Jinv
% D(q)
d11=m1*lc1^2+m2*(l1^2+lc2^2+2*l1*lc2*cos(q(2)))+I1+I2;
d12=m2*(lc2^2+l1*lc2*cos(q(2)))+I2;
d22=m2*lc2^2+I2;
Dq=[d11 d12;d12 d22];
% C(q)
h=-m2*l1*lc2*sin(q(2));
c121=h;  c112=-h;
c211=h;  c221=h;
Cq=[c121*qdot(2) c221*qdot(2)+c211*qdot(1);

```

```
    c112*qdot(1) 0];  
% D, C in workspace coordinates  
D=Jinv'*Dq*Jinv;  
C=Jinv'*Cq*Jinv+D*dJinv;  
% SPINAL ATTRACTOR MODEL  
F_SAM_L=s*([x(1)-xA(:,1) x(2)-xA(:,2)]); % linear  
F_SAM_D=gsam; %derivative  
% forward dynamics  
xdd=D\ (F_SAM_L'+(F_SAM_D-C)*xdot);  
xdxdd=[xdot;xdd];  
end
```

A.2 Code for a Traveling Peak Solution

```

%%%%%%%% TRAVELLING SPOT SIMULATION %%%%%%%%%
% Setting Parameters
A=1/4;      sigma=2; %lateral inhibition
alpha=3;    beta=1;   %time constants
g=0.55;     %adaptation gain
h=0.12/(1+g); %output function threshold
% time and space
timelim=10;
xlim=30; ylim=30;
k=10; n=2^k; m=2^k; %grid points
dx=2*xlim/n; dy=dx; %grid spacing
x=-xlim:dx:xlim-dx;
y=-ylim:dy:ylim-dy;
dt=0.1;     %time step
t=0:dt:timelim;
tspan=length(t);
[X,Y]=meshgrid(x,y);
R=sqrt(X.^2+Y.^2);
PHI=atan(Y./X);
% synaptic footprint
w_bessel=(2/(3*pi))*(besselk(0,R)-besselk(0,2*R)-...
    A*(besselk(0,R/sigma)-besselk(0,2*R/sigma)));
w_bessel(0.5*n+1,0.5*n+1)=w(0.5*n+1,0.5*n+1); % removing NaN
w=w_bessel;
% analytical solution
RFUN=@(r,A,sigma,g,h) (4/3)*r.*((besselk(0,r)*besseli(1,r))-...
    (besselk(0,2*r)*besseli(1,2*r)/2))-...
    A*((besselk(0,r/sigma)*besseli(1,r/sigma)*sigma)-...
    (besselk(0,2*r/sigma)*besseli(1,2*r/sigma)*(sigma/2))))-(h*(1+g));

```

```

deltas=fzero(@(r) RFUN(r,A,sigma,g,h),4); % solver for Eq.(4.63)
funI1=@(delta,r,s) ((1/s)*besseli(1,s*delta)*besselk(0,s*r));
funI2=@(delta,r,s) (1/((s^2)*delta))-...
    (1/s)*besseli(0,s*r)*besselk(1,s*delta);
R1=double(R>deltas);
R1(R1==0)=0.1;
R(m/2+1,n/2+1)=0.001; % avoids NaN
R2=double(R<=deltas);
Q1=(4*deltas/3)*... % solution in Eq.(4.62)
    (funI1(deltas,R1.*R,1)-funI1(deltas,R1.*R,2)...
    -A*(funI1(deltas,R1.*R,1/sigma)-...
    funI1(deltas,R1.*R,2/sigma))).*(R>deltas);
Q2=(4*deltas/3)*...
    (funI2(deltas,R2.*R,1)-funI2(deltas,R2.*R,2)...
    -A*(funI2(deltas,R2.*R,1/sigma)-...
    funI2(deltas,R2.*R,2/sigma))).*(R2);
Q=(Q1+Q2)/(1+g);
% Initialising State Variables
u=zeros(m,n,tspan);
a=zeros(m,n,tspan);
u(:,:,1)=Q; % stable initial solution
phi_p=pi; % direction of motion
t_p=ceil(1/dt); % perturbation time
a_p=2; % perturbation amplitude
% Building the Boundary Perturbation
I=zeros(m,n,tspan);
R12=((X-deltas*cos(phi_p)).^2+(Y-deltas*sin(phi_p)).^2)/(2*(0.25)^2);
I0=2*exp(-R12)/sqrt(2*pi*0.25^2); % perturbation's shape
I(:,:,1:t_p)=repmat(I0,[1 1 t_p]);
%Simulation
W=(fft2(w)); % transforming synaptic footprint
for i=1:tspan-1

```

```
FU=fft2((u(:,:,i)>=h));           % transforming output function
B=fftshift(iff2(W.*FU))*dx*dy;     % convolution
% simulating field dynamics
u(:,:,i+1)=u(:,:,i)*(1-dt*alpha)...
    +B*dt*alpha-g*a(:,:,i)*dt*alpha+I(:,:,i)*dt*alpha;
a(:,:,i+1)=a(:,:,i)*(1-dt*beta)+u(:,:,i)*dt*beta;
end
```